Report 33452F
April 1981

NASA

ADVANCED OXYGEN-HYDROCARBON ROCKET ENGINE STUDY

Final Report

By

C. J. O'Brien

&

R. L. Ewen

AEROJET LIQUID ROCKET COMPANY

Prepared For

NATIONAL AERONAUTICS AND SPACE ADMINISTRATION

NASA-Marshall Space Flight Center

Contract NAS 8-33452

1. Report No.	2. Government Accession No.	3. Recipient's Catalog No.
33452F		

4. Title and Subtitle	5. Report Date
Advanced Oxygen-Hydrocarbon Rocket Engine Study, Final Report	April 1981
	6. Performing Organization Code
7. Author(s) C. J. O'Brien and R. L. Ewen	8. Performing Organization Report No.
	10. Work Unit No.
9. Performing Organization Name and Address Aerojet Liquid Rocket Company Post Office Box 13222 Sacramento, California 95813	11. Contract or Grant No. NAS 8-33452
	13. Type of Report and Period Covered Contractor Report, Final
12. Sponsoring Agency Name and Address National Aeronautics and Space Administration Washington, D.C. 20546	14. Sponsoring Agency Code

15. Supplementary Notes

Project Manager, R. J. Richmond, Propulsion Division
NASA-Marshall Space Flight Center
Marshall Space Flight Center, Alabama 35812

16. Abstract

In the decade of the 1980's and beyond, an improved surface-to-orbit transportation system using advanced booster vehicles may be required. The potential performance advantages of using high-density-impulse rocket propellants such as LO_2/hydrocarbon have been clearly shown for such large ΔV applications. This study identifies and evaluates promising LO_2/HC rocket engine cycles, produces a consistent and reliable data base for vehicle optimization and design studies, demonstrates the significance of propulsion system improvements, and selects the critical technology areas necessary to realize an improved surface-to-orbit transportation system.

Parametric LO_2/HC engine data were generated over a range of thrust levels from 890 to 6672 kN (200K to 1.5M lbF) and chamber pressures from 6890 to 34500 kN/m^2 (1000 to 5000 psia). Engine coolants included RP-1, refined RP-1, LCH_4, LC_3H_8, LO_2, and LH_2.

LO_2/RP-1 G.G. cycles were found to be not acceptable for advanced engines. The highest performing LO_2/RP-1 staged combustion engine cycle utilizes LO_2 as the coolant and incorporates an oxidizer-rich preburner. The highest performing cycle for LO_2/LCH_4 and LO_2/LC_3H_8 utilizes fuel cooling and incorporates both fuel- and oxidizer-rich preburners. LO_2/HC engine cycles permitting the use of a third fluid (LH_2) coolant and an LH_2-rich gas generator provide higher performance at significantly lower pump discharge pressures. The LO_2/HC dual-throat engine, because of its high altitude performance, delivers the highest payload for the vehicle configuration that was investigated.

17. Key Words (Suggested by Author(s))	18. Distribution Statement
LO_2/Hydrocarbon Engines LO_2/RP-1, LO_2/LCH_4, LO_2/LC_3H_8 Engines High-Pressure Liquid Rocket Engine Design High-Pressure Heat Transfer LO_2/HC Engine Performance	Unclassified - Unlimited

19. Security Classif. (of this report)	20. Security Classif. (of this page)	21. No. of Pages	22. Price*
Unclassified	Unclassified	313	

FOREWORD

The work described herein was performed at the Aerojet Liquid Rocket Company under NASA Contract NAS 8-33452 with Mr. Robert J. Richmond, NASA-Marshall Space Flight Center, as Project Manager. The ALRC Program Manager was Mr. Jeffery W. Salmon, and the Project Engineer was Mr. Charles J. O'Brien.

The technical period of performance for the study was from 15 October 1979 to 28 November 1980.

The following ALRC engineering personnel contributed significantly to this report:

C. J. O'Brien	(Engine System)
R. L. Ewen	(Heat Transfer)
R. A. Hewitt	(Thermal Geometry)
C. E. Taylor	(Heat Transfer)
G. M. Meagher	(Performance)
R. Salkeld (Consultant)	(Vehicle System)
S. Kent	(Parametric Weight/Envelope)
R. L. Sabiers	(Turbomachinery)
G. R. Janser	(Materials)
E. W. Carter	(Materials)
J. V. Smith	(Controls)
P. E. Brown	(Structures)
G. D. Aldrich	(Structures)
B. R. Lawver	(Combustion Stability)
R. A. Boylan	(Engine Layout)

Special thanks go to Mr. Rudi Beichel, ALRC Senior Scientist, for his comments and assistance throughout the study effort. Special thanks also go to Mr. Bob Richmond, the NASA Project Manager, and to Mr. Jim Martin, NASA Langley Research Center, for their constructive criticism and assistance.

TABLE OF CONTENTS

TABLE OF CONTENTS (cont.)

TABLE OF CONTENTS (cont.)

TABLE OF CONTENTS (cont.)

LIST OF TABLES

LIST OF TABLES (cont.)

LIST OF TABLES (cont.)

LIST OF FIGURES

LIST OF FIGURES (cont.)

LIST OF FIGURES (cont.)

LIST OF FIGURES (cont.)

LIST OF FIGURES (cont.)

LIST OF FIGURES (cont.)

LIST OF FIGURES (cont.)

I. SUMMARY

A. STUDY OBJECTIVES AND SCOPE

The major objectives of this study program were to (1) identify and evaluate promising liquid oxygen/hydrocarbon (LO_2/HC) rocket engine cycles, (2) produce a consistent and reliable data base for vehicle optimization and design studies, (3) indicate the significance of propulsion system improvements, and (4) identify the critical technology areas necessary to realize an improved surface-to-orbit transportation system.

The four-task study program summarized in Figure 1 was conducted to accomplish the stated objectives. Families of high chamber pressure LO_2/HC engine cycles were examined and their regions of operation (chamber pressure, thrust level, etc.) were established from a general conceptual matrix of potential cycle candidates. Thrust chamber heat transfer analyses were performed over the parametric range of thrust levels from 890 to 6672 kN (200K to 1.5M lbF) and chamber pressures from 6890 to 34500 kN/m^2 (1000 to 5000 psia). Engine coolants included RP-1, refined RP-1, LCH_4, LC_3H_8, LO_2, and LH_2. In order to make use of the available design data from previous studies, a preliminary baseline engine thrust was established. Parametric scaling studies were conducted around this design point.

Engine performance, envelope, and weight parametric data were generated over the above parametric ranges of thrust and chamber pressure and for selected mixture ratio and consistent area ratio values. Engine fuels included RP-1, refined RP-1 (e.g., JP-7), LCH_4 and LC_3H_8.

A preliminary comparison of the engine cycles was made by utilizing a simplified vehicle trajectory performance model for a two-stage heavy-lift, ballistic vehicle.

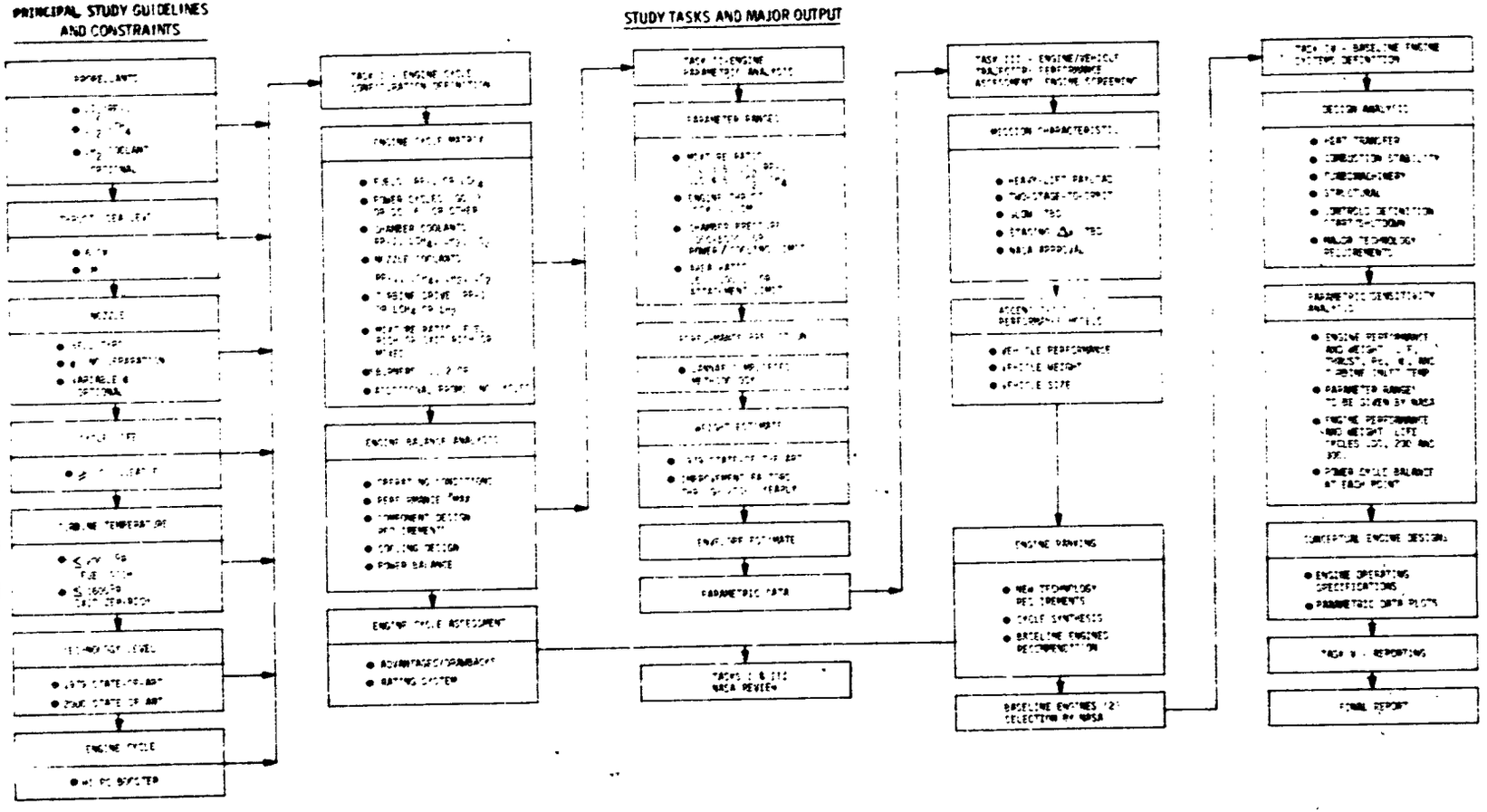

Figure 1. Overall Study Program Summary

I, A, Study Objectives and Scope (cont.)

Preliminary design analyses were conducted on the major components and subsystems of three engine cycles, and conceptual designs were prepared. Sensitivity analyses were performed which included the effects of turbine inlet temperature and number of usable life cycles.

Basic data gaps and areas requiring technology work were identified throughout the entire study effort.

B. RESULTS AND CONCLUSIONS

The highest performing LO_2/RP-1 engine cycle utilizes LO_2 or RP-1R as the coolant and incorporates an oxidizer-rich preburner. The highest performing cycle for LO_2/LCH_4 and LO_2/LC_3H_8 utilizes fuel cooling and incorporates both fuel- and oxidizer-rich preburners. LO_2/HC engine cycles permitting the use of a third fluid (LH_2) coolant and an LH_2-rich gas generator not only provide higher performance than the corresponding gas generator and staged- combustion cycles (without LH_2) but also require significantly lower pump discharge pressures. The LO_2/HC dual-throat engine, because of its high Mode 2 (altitude operation) performance, delivers the highest payload for the vehicle configuration that was investigated.

Families of LOX/RP-1, LOX/CH_4 and C_3H_8 engine cycles were identified as being acceptable candidates for future Space Transportation System (STS) application. Detailed trajectory analysis and a vehicle operational analysis, which includes engine life, reliability, safety margin, ease of maintenance, etc., need to be conducted in order to select the optimum LOX/HC engine.

Increasing the maximum allowable turbine inlet temperature for both the fuel and oxidizer rich turbines was shown to provide a large performance benefit for gas-generator and mixed cycles. A smaller benefit was shown for high-pressure, staged-combustion cycles utilizing fuel- and oxidizer-rich high-temperature turbines.

I, B, Results and Conclusions (cont.)

The performance increase for the gas generator cycles is due to the reduction in the low-performance turbine-drive-fluid which is dumped into the nozzle. The smaller performance increase for staged combustion cycles arises from a relatively small increase in chamber pressure.

The practical upper limit for both fuel-rich and oxidizer-rich turbine temperatures needs to be demonstrated before their benefit can be realized in LOX/HC engines.

A 30% reduction in engine weight by 1985 was shown to be a distinct possibility, and an even greater engine weight reduction of 40% is foreseen by the year 2000 through the use of reinforced plastic composite (RPC) materials.

MIL SPEC RP-1 cooled engines were shown to be cooling (coolant side coking) limited to a chamber pressure of about 8960 kN/m^2 (1300 psia) for the cycles investigated. With a carbon deposit on the combustion chamber walls, the cooling (coking) limit is about 13790 kN/m^2 (2000 psia). Refined RP-1 (i.e., JP-7)-cooled gas generator cycles result in a specific impulse maximum at about 17230 kN/m^2 (2500 psia); staged combustion cycles are power (pump discharge pressure) limited to about 22060 kN/m^2 (3200 psia). With a carbon deposit the refined RP-1 gas generator cycle engine attains a specific impulse maximum at a chamber pressure of about 18610 kN/m^2 (2700 psia).

LOX-cooled (LOX/RP-1) gas generator cycle engines attain a specific impulse maximum at a chamber pressure of about 17230 kN/m^2 (2500 psia); staged combustion cycle engines are power limited to about 21370 kN/m^2 (3100 psia).

I, B, Results and Conclusions (cont.)

LCH_4 and (subcooled) LC_3H_8-cooled gas generator cycle engines were shown to have a chamber pressure (specific impulse maximum) limit of about 20680 kN/m^2 (3000 psia). Staged combustion cycle engines cooled by LCH_4 and LC_3H_8 are power limited to chamber pressures of 24130 kN/m^2 (3500 psia) and 24820 kN/m^2 (3600 psia), respectively.

LH_2-cooled LO_2/HC engines of this study were shown to have a chamber pressure (power) limit of about 37920 kN/m^2 (5500 psia).

The technology recommendations resulting from this study include: (1) application of composite materials for weight reduction; (2) utilization of higher-temperature turbines for performance improvement; (3) incorporation of a stoichiometric preburner for start transient control; (4) development of the technology for high-pressure hydrocarbon and LO_2 turbopumps suitable for the engine cycles of this study; (5) generation of supercritical LCH_4 heat transfer data; and (6) further evaluation of the single-fuel, dual-throat thruster.

II. INTRODUCTION

A. BACKGROUND

In the decade of the 1980s and beyond, the nation's expanding space operations may require an improved surface-to-orbit transportation system using advanced booster vehicles with comparatively greater performance and capability than the current space shuttle concept. The mixed-mode propulsion principle clearly indicates the potential performance advantages of using high-density-impulse rocket propellants in such large ΔV applications (Ref. 1-9). For this reason, hydrocarbon fuels exhibiting increased density relative to liquid hydrogen (LH_2), though at the expense of lower specific impulse, are now being considered for the booster propulsion system of space shuttle improvements and derivatives as well as for single-stage-to-orbit and two- stage-to-orbit heavy-payload vehicles.

It is considered essential to undertake a preliminary identification and evaluation of promising liquid oxygen/hydrocarbon (LO_2/HC) rocket engine cycles in order to 1) produce a consistent and reliable data base for vehicle optimization and design studies, 2) demonstrate the significance of propulsion system improvements, and 3) identify the critical technology areas necessary to realize such advances.

B. PURPOSE AND SCOPE

The purpose of this study is to generate a consistent engine system data base for defining advantages and disadvantages, system performance and operating limits, engine parametric data, and technology requirements for candidate high-pressure LO_2/HC engine systems. The scope includes the synthesizing of optimum LO_2/HC engine power cycles and the generating of representative conceptual engine designs for an advanced surface-to-orbit transportation system.

II, B, Purpose and Scope (cont.)

The study guidelines dictated that the engine cycles to be examined must be compatible with advanced single-fuel bi- or tripropellant high-pressure LO_2/HC booster engines. "Single-fuel" refers to engines burning only one propellant combination during ascent operation, i.e., "dedicated" hydrocarbon engines. Dual-fuel engines were excluded from the study; however, "Tripropellant" engines using a supplementary fluid (e.g., LH_2) for cooling or pre-combustor power functions were included.

The general guidelines and constraints specified for the study are given in Table I. Properties of the propellants evaluated in the study are given in Tables IA and IB.

C. APPROACH

To accomplish the program objectives, an effort involving four technical tasks was conducted. Tasks accomplished are as follows:

1. Task I - Engine Cycle Configuration Definition

Formulate and assess families of high chamber pressure LO_2/HC engine cycles (Figure 2).

2. Task II - Engine Parametric Analysis

Generate performance, weight, and envelope parametric data for viable concepts based upon historical data and conceptual evaluations (Figure 3).

TABLE I

STUDY GUIDELINES AND CONSTRAINTS

Propellants	LO_2/RP-1 and LO_2/LCH_4 (liquid methane), with LH_2 as the supplementary fluid in tri-propellant engines. LO_2/LC_3H_8 (sub-cooled liquid propane) was added during Task IV.
Thrust per Engine (sea level)	600,000 lbF and 1,000,000 lbF
Expansion Nozzle Configuration	Bell-type (not necessarily fixed expansion ratio)
Nozzle Expansion Area Ratio	Consistent with booster engine mission, including the avoidance of over-expanded flow separation at sea level.
Minimum Engine Cycle Life	100 (usable)
Turbine Inlet Temperature Limits (maximum)	2000°R for fuel-rich turbine drive gases; 1600°R for oxidizer-rich turbine drive gases.
General Technology Level Assumptions	1979 state-of-the-art with yearly advance factors to 2000.
Coolants	RP-1, LCH_4, LO_2 and LH_2. Purified RP-1 (e.g., JP-7 or JP-5) was added in Task I and LC_3H_8 was added in Task IV.
Parametric Ranges:	
Chamber Pressure	1000 to 5000 psia (or power/cooling limit)
Engine Thrust	200,000 lbF to 1,500,000 lbF
Mixture Ratio	2.0 to 3.5 (LO_2/RP-1); 3.0 to 4.5 (LO_2/LCH_4)
Expansion Area Ratio	15:1 to 100:1 (or sea level flow attachment limit)
Turbine Inlet Temperature	1600°R to 3000°R (selected in Task IV)

TABLE IA

PROPERTIES OF CANDIDATE PROPELLANTS

	Oxygen[1][a]	Hydrogen[1]	RP-1[1]	JP-7[3]	Methane[1]	Propane[2]
Formula	O_2	H_2	$(CH_2)12.37$	$(CH_2)_x$	CH_4	C_3H_8
Molecular Weight	31.9988	2.01594	173.5151	14.03x	16.043	44.096
Freezing Point, °K (°F)	54.372 (-361.818)	13.835 (-434.767)	224.8 (-55)	230 (-46)	90.68 (-296.4)	85.47 (-305.8)
Boiling Point, °K (°F)	90.188 (-297.346)	20.268 (-423.187)	492.6 (427)	456-561 (360-550)	111.64 (-258.7)	231.07 (-43.7)
Critical Temperature, °K (°F)	154.581 (-181.433)	32.976 (-400.313)	679 (763)	- -	190.6 (-116.7)	369.8 (206.2)
Critical Pressure, MN/m^2 (psia)	5.043 (731.4)	1.2928 (187.51)	2.344 (340)	- -	4.60 (667)	4.24 (617.8)
Critical Density, kg/m^3 (lb/ft^3)	436.1 (27.23)	31.43 (1.962)	- -	- -	160.43 (10.015)	218.7 (13.65)
Vapor Pressure at 298.15°K, kN/m^2 (at 77°F, psia)	- -	- -	1.8 (.26)	- -	- -	- -
Density Liquid at 298.15°K, kg/m^3 (at 77°F, lb/ft^3)	1140.8[b] (71.23)	70.78[b] (4.419)	800 (49.94)	793 (49.5)	422.6[b] (26.38)	579.9[b] 728.8[d] (36.2) (45.5)
Heat Capacity, Liquid at 298.15°K, J/g-°K (at 77°F, Btu/lb-°F)	1.696[b] (.405)	9.690[b] (2.316)	1.98 (.474)	- -	3.50[b] (0.835)	2.25[b] 1.91[d] (0.536)(0.456)
Viscosity, Liquid at 298.15°K, $kN-s/m^2$ (at 77°F, $lb_m/ft-sec$)	$.1958^b$ ($1.316x10^{-4}$	0132^b ($.887x10^{-5}$)	1.53 ($1.04x10^{-3}$)	- -	0.1155^b ($7.76x10^{-5}$)	0.213^b 7.45^d ($1.43x10^{-4}$)($5.01x10^{-3}$)
Thermal Conductivity, Liq. at 298.15°K, W/m-°k (at 77°F, Btu/ft-sec-°F)	$.1515^b$ ($2.433x10^{-5}$)	$.0989^b$ ($1.589x10^{-5}$)	.137 ($2.2x10^{-5}$)	- -	$.193^b$ ($3.09x10^{-5}$)	0.128^b 0.242^d ($2.05x10^{-5}$)($3.88x10^{-5}$)
Heat of Formation, Liquid at 298.15°K, kcal/mol (at 77°F, Btu/lb)	-3.093[b] (-174.0)	-2.134[b] (-1905)	-6.2[c] (-796)	-6.3 (-808)	-21.37[b] (-2400)	-29.71[b] -32.74[d] (-1213)(-1336)
Cost, $/lb	0.033	4.50	1.00	1.00+	0.22	0.16

a Numbers in parentheses indicate references.
b At NBP
c kcal/g CH_2 unit
d At LOX NBP (-297°F)

TABLE 1B

COMPARISON OF RP-1 AND JP-7 FUELS

	Specification		Typical Value	
	RP-1	JP-7	RP-1	JP-7
Composition:				
Paraffins, %	--	--	41	50-56
Naphthenes, %	--	--	56	40-47
Aromatics, vol % (max)	5.0	5.0	3, 4.1	2.8-3.4, 3.7
Olefins, vol % (max)	1.0	--	nil, 0.77	--
Indans & Tetralins, %	--	--	--	0.5-0.7
Distillation				
Initial boiling point, °F, (min)	Report	360	349	388
10% evaporated, °F, (min)	365-410	380	379	401
20% evaporated, °F, (min)	--	403	--	410
50% evaporated, °F	Report	Report	414	414
90% evaporated, °F, (max)	Report	500	451	452
Final boiling point, °F, (max)	525	550	485	507
API Gravity, (min)	42.0	44.0	43.2	47.0
API Gravity, (max)	45.0	50.0		
Existent gum, mg/100 ml (max)	7	5	1.4	1.2
Potential gum, mg/100 ml (max)	14	10	2.9	2.0
Sulfur, total, % wt, (max)	0.05	0.01	0.026	<.006
Nitrogen, ppm	--	--	--	None detected to trace (<25)
Mercapton sulfur, % wt, (max)	0.005	0.001	0.0007	<.0007
Flash point, °F, (min)	110	140	137	156
Freezing point, °F (max)	-40	-46	<-40	-48
Heating value, net, Btu/lb (min)	18,500	18,700	18,640	18,767
Viscosity at -30°F, CS (max)	16.5	15	10.42	10.2
Copper strip corrosion, max ASTM classification	1	1B	1A	1B
Smoke point, mm, (min)	25	--	29.5	--
Luminometer No., (min)	--	75	--	88
Water separometer test, (min)	--	85	--	95
Particulate matter, mg/ℓ, (max)	--	1	--	0.1
Precipitation test, Munsell Color Code	--	<B1	--	<B1
High Temp. Research Fuel Coker Test (300°F prestress, 500°F preheater, and 600°F filter)				
Filter ΔP, in. Hg, (max)	--	3	--	0.1
Preheater deposit (Visual Comparison No.)	--	<3	--	1

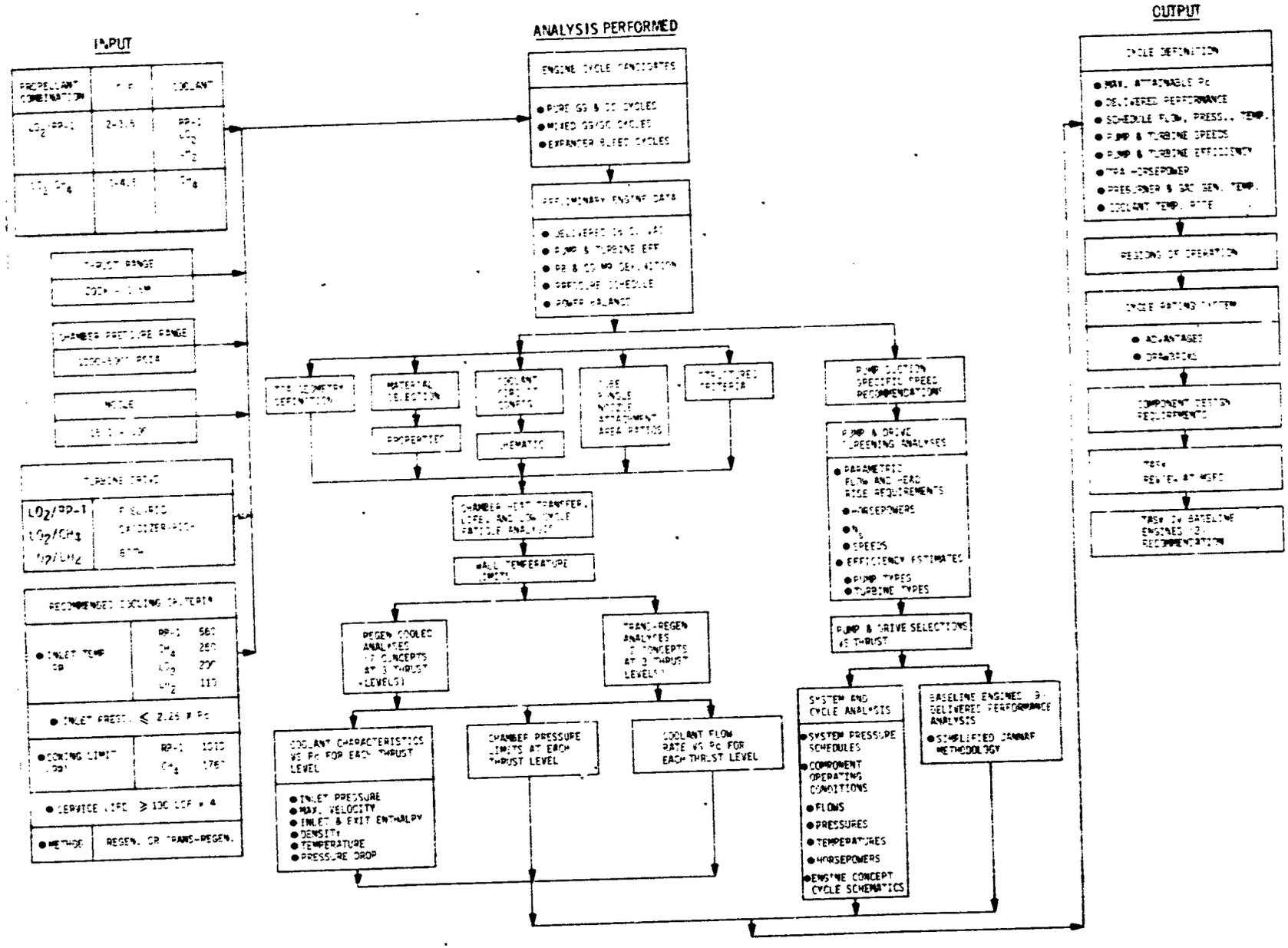

Figure 2. Task I - Engine Cycle Configuration Definition

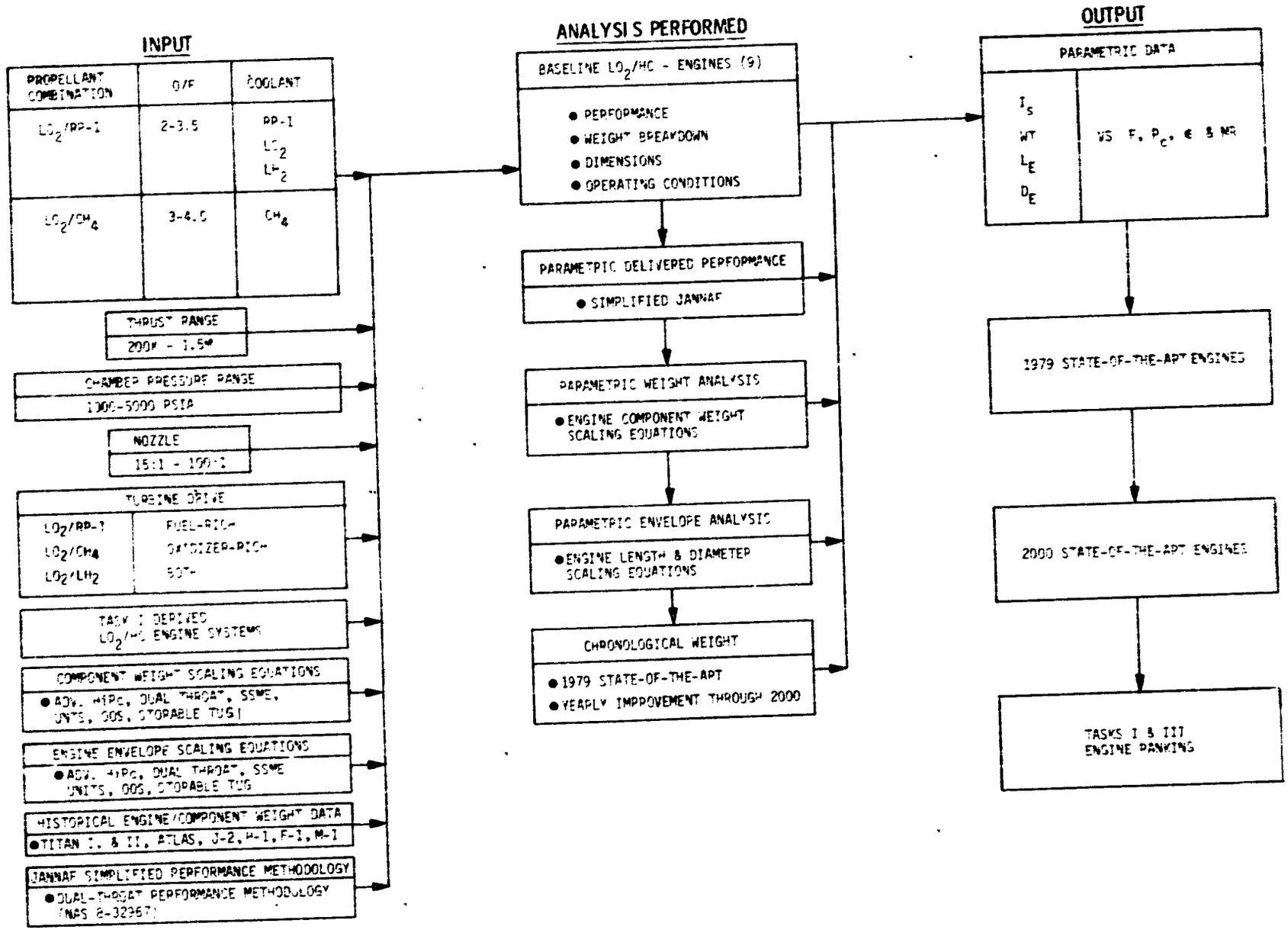

Figure 3. Task II - Engine Parametric Analysis

II, C, Approach (cont.)

3. Task III - Engine/Vehicle Trajectory Performance Assessment (Engine Screening)

Conduct a preliminary comparison of selected engine cycles by utilizing a simplified vehicle, system analysis, and trajectory performance model (Figure 4).

4. Task IV - Baseline Engine Systems Definition

Prepare preliminary designs of three baseline engine configurations. Conduct heat transfer, turbomachinery, combustion stability, structural, and controls analysis of the baseline engines and components. Conduct a parametric sensitivity analysis which includes the effects of turbine temperature and number of usable life cycles. This task is summarized in Figure 5.

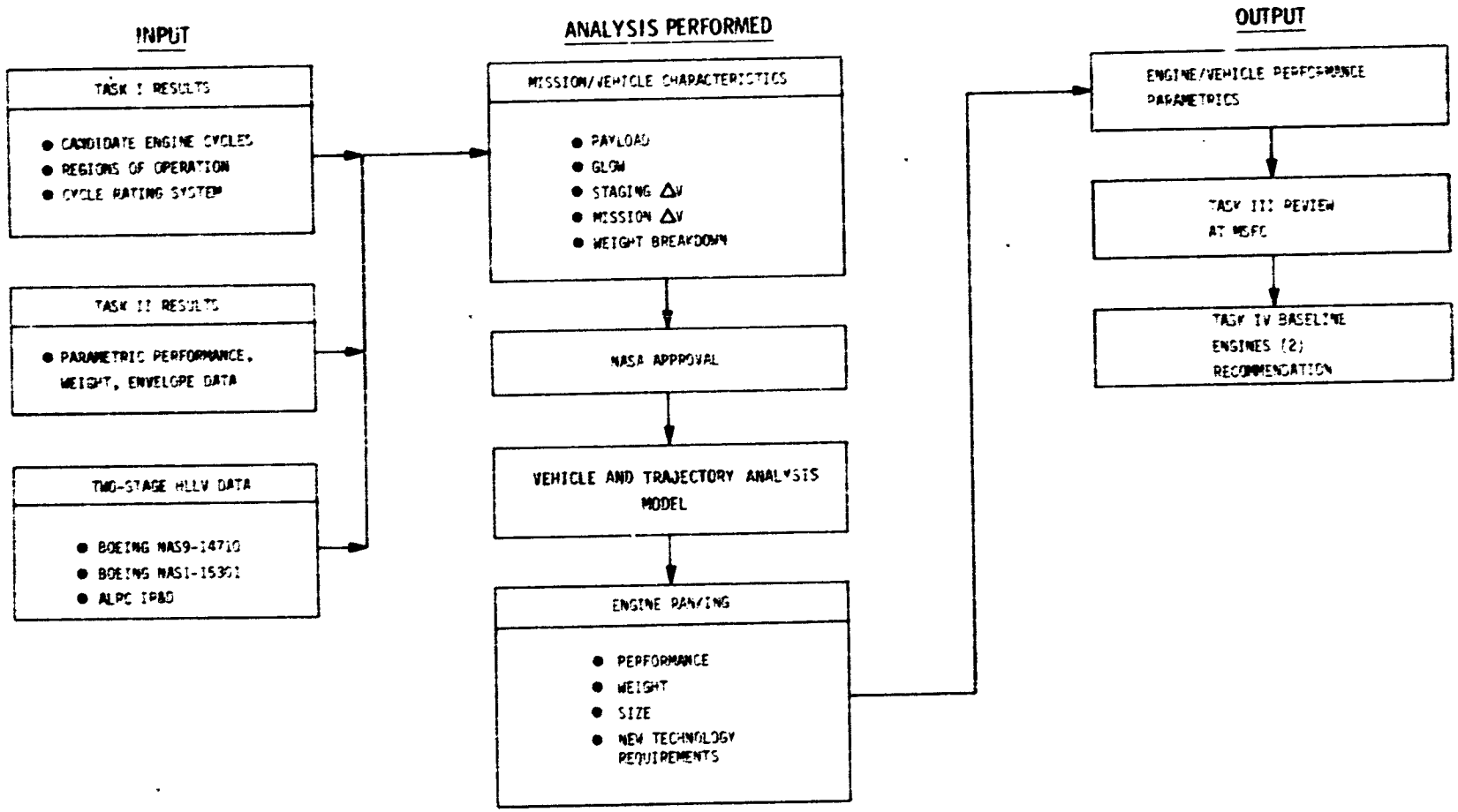

Figure 4. Task III - Engine/Vehicle Trajectory Performance Assessment (Engine Screening)

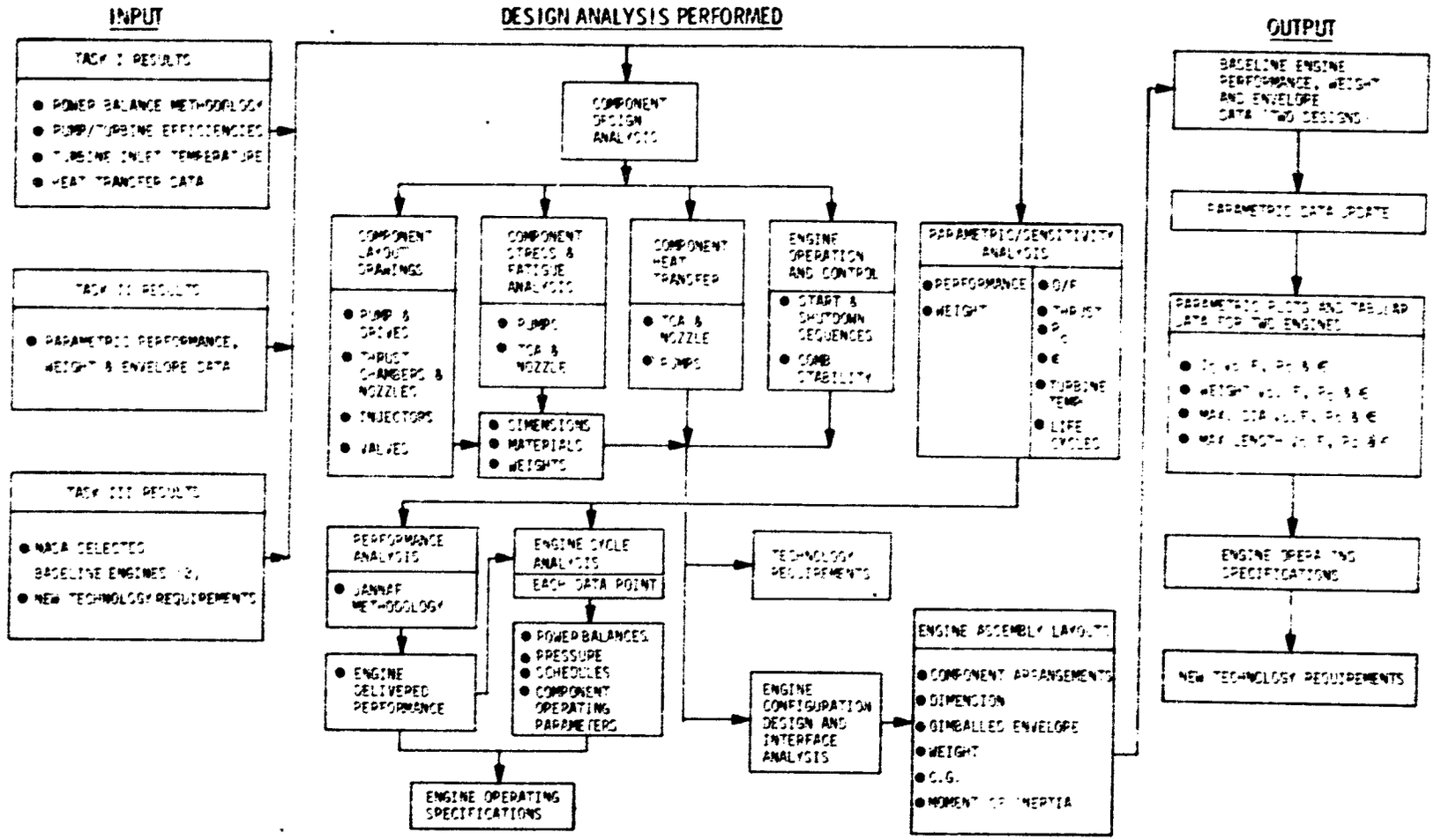

Figure 5. Task IV - Baseline Engine Systems Definition

III. ENGINE CYCLE CONFIGURATION DEFINITION

A. OBJECTIVES AND GUIDELINES

High chamber pressure LO_2/HC engine cycles from the NASA-specified cycles depicted in Figure 6 were to be evaluated. These candidates are from the NASA general conceptual matrix shown in Figure 7. The general matrix is seen to include the possibility of LH_2 cooling and the use of a fuel-rich LO_2/LH_2 turbine drive combustor (TDC).

Engine power balances and cooling design assessments were made to define chamber pressure limits. The various advantages and drawbacks of each engine cycle candidate were investigated. Analyses were conducted on the specified cycle candidates (A through I) given in Table II. Additional promising cycles (J through R) included in Table II were also examined, and two were selected for complete analysis. For each candidate propulsion system, engine balance analyses were conducted to establish engine operating conditions, performance, and component design requirements.

B. POWER CYCLE MATRIX

Power cycle candidates were evaluated by a two-step process. In the initial step, a preliminary baseline engine specification was established for a selected cycle and propellant combination. Engine flowrates were generated, coolant pressure drops were estimated (approximations based on past studies), and a pressure schedule was established for this baseline system. Heat transfer, structural, and materials analyses were then conducted over the parametric range of variables, utilizing the baseline engine as a reference.

In the second step, coolant channel pressure drop data from the heat transfer analysis were used to generate a more realistic pressure schedule for the various cycle candidates.

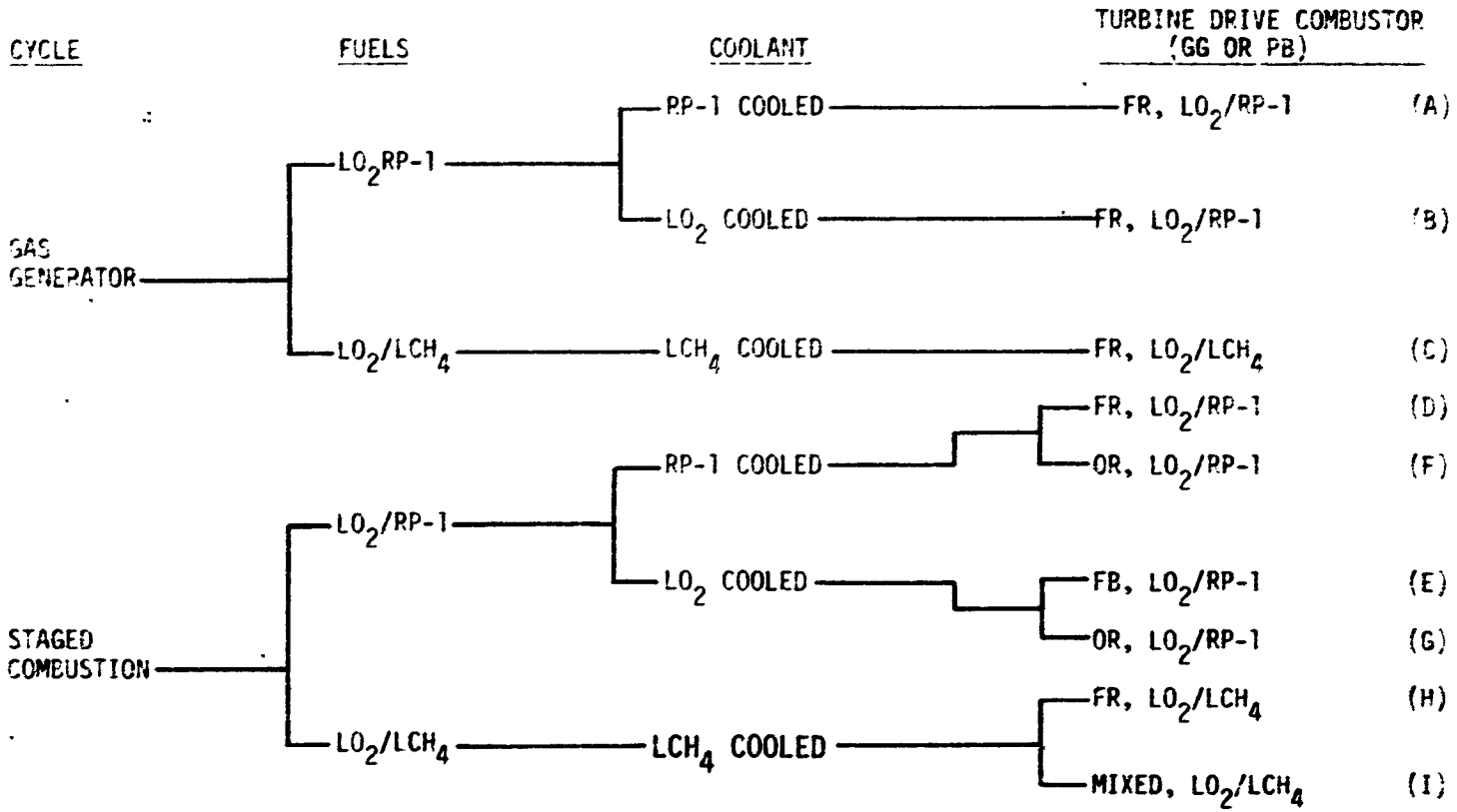

Figure 6. NASA-Specified Candidate Cycles for Advanced LO_2/HC Engines

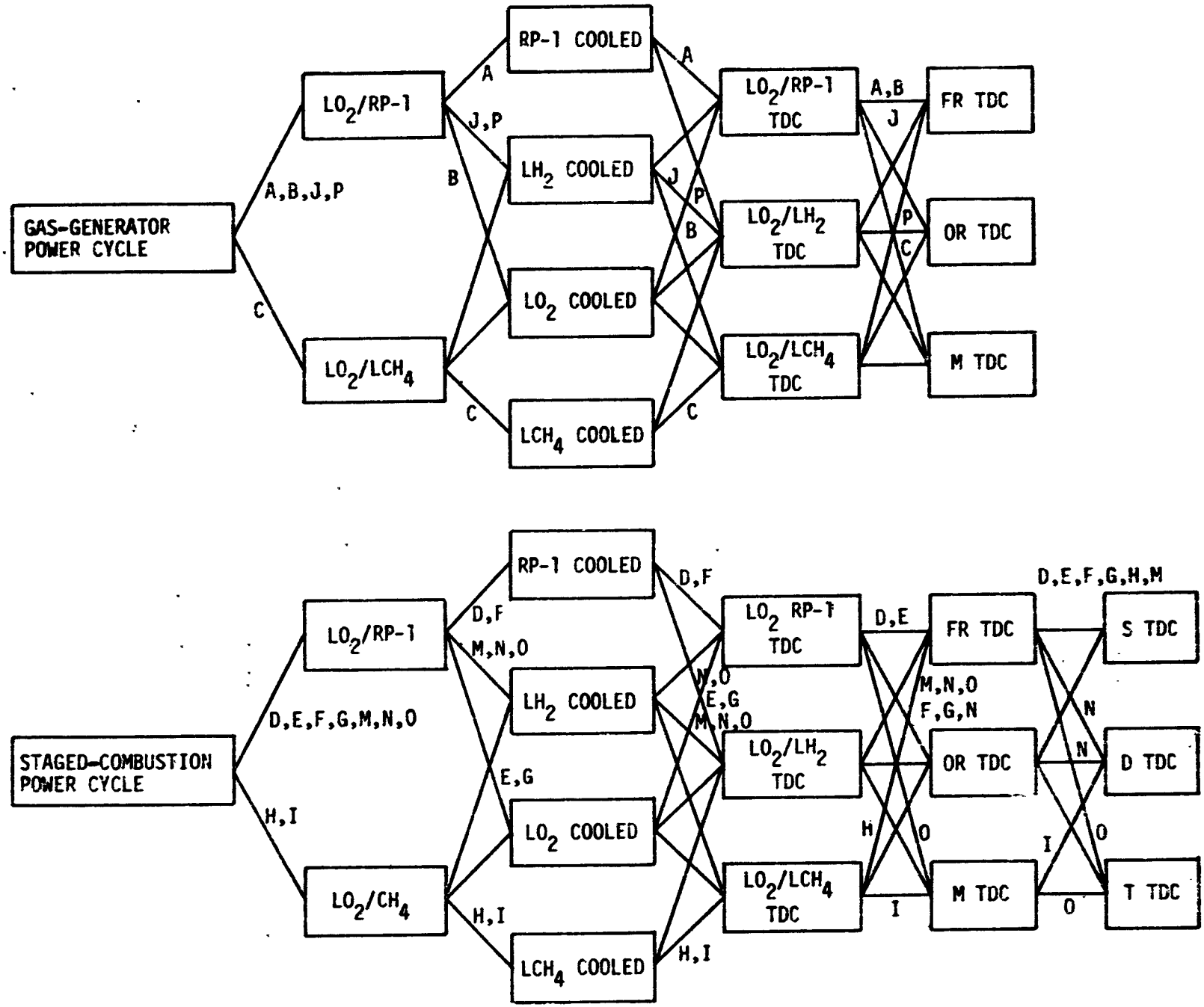

Figure 7. NASA Concept Array of Potential Cycle Choices for Advanced LO_2/HC Engines

TABLE II

CANDIDATE CYCLES INVESTIGATED

Cycle	Propellants	Coolant	Turbine Drive System
A	LO_2/RP-1	RP-1	LO_2/RP-1 fuel-rich (FR) gas generator (GG) cycle
B	LO_2/RP-1	LO_2	LO_2/RP-1 FR GG cycle
C	LO_2/LCH_4	LCH_4	LO_2/LCH_4 FR GG cycle
D	LO_2/RP-1	RP-1	LO_2/RP-1 FR preburner (PB) staged combustion (SC) cycle
E	LO_2/RP-1	LO_2	LO_2/RP-1 FR PB SC cycle
F	LO_2/RP-1	RP-1	LO_2/RP-1 oxidizer-rich (OR) PB SC cycle
G	LO_2/RP-1	LO_2	LO_2/RP-1 OR PB SC cycle
H	LO_2/LCH_4	LCH_4	LO_2/LCH_4 FR PB SC cycle
I	LO_2/LCH_4	LCH_4	LO_2/LCH_4 FR & OR PB SC cycle
J	LO_2/RP-1	LH_2	LO_2/LH_2 FR GG cycle
K	LO_2/LCH_4 Dual Throat	LH_2 & LCH_4	LO_2/LH_2 FR GG & LO_2/LCH_4 OR PB mixed cycle (GG & SC)
L*	LO_2/RP-1 Dual Throat	LH_2 & LO_2	LO_2/LH_2 FR GG & LO_2/RP-1 OR PB mixed cycle (GG & SC)
M*	LO_2/RP-1	LH_2	LO_2/LH_2 FR PB SC cycle
N*	LO_2/RP-1	LH_2	LO_2/LH_2 FR PB & LO_2/RP-1 OR PB SC cycle
O*	LO_2/RP-1	LH_2	LO_2/LH_2 FR PB & LO_2/RP-1 FR & OR PB SC cycle
P*	LO_2/RP-1	LH_2	LO_2/LH_2 OR GG cycle
Q*	LO_2/RP-1	LH_2	heated H_2 expander bleed (EB) cycle
R*	LO_2/RP-1	LH_2	heated H_2 & LO_2/RP-1 OR PB mixed cycle (EB & SC)

* Preliminary screening only

III, B, Power Cycle Matrix (cont.)

The LO_2/HC engine cycles primarily consist of either a closed-loop (staged-combustion) or an open-loop (gas-generator) system, as depicted in Figure 8. The basic components of the power cycles are turbopumps, pre-burners or gas generators, valves, lines, thrust chamber injector, and thrust chamber coolant channel circuits. The guidelines utilized throughout the parametric study for these components are given in Table III.

The initial power cycle evaluation included the nine NASA-specified cycles described in Figure 6 as cycles A through I, the five cycles labeled J, M, N, O, and P, described in Figure 7, and four additional cycles (K, L, Q, and R) described in Table II. Cycle J is similar to the Alternate Mode 1 engine concept studied in Reference 9; there it proved to be an excellent LO_2/RP-1 candidate when liquid hydrogen is available in the vehicle. This cycle was selected for additional analysis in the study. Cycles M, N, and O are chamber-pressure-limited from 6895 to 20680 kN/m^2 (Pc = 1000 to 3000 psia) when the amount of hydrogen is limited to that for a corresponding gas- generator cycle (cycle J). Cycles M, N, and O also do not meet the definition of a tri-propellant engine, given as a requirement in Section II.C., as the pre-combustor fluid is also burned in the main chamber of the engine. Consequently, these cycles were not evaluated after the initial screening.

Cycle P (cf. Figure 7) was not studied further because the oxidizer-rich LO_2/LH_2 gas generator resulted in an engine performance (specific impulse) loss of over 30 seconds (sea level and vacuum) when compared to cycle J.

The four additional cycles initially evaluated were 1) (Q), a LH_2-cooled expander bleed cycle, where the coolant jacket heated hydrogen is utilized to drive the turbine and is dumped in the nozzle at low pressure;

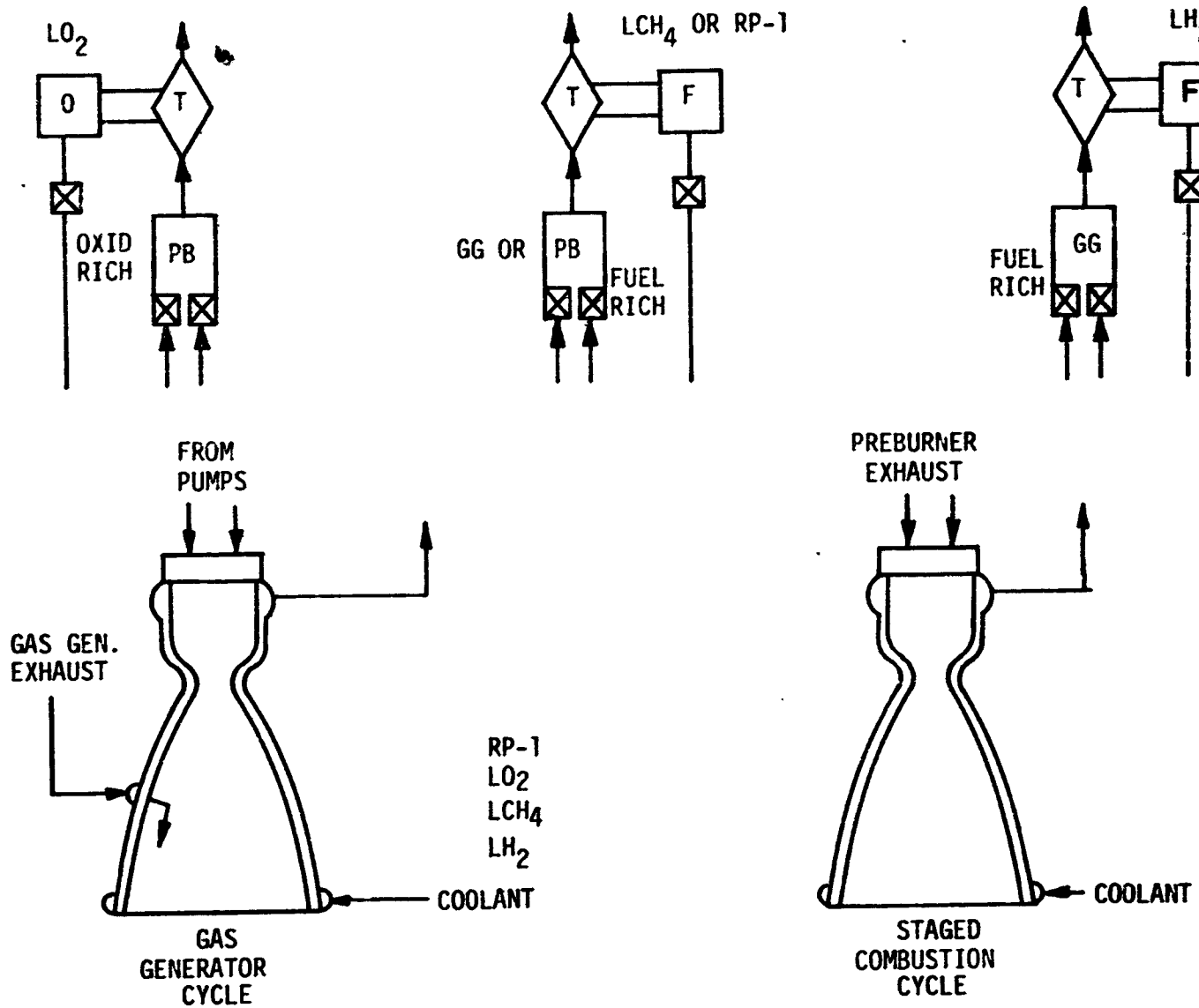

Figure 8. LOX/Hydrocarbon Engine Cycle Components

TABLE III

GUIDELINES FOR PARAMETRIC POWER CYCLE STUDY

PARAMETER	
NPSH at Engine Inlet, m (ft)	LOX: 5(16) LH_2: 31(100) RP-1: 20(65) LCH_4: 7(23) LC_3H_8: 16(54)
Propellant Pump Inlet Temperature, °K (°R) (Subcooled - propane tank cooled by LO_2 boiloff or in-tank submersion or intermediate fluid)	LOX: 90(163) LH_2: 20(37) RP-1: 289(520) LCH_4: 112(201) LC_3H_8: 90(163)
Chamber Service Free Life, cycles	$\geq$ 100
Injector Pressure Loss ($\Delta P/P_{upstream}$)	Liquid: $\geq$ 15% Gas: $\geq$ 8%
Valve Pressure Loss ($\Delta P/P_{upstream}$)	Shutoff: $\geq$ 1% Liquid Control: $\geq$ 5% Gas Control: $\geq$ 10%
Line Loss ($\Delta P/P_{upstream}$)	$\leq$ 0.5%
Main Pump Suction Specific Speed	$\approx$ 20,000
Turbine Inlet Temperature °K (°R)	Oxidizer-Rich: $\geq$ 922(1660) Fuel-Rich: $\geq$ 1033(1860)

III, B, Power Cycle Matrix (cont.)

2) (R) a LH_2-cooled expander bleed/staged-combustion mixed cycle, including an oxidizer-rich LO_2/RP-1 preburner; 3) (L), a LH_2-cooled LO_2/RP-1 dual-throat engine with a LO_2/LH_2 gas generator and a LO_2/RP-1 oxidizer-rich preburner; and 4) (K), a LH_2 and LCH_4-cooled dual-throat engine with a LO_2/LH_2 gas generator and an oxidizer-rich LO_2/LCH_4 preburner.

From a performance standpoint, both expander bleed cycles (Q and R) are competitive with corresponding gas-generator and mixed gas-generator/staged- combustion cycles but they require more hydrogen or a coolant jacket outlet temperature around 667°K (1200°R) for power balance. No further analysis was conducted on the expander bleed cycles, since the heat transfer results indicated bulk temperature values lower than the assumed 667° K, and no channel optimization was conducted to increase the bulk temperature. The hydrogen coolant exit temperature reported in Reference 9 at 811°K (1460°R) indicates that cycles Q and R should be further evaluated.

Both dual-throat engines (K and L) appeared to be excellent candidates, but only the LO_2/LCH_4 engine was selected for additional analysis. Both engines utilize LH_2 for cooling a portion of the engine and for the LO_2/LH_2 gas-generator drive. Since only a small amount of LH_2 is used, LO_2 is used to cool the remaining portion of the LO_2/RP-1 engine and LCH_4 is used to cool the remaining portion of the LO_2/LCH_4 engine. It was beyond the scope of this program to conduct a detailed heat transfer analysis of either dual-throat engine. Similar dual-throat heat transfer analyses cited in Reference 10 indicated a larger cooling requirement for the dual-throat configuration compared to conventional bell nozzles. There appeared to be less uncertainty in selecting the LO_2/LCH_4 engine as a candidate, since both LCH_4 and LO_2 are available as coolants in the high heat flux regions to complement LH_2 cooling and since only LO_2 is available for the LO_2/RP-1 engine.

C. THRUST CHAMBER HEAT TRANSFER

Cooling system design studies were conducted for a slotted zirconium-copper (Zr-Cu) chamber liner to an area ratio of 8:1 and for a two-pass Inconel 718 tube bundle for the remainder of a 40:1 nozzle. All chambers are single pass, with the coolant entering at the 8:1 area ratio. The analysis was performed for a thrust range of 890 to 8896 kN (200K to 2M lbF) and for a chamber pressure range of 6895 to 34474 kN/m^2 (1000 to 5000 psia). The following specific coolants for the various components and propellant combinations were used:

Component	Propellant Combination		
	LOX/RP-1	LOX/CH_4	LOX/C_3H_8
Chamber Coolant	LH_2 LO_2 RP-1	LH_2 LCH_4	LC_3H_8 (subcooled)
Nozzle Coolant	LO_2 RP-1		

RP-1 cooling was considered with and without carbon deposition from the combustion products on the chamber wall. Coking temperatures used in the analyses are 561°K and 700°K (550°F and 800°F). These temperatures indicate the range in thermal stability breakpoint for RP-1 and more refined petroleum fuels such as JP-5 (720°F) and JP-7 (760°F) cited in Reference 11. The more refined fuel is specified as RP-1R in this study to differentiate it from MIL SPEC RP-1. Special emphasis was placed on channel layout optimization to minimize pressure drop requirements for the propellant-cooled cases.

III, C, Thrust Chamber Heat Transfer (cont.)

Approximate chamber pressure limits defined by the chamber cooling analysis (at a pump discharge pressure limit of 55160 kN/m^2 (8000 psia) and ignoring specific impulse maxima for gas generator cycles) are summarized in Figure 9 and are listed as follows:

	Gas Generator Cycles		Staged Combustion Cycles	
Coolant	Pc, kN/m^2	Pc, psia	kN/m^2	psia
RP-1, 550°F coking	8963	1300	8963	1300
RP-1 with carbon deposit, 550°F coking	13790	2000	---	---
RP-1R, 800°F coking	20684	3000	22063	3200
RP-1R with carbon deposit, 800°F coking	24132	3500	---	---
Oxygen	28269	4100	21374	3100
Methane	29647	4300	24132	3500
Propane (sub-cooled to LOX NBP)	31026	4500	24821	3600
Hydrogen	37921	5500	---	---

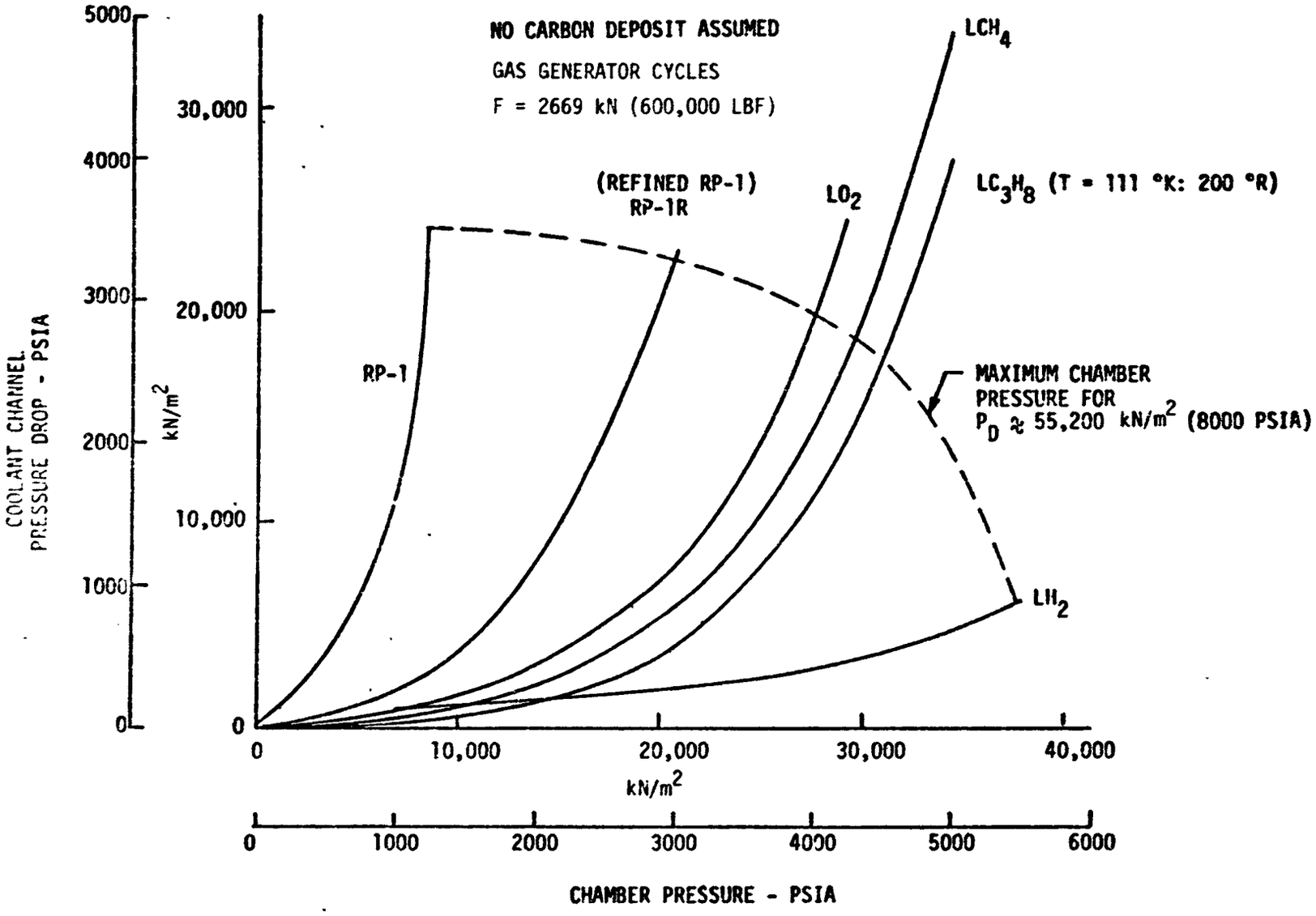

Figure 9. LO_2/HC Engine Cooling Summary

III, C, Thrust Chamber Heat Transfer (cont.)

1. Chamber Design Limits and Procedures

All chambers were designed for 100 thermal cycles with a total hold time of 10 hours, using material properties and methodologies identical to those previously used on Contract NAS 8-32967 (Ref. 10). The resulting criteria for the gas-side wall temperature are shown in Figure 10. In this figure, the difference between the maximum gas-side temperature and the average nickel closeout temperature is plotted as a function of closeout temperature. For closeout temperatures less than 239°K (-30°F), a cycle life of 100 cycles determines the allowable gas-side temperature. For closeout temperatures above 239°K, creep limits the maximum gas-side wall temperature to 811°K (1000°F). The two line segments shown in Figure 10 are input to the computer program, and the maximum gas-side wall temperature limitation automatically determines the local channel depth, provided the resultant depth/width ratio is within the 5:1 limit.

Wall strength criteria, taken from Ref. 10, are shown in Figure 11.

Convergent section contour parameters are as follows:

Contraction Ratio	2.3
Entrance radius of curvature	$3r_t$
Convergence angle	20°
Throat radius of curvature	r_t

Chamber lengths differed for propellant-cooled vs hydrogen-cooled designs and are discussed in subsequent sections.

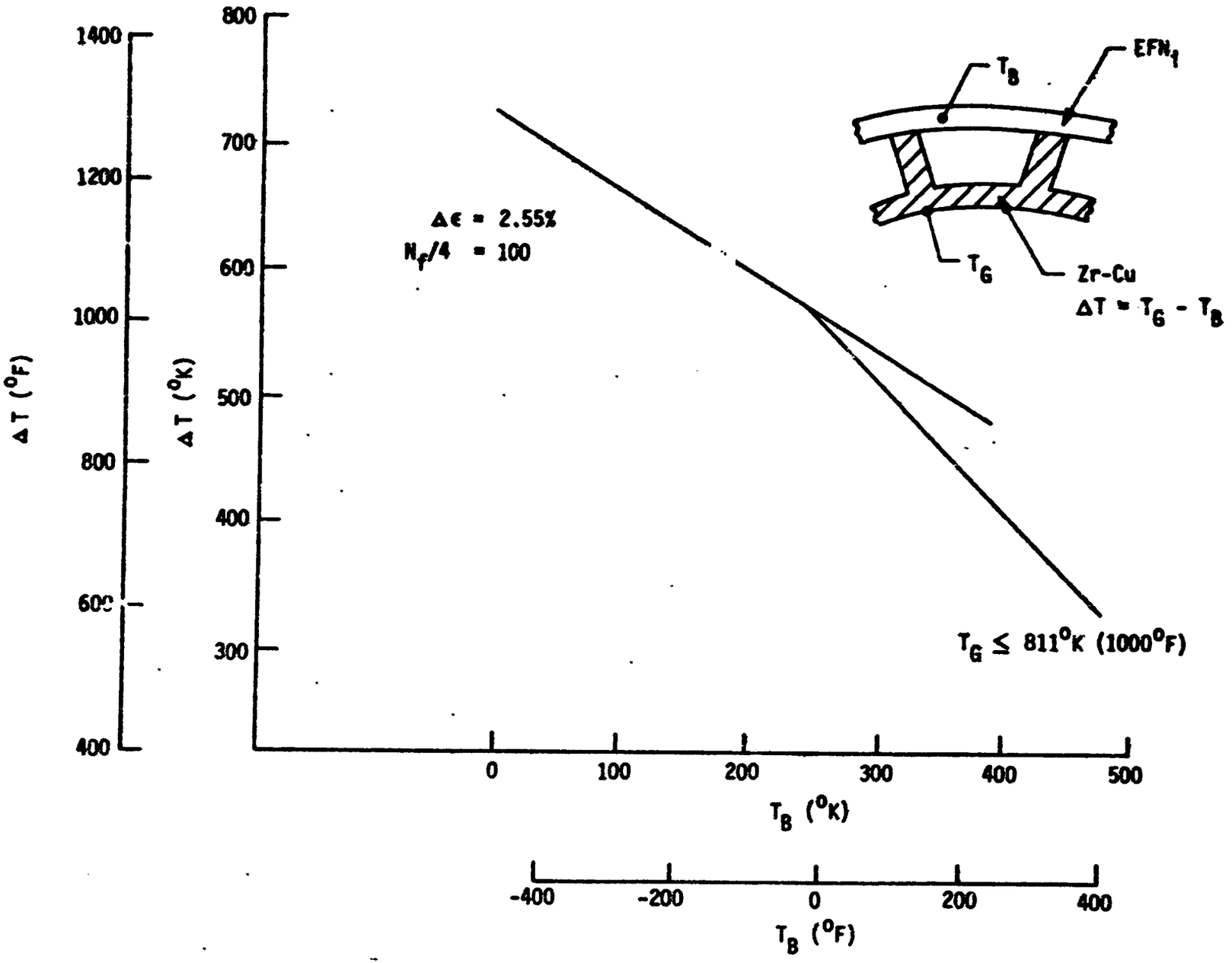

Figure 10. Cycle Life/Creep Wall Temperature Criteria

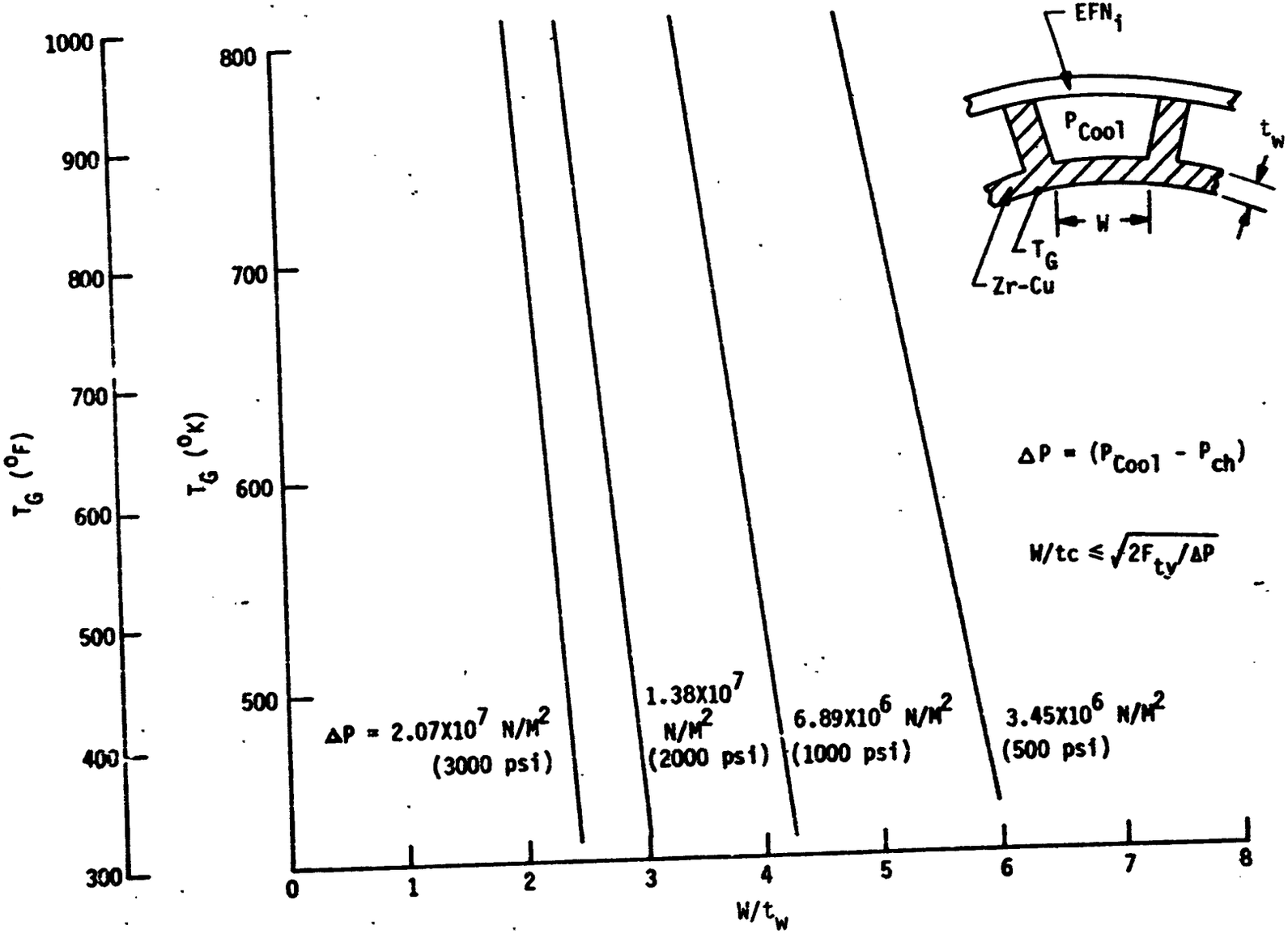

Figure 11. Zr-Cu Chamber Wall Strength Criteria

III, C, Thrust Chamber Heat Transfer (cont.)

Channel dimension limitations are as follows:

Minimum wall thickness (t_w)	.064 cm (.025 in.)
Minimum land width (L)	.102 cm (.040 in.)
Minimum channel width (W)	.102 cm (.040 in.)
Maximum channel depth/width or aspect ratio (d/w)	5:1

Channel layout details for each coolant are presented in subsequent sections.

Coolant inlet temperatures and heat transfer correlations are summarized in Table IV. An inlet pressure equal to twice the chamber pressure was assumed in all cases, and the coolant Mach number was not allowed to exceed 0.3.

All chamber designs were generated by using the SCALER Program, a program which has been developed specifically for parametric design studies. With this program, it is economically feasible to generate a relatively large number of parametric design points and still obtain a detailed, multi-station analysis of a rectangular channel at each design point. The SCALER Program scales the chamber geometry and the local gas-side heat transfer coefficients and coolant heat loads from reference input to other thrusts and chamber pressures. At each station, the program iterates to determine the channel depth required to satisfy a gas-side wall temperature limit (which can be specified as a function of closeout wall temperature consistent with cycle life and creep criteria) and an optional coolant-side wall temperature limit. The only simplifying assumption is that gas-side wall temperature differences between the reference input and scaled cases have a negligible effect on gas-side heat transfer coefficients and heat loads. Normally, gas-side wall temperature limits are known well in advance, so that local reference gas-side heat transfer analyses can be run at appropriate wall temperatures. Two-dimensional conduction effects are accounted for by using coupled fin solu-

TABLE IV

COOLANT INLET TEMPERATURES AND HEAT TRANSFER CORRELATIONS

COOLANT	INLET TEMPERATURE °K (°R)	HEAT TRANSFER CORRELATION	REFERENCE
Hydrogen	61 (110)	Hess and Kunz	12
Oxygen	111 (200)	ALRC Oxygen	13
Methane	144 (260)	ALRC Oxygen	13
Propane	111 (200)	ALRC Propane	14
RP-1 and RP-1R	311 (560)	Hines	15

tions, which also allows some variation of the coolant heat transfer coefficient around the channel perimeter.

2. Chamber Cooling

Chamber lengths for the propellant-cooled chambers were based on correlations for staged-combustion cycles, i.e.,

$$L' = 4.178\ (F/Pc)^{0.23}$$

unless the chamber geometry, defined in the previous section, required a greater length for the convergent section. In the latter case,

$$L' = 2.143\ r_t = 0.9137\ (F/Pc)^{0.5} \quad \text{LOX/RP-1}$$
$$= 0.9160\ (F/Pc)^{0.5} \quad \text{LOX/CH}_4\text{, LOX/C}_3\text{H}_8$$

The variation of L' with F/Pc for all chambers is shown in Figure 12.

Channel design optimization studies to minimize pressure drop were conducted by using the channel layout of Figure 13, which features two straddle-mill regions (constant land width) separated by a region of constant channel width ending at the throat. Three parameters were used in the optimization studies: throat channel width (W_t), barrel land width (L_b), and coolant flow fraction. As noted in Figure 13, the nozzle land width was set at 0.102 cm (0.040 in.) for all cases. These optimization studies were conducted for each coolant at selected design points (thrust and chamber pressure), as described in detail in the following sections. The optimum designs at these selected points were then used to define a channel layout prescription for a thrust and chamber pressure survey. This prescription is of the form

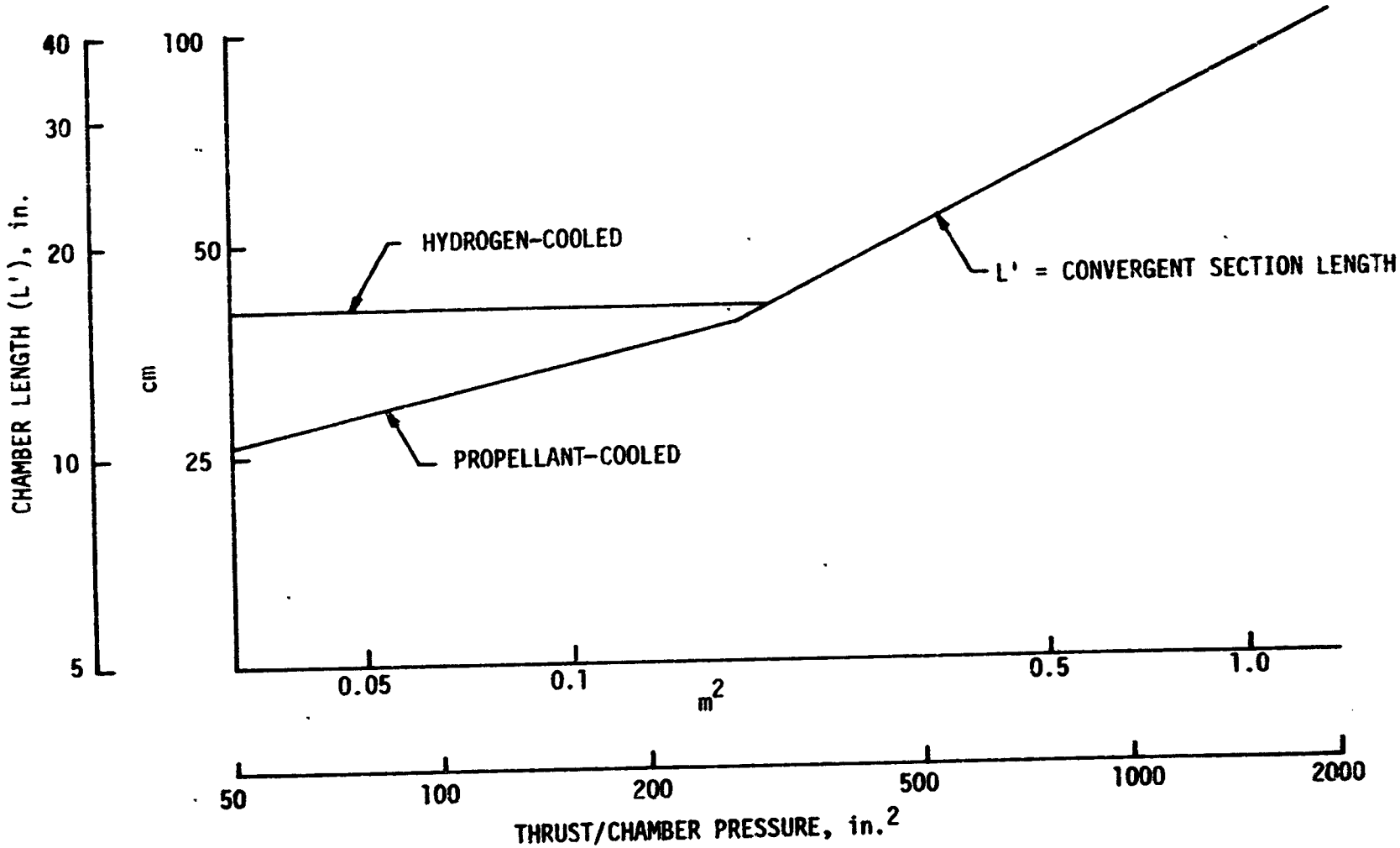

Figure 12. Chamber Length Variation With Thrust/Chamber Pressure

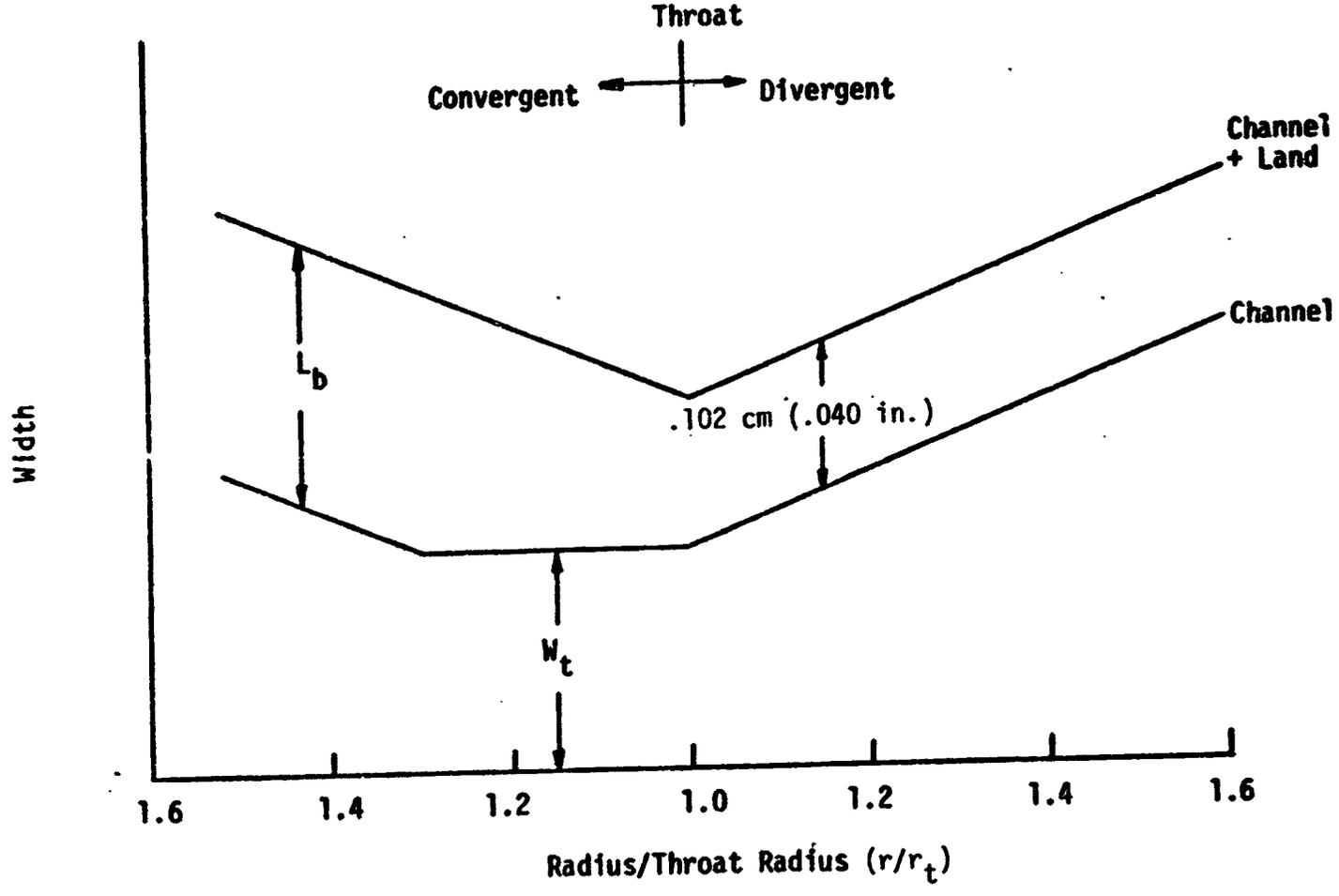

Figure 13. Channel Layout for Design Optimization Study

III, C, Thrust Chamber Heat Transfer (cont.)

$$f_c \frac{0.040 + W_t}{W^2} = C\left(\frac{P_c}{1000}\right)^n \left(\frac{10^6}{F}\right)^m$$

in which the left side is derived from the coolant mass velocity ($W/A = \rho v$) in a channel of fixed aspect ratio. A relatively constant aspect ratio near the maximum allowable is desired to provide the maximum effective coolant surface area. The coefficient C and the exponents n and m were obtained from the optimized design points. It was found that $m = 0.35$ approximates all thrust effects; values of C and n are as follows:

Coolant	C		n	
	Throat	Barrel	Throat	Barrel
RP-1 and RP-1R	14.1	11.4	0.72	0.57
Oxygen	3.84	4.89	1.00	0.59
Methane	7.76	5.39	0.79	0.79
Propane	6.24	6.86	1.17	0.84

Variations in n are to be expected in view of the effects of pressure and bulk temperature on different coolants. Optimum coolant flow fractions, defined in the optimization studies, were used to guide the thrust-chamber pressure surveys, with additional checks made during these surveys.

In general it was found that channel widths must increase as thrust increases in order to accommodate the additional channel flow, but must decrease as chamber pressure increases in order to provide a higher mass velocity at an effective channel aspect ratio.

a. RP-1 Cooling without Carbon Deposition

An additional design criterion is imposed with RP-1 cooling: the maximum local coolant-side wall temperature must not exceed the

coking or decomposition temperature of RP-1. This temperature limit is approximately 550°F for commercial RP-1. With no carbon deposition from the combustion products, it was not possible to obtain designs with reasonable pressure drops for such a limit. For example, at 6895 kN/m^2 (1000 psia) and 890 kN (200,000 lbF), a pressure drop of 11030 kN/m^2 (1600 psia) was required. This pressure drop exceeds the usual design practice for regenerative cooling, where the coolant jacket inlet pressure is maintained below 2.25 times the chamber pressure. Therefore, the use of deoxygenated and refined RP-1 (RP-1R) was investigated. This fuel would be similar to JP-7 or JP-5, both of which have decomposition temperatures approaching 700°K (800°F). Consequently, all results presented in this section are for a 700°K (800°F) coolant-side wall temperature limit. However, a special study was conducted to investigate the effects of carbon deposition at the 2669 KN (600K lbF) thrust level at both decomposition temperatures limits. This study is described in the next section.

An extensive channel layout optimization was conducted for RP-1R cooling with no carbon deposition on the gas-side surface. Table V summarizes the cases run and the resulting coolant pressure drops for the five operating points considered. A detailed parametric study was conducted at 890 kN (200K lbF) thrust and 6895 kN/m^2 (1000 psia) chamber pressure, particularly for a coolant flow fraction of 0.9. The latter results are shown in Figure 14 as a function of barrel land width for various throat channel widths. As the barrel land width increases initially, a more effective, higher aspect ratio channel results until the aspect ratio limit is reached over much of the barrel and convergent section. Note that the decrease in pressure drop in this region is relatively small since the equivalent diameter reduction tends to offset the reduction in required coolant mass velocity. After the aspect ratio limit is reached, further increases in barrel land width result in overcooling and a rapidly increasing pressure drop. For a throat channel width of 0.102 cm (0.040 in.), all results are aspect-ratio-limited, whereas the aspect ratio limit is not reached for a throat channel width of 0.20 cm (0.080 in.) even with a 0.20 cm (0.080 in.) barrel channel width.

TABLE V (1 of 3)

CHANNEL LAYOUT OPTIMIZATION FOR RP-1R COOLING

Coking Temperature 700°K (800°F) No Carbon Deposition

Thrust kN (10^6 lbF)	Pc kN/m^2 (psia)	Coolant Fraction, fc	W_t in.	L_b in.	ΔP psi
890 (0.2)	6895 (1000)	1.0	.040	.040	293
				.054	368
			.060	.040	250
				.054	225
				.068	211
				.082	202
			.080	.054	261
				.068	246
				.082	237
				.094	231
		0.95	.040	.040	271
				.054	333
				.068	478
			.060	.054	217
				.068	204
				.082	197
			.080	.068	237
				.082	230
				.094	225
		0.90	.040	.040	255
				.054	305
				.068	432
			.045	.040	225
				.050	221
				.060	234
			.050	.050	206
				.060	199
				.070	203
				.080	241

TABLE V (cont.) (2 of 3)

Thrust kN (10^6 lbF)	Pc kN/m^2 (psia)	Coolant Fraction, fc	W_t in.	L_b in.	ΔP psi
			.055	.065	197
				.074	192*
				.082	201
				.089	235
			.060	.054	215
				.068	202
				.082	195
				.089	206
			.080	.068	236
				.082	229
				.090	225
				.102	223
		0.85	.040	.040	265
				.054	300
				.068	388
			.060	.040	270
				.054	244
	10340 (1500)	0.9	.040	.075	697
			.045	.060	657
				.070	641*
				.080	645
			.050	.054	692
				.068	666
				.082	651
				.087	661
			.060	.082	704
	13790 (2000)	1.0	.040	.060	1213
				.068	1210*
				.075	1221
2669 (0.6)	6895 (1000)	0.9	.060	.040	305

TABLE V (cont.) (3 of 3)

Thrust kN (10^6 lbF)	Pc kN/m^2 (psia)	Coolant Fraction, fc	W_t in.	L_b in.	ΔP psi
				.054	325
				.068	372
				.082	488
			.075	.070	245
				.082	247
				.094	272
			.080	.082	243
				.094	237*
				.102	262
			.100	.096	255
				.103	252
				.110	251
			.120	.103	274
	13790 (2000)	0.9	.055	.070	1217
				.080	1211*
				.089	1297
			.060	.068	1215
				.082	1210
				.092	1212
			.080	.089	1261
				.094	1260
				.099	1259
			.100	.096	1461
		1.0	.060	.068	1295
				.092	1276
			.080	.094	1335

* Optimum Designs

RP-1R COOLING

F = 890 kN (200K lbF)

COOLANT FRACTION = 0.9

Pc = 6895 kN/m^2 (1000 psia)

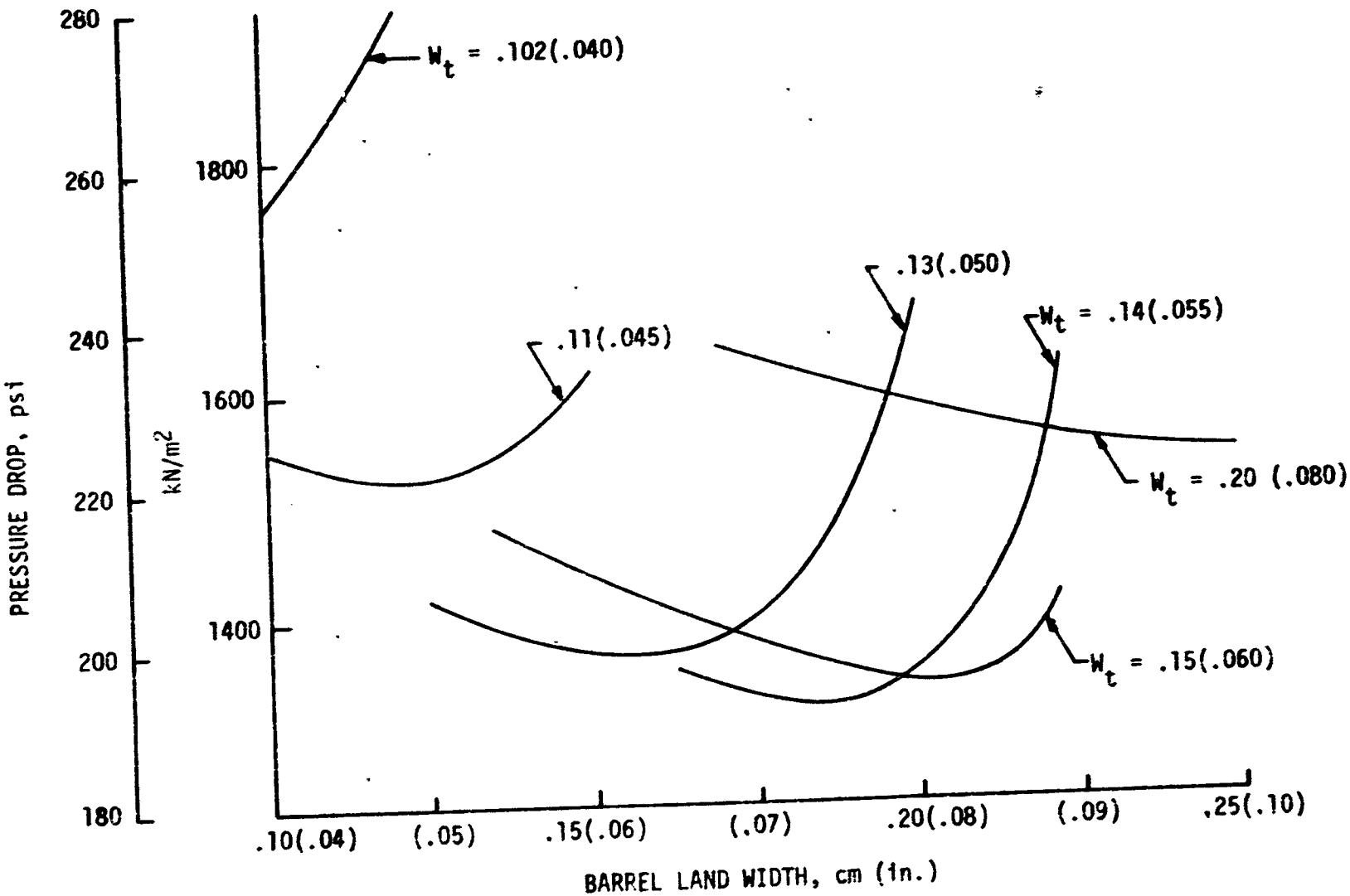

Figure 14. Barrel Land Width Optimization

Figure 15 presents the locus of minimum pressure drops from Figure 14. At low values of the throat channel width, the throat region is aspect-ratio-limited and overcooled, so the pressure drop decreases rapidly with increasing channel width. At high throat channel widths, the aspect ratio decreases and the less effective cooling (less fin effect) required an increase in pressure drop. In this case, the optimum throat design i.e., a high aspect ratio channel near the limit, occurs at a throat channel width of 0.14 cm (0.055 in.).

Although the optimization studies at other coolant flow fractions were not as detailed, it appears that the effect of coolant flow fraction on optimum pressure drop is fairly small for flow fractions between 0.9 and 1.0:

Coolant Flow Fraction	Optimum ΔP, kN/m^2 (psi)
1.00	1393 (202)
0.95	1358 (197)
0.90	1324 (192)

Limited results at lower coolant flow fractions indicate higher pressure drops.

The optimum designs for the five operating points in Table V (denoted by an asterisk) were used to define the parameters n, m, and C in the channel layout model described previously. As the chamber pressure is increased at the 890 kN (200K lbF) thrust level, the throat channel width must decrease in order to provide an increased mass velocity at an effective aspect ratio. At a chamber pressure of approximately 13100 kN/m^2 (1900 psia), the optimum channel width reaches the minimum allowable value of 0.102

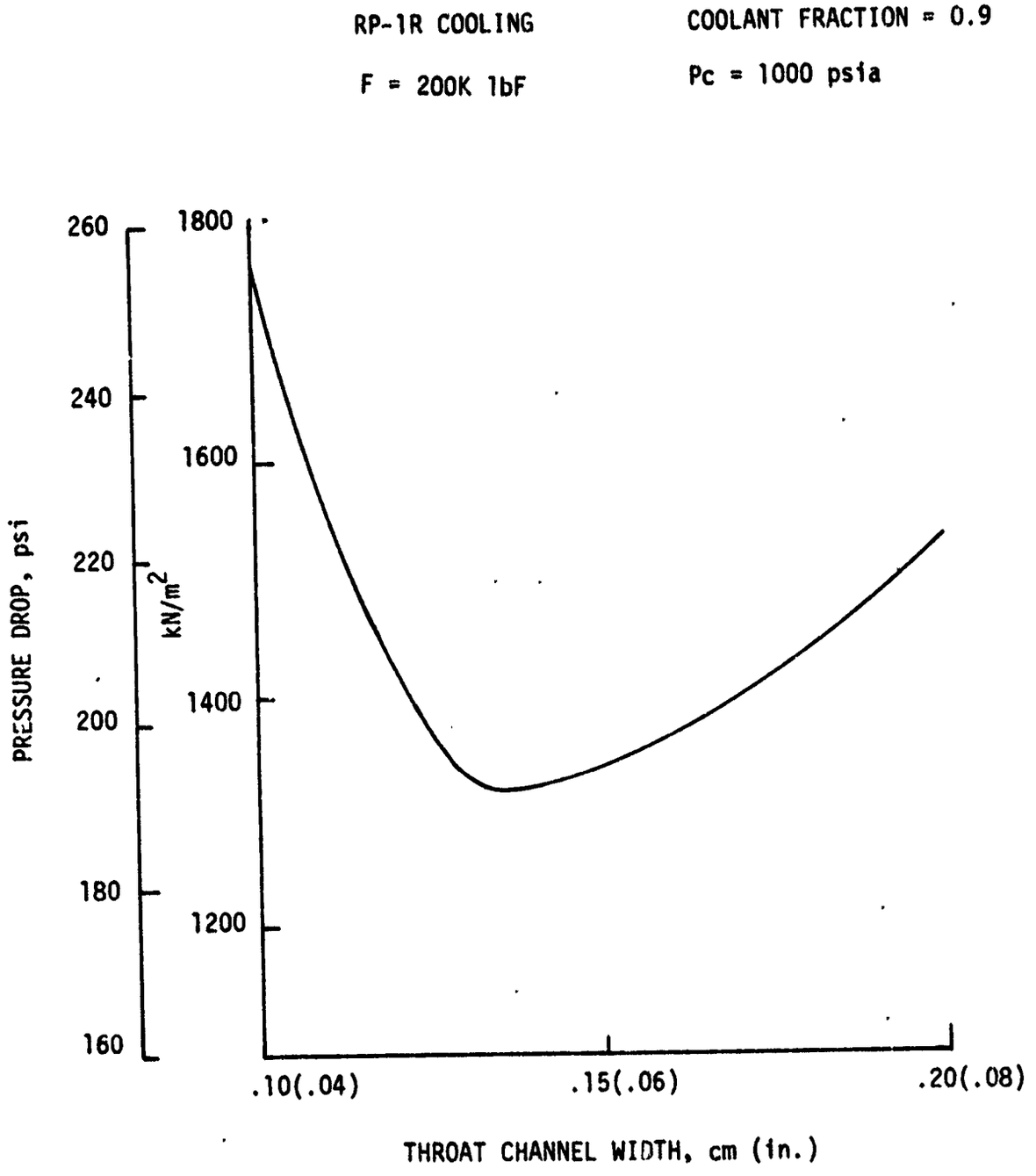

Figure 15. Throat Channel Width Optimization

cm (0.040 in.). For chamber pressures above this value, a coolant flow fraction of unity was used in order to provide as high an aspect ratio as possible.

Table VI presents the complete thrust and chamber pressure parametric study results for RP-1R cooling with no carbon deposition. Note that the effect on pressure drop of increasing thrust from 890 to 2669 kN (200 to 600K lbF) changes with chamber pressure. These trends are influenced by the 0.102 cm (0.040 in.) minimum channel width limit at the higher pressures for 890 kN (200K lbF), as noted above, and by the more detailed channel optimization at 6895 kN/m^2 (1000 psia). RP-1R cooling is practical to a chamber pressure of about 20680 kN/m^2 (3000 psia) for a coking temperature of 700°K (800°F).

b. RP-1 and RP-1R Cooling with Carbon Deposition

The effects of gas-side carbon deposition were studied at 2669 kN (600K lbF) thrust with coking temperature limits of 561 (550°F) and 700°K (800°F). The thermal resistance of the carbon layer was taken from the model of Ref 16. For LOX/RP-1 at a mixture ratio of 2.8, this yields

$$(t/k)_{carbon} = e^{9.0-0.51G} \text{ in.}^2\text{-sec-°F/Btu}$$

in which G is the local combustion product mass velocity ($\dot{w}/A$) in lbm/$in.^2$-sec. Thus the axial variation of the carbon deposition is very significant. For example, at 2669 kN (600K lbF) thrust and 17237 kN/m^2 (2500 psia) chamber pressure, the carbon resistance at the throat is only 6% of the convective resistance, while, in the barrel, it is 182% of the convective resistance. As a result, the optimum channel design required the minimum barrel land width of 0.102 cm (0.040 in.) in order to provide as wide a barrel

TABLE VI

RP-1R COOLING SUMMARY WITHOUT CARBON DEPOSITION

Coking Wall Temperature Limit = 700°K (800°F)

Thrust kN (10^6 lbF)	Pc psia	Coolant Fraction	ΔP psi	ΔT_b °F	L' in.
890 (0.2)	1000	0.9	192	191	14.14
	1500		641	203	12.88
	2000	1.0	1210	195	12.05
	2500		2322	200	11.45
	3000		4278		
2669 (0.6)	1000	0.9	237	165	22.38
	1500		614	165	18.27
	2000		1210	168	15.83
	2500		2063	169	14.74
	3000		3284		
8896 (2.0)	1000		332	147	40.86
	1500		794	148	33.36
	2000		1466	150	28.89
	2500	1.0	2517	135	25.84

channel as possible. Since the coolant flow fraction was fixed at 0.9, the channel layout optimization was simplified to allow for a variation of the throat channel width. Table VII summarizes the results obtained for the optimum channel geometries.

Figure 16 compares the various RP-1 cooling results at 2669 kN (600K lbF) thrust. The large reduction in required pressure drop due to carbon deposition is evident from the curves for a coking temperature of 700°K (800°F). Also indicated is the dramatic increase in pressure drop when the coking temperature is reduced to 561°K (550°F), particularly at higher chamber pressures. At 13790 kN/m^2 (2000 psia), the pressure drop with carbon deposition and a coking temperature of 561°K (550°F) exceeds that for one with no carbon deposition and a coking temperature of 700°K (800°F).

c. Methane Cooling

Table VIII presents the channel optimization study for methane cooling. A preliminary study with a slightly different channel layout defined approximate throat channel widths for minimum pressure drop, thereby limiting the number of cases required for the final optimization study. For example, the preliminary study indicated that reducing the throat channel width below 0.23 cm (0.090 in.) for the first operating point of Table VIII was of no benefit. It should also be remembered that the barrel land width has an upper limit defined by the case of a uniform channel width in the convergent section. This limit is pertinent in the case of a 0.25 cm (0.100 in.) throat width for the first operating point, for which the pressure drop is still decreasing with a barrel land width as large as 0.28 cm (0.110 in.). Since the limiting land width is 0.29 cm (0.113 in.), no additional cases were run.

TABLE VII

RP-1 AND RP-1R COOLING SUMMARY WITH CARBON DEPOSITION

Thrust = 2669 kN (600K lbF)

Coolant Flow Fraction = 0.9 L_b = 0.102 cm (0.040 in.)

T_{Coke} °K (°F)	Pc psia	W_t in.	ΔP psi	ΔT_b °F
561 (550)	1500	.090	296	58
	2000	.080	1415	75
700 (800)	1500	.110	65	58
	2000	.085	284	75
	2500	.055	821	90
	3000	.045	1801	105

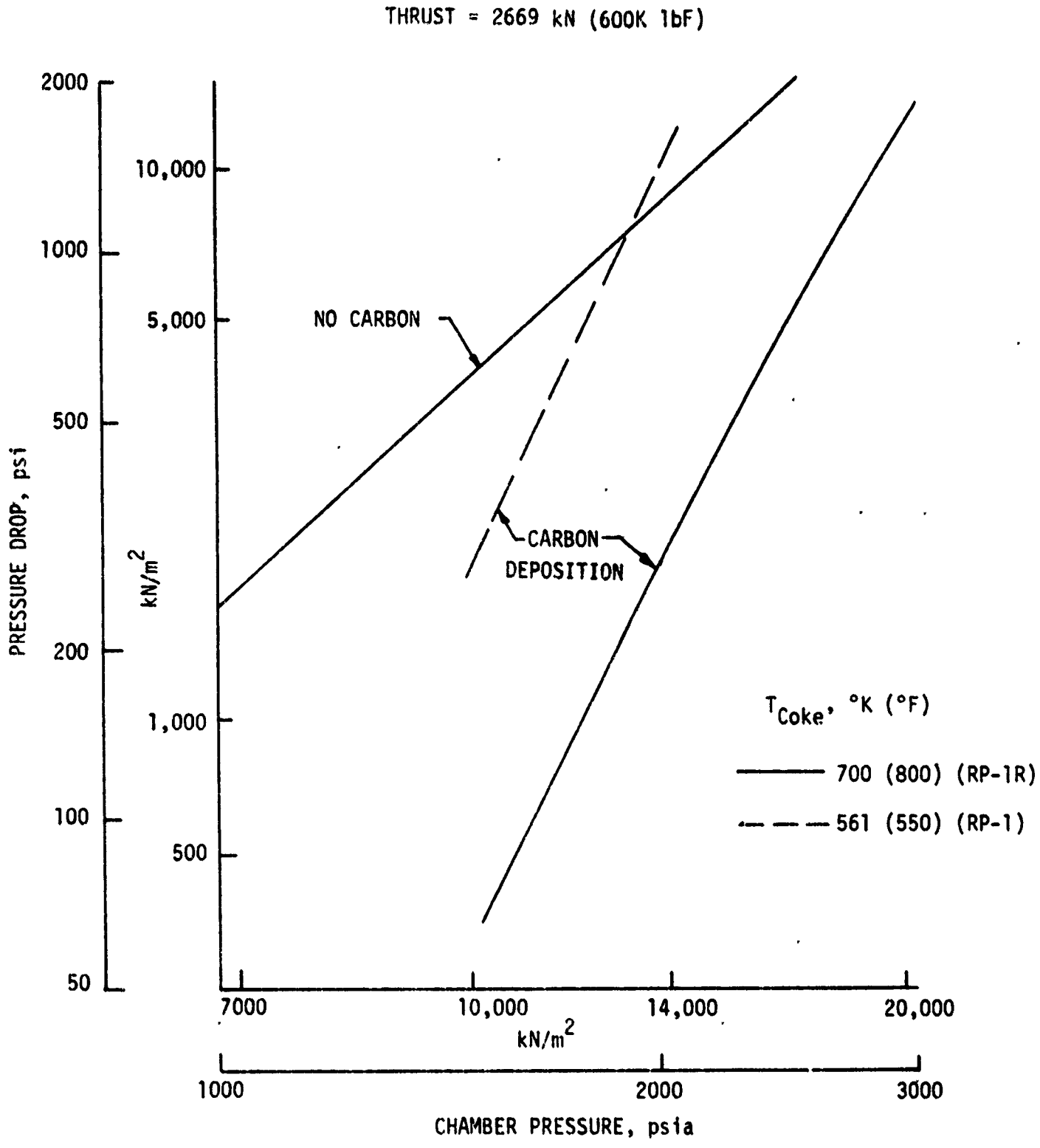

Figure 16. Effect of Carbon Deposition and Coking Temperature on RP-1 and RP-1R Cooling

TABLE VIII

CHANNEL LAYOUT OPTIMIZATION FOR METHANE COOLING

Thrust kN (10^6 lbF)	Pc psia	Coolant Fraction	W_t in.	L_b in.	ΔP psi
2669 (0.6)	2000	1.0	.090	.080	285
				.090	275*
				.100	287
			.100	.080	325
				.095	293
				.110	278
	4000	1.0	.060	.070	2545
				.080	2337*
				.090	2412
			.070	.070	3402
				.080	2990
				.090	2718
8896 (2.0)	2000	1.0	.110	.100	593
			.130	.100	407
				.110	388*
				.120	413
			.150	.100	489
		0.9	.110		497
			.130		400
			.150		484
		0.8	.110		425
			.130		423
			.150		534

Design point parametric results for methane cooling are given in Table IX. Pressure drop requirements are well below those for RP-1R and indicate that a chamber pressure as high as 31030 kN/m^2 (4500 psia) may be practical. As with RP-1R (Table VI), the effect of increasing thrust from 890 to 2669 kN (200 to 600K lbF) is dependent on chamber pressure. At low pressures, the pressure drop increases with thrust in this range, while, at high pressures, it decreases. However, a thrust increase from 2669 to 8896 kN (600K lbF to 2M lbF) results in a pressure drop increase at all chamber pressures.

d. Propane Cooling

Chamber cooling studies for a LOX/propane engine (MR = 3.1) were limited to subcooled propane cooling (111°K:200°R inlet temperature) with no gas-side carbon deposition. Channel layout optimizations were conducted for chamber pressures of 13790 and 27580 kN/m^2 (2000 and 4000 psia). No coking temperature limit was imposed, since it was noted that the coolant-side wall temperature did not exceed the accepted propane coking limit of 700°K (800°F), except at one or two stations near the injector (coolant outlet) for 13790 kN/m^2 (2000 psia). Once the optimum channel width model was established, a coolant-side wall temperature limit of 700°K (800°F) was imposed to obtain designs at 6895 and 13790 kN/m^2 (1000 and 2000 psia). In the latter case, the design represented a trivial modification of the previous designs. Since pressure drops are so low at a chamber pressure of 6895 kN/m^2 (1000 psia), a crude optimization of a uniform convergent section channel width was considered adequate. The above channel layout model indicated that as the chamber pressure is reduced, a uniform channel width is approached.

Recent long-duration heated tube tests with commercial grade propane (Ref. 14) indicate coking at wall temperatures well below 700°K (800° F). Although the data on decomposition rates are limited, especially at

TABLE IX

METHANE COOLING SUMMARY

Coolant Fraction = 1.0

Thrust kN (10^6 lbF)	Pc psia	ΔP psi	ΔT_b °F
890 (0.2)	1000	45	147
	2000	258	175
	3000	840	193
	4000	2195	197
2669 (0.6)	1000	62	129
	2000	295	138
	3000	833	147
	4000	2088	153
	5000	4885	156
8996 (2.0)	1000	84	117
	2000	388	123
	3000	1220	124
	4000	2818	124

the high coolant velocities of interest, it appears that the coolant-side wall temperature limit for commercial grade propane should be no higher than 644°K (700°F). Therefore, designs for this coking limit were developed for chamber pressures of 13790 and 20680 kN/m^2 (2000 and 3000 psia). At higher pressures, the designs noted above had coolant-side wall temperatures less than 644°K (700°F). All of the designs are summarized in Table X. Note that the use of subcooled propane provides a fairly large temperature difference between coolant-side wall temperatures and coolant bulk temperatures. Therefore, the 56°K (100°F) reduction in coking temperature did not have a drastic effect on channel designs and pressure drops. The use of NBP propane could lead to a significant loss in the cooling capability because of the coking temperature limit.

The propane pressure drop data for both coking temperatures are compared in Figure 17, with the methane pressure drop data obtained by using the ALRC oxygen correlation. Also shown is a methane data point at a chamber pressure of 13790 kN/m^2 (2000 psia) for which the new propane correlation was used. The propane correlation predicts higher methane heat transfer coefficients than the oxygen correlation and, therefore, a lower pressure drop requirement. However, the methane pressure drop remains above the corresponding propane pressure drop. It should be noted that the methane channel layout was not reoptimized for the propane correlation. Gas-side heat fluxes for a LOX/propane chamber are slightly lower than for a corresponding LOX/methane chamber. Table X indicates that a chamber pressure of about 31030 kN/m^2 (4500 psia) should be practical for LOX/propane engines.

e. Oxygen Cooling

Table XI presents the channel optimization study for oxygen cooling. As in the case of methane cooling, this study was guided by the results of a preliminary study for a slightly different channel layout.

TABLE X

PROPANE COOLING SUMMARY

F = 2669 kN (600,000 lbF) Coolant Fraction = 1.0

$T_{in.}$ = 111°K (200°R)

Coking Temp., °K (°F)	Pc psia	Throat Channel Width, in.	Barrel Land Width, in.	ΔP psi	ΔT_b °F
700 (800)	1000	.170	.149*	29	223
	2000	.100	.100	155	211
	3000	.070	.088	569	213
	4000	.055	.078	1629	216
	5000	.046	.074	3976	218
644 (700)	2000	.100	.100	204	211
	3000	.070	.088	608	213

* Uniform channel width in barrel and convergent section

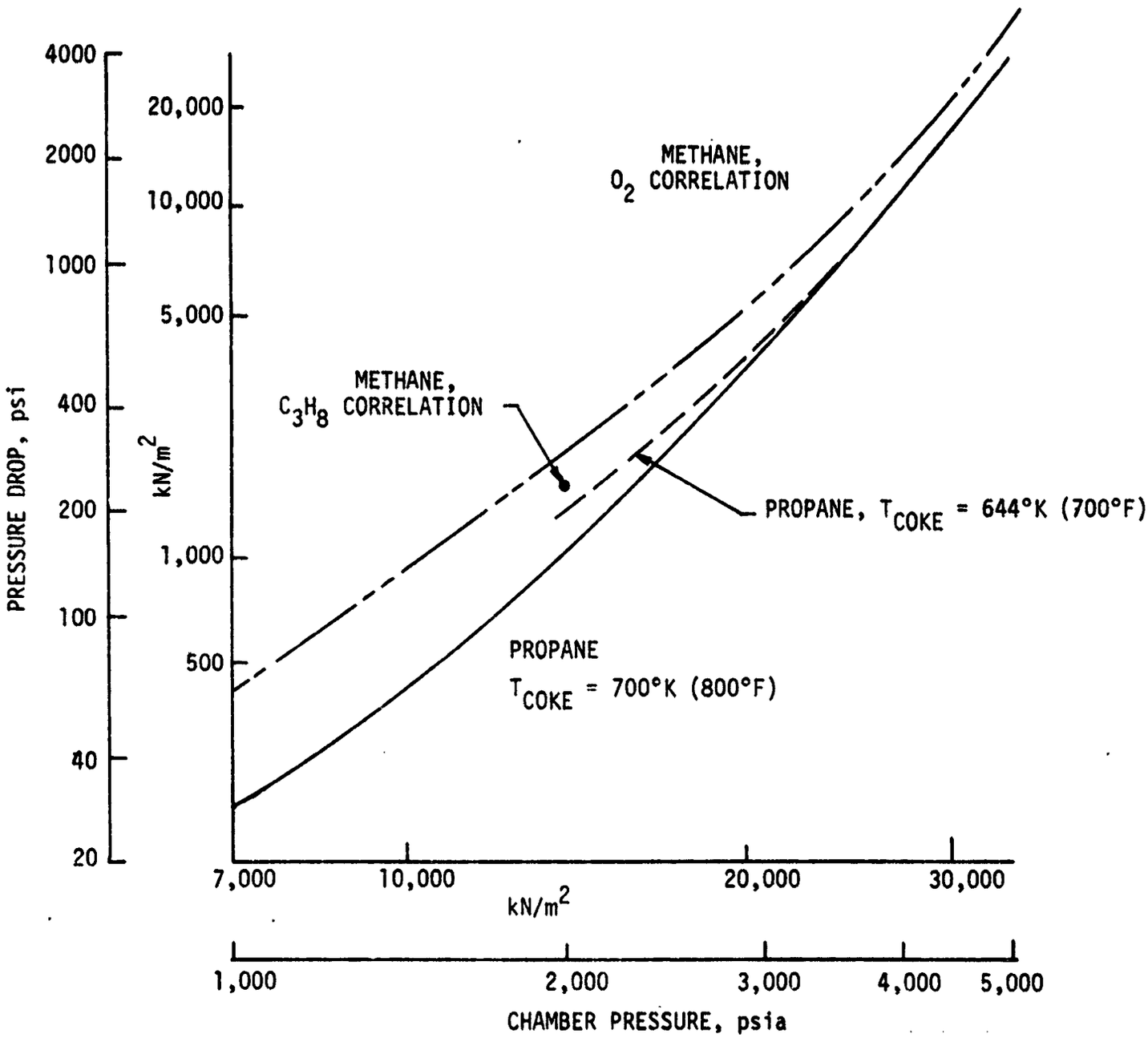

Figure 17. Comparison of Fuel-Cooled LOX/Methane and LOX/Propane Chambers

TABLE XI

CHANNEL LAYOUT OPTIMIZATION FOR OXYGEN COOLING

Thrust kN (10^6 lbF)	Pc psia	Coolant Fraction	W_t in.	L_b in.	ΔP psi
2669 (0.6)	2000	1.0	.120	.120	473
			.140	.100	462
				.120	412
				.130	395*
			.160	.130	473
	3000	1.0	.080	.090	2018
			.100	.090	1283
				.100	1203*
				.110	1280
			.120	.110	1452
8896 (2.0)	2000	1.0	.150	.130	1048
			.170	.130	630
			.190	.130	593
		.87	.150	.130	811
			.170	.120	588
				.130	559
				.140	553*
				.150	598
			.190	.130	617
		.75	.150	.130	622
			.170	.130	571
			.190	.130	675

At 8896 kN (2M lbF) thrust, a small reduction in pressure drop was obtained by using 87% of the total oxygen flow for cooling. The channel layout model resulting from the optimum cases of Table XI yields a uniform convergent section channel width for chamber pressures of 12410 kN/m^2 (1800 psia) and below.

Design point parametric results for oxygen cooling are given in Table XII. Thrust effects are similar to those noted previously for RP-1 and methane, except that the reduction in pressure drop at high chamber pressure, associated with increasing thrust from 890 to 2669 kN (200 to 600K lbF), is much less significant. Pressure drop requirements in general are somewhat higher than for methane cooling, even though the LOX/RP-1 gas-side boundary conditions considered here are slightly less severe than the LOX/CH_4 case. Table XII indicates that a chamber pressure of approximately 27580 kN/m^2 (4000 psia) should be practical.

f. Hydrogen Cooling

The initial cooling studies considered hydrogen cooling at chamber pressures of 6895, 27580, and 34470 kN/m^2 (1000, 4000, and 5000 psia). Detailed channel optimization studies were not conducted. Instead, a channel layout was selected for each chamber pressure, and the hydrogen flowrate was varied to minimize pressure drop. Nozzle land width was fixed at 0.15 cm (0.060 in.), and the throat channel and land widths were fixed at 0.102 cm (0.040 in.). At 6895 kN/m^2 (1000 psia) chamber pressure, a barrel land width of 0.15 cm (0.060 in.) was used. For the higher chamber pressures, a uniform channel width of 0.010 cm (0.040 in.) was used in the barrel and convergent sections. The chamber length prescription used above for the propellant cooling studies was not selected until after the hydrogen cooling analyses. A length (L') of 40.6 cm (16 in.) was used in the hydrogen studies, as shown in Figure 12, unless the convergent section length dictated a larger value.

TABLE XII

OXYGEN COOLING SUMMARY

Thrust kN (10^6 lbF)	Pc psia	Coolant Fraction	ΔP psi	ΔT_b °F	L' in.
890 (0.2)	1000	1.0	.78	82	14.14
	2000		376	95	12.05
	3000		1122	103	10.98
	4000		2889	107	10.28
2669 (0.6)	1000		108	72	22.38
	2000		450	73	15.83
	3000		1128	76	14.14
	4000		2874	79	13.23
8896 (2.0)	1000	0.87	125	73	40.86
	2000		553	74	28.89
	3000		1672	73	23.59
	4000		4424	73	20.43

Design point parametric results for hydrogen cooling are presented in Table XIII for LOX/RP-1 and in Table XIV for LOX/Methane. Hydrogen flowrates range from 3.4 Kg/s (7.5 lbm/sec) at low thrust, low chamber pressure to 27 Kg/s (60 lbm/sec) at high thrust, high chamber pressure. Although required pressure drops are somewhat higher for the LOX/Methane system, operation at a 37920 kN/m^2 (5500 psia) chamber pressure appears to be feasible for all thrust levels.

3. Nozzle Cooling

Two baseline tube bundle designs were developed for 2669 kN (600K lbF) thrust at 27580 kN/m^2 (4000 psia) chamber pressure: one for RP-1 cooling, and one for oxygen cooling. In both cases, a two-pass design using Inconel 718 tubes and the total propellant flow was employed. Scaling relations are proposed for extending these results to other design points.

Wall temperature criteria based on cycle life and creep are shown in Figure 18. Using the coolant inlet temperature as the limiting backside wall temperature resulted in gas-side wall temperature limits of 878°K (1120°F) for oxygen and 922°K (1200°F) for RP-1. Tube strength criteria, shown in Figure 19, were used to establish the tube wall thickness at the forward end and the axial rate of increase for a linearly tapered tube wall.

Round tubes were used for the RP-1-cooled design, so the design parameter for satisfying the wall temperature limit was the number of tubes. Because of the large flowrate involved, flattened tubes were used for the oxygen-cooled design. Therefore, along with the number of tubes, the undeformed tube diameter at the forward end was a design parameter. A linearly tapered tube (undeformed) was assumed, with the aft end diameter equal to twice the forward diameter. Designs were generated for 200 and 250

TABLE XIII

HYDROGEN COOLING SUMMARY FOR LOX/RP-1 ENGINES

Thrust kN (10^6 lbF)	Pc psia	Coolant Flow, lb/sec	ΔP psi	ΔT_b °F
890 (0.2)	1000	7.5	53	655
	4000	15	440	445
	5000	20	799	355
2669 (0.6)	1000	15	137	787
	4000	25	405	491
	5000	30	680	429
4448 (1.0)	1000	20	256	946
	4000	30	429	559
	5000	35	770	498
8896 (2.0)	1000	40	607	879
	4000	50	715	594
	5000	60	850	478

TABLE XIV

HYDROGEN COOLING SUMMARY FOR LOX/CH_4 ENGINES

Thrust kN (10^6 lbF)	Pc psia	Coolant Flow, lb/sec	ΔP psi	ΔT_b °F
890 (0.2)	1000	7.5	72	740
	4000	14.6	611	495
	5000	19.4	1105	395
2669 (0.6)	1000	15.0	199	900
	4000	24.7	563	558
	5000	29.5	1041	484
4448 (1.0)	1000	25.0	334	852
	4000	29.7	767	642
	5000	34.6	1369	568
8896 (2.0)	1000	40.0	893	1004
	4000	49.6	983	684
	5000	59.4	1122	551

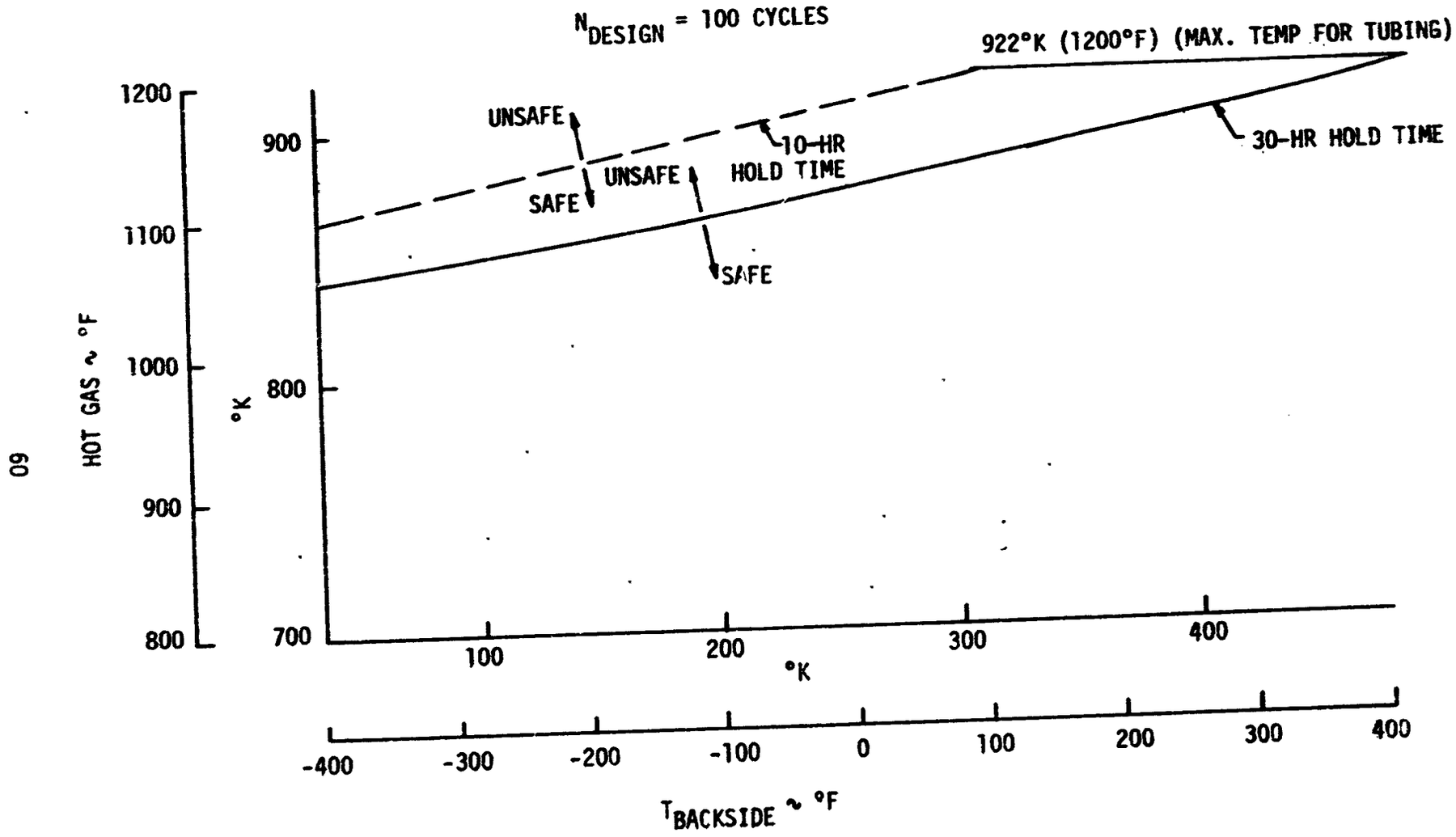

Figure 18. Allowable Hot Gas-Side Wall Temperature Vs. Backside Wall Temperature for Inconel 718 Tubes

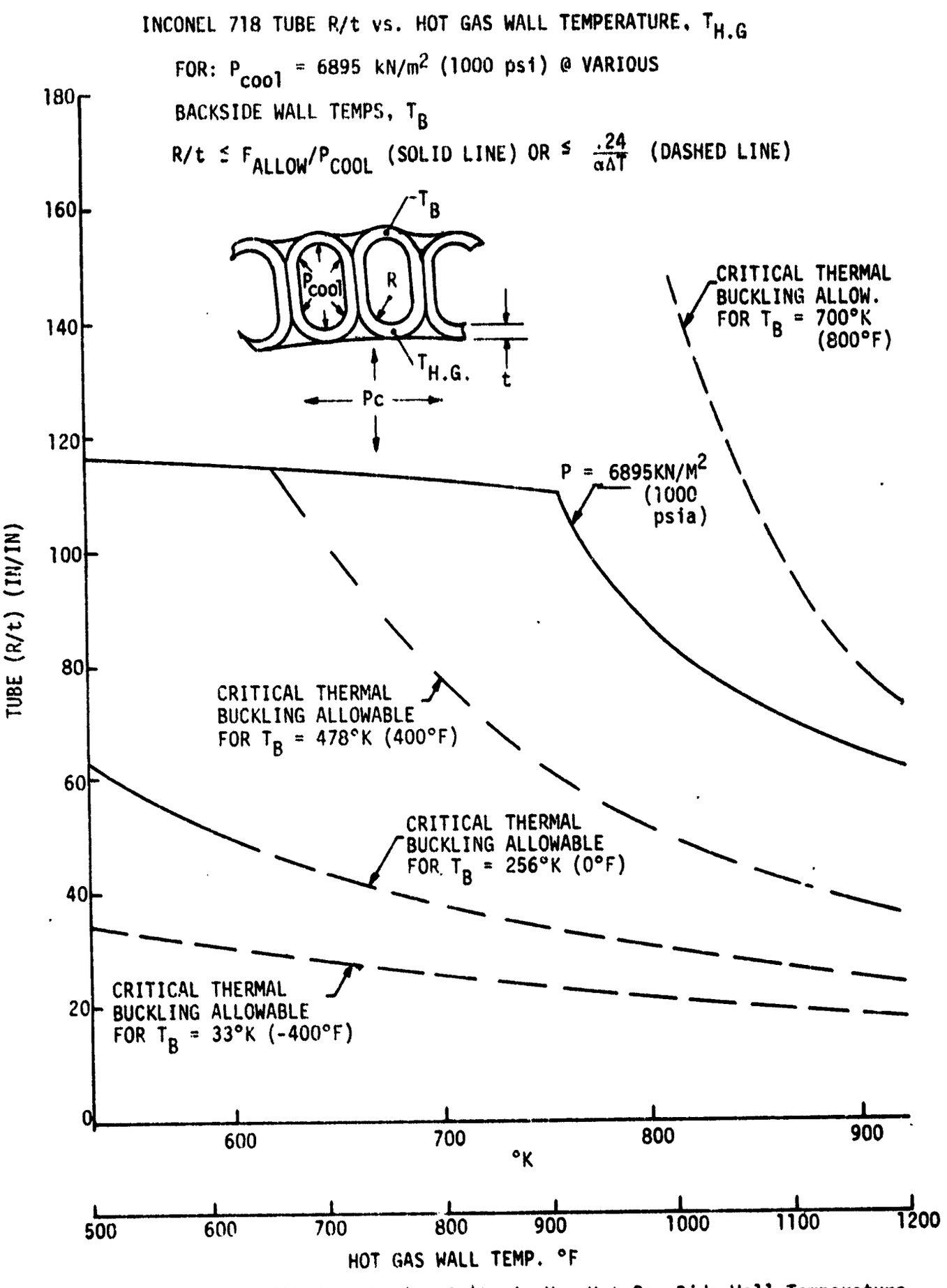

Figure 19. Inconel 718 Tube Design Criteria Vs. Hot Gas-Side Wall Temperature

tubes, with the latter providing a lower pressure drop. Details of the baseline tube bundle for both coolants are given in Table XV.

Previous nozzle tube bundle design studies, particularly those of Ref. 10, were used to develop the following scaling relationships for coolant pressure drop and bulk temperature rise:

$$\Delta P \sim P_c^{3.5} \; F^{0.25}$$

$$\Delta T_b \sim P_c^{0.05}/F^{0.075}$$

D. CYCLE POWER BALANCE

Utilizing the parametric heat transfer and performance data from this study, power balance data were generated for the eleven engine cycles (A - K) given in Table II. The cycles labeled A through I (shown in Figure 6) are those specified by the contract. Cycles J and K were selected as the most promising additional candidates from the preliminary cycle studies previously cited in Section III,B.

Engine specification data based on the parametric performance data for LO_2/RP-1, LO_2/LCH_4, and LO_2/LC_3H_8 are given in Tables XVI, XVII, and XVIII, respectively. These data were used for the power balance evaluation of staged-combustion cycle engines and for the thrust chamber portion of open-loop (e.g., gas-generator) cycle engines. In many cases, power balances were not achieved at the higher chamber pressures (Pc = 20680 to 34470 kN/m^2 (3000 to 5000 psia)) due to cooling limitations (i.e., high coolant channel pressure drops). Split flow pumps were utilized in the analysis where they proved beneficial in lowering the horsepower requirements. The power cycles and the power balance data are summarized in Table XIX and in the following paragraphs.

TABLE XV

BASELINE NOZZLE TUBE BUNDLE DESIGNS

F = 2669 kN (600K lbF) Pc = 27580 kN/m^2 (4000 psia)

Coolant	RP-1	Oxygen
No. of Tubes	326	250
Type of Tubes	Round	Flattened
Undeformed Diameter, cm (in.)		
Forward	.73 (.287)	2.01 (.790)
Aft	1.63 (.643)	4.01 (1.580)
Wall Thickness, cm (in.)		
Forward	.04 (.017)	.05 (.020)
Aft	.12 (.046)	.14 (.054)
Pressure Drop, kN/m^2 (psi)	3034 (440)	531 (77)
Bulk Temperature Rise, °K (°F)	314 (106)	287 (56)
Max. Wall Temperature, °K (°F)	922 (1200)	878 (1120)

TABLE XVI

LO_2/RP-1 THRUST CHAMBER ASSEMBLY SPECIFICATION DATA

(SI Units)

PARAMETER					
Chamber Pressure, kN/m^2	34470	27580	20680	13790	6890
Thrust, S.L. kN	2669	2669	2669	2669	2669
Thrust, vac, kN	2947	2964	2987	3022	3094
Mixture Ratio	2.8	2.8	2.8	2.8	2.8
Area Ratio	61.7	51.9	41.3	29.8	17.2
ODE Is, S.L. sec	334.4	330.7	325.3	313.6	293.5
ODE Is, vac, sec	368.1	365.9	362.5	353.7	339.5
Is Efficiency, %(V)	96.7	96.6	96.4	96.8	96.7
Deliv. Is, S.L. sec	322.3	318.2	312.2	302.4	283.0
Deliv. Is, vac, sec	355.9	353.4	349.4	342.4	328.1
Total Flowrate, kg/s	844.4	855.3	871.8	900.0	961.7
LO_2 Flowrate kg/s	622.2	630.2	642.3	663.2	708.6
Fuel Flowrate kg/s	222.2	225.1	229.4	236.8	253.1
c*, m/s	1816	1812	1805	1797	1783
Throat Area, cm^2	446	561	762	1173	2487
Throat Diam., cm	23.8	26.7	31.14	38.6	56.3
Exit Area, cm^2	27477	29161	31458	34955	42781
Exit Diam., cm	187	193	200	211	233
Exit Pressure, kN/m^2	41	41	41	41	41

TABLE XVI (cont.)

LO_2/RP-1 THRUST CHAMBER ASSEMBLY SPECIFICATION DATA

(English Units)

PARAMETER					
Chamber Pressure, psia	5000	4000	3000	2000	1000
Thrust, S.L. lbF	600,000	600,000	600,000	600,000	600,000
Thrust, vac, lbF	662,617	666,433	671,605	679,365	695,618
Mixture Ratio	2.8	2.8	2.8	2.8	2.8
Area Ratio	61.7	51.9	41.3	29.8	17.2
ODE Is,S.L. sec	334.4	330.7	325.3	313.6	293.5
ODE Is, vac, sec	368.1	365.9	362.5	353.7	339.5
Is Efficiency, %(V)	96.7	96.6	96.4	96.8	96.7
Deliv. Is,S.L. sec	322.3	318.2	312.2	302.4	283.0
Deliv. Is, vac, sec	355.9	353.4	349.4	342.4	328.1
Total Flowrate, lb/s	1861.62	1885.61	1921.84	1984.13	2120.14
LO_2 Flowrate, lb/s	1371.72	1389.39	1416.10	1461.99	1562.21
Fuel Flowrate, lb/s	489.90	496.21	505.75	522.14	557.93
c*, ft/s	5958	5945	5922	5897	5850
Throat Area, in^2	69.10	86.92	118.05	181.8	385.5
Throat Diam., in.	9.38	10.52	12.26	15.21	22.15
Exit Area, in^2	4259	4520	4876	5418	6631
Exit Diam., in.	73.6	75.9	78.8	83.1	91.9
Exit Pressure, psia	6.0	6.0	6.0	6.0	6.0

TABLE XVII

LO_2/LCH_4 THRUST CHAMBER ASSEMBLY SPECIFICATION DATA

(SI Units)

PARAMETER					
Chamber Pressure, kN/m^2	34470	27580	20680	13790	6890
Thrust, S.L., kN	2669	2669	2669	2669	2669
Thrust, vac, kN	2958	2973	2996	3035	3117
Mixture Ratio	3.5	3.5	3.5	3.5	3.5
Area Ratio	63.9	53.2	42.2	30.5	17.6
ODE Is, S.L. sec	343.1	338.3	332.4	321.5	301.2
ODE Is, vac, sec	378.8	375.4	371.6	363.8	349.8
Is Efficiency, %(V)	96.4	96.6	96.5	96.7	96.5
Deliv. Is, S.L. sec	329.6	325.4	319.4	309.4	289.0
Deliv. Is, vac, sec	365.3	362.5	358.5	351.7	337.5
Total Flowrate, kg/s	825.7	836.4	852.1	879.6	941.7
LO_2 Flowrate, kg/s	642.2	650.5	662.7	684.2	732.5
Fuel Flowrate, kg/s	183.5	185.9	189.4	195.5	209.3
c*, m/s	1865	1861	1856	1848	1834
Throat Area, cm^2	446	565	765	1179	2505
Throat Diam., cm	23.9	26.8	31.2	38.7	56.5
Exit Area, cm^2	28548	30032	32258	35955	44084
Exit Diam., cm	191	196	203	214	237
Exit Pressure, kN/m^2	41	41	41	41	41

TABLE XVII (cont.)

LO_2/LCH_4 THRUST CHAMBER ASSEMBLY SPECIFICATION DATA

(English Units)

PARAMETER					
Chamber Pressure, psia	5000	4000	3000	2000	1000
Thrust, S.L. lbF	600,000	600,000	600,000	600,000	600,000
Thrust, vac, lbF	665,090	668,416	673,553	682,193	700,698
Mixture Ratio	3.5	3.5	3.5	3.5	3.5
Area Ratio	63.9	53.2	42.2	30.5	17.6
ODE Is, S.L. sec	343.1	338.3	332.4	321.5	301.2
ODE Is, vac, sec	378.8	375.4	371.6	363.8	349.8
Is Efficiency, %(V)	96.4	96.6	96.5	96.7	96.5
Deliv. Is, S.L. sec	329.6	325.4	319.4	309.4	289.0
Deliv. Is, vac, sec	365.3	362.5	358.5	351.7	337.5
Total Flowrate, lb/s	1820.39	1843.88	1878.52	1939.24	2076.12
LO_2 Flowrate, lb/s	1415.86	1434.13	1461.07	1508.30	1614.76
Fuel Flowrate, lb/s	404.53	409.75	417.45	430.94	461.36
c*, ft/s	6119	6107	6088	6063	6017
Throat Area, in^2	69.2	87.5	118.5	182.7	388.3
Throat Diam., in.	9.39	10.56	12.28	15.25	22.24
Exit Area, in^2	4425	4655	5000	5573	6833
Exit Diam., in.	75.1	77.0	79.8	84.2	93.3
Exit Pressure, psia	6.0	6.0	6.0	6.0	6.0

TABLE XVIII

LO_2/LC_3H_8 THRUST CHAMBER ASSEMBLY SPECIFICATION DATA

(SI Units)

PARAMETER					
Chamber Pressure, kN/m^2	34470	27580	20680	13790	6890
Thrust, S.L. kN	2669	2669	2669	2669	2669
Thrust, vac, kN	2949	2968	2993	3030	3112
Mixture Ratio	3.1	3.1	3.1	3.1	3.1
Area Ratio	61.9	52.4	41.7	30.1	17.3
ODE Is, S.L. sec	340.0	334.9	328.2	317.9	297.2
ODE Is, vac, sec	374.6	371.3	366.8	359.5	344.6
Is Efficiency, %(V)	97.2	97.2	96.9	97.0	96.6
Deliv. Is, S.L. sec	329.6	324.5	317.1	307.2	285.3
Deliv. Is, vac, sec	364.2	360.9	355.6	348.8	332.7
Total Flowrate, kg/s	825.7	838.7	858.3	885.9	953.9
LO_2 Flowrate, kg/s	624.3	634.1	648.9	669.9	721.3
Fuel Flowrate, kg/s	201.4	204.6	209.3	216.1	259.9
c*, m/s	1864	1857	1850	1843	1828
Throat Area, cm^2	446	565	768	1184	2530
Throat Diam., cm	23.9	26.8	31.3	38.8	56.7
Exit Area, cm^2	27632	29587	32006	35645	43761
Exit Diam., cm	188	194	202	213	236
Exit Pressure, kN/m^2	41	41	41	41	41

TABLE XVIII (cont.)

LO_2/LC_3H_8 THRUST CHAMBER ASSEMBLY SPECIFICATION DATA

(English Units)

PARAMETER					
Chamber Pressure, psia	5000	4000	3000	2000	1000
Thrust, S. L. lbF	600,000	600,000	600,000	600,000	600,000
Thrust, vac, lbF	662,985	667,304	672,848	681,250	699,685
Mixture Ratio	3.1	3.1	3.1	3.1	3.1
Area Ratio	61.9	52.4	41.7	30.1	17.3
ODE Is,S.L. sec	340.0	334.9	328.2	317.9	297.2
ODE Is, vac, sec	374.6	371.3	366.8	359.5	344.6
Is Efficiency, %(V)	97.2	97.2	96.9	97.0	96.6
Deliv. Is,S.L. sec	329.6	324.5	317.1	307.2	285.3
Deliv. Is, vac, sec	364.2	360.9	355.6	348.8	332.7
Total Flowrate, lb/s	1820.39	1849.00	1892.15	1953.13	2103.05
LO_2 Flowrate, lb/s	1376.39	1398.02	1430.65	1476.75	1590.11
Fuel Flowrate, lb/s	444.00	450.98	461.50	476.37	512.94
c*, ft/s	6115	6092	6069	6047	5998
Throat Area, $in.^2$	69.2	87.5	119.0	183.5	392.1
Throat Diam., in.	9.39	10.56	12.31	15.29	22.34
Exit Area, $in.^2$	4283	4586	4961	5525	6783
Exit Diam., in.	73.9	76.4	79.5	83.9	92.9
Exit Pressure, psia	6.0	6.0	6.0	6.0	6.0

TABLE XIX (1 of 6)

POWER CYCLE DATA SUMMARY FOR LOX/HYDROCARBON ROCKET ENGINES

SEA LEVEL THRUST - 600,000 lbF

Engine Config.	Engine Cycle	Hydrocarbon Fuel	Chamber Coolant	Turbine Drive	Turbine Inlet Temp. (°R)	Fuel Pump Dischg. Press (psia)	LOX Pump Dischg. Press (psia)	Chamber Pressure (psia)	Mixture Ratio	Specific Impulse S.L. (sec)	Specific Impulse Vac. (sec)
A	GG	RP-1	RP-1	FR	1860	2824	1210	1000	2.61	277.3	322.1
A'	GG	RP-1R	RP-1R	FR	1860	1441	1210	1000	2.66	278.0	232.2
						3629	2421	2000	2.49	291.2	331.1
						5095	3025	2500	2.40	293.0	331.5
						6931	3629	3000	2.30	293.1	330.1
						11400	4880	4000	2.12	290.8	325.5
					2260	3629	2421	2000	2.62	295.2	335.3
						5095	3025	2500	2.57	298.4	337.1
A	GG	RP-1	RP-1*	FR	1860	3717	2421	2000	2.49	291.1	331.0
					2260	3717	2421	2000	2.62	295.2	335.3
A'	GG	RP-1R	RP-1R*	FR	1860	2671	2421	2000	2.52	292.4	332.3
						3762	3025	2500	2.44	294.7	333.1
						5406	3629	3000	2.35	295.1	332.1
					2260	2671	2421	2000	2.64	296.0	336.1
						3762	3025	2500	2.59	300.0	339.3
						5406	3629	3000	2.53	302.5	341.0
					2960	5406	3629	3000	2.71	307.0	344.7
B	GG	RP-1	LOX	FR	1860	1194	1320	1000	2.66	278.0	232.2
						2389	2878	2000	2.59	291.6	331.6
						3583	4774	3000	2.33	294.6	331.6
						4777	7797	4000	2.13	291.3	326.2
						5972	11890	5000	1.91		
					2260	2389	2878	2000	2.63	295.5	335.6
						3583	4774	3000	2.53	301.2	338.5
						4777	7797	4000	2.39	301.5	336.8

*CARBON DEPOSIT ON CHAMBER WALL

TABLE XIX (cont.) (2 of 6)

POWER CYCLE DATA SUMMARY FOR LOX/HYDROCARBON ROCKET ENGINES

SEA LEVEL THRUST - 600,000 lbF

Engine Config.	Engine Cycle	Hydrocarbon Fuel	Chamber Coolant	Turbine Drive	Turbine Inlet Temp. (°R)	Fuel Pump Dischg. Press (psia)	LOX Pump Dischg. Press (psia)	Chamber Pressure (psia)	Mixture Ratio	Specific I S.L. (sec)	mpulse Vac. (sec)
B	GG	RP-1	LOX*	FR	1860	2389	2522	2000	2.53	292.5	332.5
						3583	4269	3000	2.36	295.8	322.9
						4777	6700	4000	2.18	293.9	328.8
						5972	11147	5000	1.94	285.9	319.0
					2260	2389	2522	2000	2.64	296.1	336.2
						3583	4269	3000	2.55	302.0	339.3
						4777	6700	4000	2.43	303.4	338.4
					2960	2389	2522	2000	2.75	299.3	339.6
						3583	4269	3000	2.72	307.3	344.9
						4777	6700	4000	2.68	311.0	346.7
C	GG	LCH_4	LCH_4	FR	1860	1263	1210	1000	3.37	285.7	334.5
						2700	2421	2000	3.22	302.5	345.2
						4447	3629	3000	3.07	308.4	348.0
						6921	4879	4000	2.88	309.3	346.8
						10961	6172	5000	2.65	306.7	342.9
					2260	2700	2421	2000	3.35	304.7	347.5
						4447	3629	3000	3.25	312.0	351.6
						6921	4879	4000	3.14	314.5	352.3
						10961	6172	5000	2.98	314.1	350.6
					2960	2700	2421	2000	3.44	306.2	348.8
						4447	3629	3000	3.40	314.5	354.0
						6921	4879	4000	3.36	318.5	356.0
						10961	6172	5000	3.29	319.8	356.1
C (200K)	GG	LCH_4	LCH_4	FR	1860	7030	4879	4000	2.88	308.5	346.2
C (1.5M)	GG	LCH_4	LCH_4	FR	1860	7662	4879	4000	2.85	308.9	346.5

*CARBON DEPOSIT ON CHAMBER WALL

TABLE XIX (cont.) (3 of 6)

POWER CYCLE DATA SUMMARY FOR LOX/HYDROCARBON ROCKET ENGINES

SEA LEVEL THRUST - 600,000 lbF

Engine Config.	Engine Cycle	Hydrocarbon Fuel	Chamber Coolant	Turbine Drive	Turbine Inlet Temp. (°R)	Fuel Pump Dischg. Press (psia)	LOX Pump Dischg. Press (psia)	Chamber Pressure (psia)	Mixture Ratio	Specific Impulse S.L. (sec)	Specific Impulse Vac. (sec)
C'	GG	LC_3H_8	LC_3H_8	FR	1860	1230	1210	1000	2.99	282.0	329.6
						2558	2421	2000	2.85	299.5	341.2
						4179	3629	3000	2.71	305.1	343.7
						6455	4879	4000	2.56	307.3	343.8
						10038	6172	5000	2.38	305.9	340.6
D	SC	RP-1	RP-1	FR	1860	3312	1210/1680	1000	2.80	283.0	328.1
D'	SC	RP-1R	RP-1R	FR	1860	1840	1210/1592	1000	2.80	283.0	328.1
						5303	2421/4054	2000		302.4	342.4
						8188	3025/6063	2500		307.8	346.4
						12845	3629/9468	3000		312.2	349.4
					2260	4610	2421/3364	2000		302.4	342.4
						6645	3025/4528	2500		307.8	346.4
						9340	3629/5981	3000		312.2	349.4
						16909	4879/10259	4000		318.2	353.4
					2960	4215	2421/2972	2000		302.4	342.4
						8072	3629/4718	3000		312.2	349.4
						13398	4879/6765	4000		318.2	353.4
D	SC	RP-1	RP-1*	FR	1860	5407	2421/4071	2000	2.8	302.4	342.4
					2260	4698	2421/3366	2000			
D'	SC	RP-1P	RP-1R*	FR	1860	1650	1210/1582	1000	2.8	283.0	328.1
						4163	2421/3873	2000		302.4	342.4
						6397	3025/5607	2500		307.8	346.4
						10284	3629/8437	3000		312.2	349.4

*CARBON DEPOSIT ON CHAMBER WALL

TABLE XIX (cont.) (4 of 6)

POWER CYCLE DATA SUMMARY FOR LOX/HYDROCARBON ROCKET ENGINES

SEA LEVEL THRUST - 600,000 lbF

Engine Config.	Engine Cycle	Hydrocarbon Fuel	Chamber Coolant	Turbine Drive	Turbine Inlet Temp. (°R)	Fuel Pump Dischg. Press (psia)	LOX Pump Dischg. Press (psia)	Chamber Pressure (psia)	Mixture Ratio	Specific S.L. (sec)	Impulse Vac. (sec)
D'	SC	RP-1P	RP-1P*	FR	2260	3570	2421/3284	2000	2.8	302.4	342.4
						5170	3025/4386	2500		307.8	346.4
						7572	3629/5738	3000		312.2	349.4
					▼	16909	4879/10259	4000		318.2	353.4
					2960	6481	3629/4653	3000		312.2	349.4
▼	▼	▼	▼	▼	▼	13398	4879/6765	4000	▼	318.2	353.4
E	SC	RP-1	LOX	FP	1860	1589	1320/1589	1000	2.8	283.0	328.1
						3966	2878/3966	2000		302.4	342.4
					▼	8524	4774/8524	3000		312.2	349.4
					2260	3324	2878/3324	2000		302.4	342.4
						5709	4774/5709	3000		312.2	349.4
						9517	7797/9517	4000		318.2	353.4
					▼	18544	11890/18544	5000		322.3	355.9
					2960	4635	4774/4635	3000		312.2	349.4
						6570	7797/6570	4000		318.2	353.4
▼	▼	▼	▼	▼	▼	8893	11890/8893	5000	▼	322.3	355.9
E	SC	RP-1	LOX*	FP	2260	8995	6700/8995	4000	2.8	318.2	353.4
▼	▼	▼	▼	▼	2960	6485	6700/6485	▼	▼	▼	▼
F	SC	RP-1	RP-1	OR	1660	2825/1549	1567	1000	2.8	283.0	328.1
F'	SC	RP-1P	RP-1P	OR	1660	1441/1505	1523	1000	2.8	283.0	328.1
						3629/3415	3452	2000		302.4	342.4
						5095/4648	4700	2500		307.8	346.4
						6931/6222	6281	3000		312.2	349.4
▼	▼	▼	▼	▼	▼	11400/12289	12429	4000	▼	318.2	353.4

*CARBON DEPOSIT ON CHAMBER WALL

TABLE XIX (cont.) (5 of 6)

POWER CYCLE DATA SUMMARY FOR LOX/HYDROCARBON ROCKET ENGINES

SEA LEVEL THRUST - 600,000 lbF

Engine Config.	Engine Cycle	Hydrocarbon Fuel	Chamber Coolant	Turbine Drive	Turbine Inlet Temp. (°R)	Fuel Pump Dischg. Press (psia)	LOX Pump Dischg. Press (psia)	Chamber Pressure (psia)	Mixture Ratio	Specific I. S.L. (sec)	Impulse Vac. (sec)
G	SC	RP-1	LOX	OR	1660	1194/1504	1631	1000	2.8	283.0	328.1
						2389/3391	3885	2000		302.4	342.4
						3583/6045	7248	3000		312.2	349.4
						4777/11881	14936	4000		318.2	353.4
					2600	4777/7791	10826	4000			
G	SC	RP-1	LOX*	OR	1660	4777/10576	12527	4000	2.8	318.2	353.4
G'	SC	LC_3H_8	LOX	OR	1660	1194/1502	1630	1000	3.1	285.3	332.7
						2389/3382	3876	2000		307.2	348.8
						3583/6012	7216	3000		317.1	355.6
						4777/11652	14706	4000		324.5	360.9
H	SC	LCH_4	LCH_4	FR	1860	1607	1210/1536	1000	3.5	289.0	337.5
						3945	2421/3627	2000		309.4	351.7
						7896	3629/7015	3000		319.4	358.5
					2960	5517	3629/4648				
					2260	8315	4246/6889	3500		323.1	361.0
					2960	6994	4246/5576				
					2960	7972	4626/6164	3800		324.9	362.1
					2260	10794	4879/6831	4000		325.4	362.5
					2960	8728	4879/6575				
I	SC	LCH_4	LCH_4	FR/OR	1860/1660	1525	1485	1000	3.5	289.0	337.5
						3481	3206	2000		309.4	351.7
						6253	5381	3000		319.4	358.5
						10959	8795	4000		325.4	362.5
					2260/1660	9146	8339				
					2960/1660	8210	9704				

*CARBON DEPOSIT IN CHAMBER WALL

TABLE XIX (cont.) (6 of 6)

POWER CYCLE DATA SUMMARY FOR LOX/HYDROCARBON ROCKET ENGINES

SEA LEVEL THRUST - 600,000 lbF

Engine Config.	Engine Cycle	Hydrocarbon Fuel	Chamber Coolant	Turbine Drive	Turbine Inlet Temp. (°R)	Fuel Pump Discha. Press (psia)	LOX Pump Discha. Press (psia)	Chamber Pressure (psia)	Mixture Ratio	Specific Impulse S.L. (sec)	Specific Impulse Vac. (sec)
↕	GG	LC_3H_8	LC_3H_8	FP/OP	1860/1660	1476	1501	1000	3.1	285.3	332.7
						3283	3288	2000		307.2	348.8
						5791	5526	3000		317.1	355.6
▼	▼	▼	▼	▼	▼	9845	8851	4000	▼	324.5	360.9
↕	GG	RP-1	LH_2	HP	1840	1194/1325	1213	1000	(2.8)	293.3	328.5
						2389/2566	2421	2000	↕	302.4	342.5
						3583/3826	3629	3000		311.9	349.2
						4777/5093	4839	4000		317.3	352.7
▼	▼	▼	▼	▼	▼	5972/6740	6172	5000	▼	321.1	354.9
↕ (D-T)	GG/GG	LCH_4	LH_2/LCH_4	HP/OP	[illegible]	7429/1655	7429	2000/4000	(3.5)	319.0	357.9 (I)
								4000 (II)			380.2(II)

III, D, Cycle Power Balance (cont.)

1. Cycle A

The schematic for engine cycle A is given in Figure 20. As shown in the figure, the engine is fuel-cooled from a low area ratio (8:1) to the injector. The coolant then enters the nozzle (ϵ = 8:1 to about 40:1). A small portion of the fuel bypasses the coolant jacket and flows directly to the gas generator, and a small portion of the oxidizer bypasses the main injector circuit and flows to the gas generator. The fuel-rich gas generator provides the drive fluid for the two turbines shown in series in the schematic. Other turbine arrangements are possible, depending upon the horsepower requirements and speeds of the pumps. Since the series turbine arrangement offers a slight horsepower advantage over a parallel turbine arrangement, it was selected for the purposes of obtaining the parametric cycle data. Split flow pumps were also utilized to minimize horsepower requirements. The pump discharge pressure for the gas generator fluids was chosen equal to that for the oxidizer pump.

Another cooling scheme was investigated to further optimize the engine cycle power balance. Liquid oxygen was substituted for fuel as the nozzle coolant from 8:1 to the nozzle area ratio. The differences in fuel pump discharge pressure and performance are seen to be small when oxygen is used as the nozzle coolant:

Chamber Pressure kN/m^2	(psia)	ΔP_{DF} kN/m^2	(psi)	ΔIs(S.L.) (sec)	ΔIs(vac) (sec)
13790	2000	-269	(-39)	0	0
20680	3000	-1124	(-163)	0.2	0.2
27580	4000	-3082	(-447)	0.4	0.3

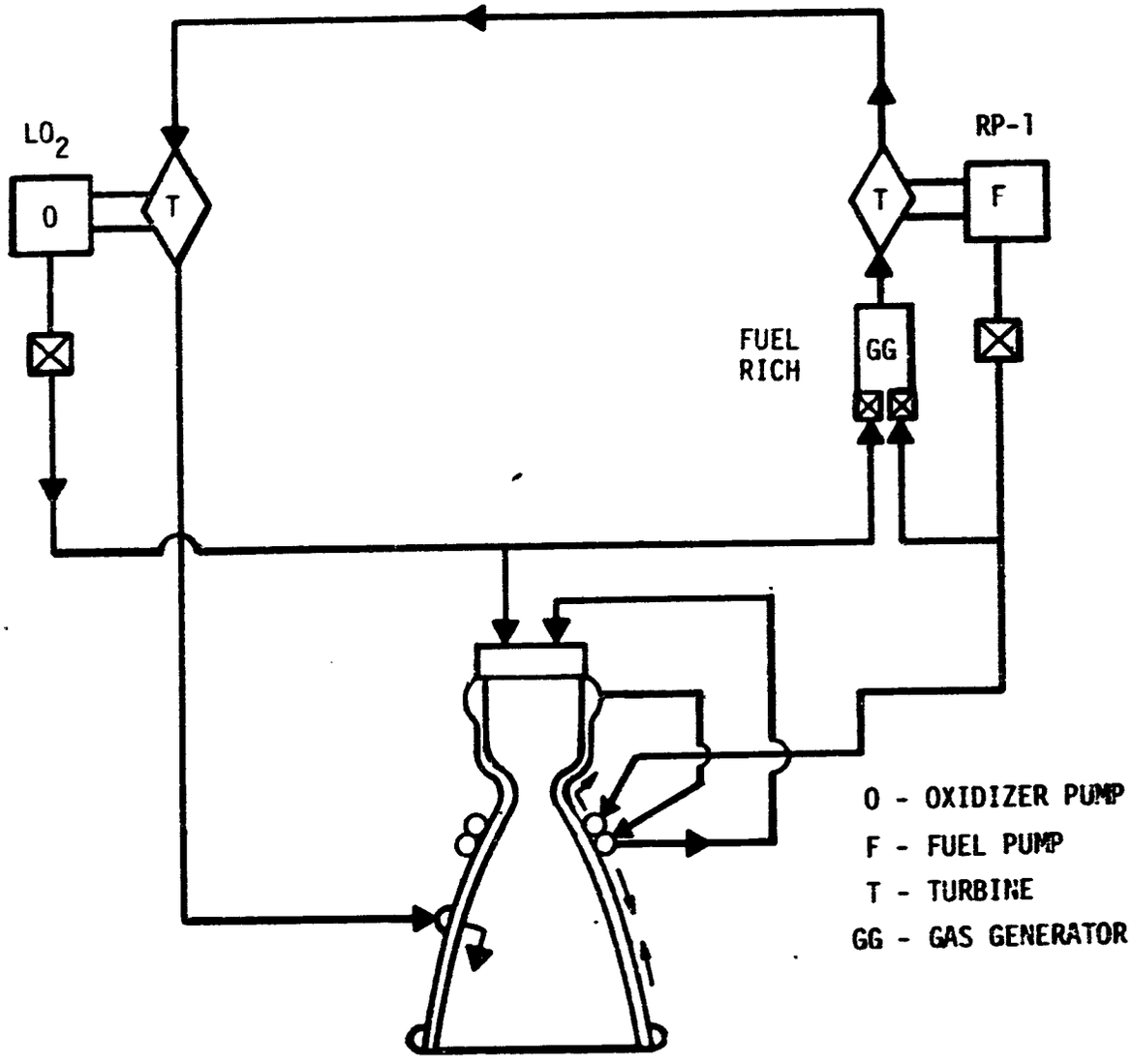

Figure 20. RP-1 Fuel-Rich Gas-Generator Cycle A Schematic

III, D, Cycle Power Balance (cont.)

A small thrust contribution is obtained by dumping the turbine exhaust into the nozzle and expanding the gas along with the exhaust from the thrust chamber. This thrust contribution and the overall engine specifications are summarized in Tables XIX and XX for the LOX-cooled nozzle cases, as these represent a slightly higher chamber pressure capability for this cycle. The pump discharge pressure requirement as a function of chamber pressure is illustrated in Figure 21, and the delivered performance versus chamber pressure is plotted in Figure 22.

Calculations were initially made from coolant pressure drop data, obtained by assuming no carbon deposit on the hot gas-side chamber wall, and by assuming a maximum local coolant-side wall temperature of 550°F (the decomposition temperature for MIL SPEC RP-1). With no carbon deposition, the RP-1 coolant pressure drop at a chamber pressure of 6895 kN/m^2 (1000 psia) and an engine thrust level of 890 kN (200K lbF) is 11030 kN/m^2 (1600 psia). Since it would not be possible to achieve an engine power balance with RP-1 at much higher chamber pressures (cf. the slope of curve 5 in Figure 21), a more refined petroleum fraction (RP-1R) was utilized in most of the calculations. The more refined fuel is similar to JP-5 or JP-7, which have breakpoint temperatures approaching 700°K (800°F).

The conclusions to be drawn from examination of Figure 21 are as follows: (1) MIL SPEC RP-1-cooled engines (curve 5) are limited to a chamber pressure slightly above 6895 kN/m^2 (1000 psia) when there is no carbon deposit on the wall; (2) MIL SPEC RP-1-cooled engines (curve 3) can achieve a chamber pressure in excess of 13790 kN/m^2 (2000 psia) if a uniform carbon deposit is maintained on the chamber wall; (3) an RP-1R-cooled engine (curve 2) is limited to a chamber pressure slightly in excess of 20680 kN/m^2 (3000 psia) without a carbon deposit; (4) an RP-1R-cooled engine (curve 1) can achieve a chamber pressure in excess of 24130 kN/m^2 (3500 psia) if a carbon deposit is maintained on the chamber wall; and (5) the LOX pump discharge pressure (curve 4) is not the controlling element in the power balances for this cycle.

TABLE XX (1 of 2)

ENGINE CYCLE & PARAMETRIC DATA

LOX/PP-1 & PP-1R

PARAMETER						HIGH TEMPERATURE TURBINE		
Chamber Pressure, psia	1000*	1000	2000*	2000	2000	3000	2000*	2000
S.L. Engine Thrust, lbF	604,775	601,750	606,079	605,924	605,338	604,810	605,051	604,254
Vac. Engine Thrust, lbF	702,481	699,525	689,193	689,006	687,898	686,982	687,241	686,090
Area Ratio	17.2	17.2	29.8					
Del. S.L. Is, sec	277.3	278.0	291.1	291.2	295.5	297.4	296.2	298.0
Del. Vac, Is, sec	322.1	322.2	331.0	331.1	335.4	337.5	336.2	338.1
Engine Flowrate, lb/s	2180.94	2164.54	2082.03	2081.03	2069.83	2048.93	2049.63	2041.43
TCA Mixture Ratio	2.8	2.8	2.8					
TCA S.L. Is, sec	283.0	283.0	302.4					
TCA Vac. Is, sec	328.1	328.1	342.4					
GG Mixture Ratio	.335	.335	.315	.315	.315	.475	.475	.475
GG Flowrate	60.80	44.40	97.90	96.90	85.70	64.80	65.50	57.30
GG S.L. Is, sec	39.4	39.4	61.1	61.1	61.1	74.2	74.2	74.2
GG Vac. Is, sec	88.0	88.0	99.5	99.5	99.5	117.5	117.5	117.5
Coolant ΔP, psi	1600	165	1296**	1210	266**	1210	1296**	266**
Turbine Inlet Temp., °R	1860	1860	1860	1860	1860	2260	2260	2260
Turbine Power, hp	20,230	14,770	31,700	31,370	27,740	30,850	31,180	27,280
Fuel Pump Dischg. P. psia	2824	1441	3717	3629	2671	3629	3717	2671
Ox Pump Dischg. P. psia	1210	1210	2421	2421	2421	2421	2421	2421

* MIL SPEC PP-1

** CARBON DEPOSITION ON CHAMBER WALL

TABLE XX (cont.) (2 of 2)

ENGINE CYCLE A PARAMETRIC DATA

LOX/RP-1 & RP-1P

PARAMETER	HIGH TEMP. TURBINE								
Chamber Pressure, psia	2500	2500	2500	2500	3000	3000	3000	3000	4000
S.L. Engine Thrust, lbF	608,655	607,589	606,862	607,026	593,064	610,473	610,197	605,957	618,939
Vac. Engine Thrust, lbF	688,424	686,759	685,567	686,546	667,931	687,015	687,358	680,369	692,794
Area Ratio	35.9				41.3				51.9
Del. S.L. Is, sec	293.0	294.7	298.4	300.0	293.1	295.3	302.5	302.0	290.8
Del. Vac. Is, sec	331.4	333.1	337.1	339.3	330.1	332.1	341.0	344.7	325.5
Engine Flowrate, lb/s	2077.32	2061.72	2033.72	2023.42	2086.75	2068.70	2017.18	1973.80	2128.40
TCA Mixture Ratio	2.8				2.8				2.8
TCA S.L. Is, sec	307.8				312.2				318.2
TCA Vac. Is, sec	346.4				349.4				353.4
GG Mixture Ratio	.310	.310	.470	.470	.305	.305	.465	1.0	.315
GG Flowrate	128.0	112.4	84.40	74.10	164.90	146.85	95.33	51.95	242.80
GG S.L. Is, sec	66.8	66.8	81.2	81.2	70.9	70.9	86.4	115.8	78.7
GG Vac. Is, sec	102.8	102.8	121.7	121.7	105.0	105.0	124.9	166.8	109.6
Coolant ΔP, psi	2063	750**	2063	750**	3280	1778**	1778**	1778**	6500
Turbine Inlet Temp., °R	1860	1860	2260	2260	1860	1860	2260	2960	1860
Turbine Power, hp	41,180	36,150	40,280	35,370	52,480	46,740	45,380	44,430	78,610
Fuel Pump Dischg. P. psia	5095	3762	5095	3762	6931	5406	5406	5406	11,400
Ox Pump Dischg. P. psia	3025	3025	3025	3025	3629	3629	3629	3629	4880

*MIL SPEC RP-1

**CARBON DEPOSITION ON CHAMBER WALL

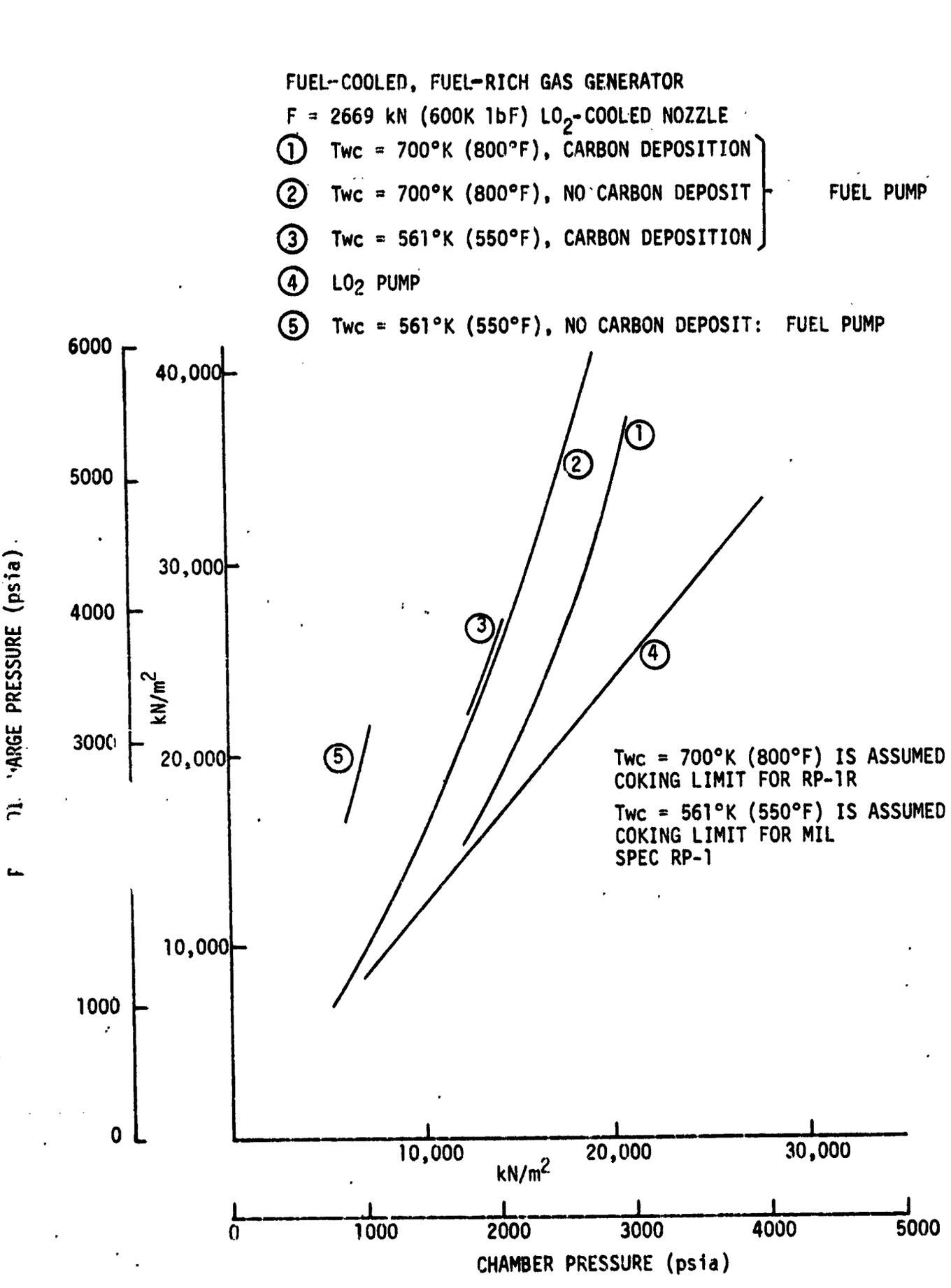

Figure 21. LO_2/RP-1 Engine Cycle A Pump Discharge Pressure Requirements

C-2

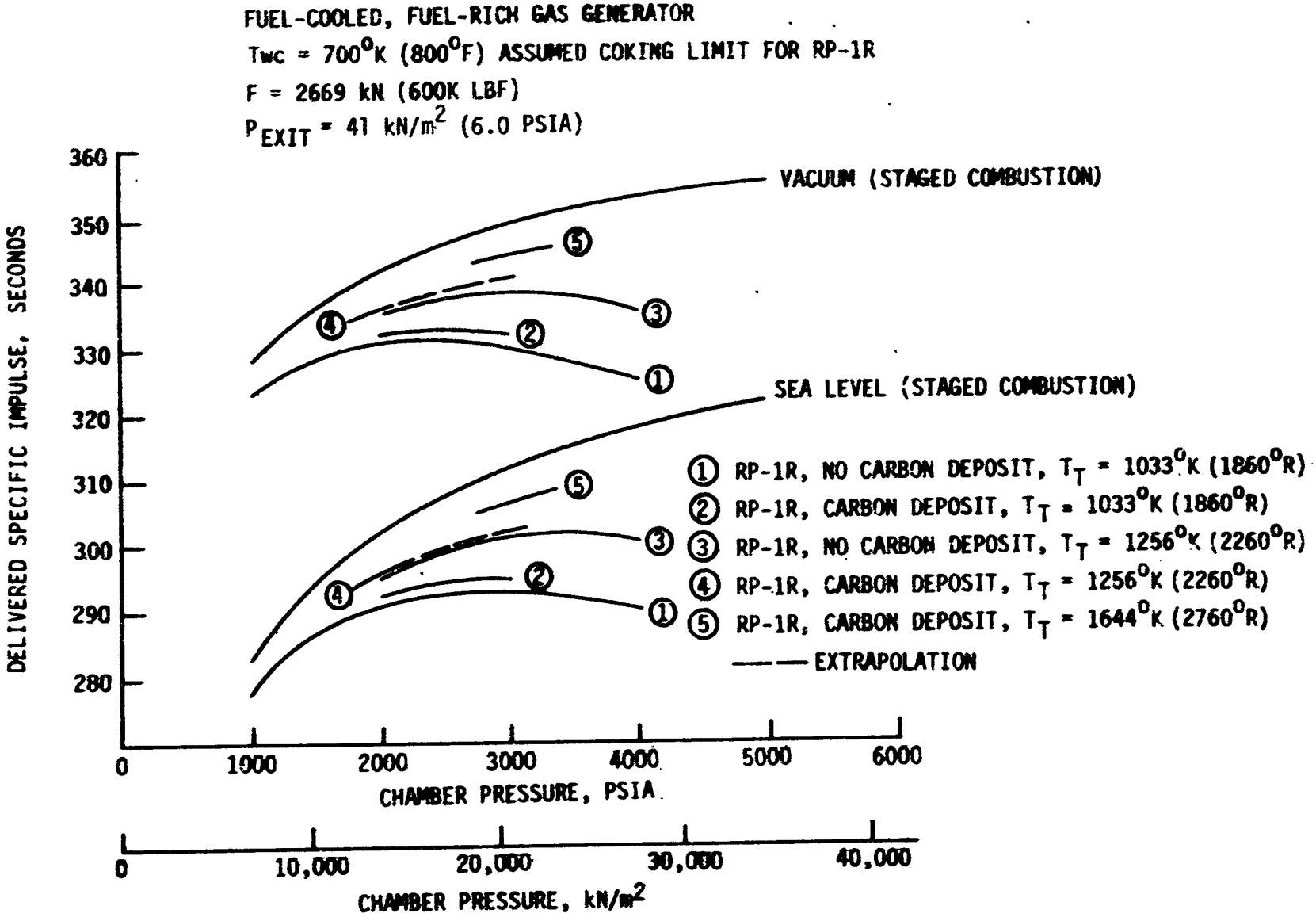

Figure 22. LO_2/RP-1 Engine Cycle A Performance

Figure 22 depicts the performance for the various cycle A engines in comparison to a staged-combustion cycle engine (shown in Table XVI). The conclusions from Figure 22 are that (1) a carbon deposit slightly influences (increases) the performance of the LOX/RP-1 gas-generator cycle engine (due to a reduction in gas-generator flowrate); (2) the turbine inlet temperature has a large effect on gas-generator engine performance (due to the variation in gas-generator flowrate); and (3) it is the gas-generator cycle losses which determine the chamber pressure operation (e.g., Pc = 3000 psia for curve 1 gives maximum performance) rather than the pump discharge pressure limit (e.g., Pd = 35160 kN/m^2 (8000 psia), which represents the current state of the art in rocket engines).

2. Cycle B

Engine cycle B differs from cycle A in that LO_2 is used as the coolant. The schematic is given in Figure 23. The power balance results are summarized in Tables XIX and XXI and in Figures 24 and 25.

Figure 24, when compared with Figure 21, shows the potential benefit of using LO_2, rather than RP-1, as the coolant. If the 1980 state-of-the-art of rocket engine turbopumps is assumed to be 8,000 psia pump discharge pressure, then LO_2 is capable of cooling a LO2/RP-1 engine with a chamber pressure of 27580 kN/m^2 (4000 psia) (curve 2) compared to 1000 psia for RP-1 and to 2500 for RP-1R, respectively. When a carbon deposit is assumed, LO_2 is capable of cooling an engine with a chamber pressure of about 30340 kN/m^2 (4400 psia) (curve 1).

Similar trends in performance as were seen in Figure 22 are shown in Figure 25. A carbon deposit provides a small increase in performance (about 1 second), and an increased turbine inlet temperature shows a large

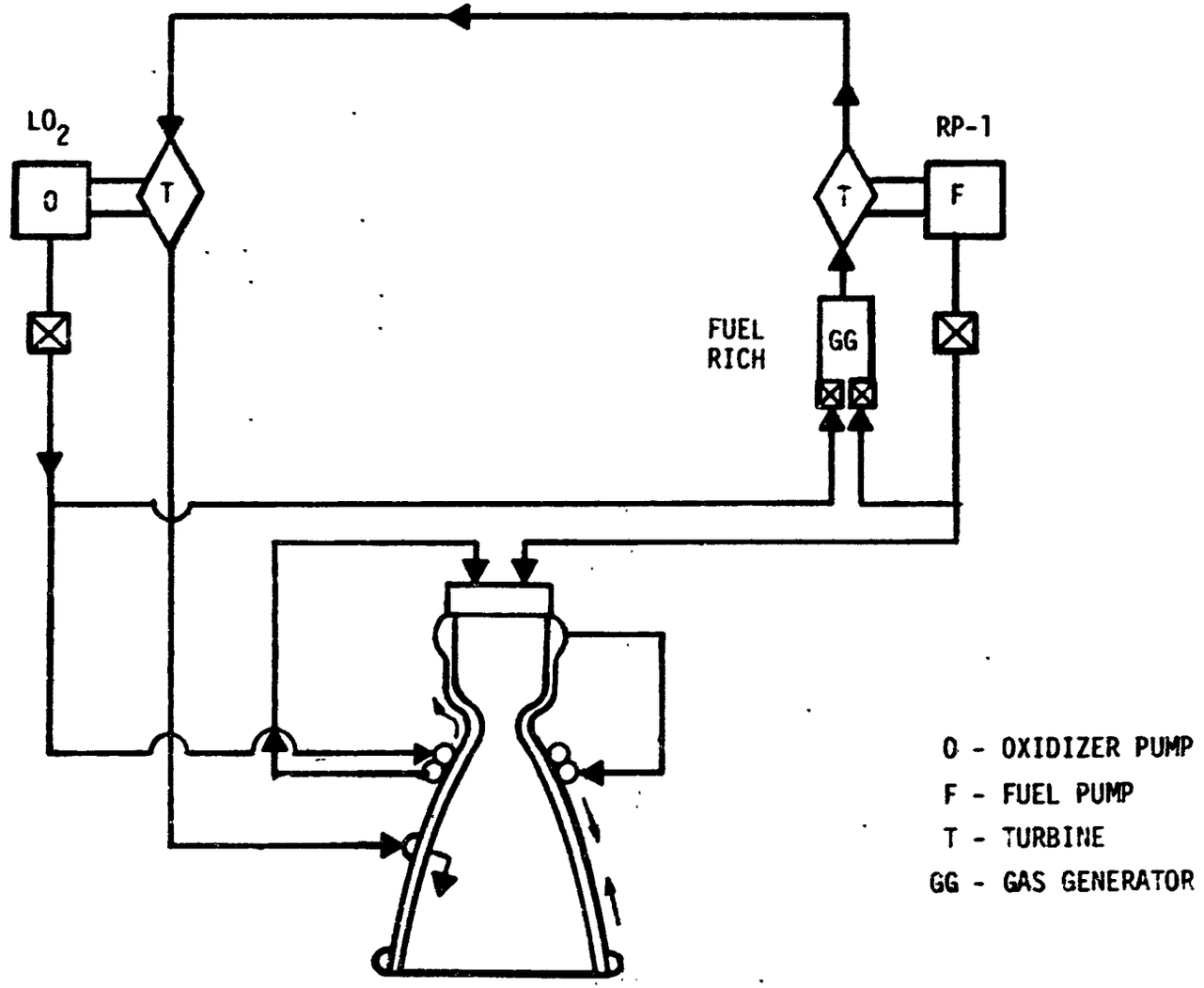

Figure 23. RP-1 Fuel-Rich Gas-Generator Cycle B Schematic

TABLE XXI (1 of 2)

ENGINE CYCLE B PARAMETRIC DATA

LOX/RP-1

PARAMETER			HIGH TEMPERATURE TURBINE					HIGH TEMP. TURBINE
Chamber Pressure, psia	1000	2000	2000	2000	2000	2000	3000	3000	3000
S.L. Engine Thrust, lbF	601,631	605,598	605,112	604,631	604,269	603,137	610,785	609,845	608,484
Vac. Engine Thrust, lbF	699,450	688,670	687,863	686,681	686,104	684,348	687,49F	686,333	683,838
Area Ratio	17.2	29.8					41.3		
Del. S.L. Is, sec	278.0	291.6	292.5	295.5	296.1	299.3	294.6	295.8	301.2
Del. Vac. Is, sec	323.2	331.6	332.5	335.6	336.2	339.6	331.6	338.9	338.5
Engine Flowrate, lb/s	2164.14	2076.81	2068.76	2046.13	2040.76	2015.16	2073.27	2061.68	2020.20
TCA Mixture Ratio	2.8	2.8					2.8		
TCA S.L. Is, sec	283.0	302.4					312.2		
TCA Vac. Is, sec	328.1	342.4					349.4		
GG Mixture Ratio	.335	.315	.315	.475	.475	1.0	.305	.305	.365
GG Flowrate	44.00	92.68	84.63	62.00	56.63	31.03	151.42	139.83	98.35
GG S.L. Is, sec	38.4	61.1	61.1	74.2	74.2	99.5	70.9	70.9	86.4
GG Vac. Is, sec	87.5	99.5	99.5	117.5	117.5	157.7	105.0	105.0	124.8
Coolant ΔP, psi	118	470	120*	470	120*	120*	1156	658*	1156
Turbine Inlet Temp, °R	1860	1860	1860	2260	2260	2960	1860	1860	2260
Turbine Power, hp	14,640	30,010	27,400	29,520	26,950	26,550	48,200	44,560	46,920
Fuel Pump Dischg. P. psia	1194	2389	2389	2389	2389	2389	3583	3583	3583
Ox Pump Dischg. P. psia	1320	2878	2522	2878	2522	2522	4774	4269	4774

*CARBON DEPOSITION ON CHAMBER WALL

TABLE XXI (cont.) (2 of 2)

ENGINE CYCLE B PARAMETRIC DATA

LOX/RP-1

PARAMETER	HIGH TEMP. TURBINE				HIGH TEMP. TURBINE				
Chamber Pressure, psia	3000	3000	4000	4000	4000	4000	4000	5000	5000
S.L. Engine Thrust, lbF	607,823	605,796	618,328	616,396	614,285	613,232	609,268	-	627,413
Vac. Engine Thrust, lbF	682,896	679,919	692,408	689,592	686,206	683,974	679,206	-	700,052
Area Ratio	41.3	———	51.9	———	———	———	———	61.7	———
Del. S.L. Is, sec	302.0	307.3	291.3	293.9	301.5	303.4	311.0	-	285.9
Del. Vac. Is, sec	339.3	344.9	326.2	328.8	336.8	338.4	346.7	-	319.0
Engine Flowrate, lb/s	2012.66	1971.35	2122.65	2097.30	2037.43	2021.20	1959.06	2211.92	2194.52
TCA Mixture Ratio	2.8	———	2.8	———	———	———	———	2.8	———
TCA S.L. Is, sec	312.2	———	318.2	———	———	———	———	322.3	———
TCA Vac. Is, sec	349.4	———	353.4	———	———	———	———	355.9	———
GG Mixture Ratio	.465	1.0	.30	.30	.46	.46	1.0	.297	.297
GG Flowrate	90.81	49.50	237.05	211.70	151.83	135.60	73.46	350.30	332.90
GG S.L. Is, sec	86.4	115.6	77.3	77.3	94.1	94.1	125.6	-	82.1
GG Vac. Is, sec	124.8	166.8	109.2	109.2	129.9	129.9	172.5	-	112.5
Coolant ΔP, psi	658*	658*	2951	1870*	2951	1870*	1870*	5800	5068*
Turbine Inlet Temp, °R	2260	2960	1860	1860	2260	2260	2960	1860	1860
Turbine Power, hp	43,330	42,340	75,340	67,270	72,610	64,830	62,840	111,550	106,000
Fuel Pump Dischg. P. psia	3583	3583	4777	4777	4777	4777	4777	5972	5972
Ox Pump Dischg. P. psia	4269	4269	7797	6700	7797	6700	6700	11,890	11,147

*CARBON DEPOSITION ON CHAMBER WALL

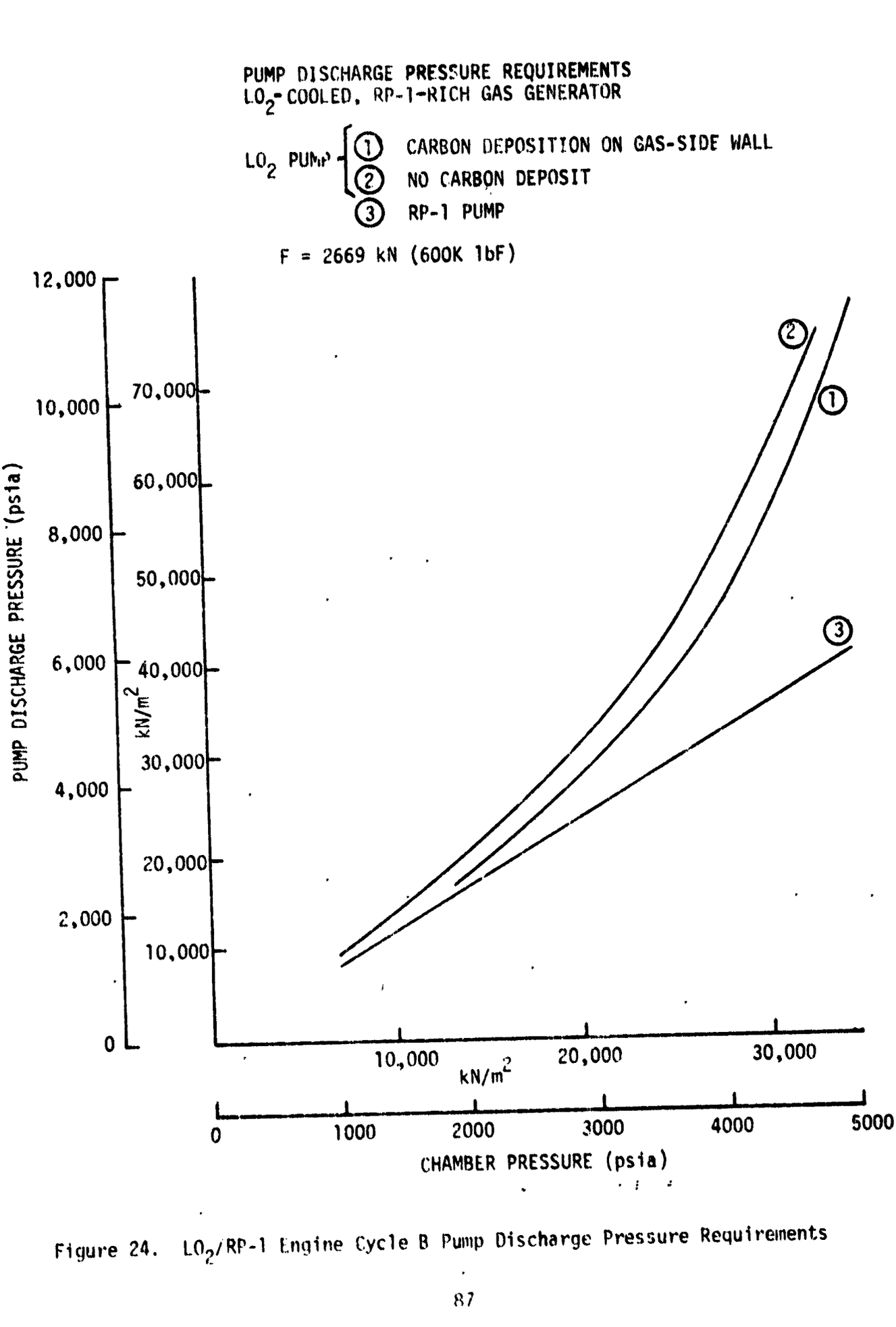

Figure 24. LO_2/RP-1 Engine Cycle B Pump Discharge Pressure Requirements

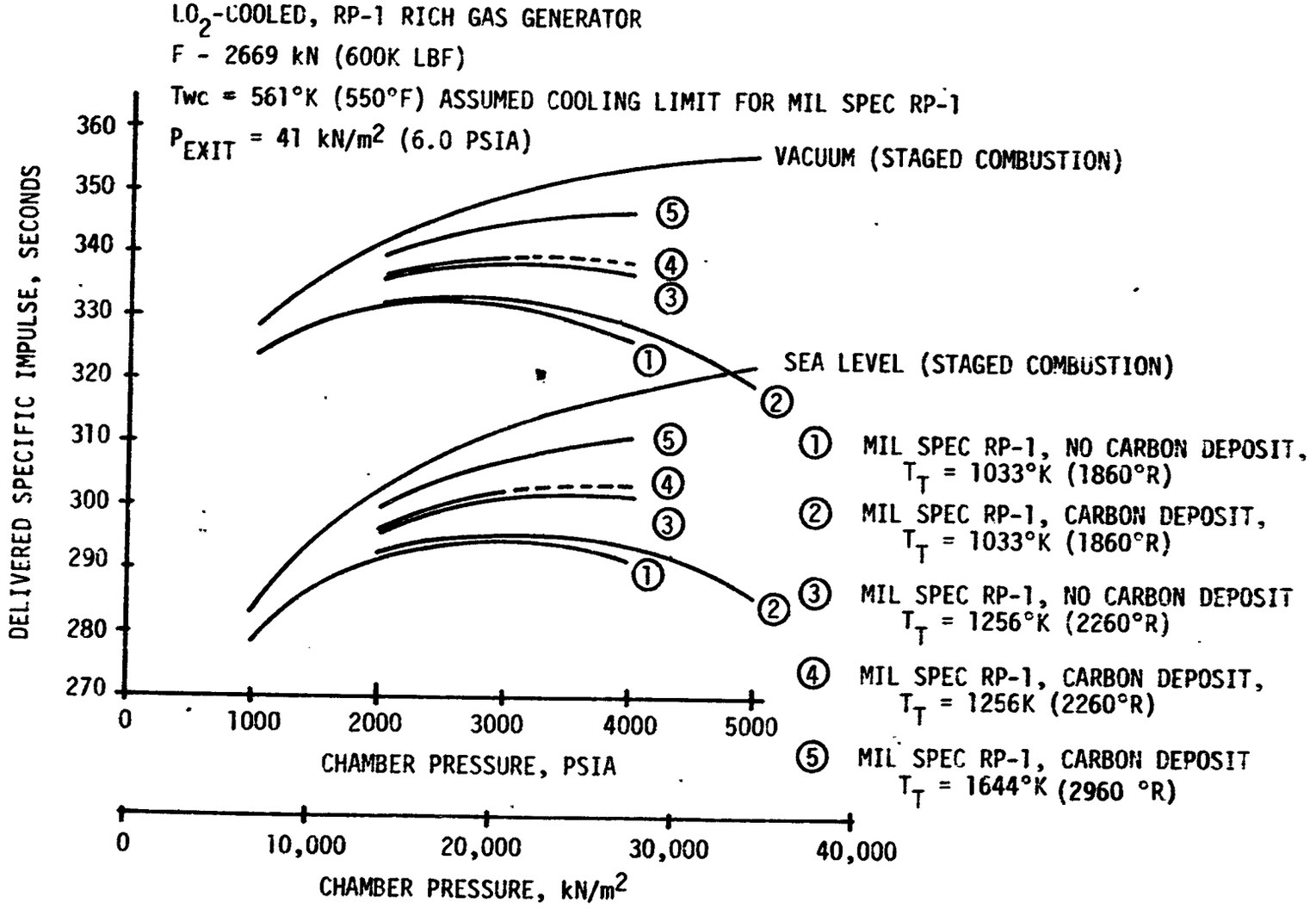

Figure 25. LO_2/RP-1 Engine Cycle B Performance

increase in performance (from 4 to 20 seconds). It should also be noted that the uncoated chamber reaches its maximum sea level performance at a chamber pressure of about 20680 kN/m^2 (3000 psia), which is essentially the same for cycle A. A carbon deposit and/or an increase in turbine inlet temperature is seen to shift the maximum performance to higher chamber pressures. The same trend was indicated in Figure 22 for the RP-1-cooled gas-generator cycle engine.

3. Cycle C

Cycle C is identical to cycle A, with the exception that methane is used as the fuel. The schematic of the cycle is given in Figure 26. Power balance data for the methane-cooled gas-generator cycle are summarized in Tables XIX and XXII and Figures 27 and 28. For an assumed pump discharge pressure limit (1980 state of the art) of 55160 kN/m^2 (8000 psia), a methane cooled gas-generator cycle engine is limited to a chamber pressure of 29650 kN/m^2 (4300 psia). A carbon deposit on the chamber wall, as seen for cycles A and B, would allow an even higher chamber pressure.

Modification of cycle C to include an oxygen-cooled nozzle has essentially no effect on the fuel pump discharge pressure (-386 kN/m^2 [-56 psia] at Pc = 4000 psia) and no effect on performance.

Performance data for three turbine inlet temperatures are given in Figure 28. The initial increase in turbine inlet temperature from 1033 to 1256°K (1860 to 2260°R) offers an increase in performance of about 4-8 seconds. Further increase in temperature to 1644°K (2960°R) is seen to give only about 2-4 seconds in additional engine performance.

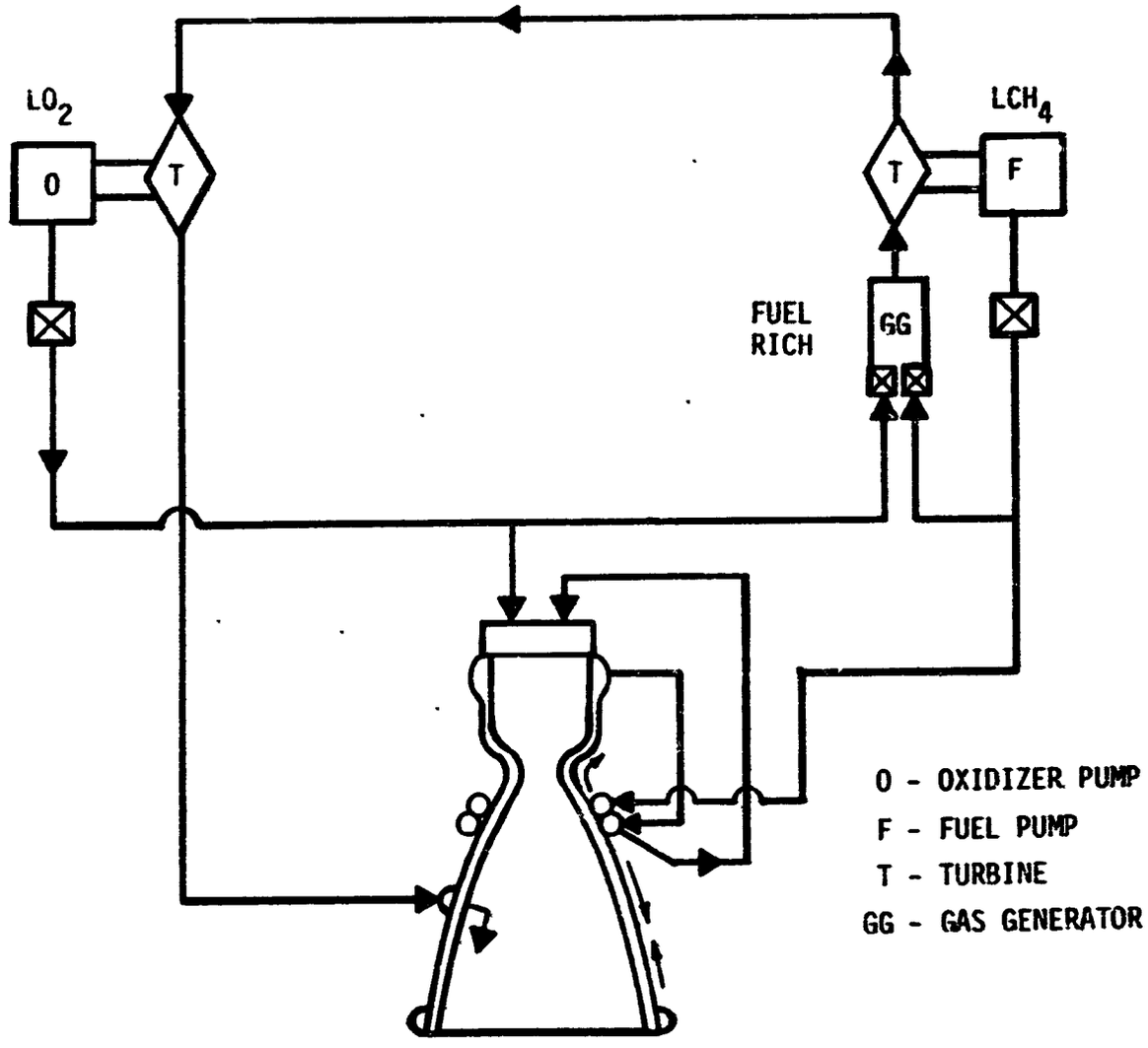

Figure 26. LCH_4 Fuel-Rich Gas-Generator Cycle C Schematic

TABLE XXII (1 of 2)

ENGINE CYCLE C PARAMETRIC DATA

LOX/LCH4

PARAMETER	HIGH TEMP. TURBINE				HIGH TEMP. TURBINE			
Chamber Pressure, psia	1000	2000	2000	2000	3000	3000	3000	4000
S.L. Engine Thrust, lbF	601,516	604,861	604,037	603,664	608,973	607,595	606,315	614,709
Vac. Engine Thrust, lbF	704,260	690,241	688,884	687,649	687.168	684.713	682,466	689,237
Area Ratio	17.6	30.5			42.2			53.2
Del. S.L. Is, sec	285.7	302.5	304.7	306.2	308.4	312.0	314.5	309.3
Del. Vac. Is, sec	334.5	345.2	347.5	348.8	348.0	351.6	354.0	346.8
Engine Flowrate, lb/s	2105.41	1999.54	1982.40	1971.47	1974.62	1947.42	1927.87	1987.42
TCA Mixture Ratio	3.5	3.5			3.5			3.5
TCA S.L. Is, sec	289.0	309.4			319.4			325.4
TCA Vac. Is, sec	337.5	351.7			358.5			362.5
GG Mixture Ratio	.43	.42	.75	1.44	.41	.71	1.42	.40
GG Flowrate	29.29	60.30	43.16	32.23	94.10	68.90	49.35	143.54
GG S.L. Is, sec	52.9	81.0	95.1	110.4	94.1	109.6	127.2	102.0
GG Vac. Is, sec	119.1	133.6	155.7	170.6	140.8	163.1	180.9	145.1
Coolant ΔP, psi	62	295			833			2088
Turbine Inlet Temp. °R	1860	1860	2260	2960	1860	2260	2960	1560
Turbine Power, hp	17,130	34,020	33,470	33,120	53,130	51,830	50,900	77,800
Fuel Pump Dischg. P. psia	1263	2700			4447			5921
Ox Pump Dischg. P. psia	1210	2421			3629			4879

TABLE XXII (cont.) (2 of 2)

ENGINE CYCLE C PARAMETRIC DATA

LOX/LCH_4

PARAMETER	HIGH TEMP. TURBINE		THRUST VARIATION		HIGH TEMP. TURBINE	
Chamber Pressure, psia	4000	4000	4000	4000	5000	5000	5000
S.L. Engine Thrust, lbF	612,052	609,908	204,937	1,538,674	622,868	618,746	614,940
Vac. Engine Thrust, lbF	685,615	681,719	229,981	1,725,965	696,385	690,647	684,741
Area Ratio	53.2				63.9		
Del. S.L. Is, sec	314.5	318.5	308.5	308.9	306.7	314.1	319.8
Del. Vac. Is, sec	352.3	356.0	346.2	346.5	342.9	350.6	356.1
Engine Flowrate, lb/s	1946.11	1914.94	664.30	4981.14	2030.87	1969.90	1922.89
TCA Mixture Ratio	3.5				3.5		
TCA S.L. Is, sec	325.4		324.7	325.9	329.6		
TCA Vac. Is, sec	362.5		361.8	363.0	365.3		
GG Mixture Ratio	.68	1.40	.40	.40	.39	.65	1.37
GG Flowrate	102.23	71.06	48.35	378.50	210.48	149.51	132.50
GG S.L. Is, sec	118.6	138.2	102.0	102.0	108.1	125.1	145.8
GG Vac. Is, sec	167.8	187.6	145.1	145.1	148.7	171.2	192.4
Coolant ΔP, psi	2088		2195	2818	4885		
Turbine Inlet Temp. °R	2260	2960	1860	1860	1860	2260	2960
Turbine Power, hp	75,170	73,190	26,210	205,150	113,440	108,550	104,760
Fuel Pump Dischg. P. psia	6921		7030	7662	10,961		
Ox Pump Dischg. P. psia	4879		4879	4879	6172		

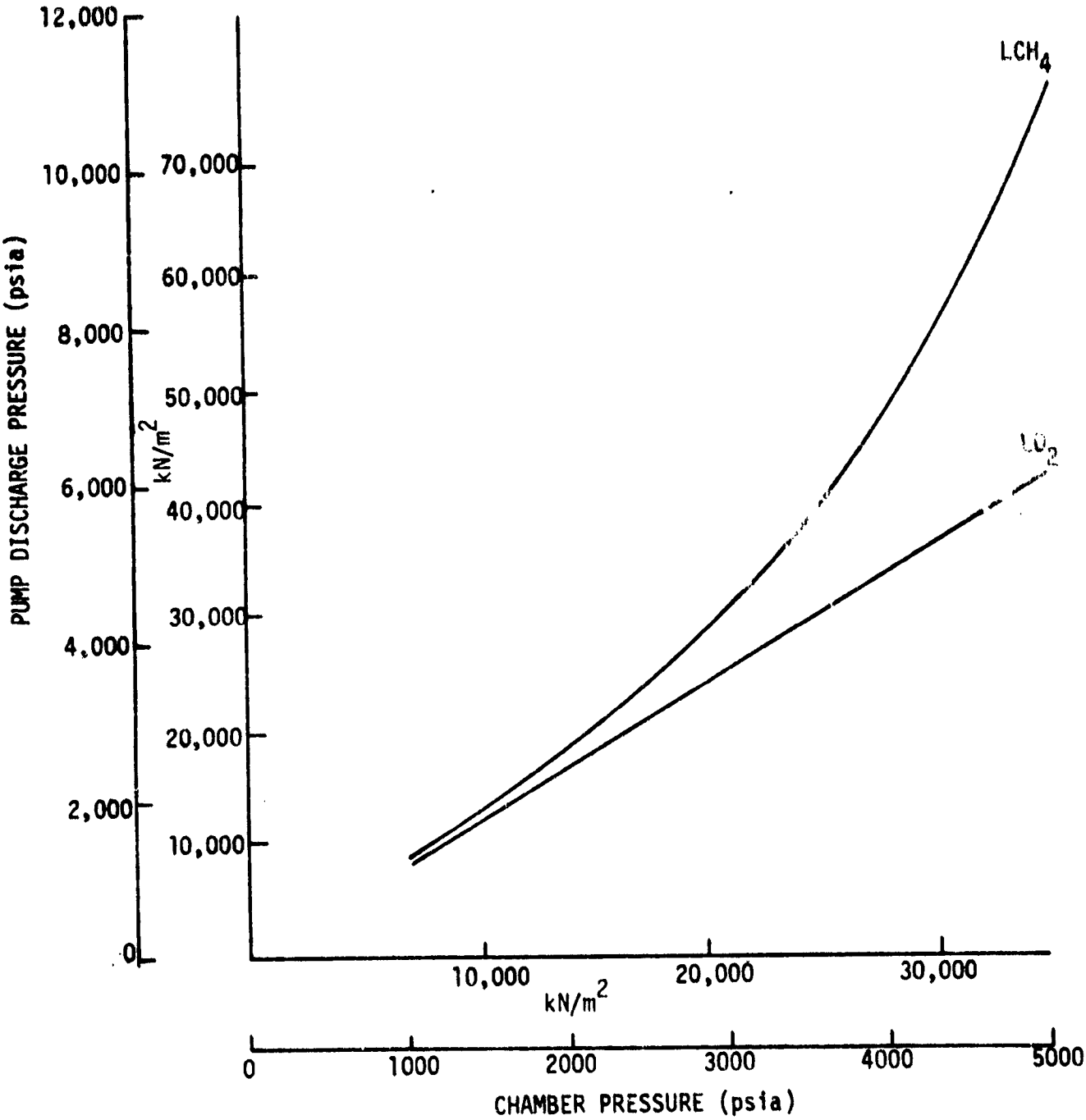

Figure 27. LO_2/LCH_4 Engine Cycle C Pump Discharge Pressure Requirements

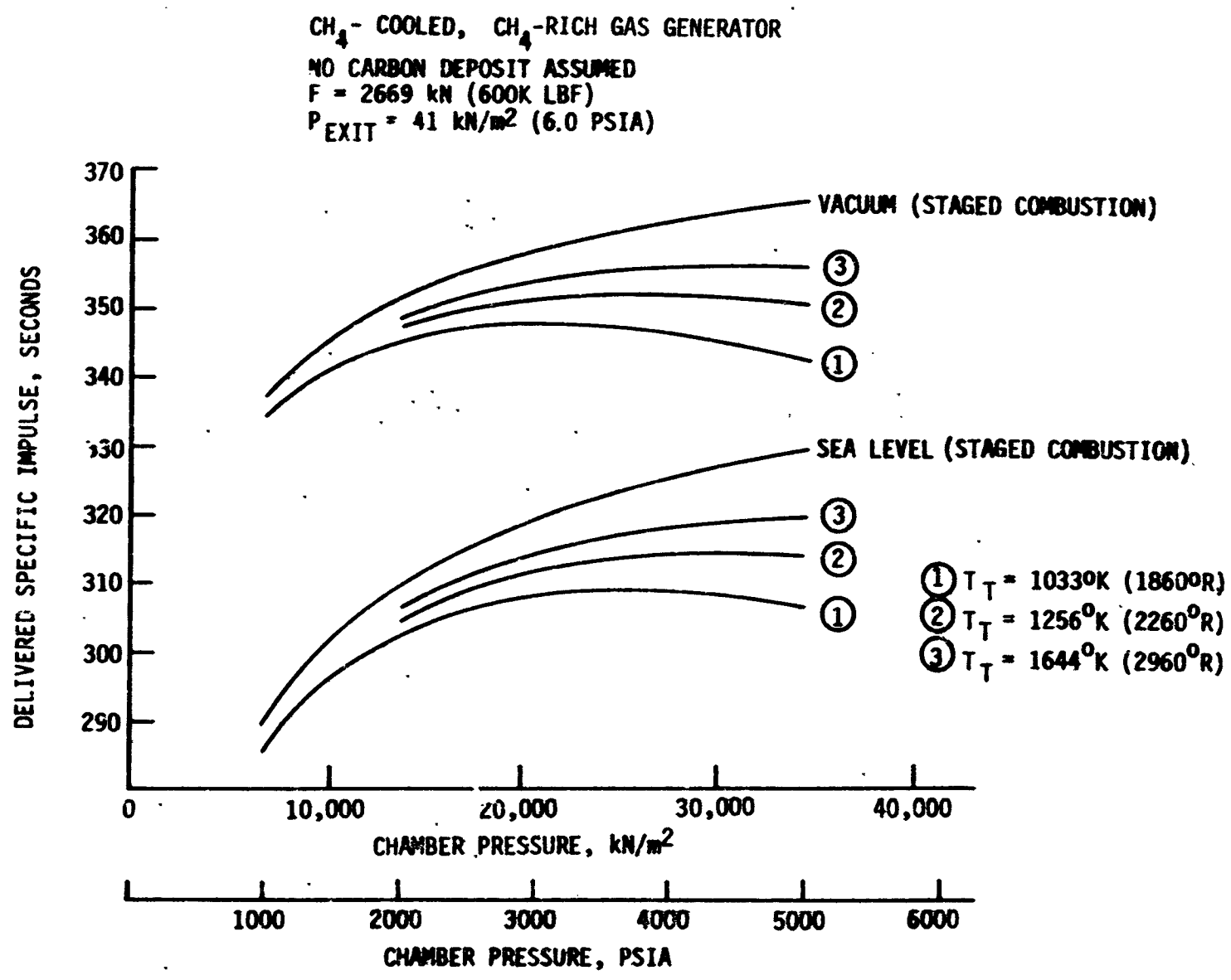

Figure 28. LO_2/LCH_4 Engine Cycle C Performance

III, D, Cycle Power Balance (cont.)

The maximum in sea level performance for cycle C occurs at about 24130 kN/m^2 (3500 psia) chamber pressure and the maximum in vacuum performance at about 20690 kN/m^2 (3000 psia). The change in performance between 20680 and 27580 kN/m^2 (3000 and 4000 psia) chamber pressure is small, however, because of the increased amount of turbine-drive fluid required. The performance at sea level and the performance at vacuum between 3000 and 4000 psia must, therefore, be compared with the engine factors that influence life and reliability in order to optimize the engine system.

4. Cycle C'

Subcooled propane replaces liquid methane in cycle C', otherwise the schematics for cycle C' and cycle C are identical (cf. Figure 26). Subcooled propane is stored in the vehicle at the liquid oxygen normal boiling point (NBP) to take advantage of its increased density (729 Kg/m^3: 45.5 lb/ft^3) compared to NBP propane (578 Kg/m3: 36.1 lb/ft^3). Because the propane is subcooled from its NBP temperature of 231 to 91°K (416 to 163°R), its heat transfer capacity is also increased. Methane, with a much smaller liquidus range than propane, cannot be utilized in such a subcooled manner.

Tables XIX and XXIII and Figure 29 and 30 summarize the parametric data generated for the LOX/LC_3H_8 gas-generator cycle engine C'. Figure 29 shows that this engine can achieve a chamber pressure of 31030 kN/m^2 (4500 psia) with a 55160 kN/m^2 (8000 psia) pump discharge pressure limit. As shown in Figure 30, the maximum in sea level performance is achieved at 27580 kN/m^2 (4000 psia) (or higher) chamber pressure. The figure also indicates the maximum in vacuum specific impulse at a chamber pressure of about 20690 kN/m^2 (3000 psia).

5. Cycle D

The schematic for the LO_2/RP-1 staged-combustion cycle D engine is given in Figure 31. The figure shows that the engine, like the

TABLE XXIII

ENGINE CYCLE C' PARAMETRIC DATA

LOX/LC_3H_8

PARAMETER					
Chamber Pressure, psia	1000	2000	3000	4000	5000
S.L. Engine Thrust, lbF	601,402	604,523	608,308	612,812	619,108
Vac. Engine Thrust, lbF	702,915	688,692	685,269	685,599	689,337
Area Ratio	17.3	30.1	41.7	52.4	61.9
Del. S.L. Is, sec	282.0	299.5	305.1	307.3	305.9
Del. Vac Is, sec	329.6	341.2	343.7	343.8	340.6
Engine Flowrate, lb/s	2132.63	2018.44	1993.80	1994.18	2023.89
TCA Mixture Ratio	3.1				
TCA S.L. Is, sec	285.3	307.2	317.1	324.5	329.6
TCA Vac. Is, sec	332.7	348.8	355.6	360.9	364.2
GG Mixture Ratio	.38	.36	.35	.33	.31
GG Flowrate	29.58	65.32	101.65	145.18	203.50
GG S.L. Is, sec	47.8	69.8	81.2	88.7	94.0
GG Vac. Is, sec	107.5	115.0	121.6	126.2	129.4
Coolant ΔP, psi	29	155	569	1629	3976
Turbine Inlet Temp. °R	1860				
Turbine Power, hp	14,070	27,260	41,830	59,420	82,940
Fuel Pump Dischg. P. psia	1230	2558	4179	6455	10,038
Ox Pump Dischg. P. psia	1210	2421	3629	4879	6172

NO CARBON DEPOSIT ASSUMED

LC_3H_8-COOLED C_3H_8 - RICH GAS GENERATOR

LO_2-COOLED NOZZLE ($\epsilon \geq 8:1$)

F = 2669 kN (600K lbF)

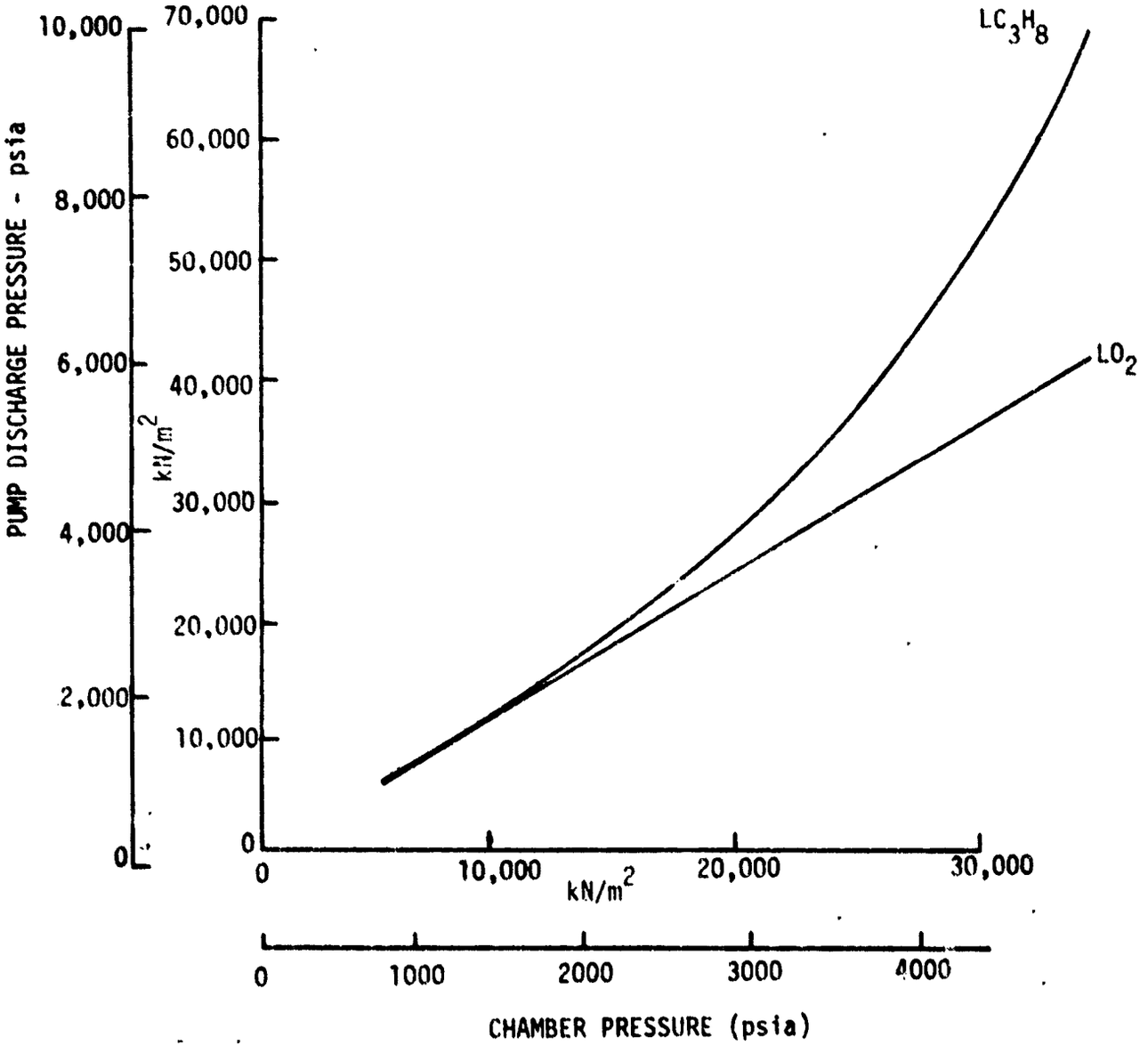

Figure 29. LO_2/LC_3H_8 Engine Cycle C' Pump Discharge Pressure Requirements

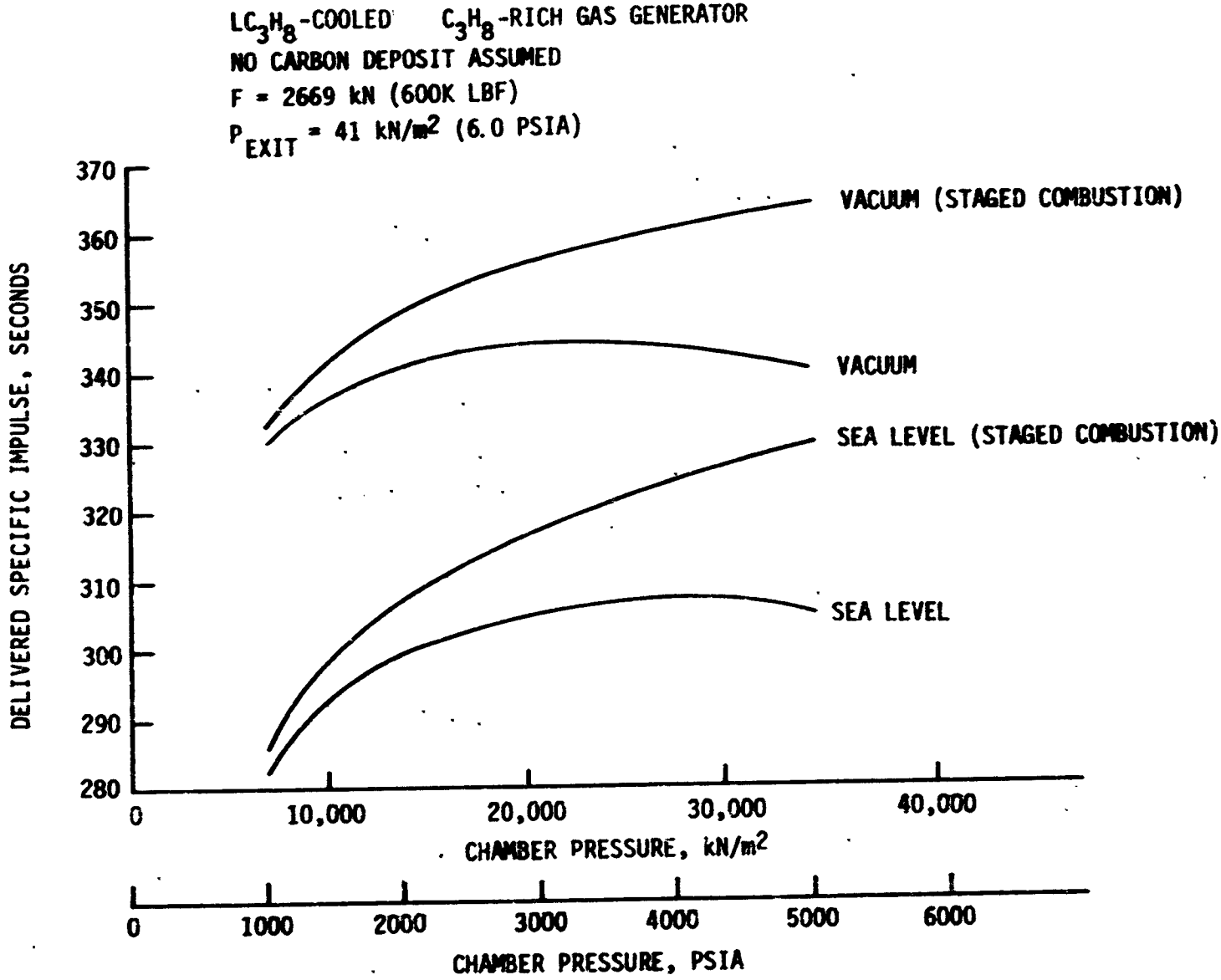

Figure 30. LO_2/LC_3H_8 Engine Cycle C' Performance

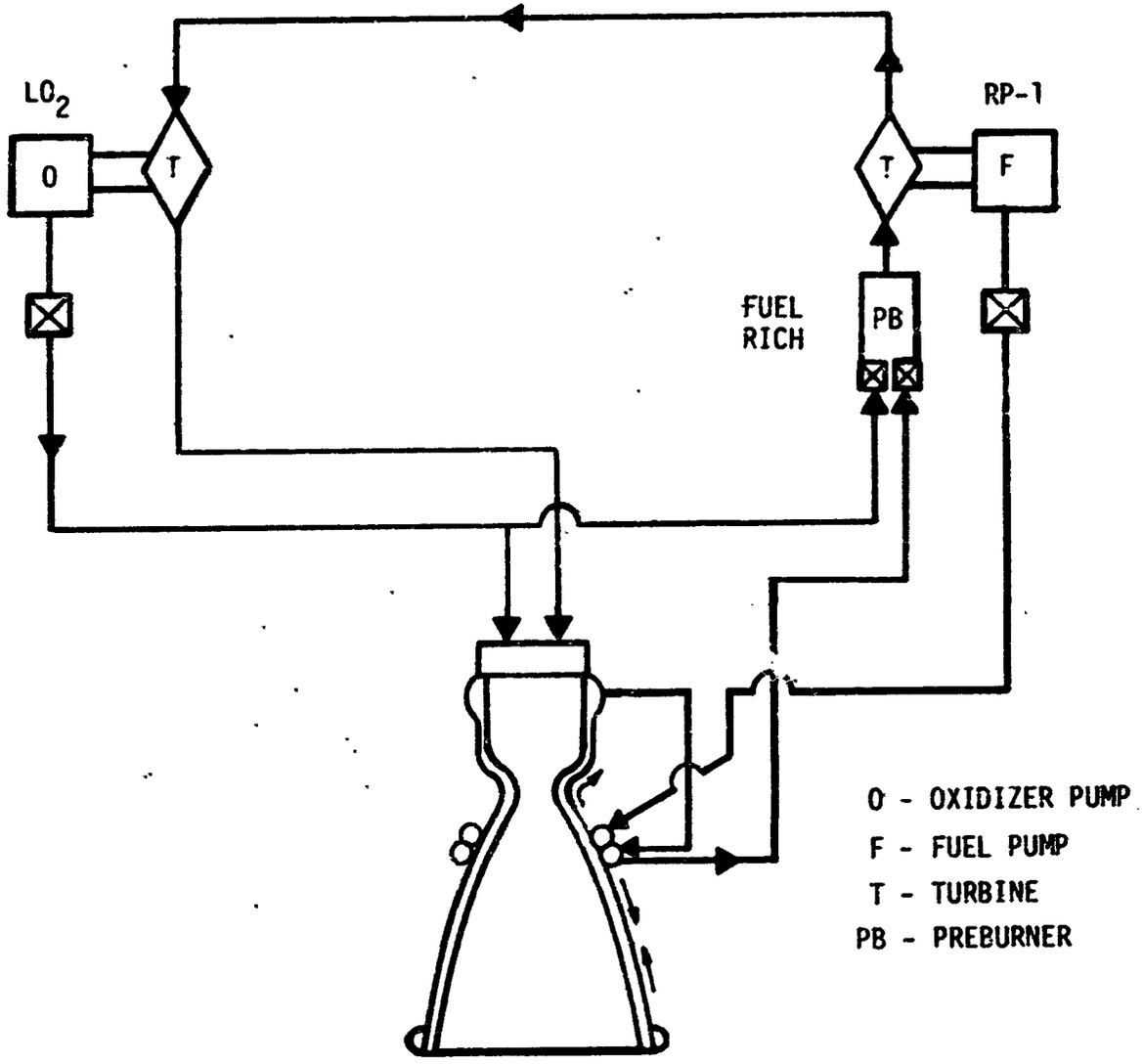

Figure 31. RP-1 Fuel-Rich Preburner Staged-Combustion Cycle D Schematic

previously described cycles, is fuel-cooled through two circuits. All of the fuel returning from the two-pass nozzle coolant circuit enters the preburner and is partially burned with a small amount of oxidizer. The preburner exhaust drives the turbines (in series) and flows to the main combustion chamber where it is further burned with the remaining oxidizer to generate the engine thrust.

Substitution of oxygen for the fuel in the nozzle coolant circuit provides a slight benefit by lowering the fuel pump discharge pressure. This benefit is 1731 and 3861 kN/m^2 (251 and 560 psi), respectively, at chamber pressures of 20680 and 27580 kN/m^2 (3000 and 4000 psia).

The power balance data for cycle D are summarized in Tables XIX and XXIV and in Figure 32. Since the staged-combustion cycle is a closed-loop cycle, all its variations at the same chamber pressure deliver the same performance. The performance data have previously been summarized (cf. Figures 22 and 25 and Table XVI).

As shown in Figure 32, the LO_2/RP-1, RP-1-cooled, staged-combustion cycle D is limited to chamber pressures between 17240 and 22750 kN/m^2 (2500 and 3300 psia) if an upper limit of 55160 kN/m^2 (8000 psia) pump discharge pressure is assumed.

6. Cycle E

Cycle E (Figure 33) differs from cycle D by utilizing LO_2 rather than RP-1 or RP-1R as the coolant. A modest increase in chamber pressure from 2500 (curve 1, Figure 32) to 2900 psia (curve 1, Figure 34) is achieved by changing coolants. The effects of carbon deposit and turbine inlet temperature are also indicated in Figure 34 and in Table XIX.

TABLE XXIV (1 of 3)

ENGINE CYCLE D PARAMETRIC DATA

LOX/RP-1 & RP-1R

PARAMETER					HIGH TEMP. TURBINE		HIGH TEMP. TURBINE	
Chamber Pressure, psia	1000*	1000	1000	2000*	2000*	2000	2000	2000
Mixture Ratio	2.8			2.8				
Del. S.L. Is, sec	283.0			302.4				
Del. Vac, Is, sec	328.1			342.4				
Engine Flowrate, lb/s	2120.14			1984.13				
Preburn. Mixture Ratio	.325			.305	.47	.305	.465	1.0
Preburn. Flowrate, lb/s	739.26			681.39	767.55	681.39	764.94	1044.28
Turbine Inlet Temp. °R	1860			1860	2260	1860	2260	2960
Turbine Power, hp	22,050	16,320	15,570	37,540	34,840	37,160	34,510	33,360
Coolant P. psi	1600	237	60**	1296**	1296**	1210		
Fuel Pump Dischg. P. psia	3312	1840	1650	5407	4698	5303	4610	4215
Ox Pump Dischg. P. psia	1210			2421				
Ox P.B. Pump Dischg. P. psia	1680	1592	1582	4071	3366	4054	3364	2972

*MIL SPEC RP-1

**CARBON DEPOSITION ON CHAMBER WALL

TABLE XXIV (cont.) (2 of 3)

ENGINE CYCLE D PARAMETRIC DATA

LOX/RP-1 & RP-1R

PARAMETER		HIGH TEMP. TURBINE		HIGH TEMP. TURBINE		HIGH TEMP. TURBINE		HIGH TEMP. TURBINE	
Chamber Pressure, psia	2000	2000	2500	2500	2500	2500	3000	3000	3000
Mixture Ratio	2.8	———	2.8	———	———	———	2.8	———	———
Del. S.L. Is, sec	302.4	———	307.8	———	———	———	312.2	———	———
Del. Vac. Is, sec	342.4	———	346.4	———	———	———	349.4	———	———
Engine Flowrate, lb/s	1984.13	———	1949.32	———	———	———	1921.84	———	———
Preburn. Mixture Ratio	.305	.47	.297	.462	.299	.46	.297	.455	1.0
Preburn. Flowrate, lb/s	681.39	767.55	665.34	749.98	666.36	748.95	655.96	735.87	1011.50
Turbine Inlet Temp. °R	1860	2260	1860	2260	1860	2260	1860	2260	2960
Turbine Power, hp	32,910	30,680	51,900	45,920	45,200	40,500	73,510	59,670	55,260
Coolant ΔP. psi	266**	———**	2063	———	750**	———**	3280	———	———
Fuel Pump Dischg. P. psia	4163	3570	8188	6645	6397	5170	12,845	9340	8072
Ox Pump Dischg. P. psia	2421	———	3025	———	———	———	3629	———	———
Ox P.B. Pump Dischg. P. psia	3873	3284	6063	4528	5607	4386	9468	5981	4718

*MIL SPEC RP-1

**CARBON DEPOSITION ON CHAMBER WALL

TABLE XXIV (cont.) (3 of 3)

ENGINE CYCLE D PARAMETRIC DATA

LOX/RP-1 & RP-1R

PARAMETER		HIGH TEMP. TURBINE			
Chamber Pressure, psia	3000	3000	3000	4000	4000
Mixture Ratio	2.8			2.8	
Del. S.L. Is, sec	312.2			318.2	
Del. Vac. Is, sec	349.4			353.4	
Engine Flowrate, lb/s	1921.84			1885.7	
Preburn. Mixture Ratio	.297	.455	1.0	.455	1.0
Preburn. Flowrate, lb/s	655.96	735.87	1011.50	721.97	992.40
Turbine Inlet Temp. °R	1860	2260	2960	2260	2960
Turbine Power, hp	63,830	53,220	49,570	96,060	82,700
Coolant ΔP. psi	1778**	**	**	6500	6500
Fuel Pump Dischg. P. psia	10,284	7572	6481	16,909	13,398
Ox Pump Dischg. P. psia	3629			4879	
Ox P.B. Pump Dischg. P. psia	8437	5738	4653	10,259	6765

*MIL SPEC RP-1

**CARBON DEPOSITION ON CHAMBER WALL

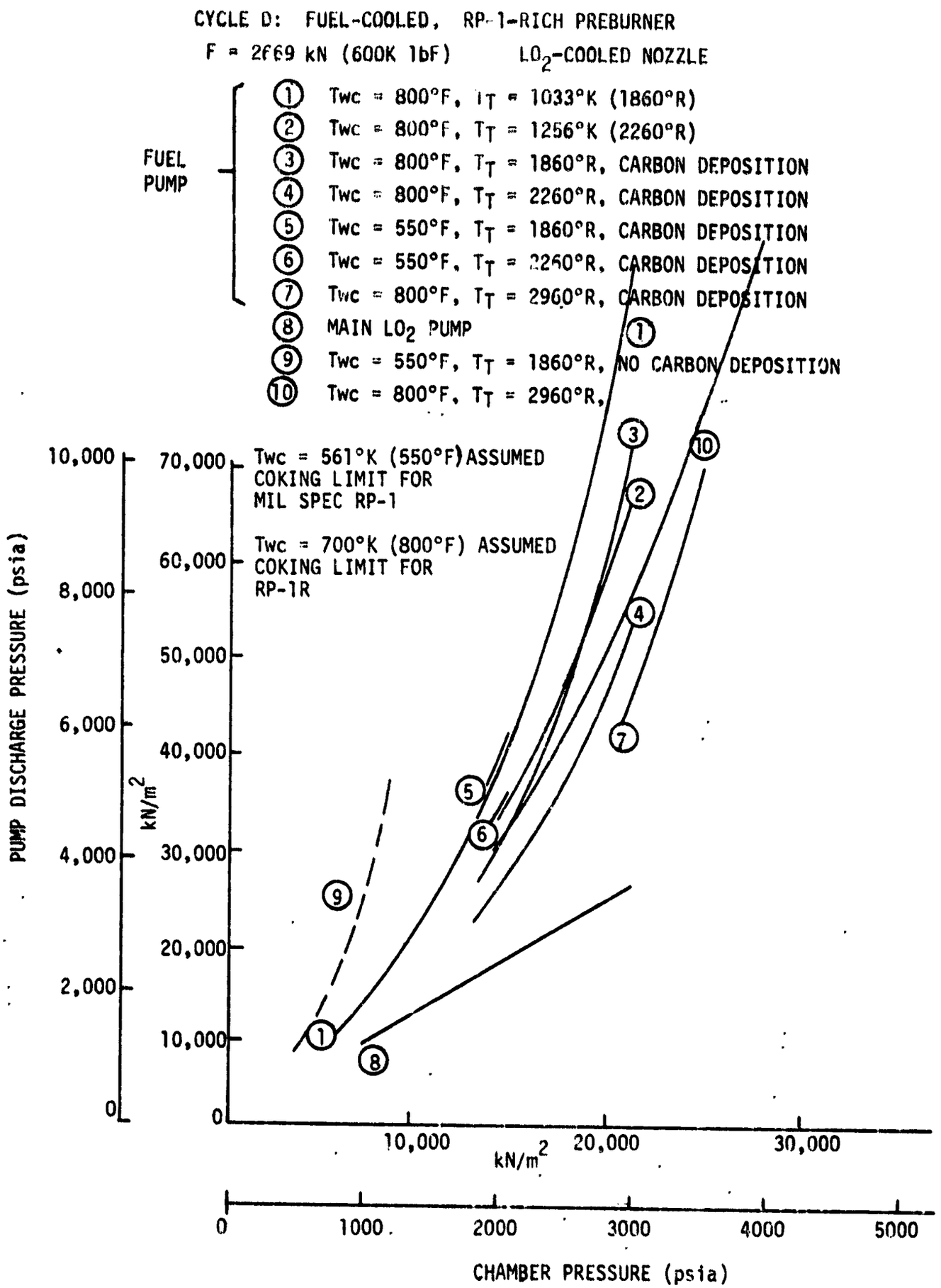

Figure 32. LO_2/RP-1 Engine Cycle D Pump Discharge Pressure Requirements

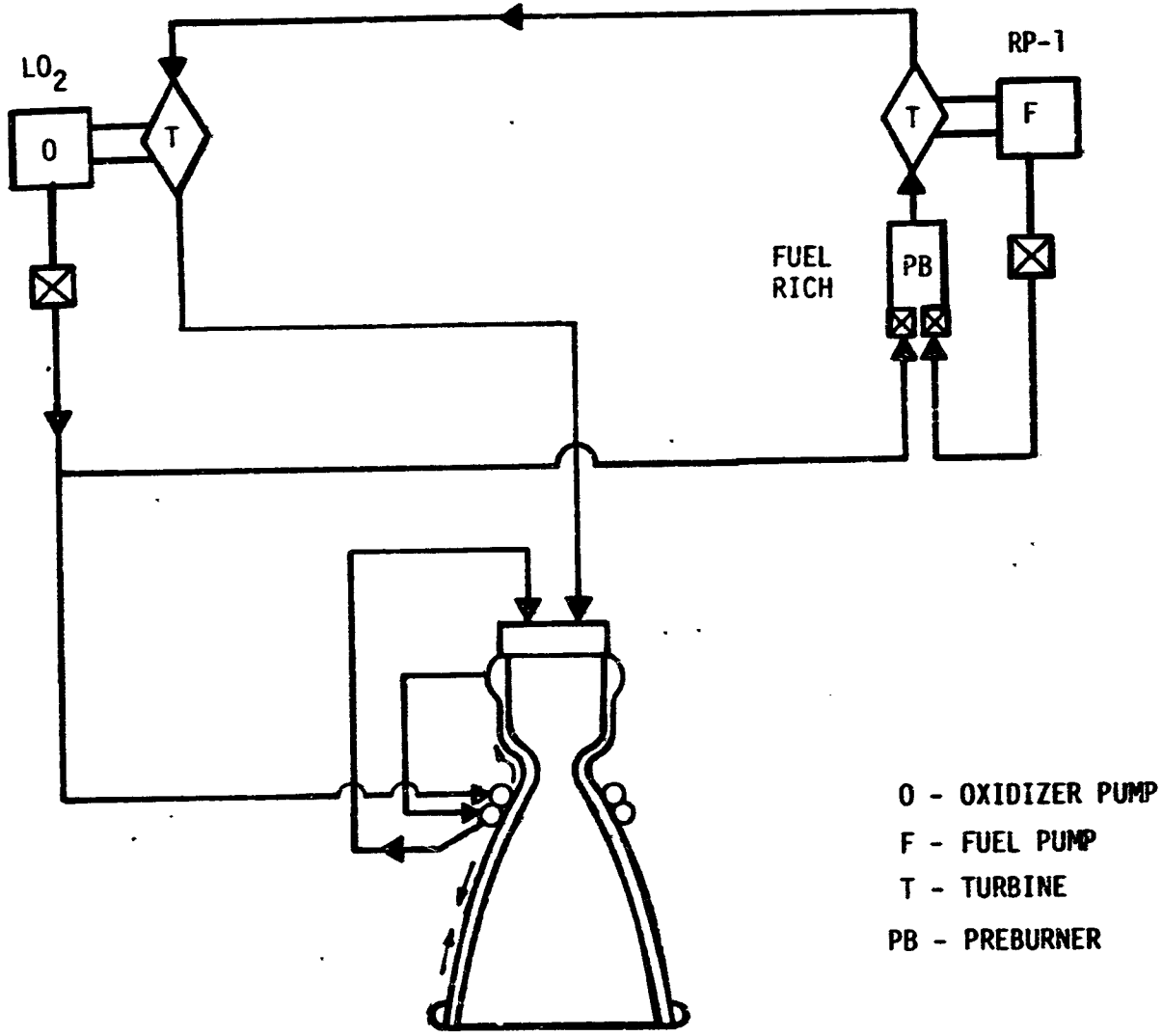

Figure 33. RP-1 Fuel-Rich Preburner Staged-Combustion Cycle E Schematic

LO_2-COOLED, RP-1-RICH PREBURNER

F = 2669 kN (600K lbF)

① RP-1 PUMP NO CARBON DEPOSIT T_{TI} = 1033°K (1860°R)
② LO_2 PUMP NO CARBON DEPOSIT
③ RP-1 PUMP NO CARBON DEPOSIT T_{TI} = 1256°K (2260°R)
④ RP-1 PUMP NO CARBON DEPOSIT T_{TI} = 1644°K (2960°R)
⑤ RP-1 PUMP WITH CARBON DEPOSIT T_{TI} = 1256°K (2260°R)
⑥ RP-1 PUMP WITH CARBON DEPOSIT T_{TI} = 1644°K (2960°R)
⑦ LO_2 PUMP WITH CARBON DEPOSIT

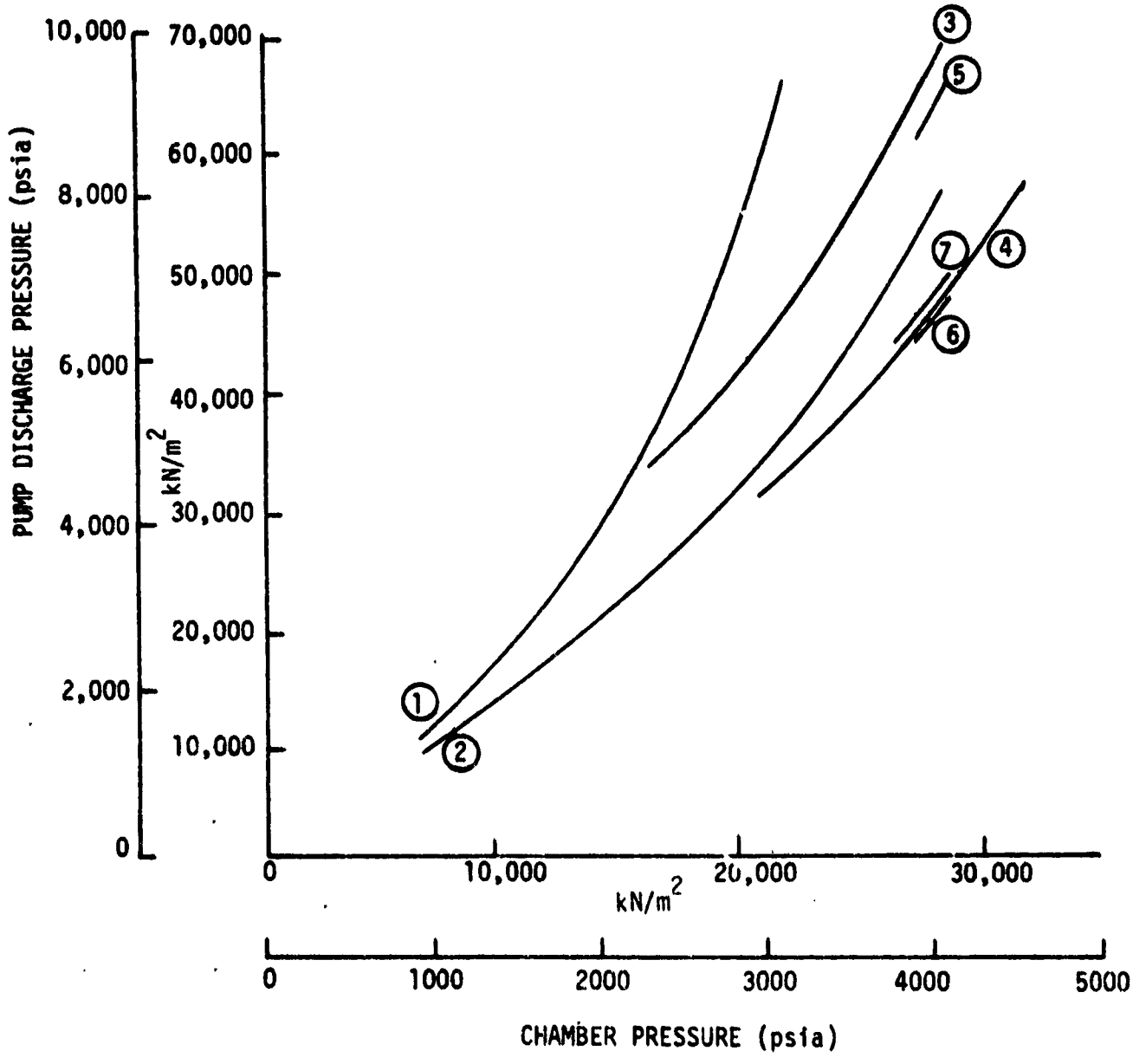

Figure 34. LO_2/RP-1 Engine Cycle E Pump Discharge Pressure Requirements

III, D, Cycle Power Balance (cont.)

7. Cycle F

Cycle F differs from cycle D in the use of a LO_2-rich preburner in place of the RP-1-rich preburner. The cycle schematic is depicted in Figure 35, and the power balance summary is given in Figure 36 and Table XIX. The required pump discharge pressure for the three staged-combustion cycles (cycles D, E, and F) at a chamber pressure of 17240 kN/m^2 (2500 psia) are as follows:

Cycle	P_D kN/m^2 (psia)	Coolant	Preburner
D	56540 (8200)	RP-1R	RP-1-rich
E	39990 (5800)	LO_2	RP-1-rich
F	35160 (5100)	RP-1R	LO_2-rich

Because of its high mass flow, the LO_2-rich preburner provides more horsepower, resulting in a lower pump discharge pressure requirement. The maximum chamber pressure for this cycle is seen to be 22410 kN/m^2 (3250 psia) for a pump discharge pressure of 55160 kN/m^2 (8000 psia).

The influence of carbon deposit and turbine inlet temperature was not computed for this cycle. The effect of these variables should be similar to that previously shown.

8. Cycle G

The utilization of both a LO_2-rich preburner and LO_2 cooling is indicated in the schematic (Figure 37) for a cycle G, LO_2/RP-1 staged- combustion cycle. Figure 38 and Table XIX present the power balance results for this cycle. At a chamber pressure of 17240 kN/m^2 (2500 psia),

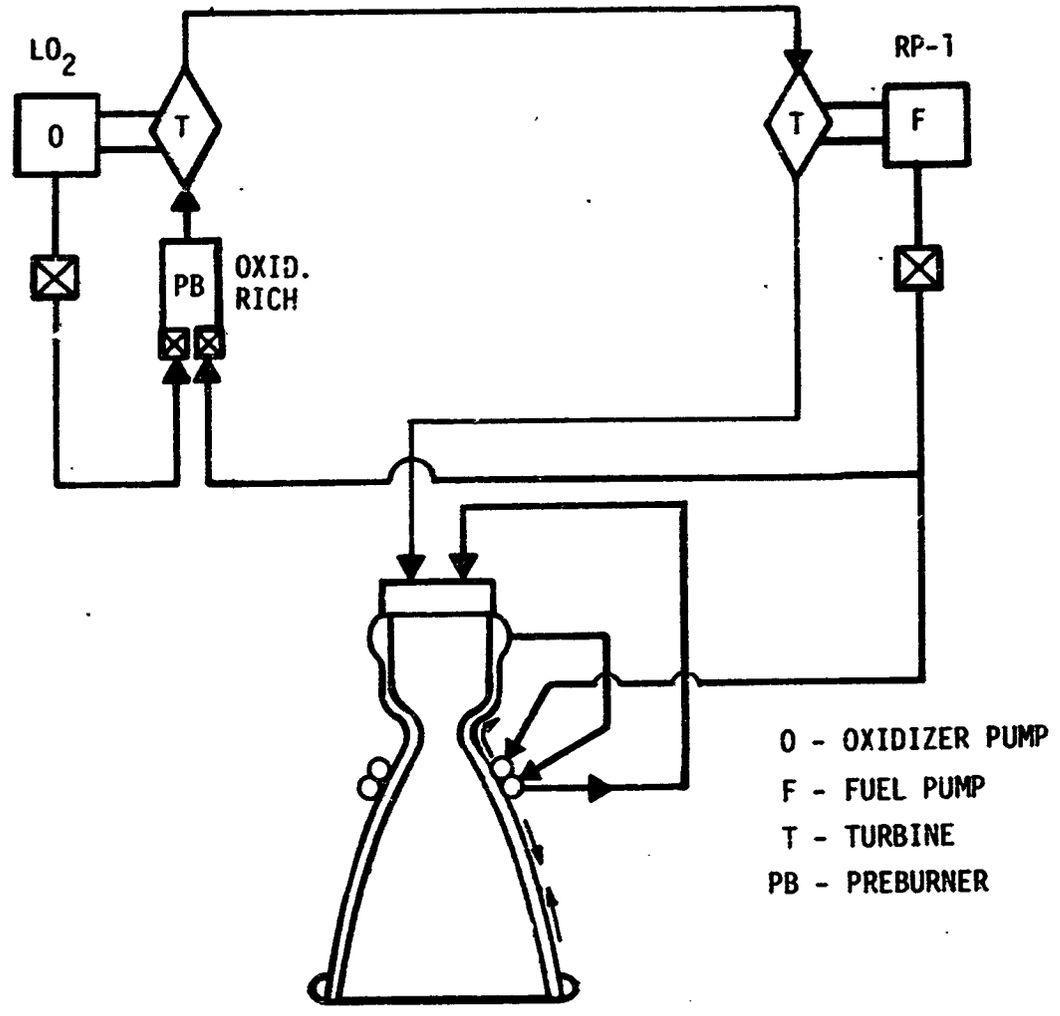

Figure 35. LO_2/RP-1 Oxidizer-Rich Preburner Staged-Combustion Cycle F Schematic

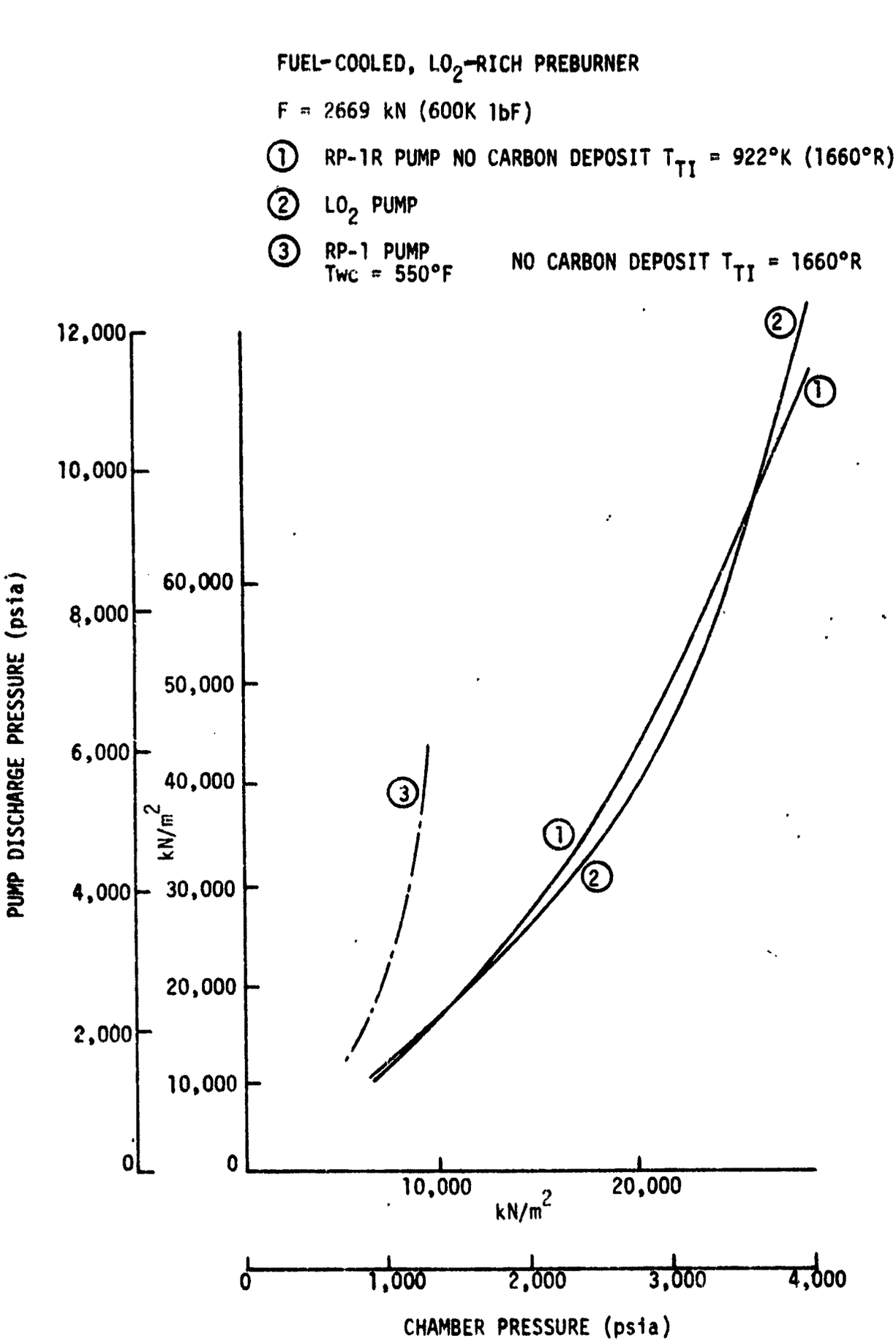

Figure 36. LO_2/RP-1 Engine Cycle F Pump Discharge Pressure Requirements

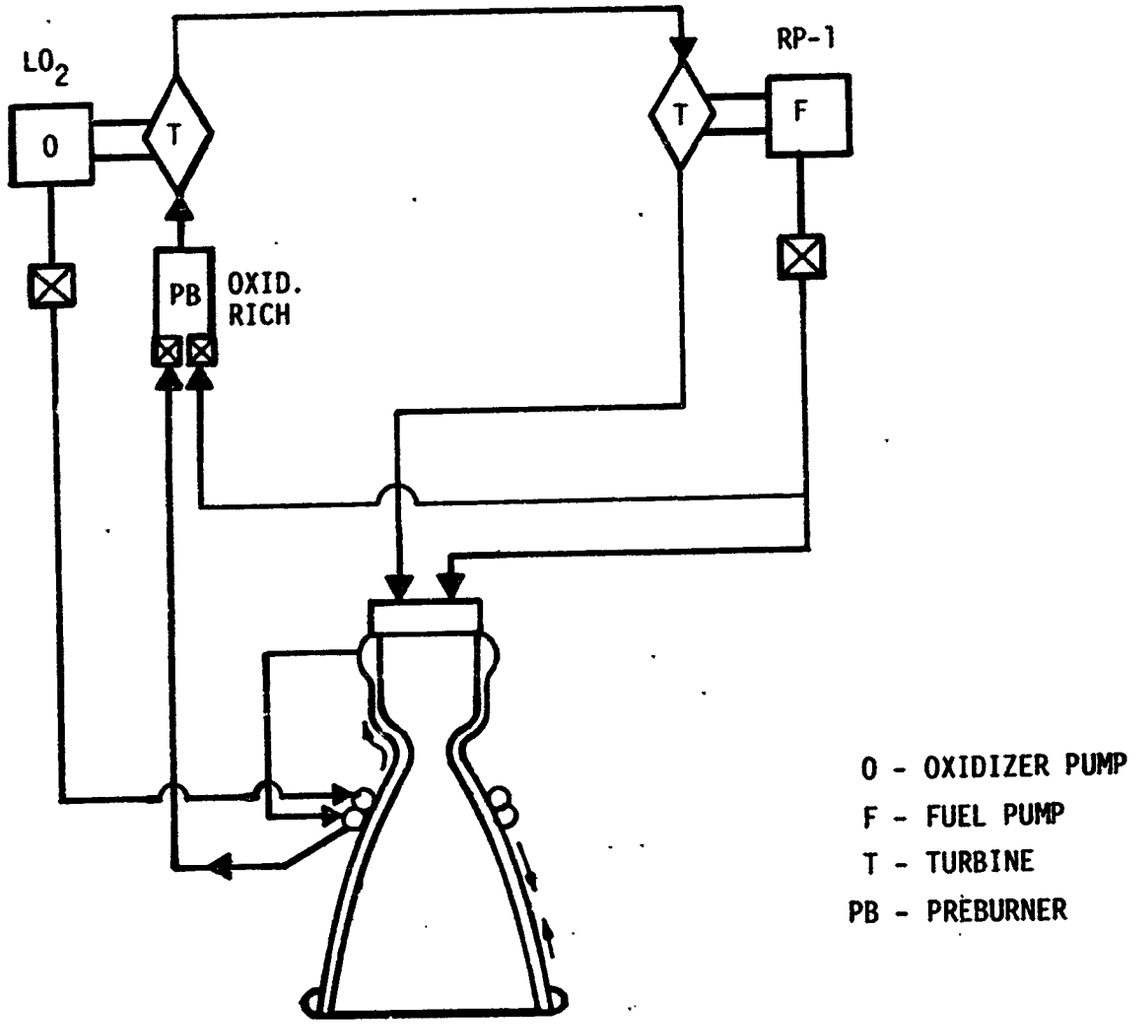

Figure 37. LO_2/RP-1 Oxidizer-Rich Preburner Staged-Combustion Cycle G Schematic

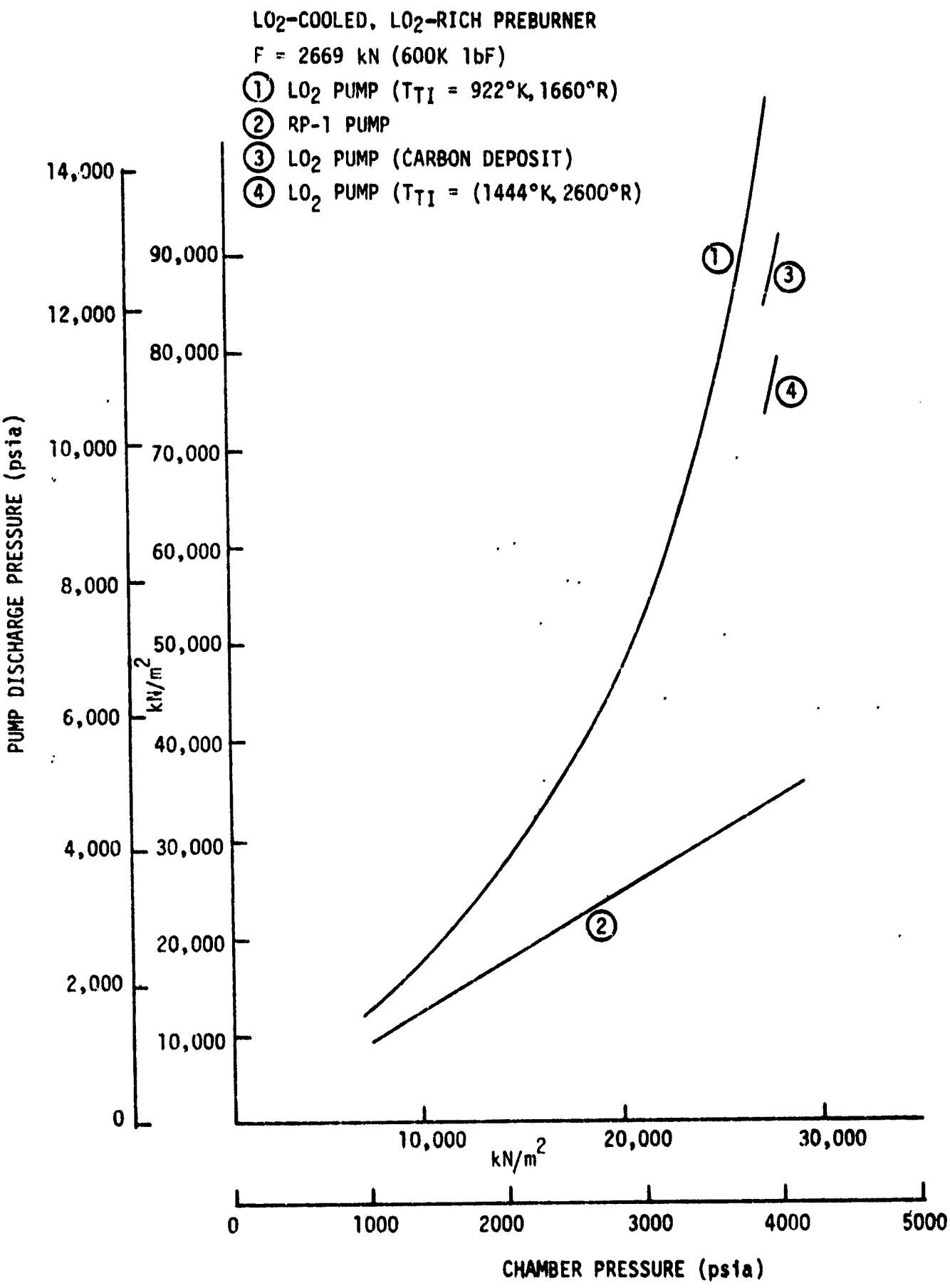

Figure 38. LO_2/RP-1 Engine Cycle G Pump Discharge Pressure Requirements

the pump discharge pressure requirement is 35850 kN/m^2 (5200 psia), similar to that for cycle F. The maximum chamber pressure allowed by this cycle is 21720 kN/m^2 (3150 psia) if a 1980 state-of-the-art pump discharge limit of 55160 kN/m^2 (8000 psia) is assumed.

The effects of a chamber wall carbon deposit and of a higher turbine inlet temperature are also shown in Figure 38 at a chamber pressure of 27580 kN/m^2 (4000 psia). The state-of-the-art turbine inlet temperature for rocket engine oxidizer-rich preburners is 932°K (1678°R) at a pressure of 31410 kN/m^2 (4556 psia) based on the ARES program (Ref. 17). However, an advanced ARES program (Ref.18) utilized an oxidizer-rich monopropellant (98% H_2O_2) preburner (no turbine) operating at 31030 kN/m^2 (4500 psia) and 1244°K (2240°R). Since the upper limit of feasible oxidizer-rich turbine-inlet temperatures has not been established, a temperature of 1444°K (2600°R) was selected for the one example shown in Figure 38.

9. Cycle G'

Subcooled propane is used in cycle G', replacing the RP-1 of cycle G. Otherwise these cycles are identical. The power balance results are summarized in Table XIX and in Figure 39. The allowable chamber pressure for a pump discharge pressure of 55160 kN/m^2 (8000 psia) is seen to be 22060 kN/m^2 (3200 psia).

The conclusions to be made concerning staged-combustion cycles D through G' are: (1) an oxidizer-rich preburner offers a significant improvement (lower pump discharge pressures lead to longer life turbopumps); (2) LO_2 cooling significantly reduces the pump discharge pressure requirements of a fuel-rich preburner cycle; and (3) higher turbine inlet temperatures can lead to a lower pump discharge pressure (longer life) and/or to a higher chamber pressure.

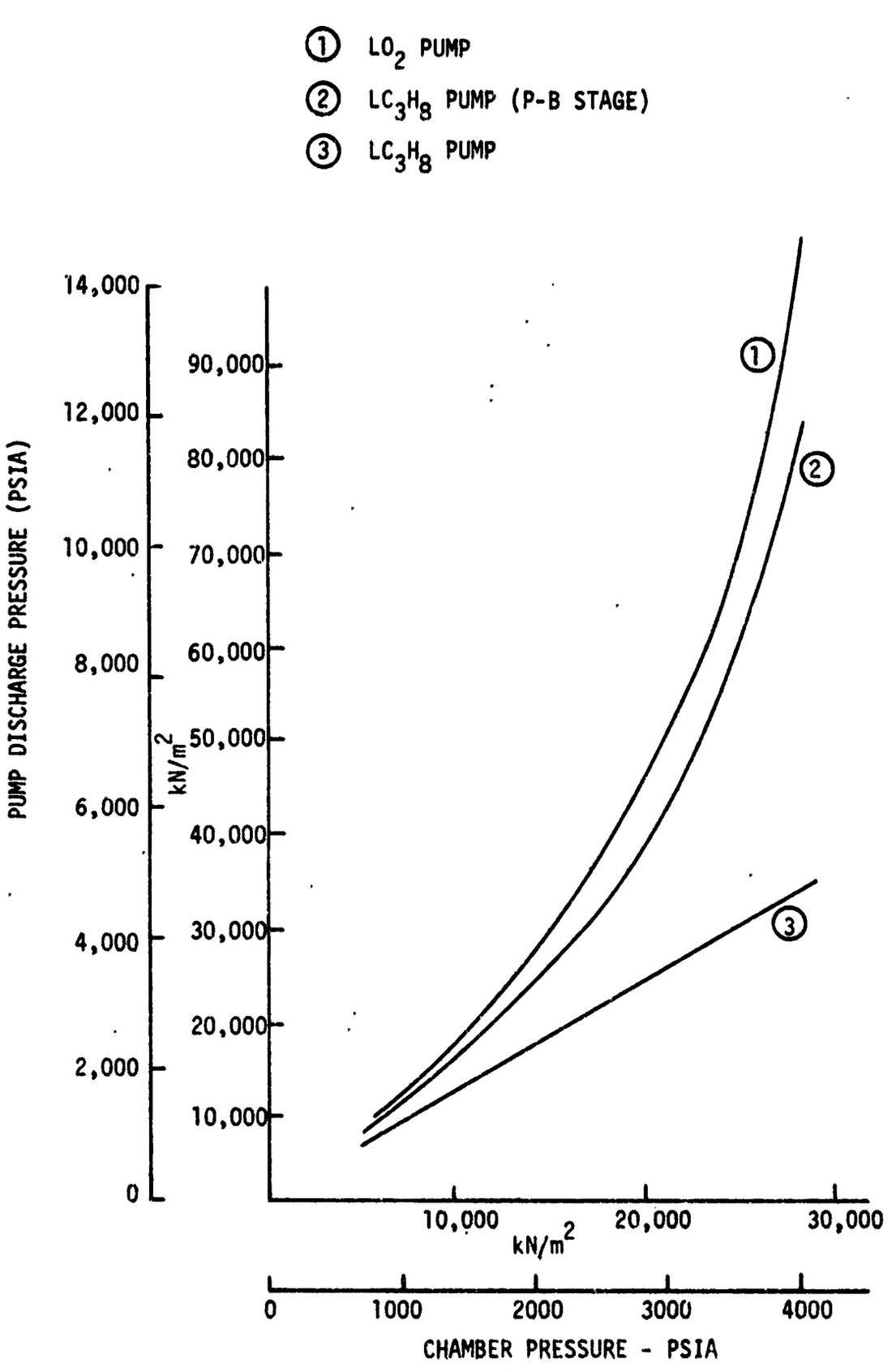

Figure 39. LO_2/LC_3H_8 Engine Cycle G' Pump Discharge Pressure Requirements

III, D, Cycle Power Balance (cont.)

10. Cycle H

The schematic for the LO_2/LCH_4 staged-combustion cycle H is shown in Figure 40. The schematic is identical to that for cycle D, with methane replacing RP-1. The results of the power balance analysis are summarized in Table XIX and in Figure 41.

If a pump discharge pressure limit of 55160 kN/m^2 (8000 psia) is assumed to be 1980 state of the art, the chamber pressure limit for cycle H is 20680 kN/m^2 (3000 psia) (see Figure 41). This limit is increased to 26200 kN/m^2 (3800 psia) if the turbine inlet temperature can be increased to 1644°K (2960°R).

No calculations were made for cycle H assuming a carbon deposit on the chamber wall. Although some deposit probably exists, it is expected to be much lighter than that found from the combustion of LO2 and RP-1.

11. Cycle I

Cycle I differs from cycle H in the addition of an oxidizer-rich preburner, as shown in Figure 42. The power balance data are summarized in Table XIX and Figure 43. The chamber pressure limit is seen to be 24130 kN/m^2 (3500 psia) (curve 1 in Figure 43) compared to 20680 kN/m^2 (3000 psia) (curve 1 in Figure 41). The benefit of the addition of an oxidizer-rich preburner to cycle H is directly translatable into a performance increase of 3.2 seconds (sea level) and 2.3 seconds (vacuum) because of the chamber pressure increase to 24130 kN/m^2 (3500 psia).

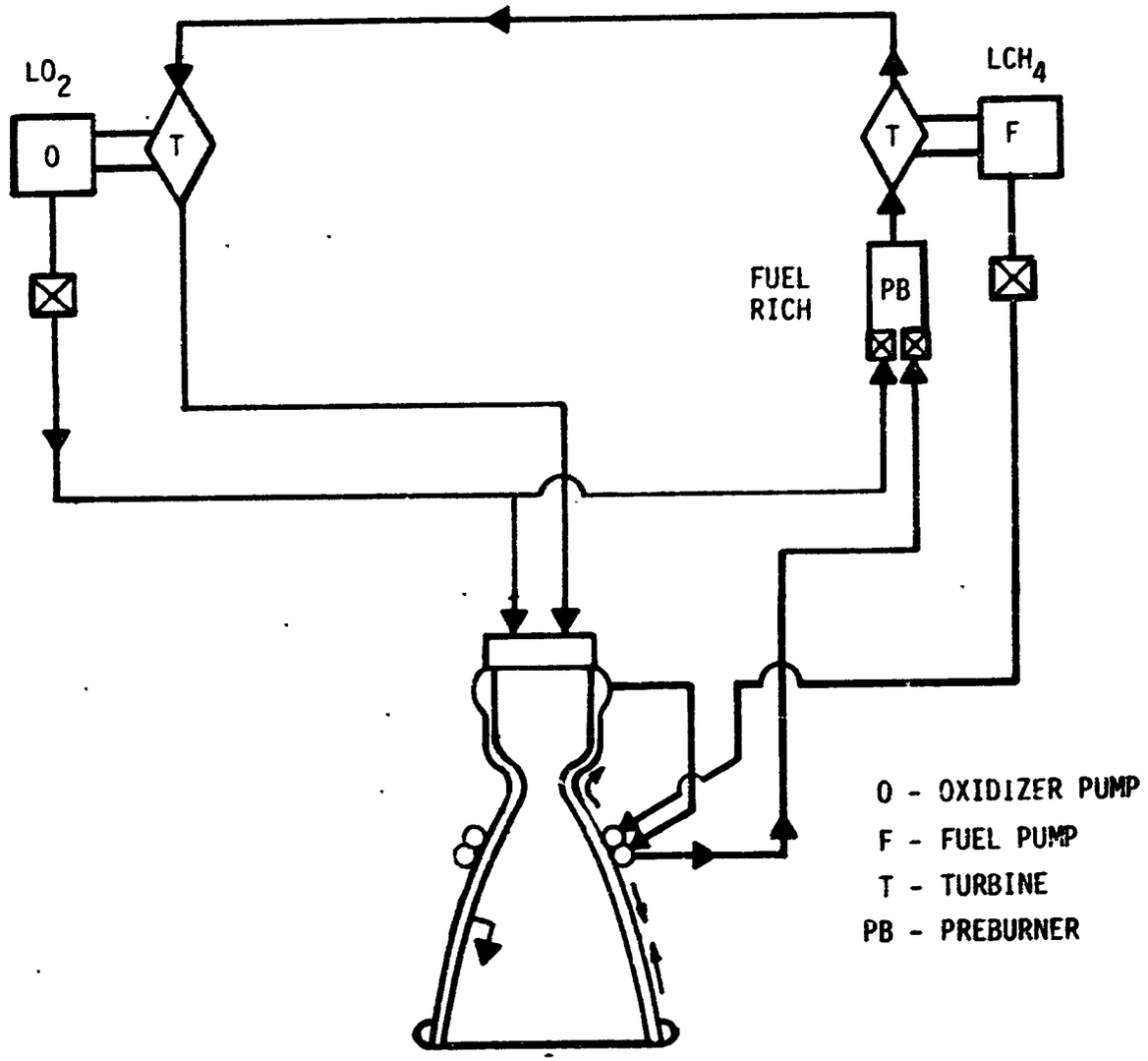

Figure 40. LCH_4 Fuel-Rich Preburner Staged-Combustion Cycle H Schematic

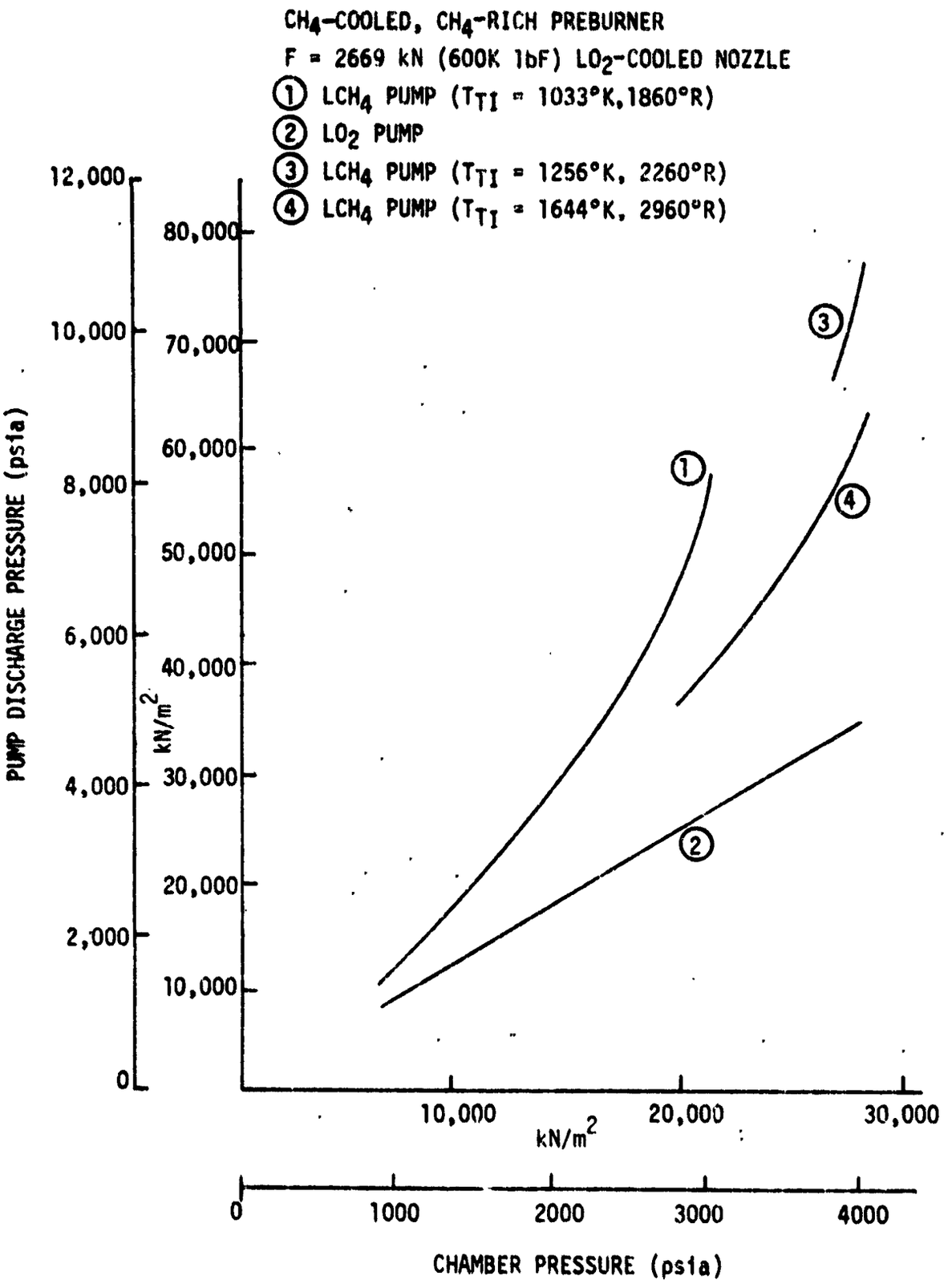

Figure 41. LO_2/LCH_4 Engine Cycle H Pump Discharge Pressure Requirements

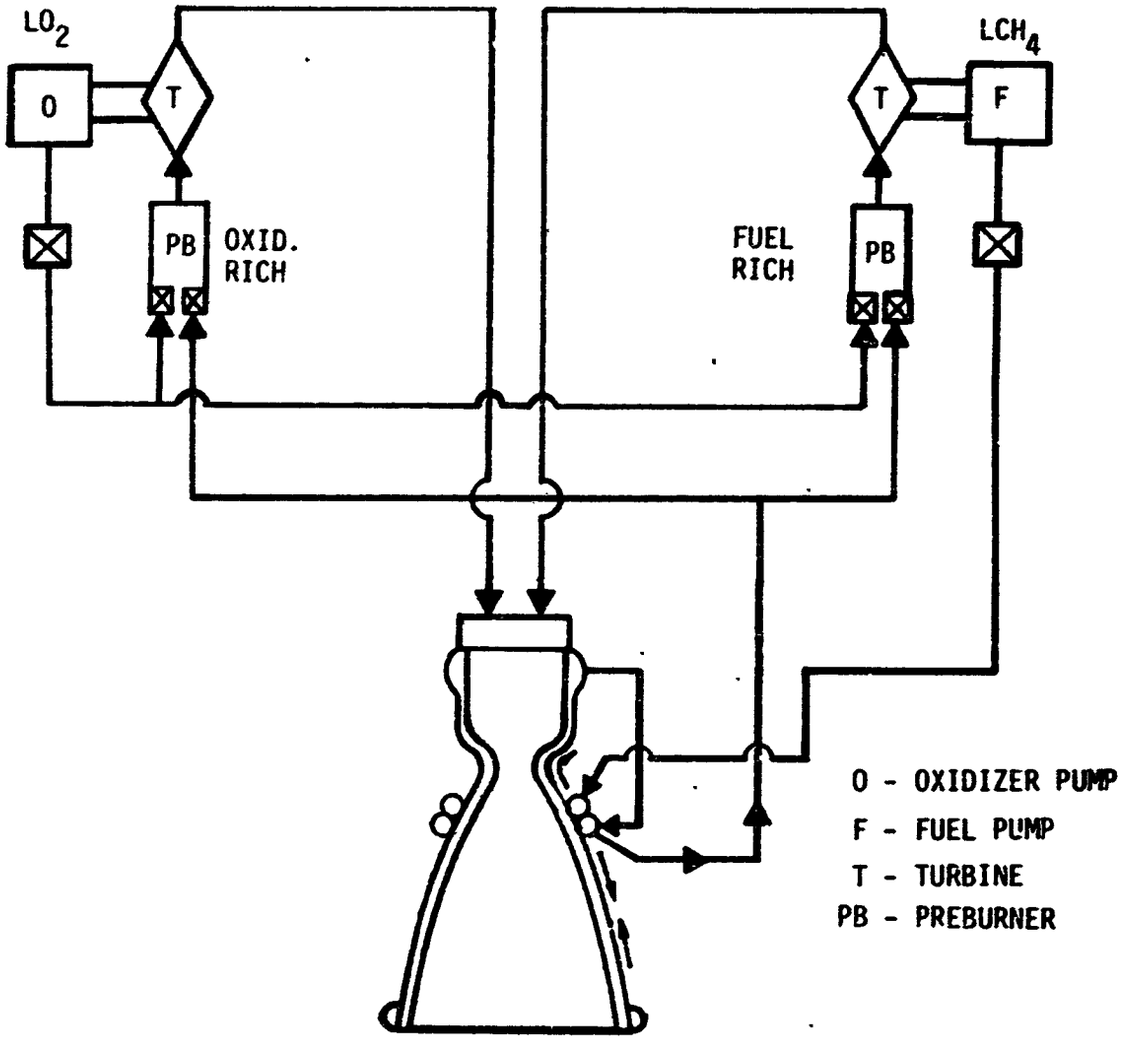

Figure 42. LCH_4 Mixed Preburner Staged-Combustion Cycle I Schematic

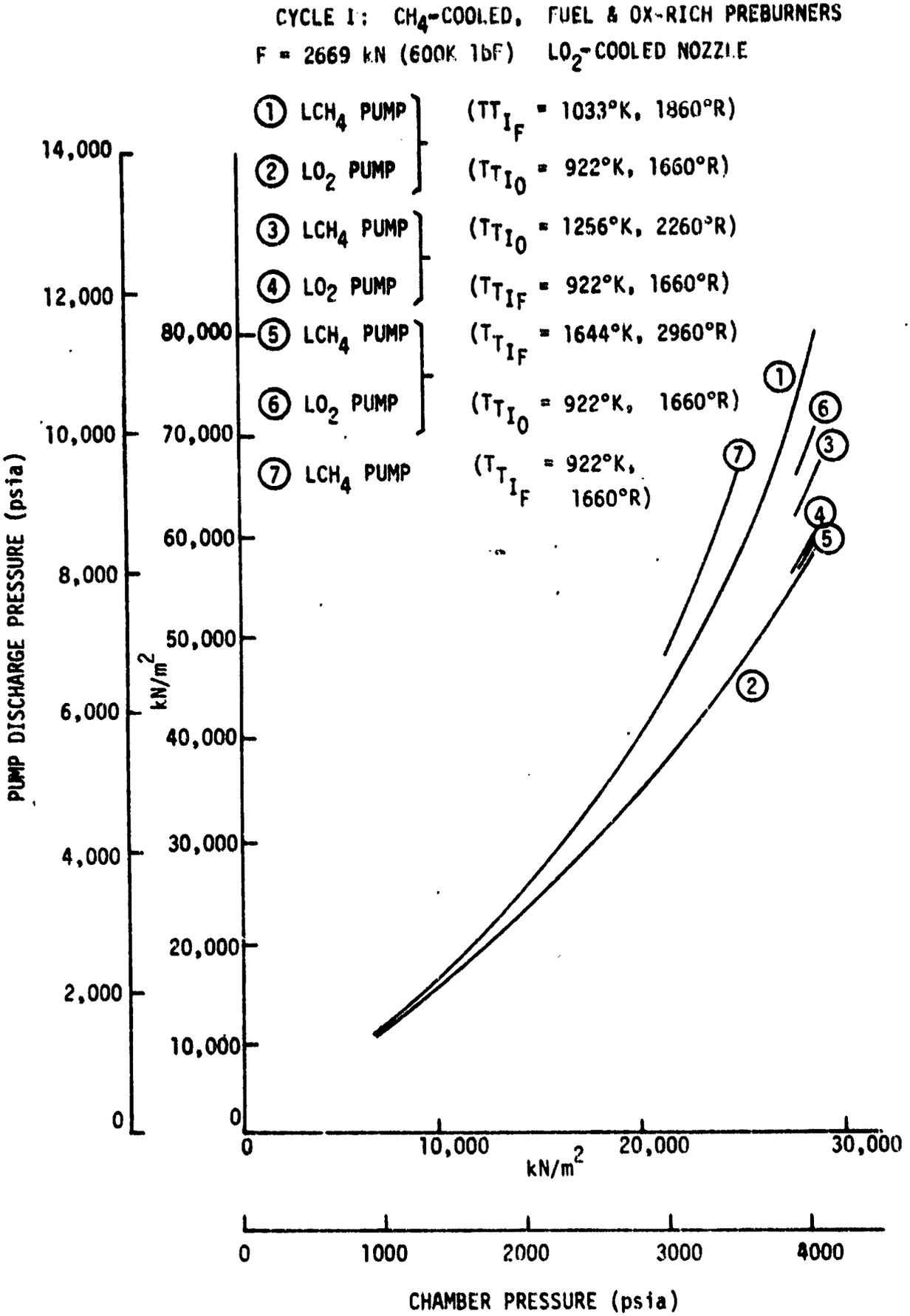

Figure 43. LO_2/LCH_4 Engine Cycle I Pump Discharge Pressure Requirements

III, D, Cycle Power Balance (cont.)

The influence of turbine inlet temperature is indicated in the figure at a chamber pressure of 27580 kN/m^2 (4000 psia). An increase in the fuel-rich turbine inlet temperature to 1644°K (2960°R) significantly lowers the fuel pump discharge pressure. However, if the oxidizer-rich turbine inlet temperature is maintained constant at 922°K (1660°R), as shown in Figure 43, the reduction in flow through the oxidizer-rich turbine results in a higher LO_2 pump discharge pressure (curve 6) corresponding to the lower fuel discharge pressure (curve 5). Consequently, a modest increase in fuel-rich turbine inlet temperature (curves 3 and 4) is preferable in this case. The other option, i.e., to increase the oxidizer-rich turbine temperature, will be discussed in Section VI,H.

12. Cycle I'

Cycle I' is the subcooled propane version of cycle I, where propane is substituted for methane fuel. The summary of the power balance data for this cycle is given in Table XIX and in Figure 44. The maximum chamber pressure achievable at a pump discharge pressure of 55160 kN/m^2 (8000 psia) is seen to be 24820 kN/m^2 (3600 psia).

13. Cycle J

The schematic for a LH_2-cooled, LH_2 fuel-rich gas-generator, LO_2/RP-1 engine cycle is depicted in Figure 45. The results from the power balance analysis for this cycle are summarized in Figures 46 and 47 and in Table XIX.

Cycle J is capable of generating a chamber pressure of 34470 kN/m^2 (5000 psia) at a pump discharge pressure 46200 kN/m^2 (6700 psia), well below the 55160 kN/m^2 (8000 psia) 1980 state-of-the-art value. The

LC_3H_8-COOLED FUEL & OX - RICH PREBURNERS

F = 2669 kN (600K lbF)

① LC_3H_8 PUMP (HI P STAGE)

② LO_2 PUMP

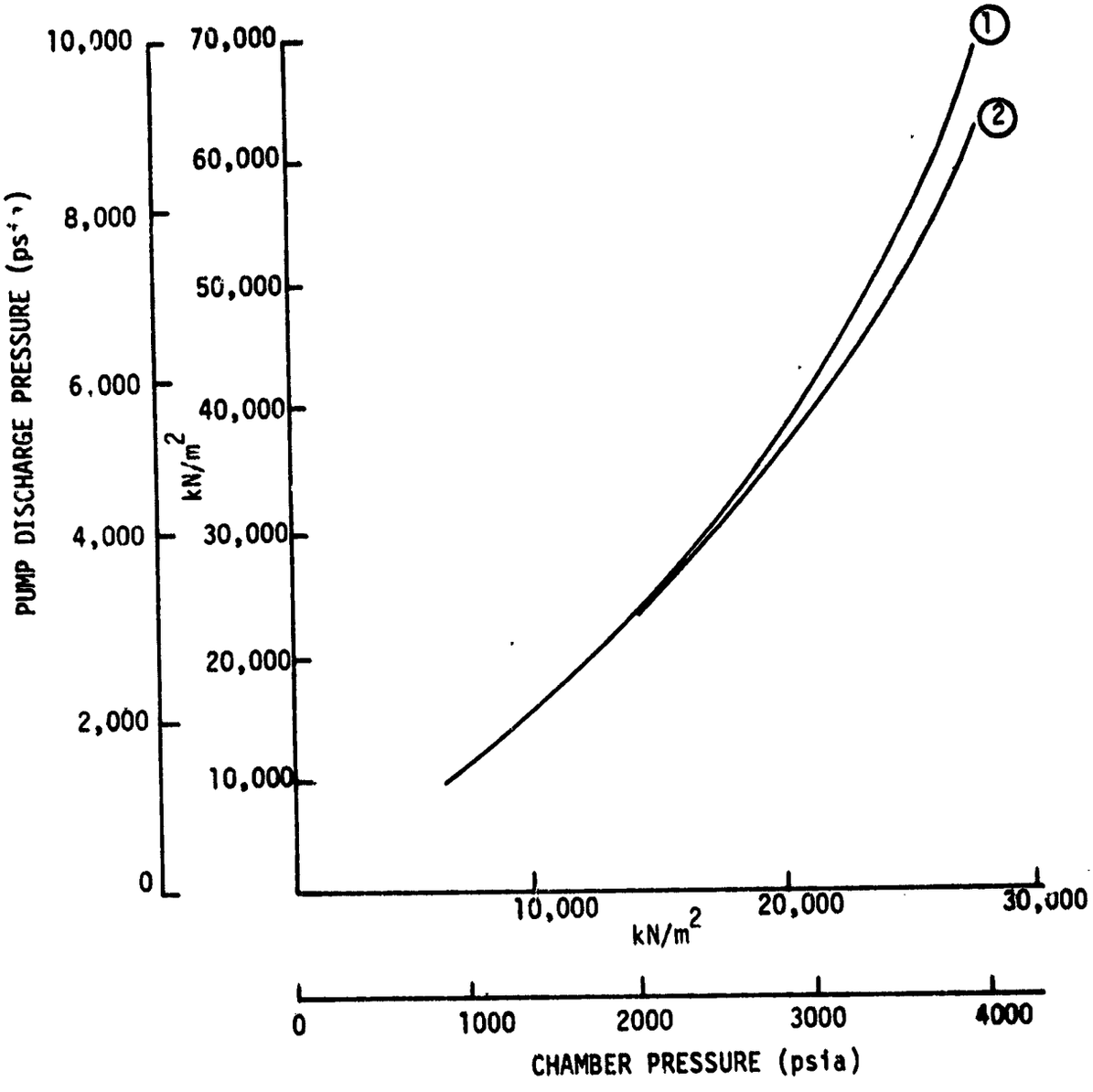

Figure 44. LO_2/LC_3H_8 Engine Cycle I' Pump Discharge Pressure Requirements

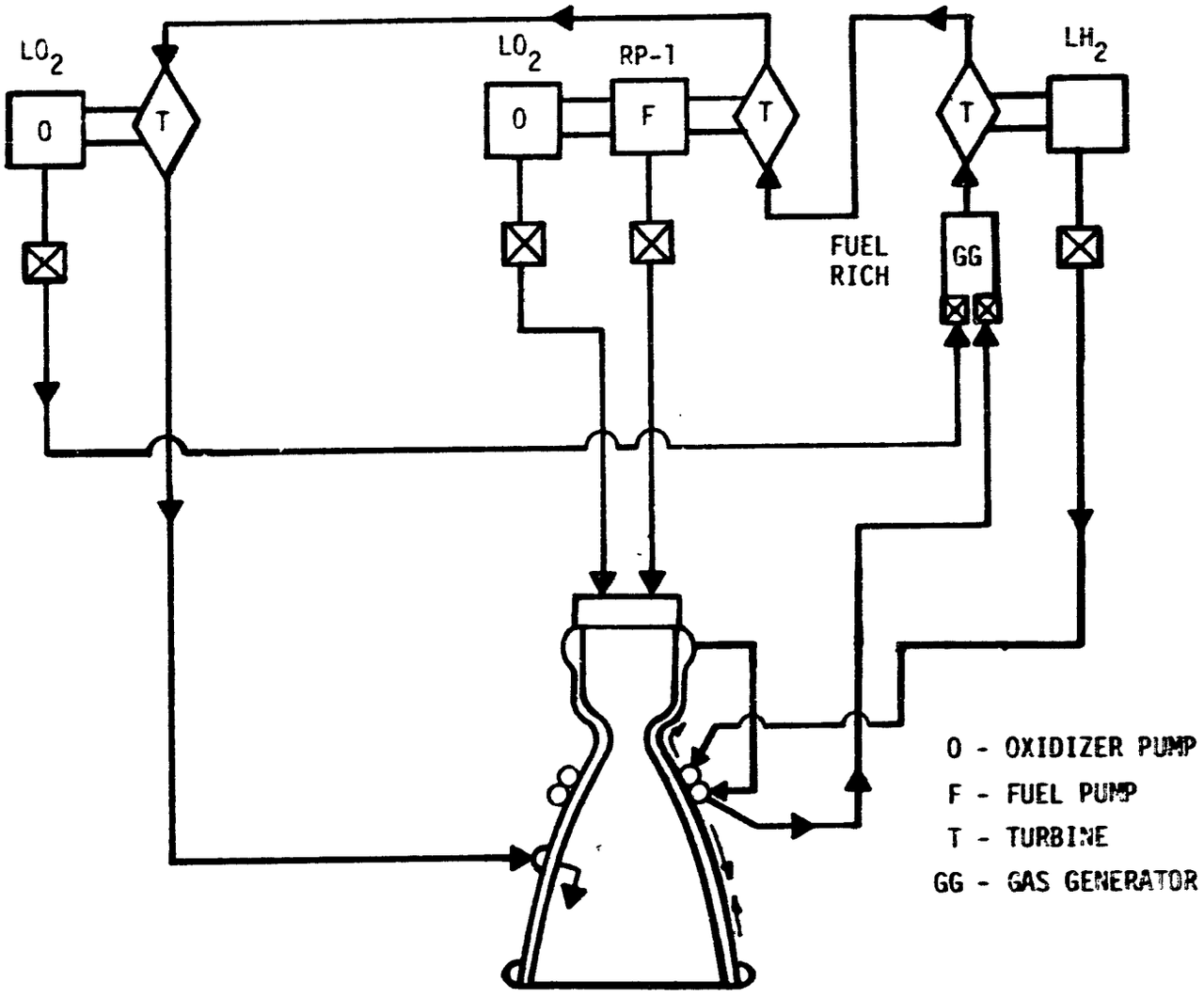

Figure 45. LO_2/RP-1 Engine Fuel-Rich LH_2 Gas-Generator Cycle J Schematic

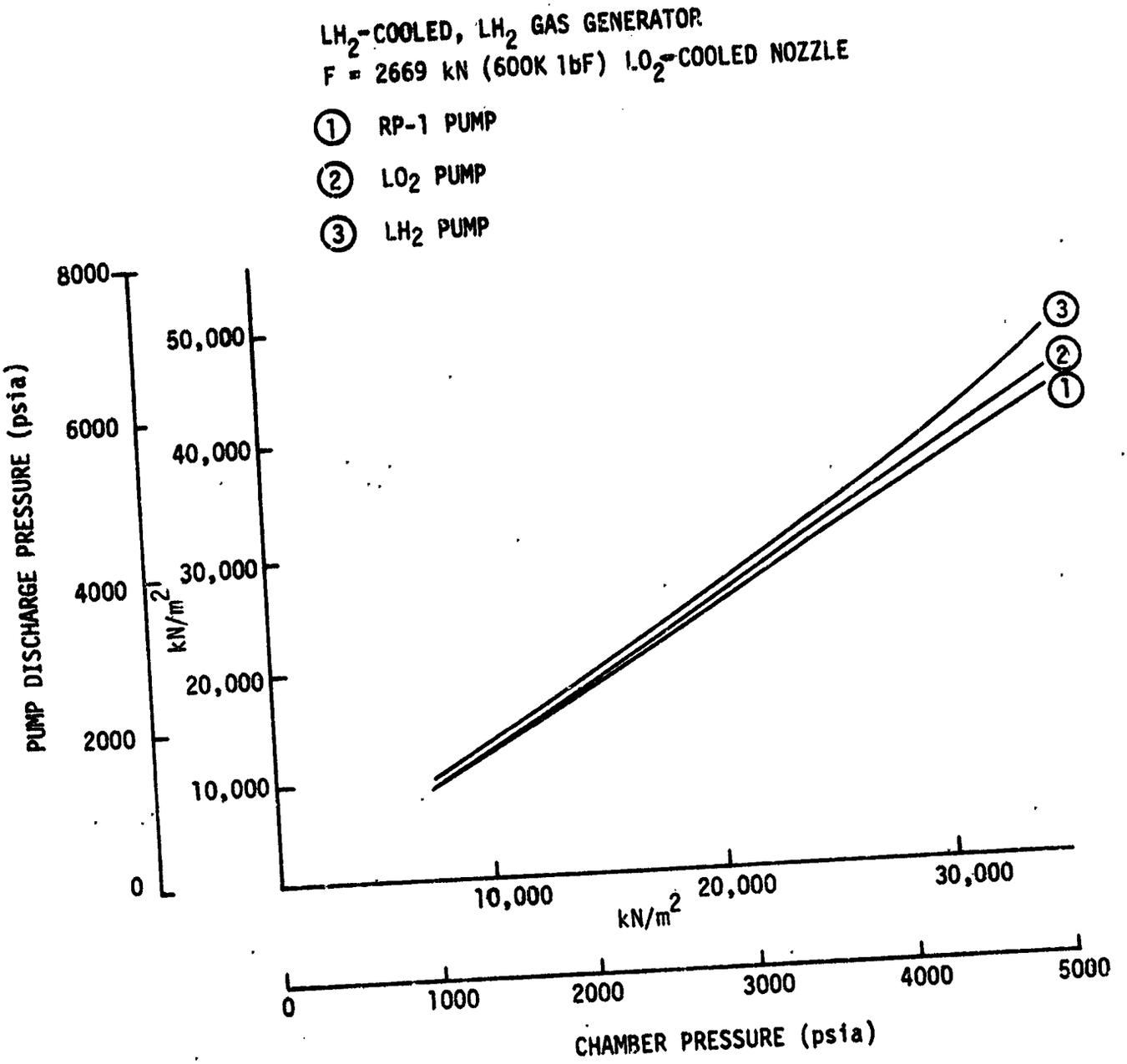

Figure 46. LO_2/RP-1 + LH_2 Engine Cycle J Pump Discharge Pressure Requirements

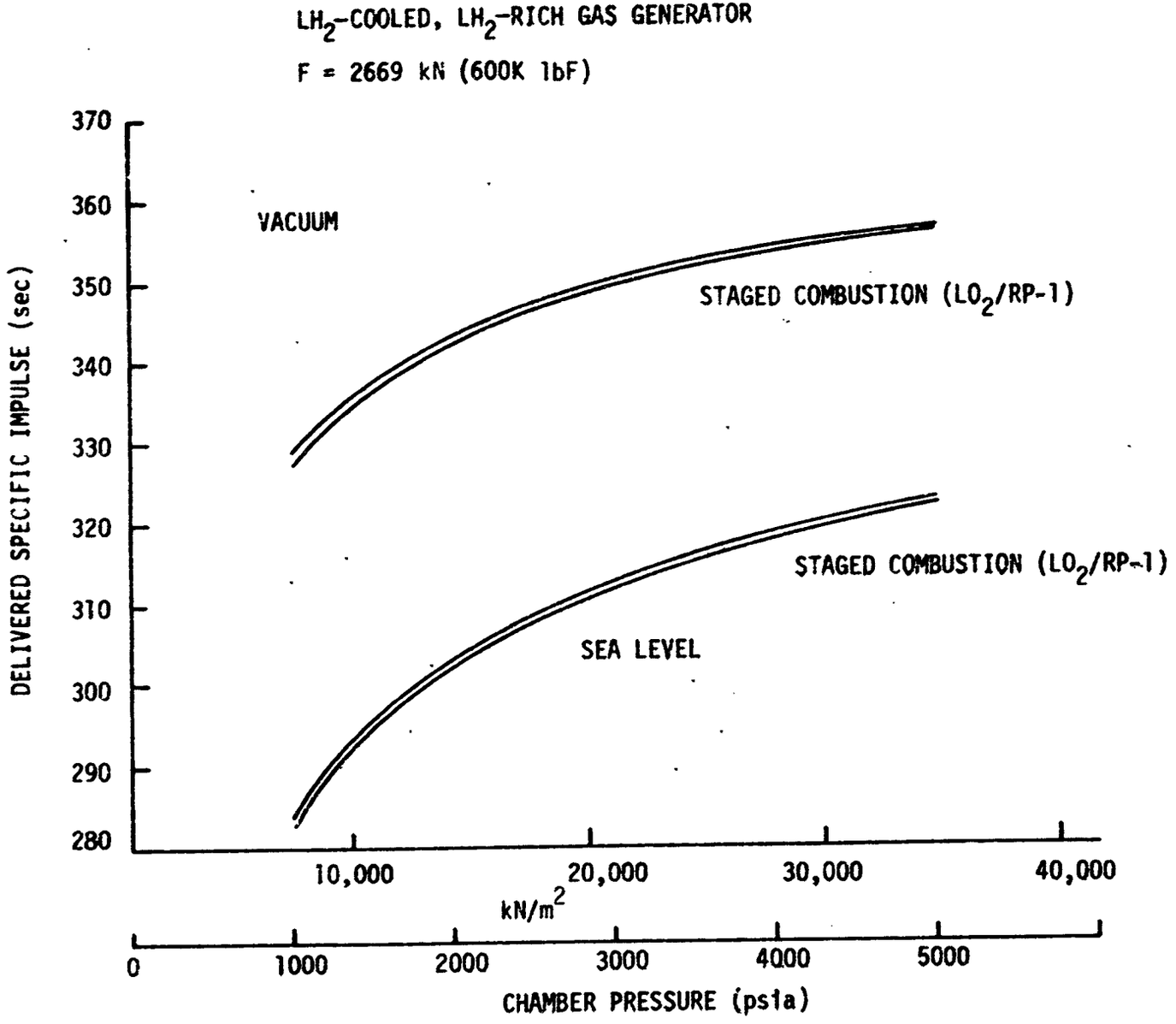

Figure 47. LO_2/RP-1 + LH_2 Engine Cycle J Performance

delivered performance for the engine slightly exceeds that for a staged-combustion LO_2/RP-1 engine because of the addition of the H_2 fuel-rich turbine exhaust in the thrust chamber nozzle.

14. Cycle K

A LO_2/LCH_4 dual-throat engine schematic is shown in Figure 48. This engine utilizes both LH_2 and LCH_4 as coolants and both an oxidizer-rich preburner and a H_2 fuel-rich gas generator. The cycle shown in the schematic is representative of this class of engines, but a detailed heat transfer and thrust split analysis is required to fully optimize this type of engine for a two-stage mission. Sufficient data exist for similar tri-propellant engines to allow a power balance and performance analysis of this bipropellant engine with a hydrogen-rich gas-generator drive. The specification for cycle K is given in Table XXV.

15. Thrust Level Variation

The parametric heat transfer data and the parametric performance data generated in this study show some variation with thrust levels from 890 to 6672 kN (200K to 1M lbF). Some of this variation is real, and some of it is the result of approximations used in the parametric scaling relationships required to facilitate the generation of a wide variety of design data.

Past experience has shown that engine cycles can be rated at a given thrust level (e.g., 600K lbF) and that the rating will be valid for other thrust levels (i.e., 200K to 1M lbF). To validate this premise, power balance calculations were made for cycle C at thrust levels of 890, 2669, and 6672 kN (200, 600K, and 1M lbF). The results are given in Table XIX. Table XXVI summarizes the pertinent data.

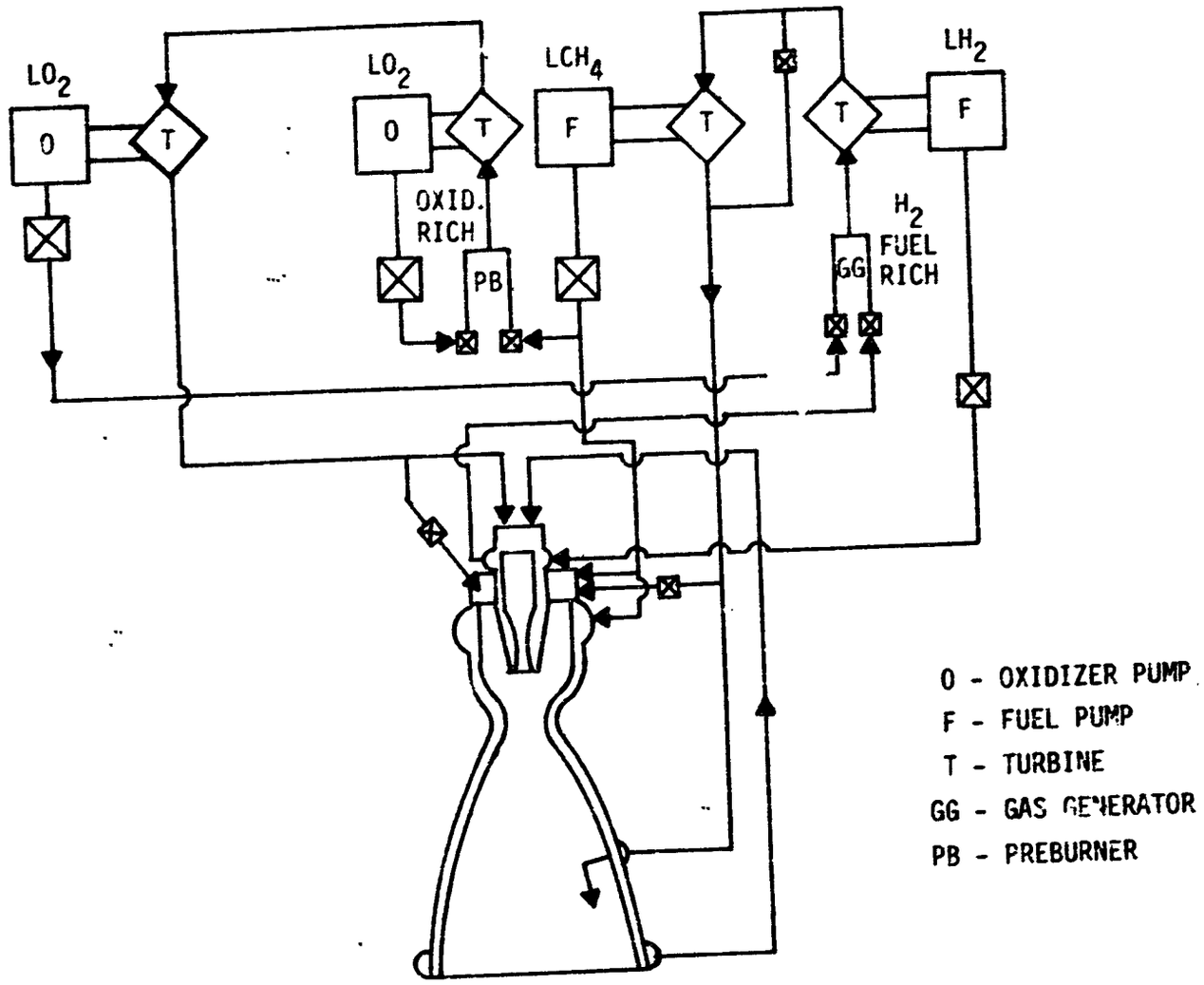

Figure 48. LO_2/LCH_4 Dual Throat Engine Mixed Gas-Generator/Staged-Combustion Cycle K Schematic

TABLE XXV

LO_2/LCH_4 ENGINE CYCLE K SPECIFICATION

PARAMETER	MODE I	MODE II
Sea Level Thrust, lbF	610,745	--
Vacuum Thrust, lbF	685,270	225,960
Sea Level Is, sec	319.0	--
Vacuum Is, sec	357.9	380.2
Mixture Ratio (LO_2/LCH_4)	3.5	3.5
Mixture Ratio (LO_2/LH_2)	0.8	0.8
Chamber Pressure, psia	2800/4000	4000
Area Ratio	42	187
TCA Sea Level Is, sec	320.9	--
TCA Vacuum Is, sec	359.3	383.6
GG Sea Level Is, sec	238.8	--
GG Vacuum Is, sec	300.7	338.1
Flowrate, lb/sec	1914.61	594.36
TCA LO_2 Flowrate, lb/sec	1454.14	427.28
TCA LCH_4 Flowrate, lb/sec	415.47	122.08
GG LO_2 Flowrate, lb/sec	20.00	20.00
GG LH_2 Flowrate, lb/sec	25.00	25.00
Throat Area, in^2	115.22	26.06
Exit Area, in^2	4869.72	4869.73
Exit Pressure, psia	7.3	1.5
LCH_4 Pump Dischg. Pressure, psia	7429	7429
LO_2 Pump Dischg. Pressure, psia	7429	7429
LH_2 Pump Dischg. Pressure, psia	1655	1655

TABLE XXVI

THRUST LEVEL EFFECT ON PERFORMANCE

Thrust kN (lbF)	Chamber Pressure kN/m^2 (psia)	Pump Dischg. Pressure kN/m^2 (psia)	Sea Level Is (sec)	Vacuum Is (sec)
890 (200,000)	27580 (4000)	48470 (7030)	315.8	353.5
2669 (600,000)	" (4000)	47720 (6921)	316.5	354.1
6672 (1,500,000)	" (4000)	52830 (7662)	316.5	354.1

It is seen that there is little variation in the performance of the engines over this wide range of thrust levels. There is a variation in pump discharge pressure on the order of 10%, but some of this variation can be reduced through thrust chamber design changes to decrease the coolant pressure drop.

E. ENGINE CYCLE RATING SYSTEM

In order to select two of the candidate cycles for preliminary design analysis and engine definition in Task IV of this program, it was necessary to establish cycle rating criteria. These criteria, summarized in the following paragraphs, also include the LOX/propane propellant system added in the conduction of Task IV. Final ranking and selection of the cycles is deferred to Section V.D. where the mission analysis results will be presented.

Engine cycle rating parameters were established according to the system shown in Figure 49. The desired condition and the effect of the parameter on the engine and/or vehicle are listed in the figure. The listed rating points for each parameter are subjective and depend upon the assumptions chosen for the study. In general, the assumptions reflect good design practice for a reusable, long-life rocket engine system that makes maximum use of the chemical energy of the propellants to obtain an optimum power cycle.

Engine performance is given the highest rating point potential of fifteen because of the impact of Stage 1 performance on the mission capability (payload) for a two-stage vehicle. Engine weight does not affect the mission results to a great degree, and, accordingly, is assigned a one-point maximum rating for the lowest engine weight.

PARAMETER	ENGINE CYCLE		EFFECT	POINTS
	SC	GG		
ENGINE PERFORMANCE	HIGH	LOWER	PAYLOAD CAPABILITY	15
ENGINE WEIGHT	HIGH	LOWER	PAYLOAD CAPABILITY	1
PUMP DISCHARGE PRESSURE	HIGH	LOWER	TPA CYCLE LIFE	2
CHAMBER PRESSURE	HIGH	LOWER	PAYLOAD CAPABILITY ENGINE ENVELOPE	3
TANK MIXTURE RATIO	OPTIMUM	NOT OPTIMUM	PAYLOAD CAPABILITY	1
TURBINE TEMPERATURE	HIGH	LOWER	TPA CYCLE LIFE COOLING SYSTEM COMPLEXITY	N/A
	HIGH	HIGH	POWER REQUIREMENT PAYLOAD CAPABILITY	
LO_2/HC FUEL-RICH TURBINE	COKING	COKING	TPA/INJECTOR CYCLE LIFE PURGE SYSTEM REQUIREMENT LOW PERFORMANCE	3
LO_2/H_2 FUEL-RICH TURBINE	LOW P_2/P_1	HIGH P_2/P_1	STAGED TURBINE HIGH PERFORMANCE LOW PUMP DISCHARGE PRESSURE	
INTER-PROPELLANT SEAL REQUIREMENT FOR TPA	NO/YES	YES	TPA CYCLE LIFE & PERFORMANCE	2
COOLANT REQUIREMENT	HIGHER	LOWER	HOT GAS MANIFOLD COOLING IF TURBINE TEMP.>922°K (1200°F)	3

INDICATES DESIRABLE CONDITION

Figure 49. Engine Cycle Rating Parameters

III, E, Engine Cycle Rating System (cont.)

Pump discharge pressure and chamber pressure were viewed as life cycle influencing parameters, and, as such, lower pressures were awarded higher points. Hydrocarbon coking on the turbine blades was envisioned as an unacceptable commodity. No coking, therefore, was assigned three points.

Interpropellant seals in turbomachinery require large amounts of inert gas, such as helium, and significantly increase the weight of the turbopump system. Therefore, two rating points were assigned to a cycle without the requirement for an interpropellant seal.

A shift in mixture ratio from the optimum staged-combustion cycle value, such as required by a gas-generator cycle, was penalized slightly, with optimum mixture ratio assigned one point. Coolants such as LO_2, LCH_4, and LC_3H_8 were assigned two points, and LH_2 coolant was assigned three points. The questionable coolant RP-1R was given one rating point.

Both low- and high-temperature turbines are listed as desirable in the figure in view of the fact that this study indicates a marked benefit of a high-temperature turbine temperature on some cycles. Since the cycle ranking was based on turbine temperatures of 1033°K (1860°R), no point rating was assigned to this parameter.

1. Preliminary Cycle Ranking

A chamber pressure ranking of the cycles is given in Figure 50. The ranking is based on an upper limit of pump discharge pressure of 55160 kN/m^2 (8000 psia) for staged-combustion cycles and the optimum performance for gas-generator cycles. The pump discharge pressure limit is the 1980 state of the art for rocket turbopumps. The ranking is also based on 1980 state-of-the-art fuel-rich and oxidizer-rich turbine temperatures of 1033 and 922°K (1860 and 1660°R), respectively. The RP-1-cooled engines (cycles A, D, and F) are seen to be limited to very low chamber pressures.

ASSUMPTIONS

TURBINE TEMP: FR 1860°R: OR 1660°R

ENGINES OPTIMIZED FOR EITHER:

POWER LIMIT ($P_D \leq$ 8000 PSIA)

PEAK Is (GG CYCLES)

RP-1 COKING TEMP.

PUMP DISCHARGE PRESSURE ≤ 8000 PSIA

CODE: COOLANTS: RP-1P*, RP-1, LO_2, LCH_4, LH_2, LC_3H_8

FP = FUEL-RICH OP = OXIDIZER-RICH

GG = GAS GENERATOR PB = PREBURNER

HP = HYDROGEN-RICH

*REFINED RP-1

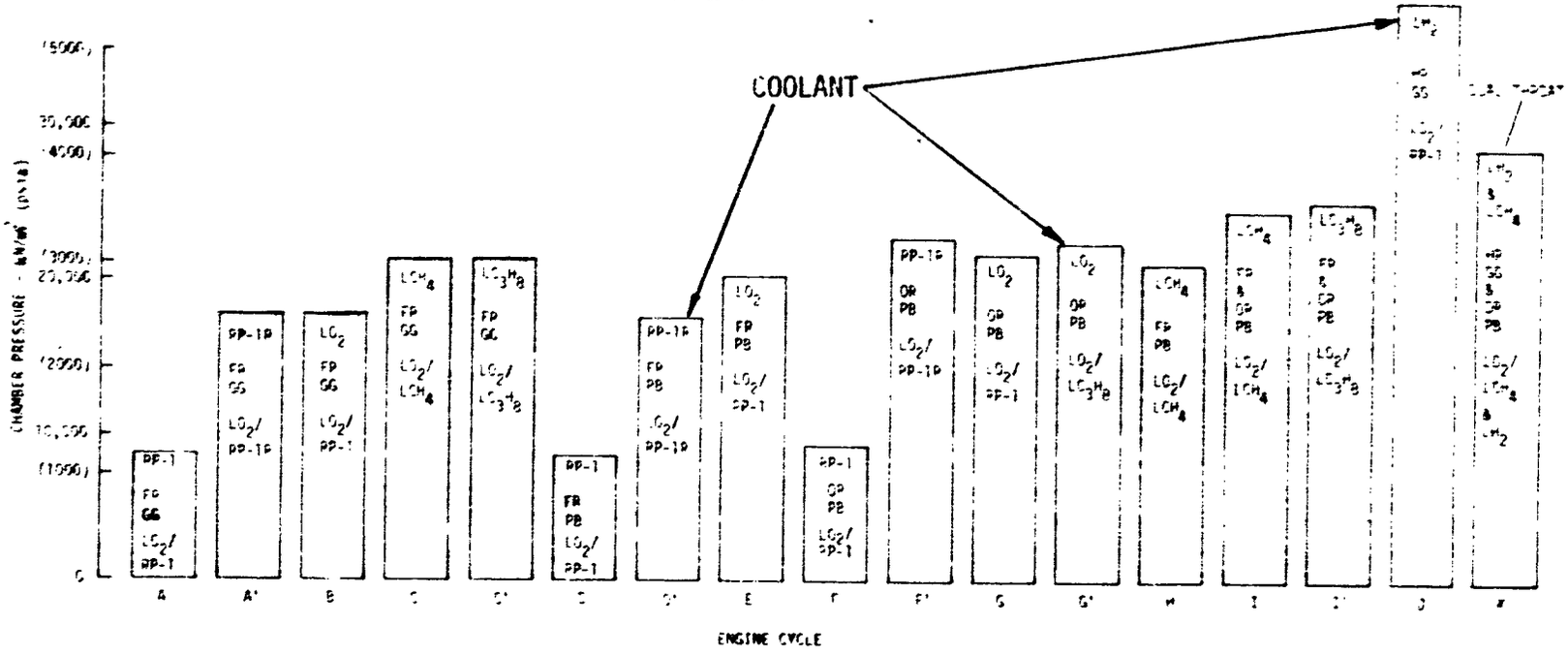

Figure 50. Chamber Pressure Ranking of LO_2/HC Engine Cycles

The chamber pressure ranking from Figure 50 can be converted into a performance ranking for the cycles, as shown in Figure 51. The performance values show less variation than the chamber pressures due to the high delivered performance for the staged-combustion cycles, even at lower chamber pressures. The cycle with the highest performance potential is seen to be the dual-throat cycle. The variable geometry (without moving parts) allows the achievement of a high performance at altitude.

2. Preliminary Cycle Comparison

It is interesting to compare the best-performing cycles (dual throat not included) as a function of chamber pressure and power limits, as shown in Figure 52. The lowest-performing cycle (B) achieves its maximum performance at a pump discharge pressure of 33090 kN/m^2 (4800 psia). If the best staged-combustion cycle (F'), utilizing the same LOX/RP-1 propellants, is compared with cycle B at the same pump discharge pressure (Pc = 16550 kN/m^2 [2400 psia]), it is seen that a performance difference of about 12 sec exists. Operating cycle F' at its pump discharge pressure limit of 55160 kN/m^2 (8000 psia) results in a difference of 18 sec between the cycles.

The gas-generator cycles C and C', using LOX/methane and LOX/propane, respectively, are seen to compare favorably with the LOX/RP-1 staged-combustion cycle F'. Additional performance can be gained through the utilization of the staged-combustion cycles I and I' for these propellant combinations. The gains amount to about 12 to 16 sec in specific impulse between cycles C, C' and I, I'. Selection of one of the fuels, methane or propane, on the basis of performance is difficult, as the differences amount to about 3 sec for gas-generator cycles C and C' and to about 2 sec for staged-combustion cycles I and I'.

The liquid-hydrogen-cooled cycle J is seen to be competitive with cycles I and I' when sea level performance is compared. The vacuum performance shown in Figure 51 slightly favors cycles I and I'.

ASSUMPTIONS

TURBINE TEMP: FR 1860°R; OR 1660°R

ENGINES OPTIMIZED FOR EITHER:

POWER LIMIT ($P_D \leq 8000$ PSIA)

PEAK Is (GG CYCLES)

RP-1 COKING TEMP.

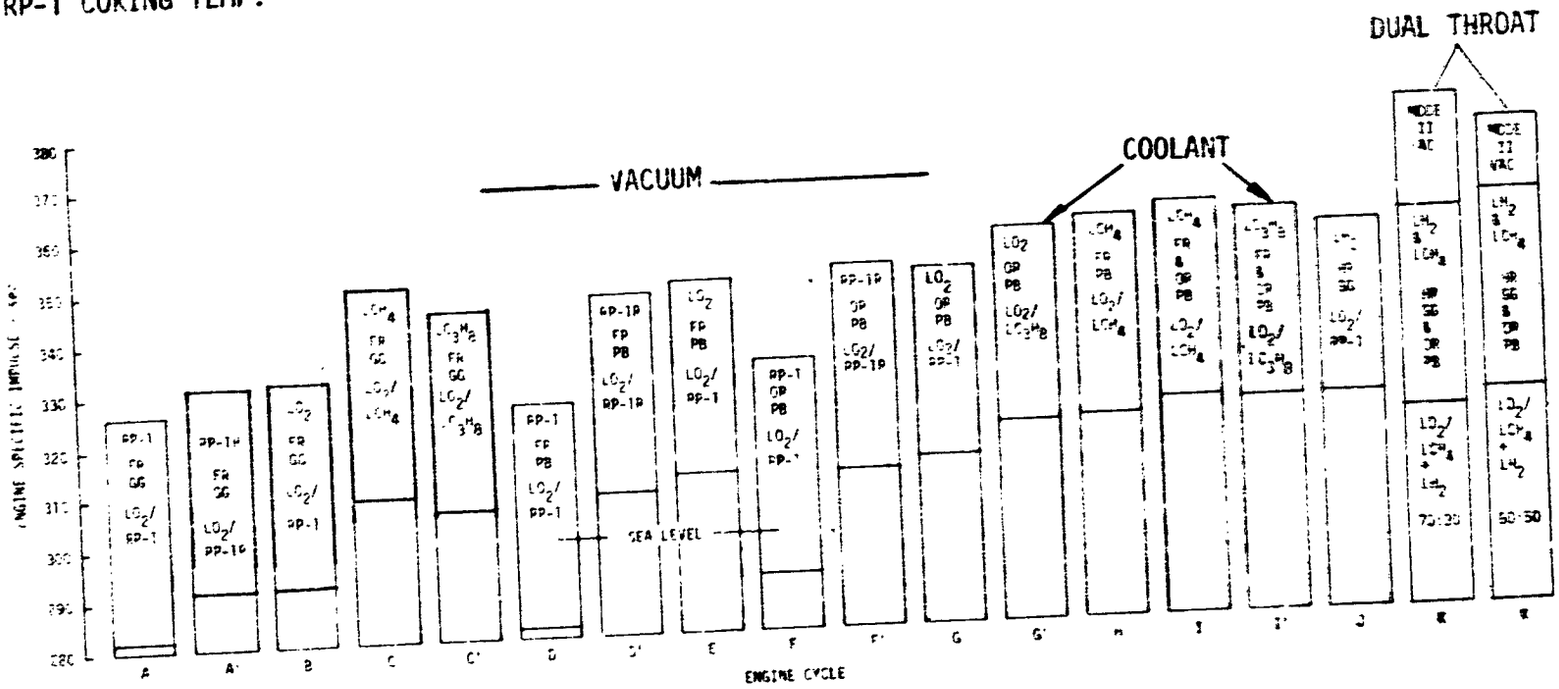

Figure 51. Performance Ranking of LO_2/HC Engine Cycles

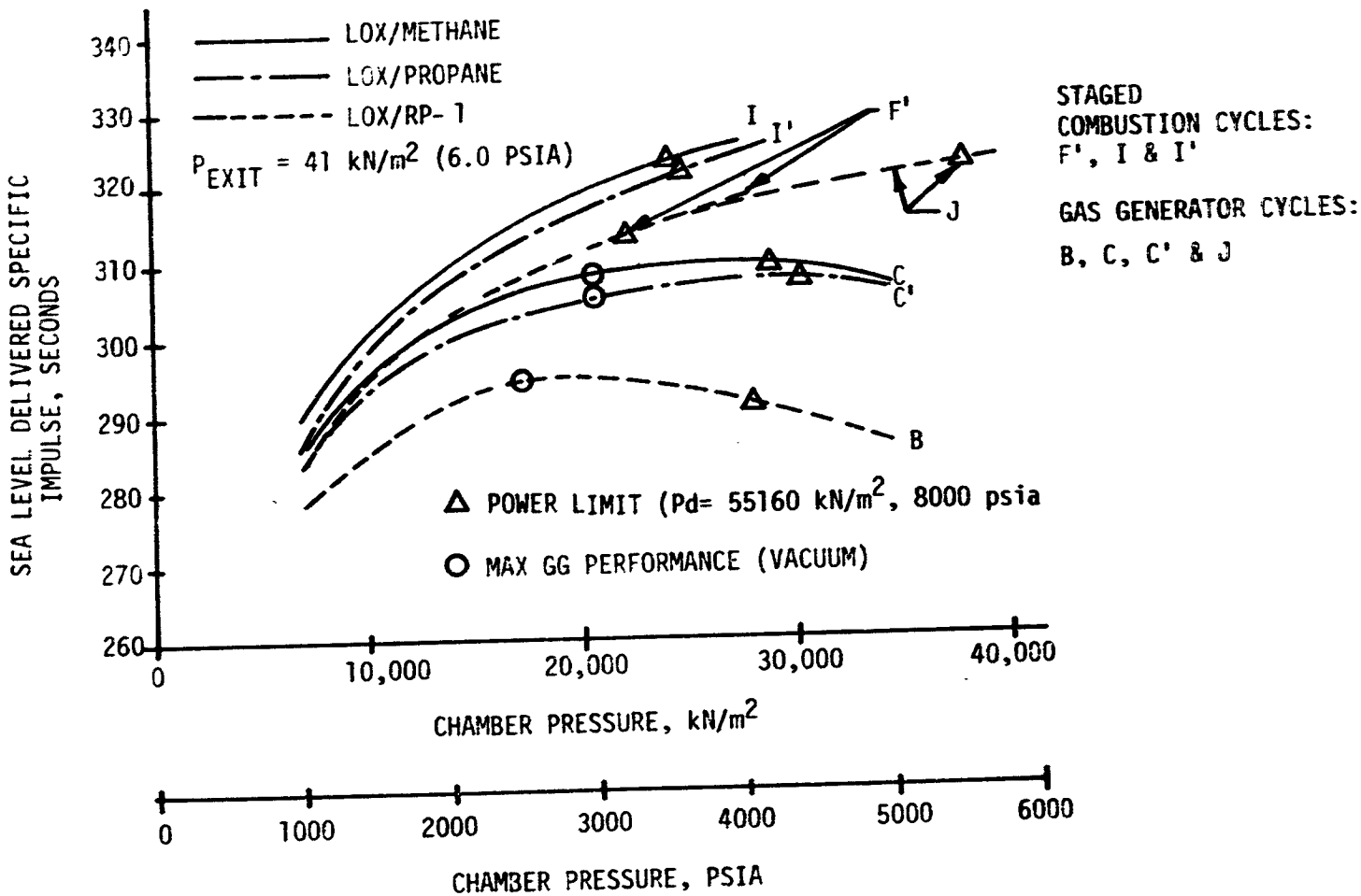

Figure 52. Comparison of Engine Cycles as a Function of Chamber Pressure

IV. ENGINE PARAMETRIC ANALYSIS

A. OBJECTIVES AND GUIDELINES

Performance, weight, and envelope parametric data were to be developed for the high-pressure LO_2/HC engine systems derived in the previous section. The following parameter range guidelines were utilized:

Propellant mixture ratio (O/F):

LO_2/RP-1	2 to 3.5
LO_2/LCH_4	3 to 4.5
LO_2/LC_3H_8	2 to 4

Engine Thrust: 890 to 6672 kN (200K to 1.5M lbF)

Chamber Pressure: 6895 to 34,470 kN/m^2 (1,000 to 5,000 psia) (or power/cooling limit)

Area Ratio (ϵ): 15:1 to 100:1 (or sea level flow attachment limit)

Performance prediction methods were consistent with the JANNAF simplified methodology. Engine weight estimates were based on the 1979 state of the art, with yearly improvement factors through the year 2000.

B. ENGINE PERFORMANCE

The first step in the JANNAF performance prediction procedure is to determine the one-dimensional equilibrium specific impulse (Isp_{ODE}) which is a function of propellant combination and mixture ratio, nozzle area ratio (ϵ), chamber pressure, and the propellant temperature (tank conditions). Isp_{ODE} data were obtained by using the TDK program (Ref. 19).

IV, B, Engine Performance (cont.)

The predicted delivered specific impulse (Isp_{DEL}) is obtained by calculating the efficiency of the known loss mechanisms that degrade the ideal (Isp_{ODE}) performance. For this analysis, these loss mechanisms were divided in four major categories: 1) energy release efficiency (η_{ERE}); 2) reaction kinetics efficiency (η_K); 3) two-dimensional divergence efficiency (η_{2D}); and 4) loss due to the thrust decrement within the boundary layer.

A computer program was developed to help facilitate the parametric analysis by representing each loss mechanism in a subroutine with the appropriate data base, except for the energy release efficiencies which were specified as 98% for LOX/RP-1 and 98.5% for LOX/LCH_4 and for LOX/LC_3H_8.

The kinetic efficiency was obtained by comparing the one dimensional kinetics specific impulse (Isp_{ODK}), calculated using the TDK computer program (Ref. 19), to the Isp_{ODE} ($\eta_K = Isp_{ODK}/Isp_{ODE}$). The two-dimensional efficiency was obtained from charts which gave the η_{2D} for optimum Rao nozzles as described in Reference 20. These charts were tabularized to facilitate their use in the performance program. The boundary loss was obtained by implementing the turbulent boundary layer chart procedures also given in Reference 20. The boundary layer efficiency was calculated by assuming an adiabatic wall and propellants at the tank enthalpy. Past analyses have shown this approach to be quicker and to result in the same efficiency as the more rigorous method of calculating the enthalpy transfer to the regenerative coolant and then finding a new Isp_{ODE} by using the increased propellant enthalpy.

1. Parametric Performance Data

All of the parametric performance data presented in the this section are for staged-combustion cycle engines or for the thrust chamber of

open-loop (e.g., gas-generator) cycle engines. Corrections such as described in Section III.D. must be made for open-loop cycle engines.

The performance data for LOX/RP-1, LOX/LCH_4, and LOX/LC_3H_8 are summarized in Figures 53-64. Figures 53, 57, and 61 show the influence of chamber pressure on engine performance. An expansion to a constant one dimensional exit pressure of 41 kN/m^2 (6 psia) was assumed for all cases to ensure that flow separation would not occur under sea level operating conditions. The pressure selection affords a reasonable tradeoff in sea level and vacuum performance for booster engines. This resulted in an area ratio change with chamber pressure and an increase with chamber pressure of both vacuum and sea level specific impulse. In general, methane and propane, respectively, provide approximately a 3% and 2% improvement in maximum specific impulse compared to RP-1, as can be seen in a comparison of Figures 53-56, 57-60, and 61-64.

The effect of mixture ratio on specific impulse is shown in Figures 54, 58, and 62 for the propellant combinations. In all cases, chamber pressure is constant at 27580 kN/m^2 (4000 psia), thrust is constant at 2669 kN (600K lbF), and the area ratio is varied to provide an expansion to an exit pressure of 41 kN/m^2 (6 psia). The maximum specific impulse for LOX/RP-1 occurs at a mixture ratio of approximately 2.8 while that for LOX/CH_4 and LOX/C_3H_8 occurs at a mixture ratio of approximately 3.5 and 3.1, respectively. At any mixture ratio shown, the specific impulse values of LOX/LCH_4 and LOX/LC_3H_8 are about equal to, or greater than, that produced by LOX/RP-1.

As seen in Figures 55, 59, and 63, the effect of thrust level variations over the range from 890 to 6672 kN (200K lbF to 1.5M lbF) on specific impulse is relatively small. Over this range of thrust, specific impulse values increase less than 0.5%.

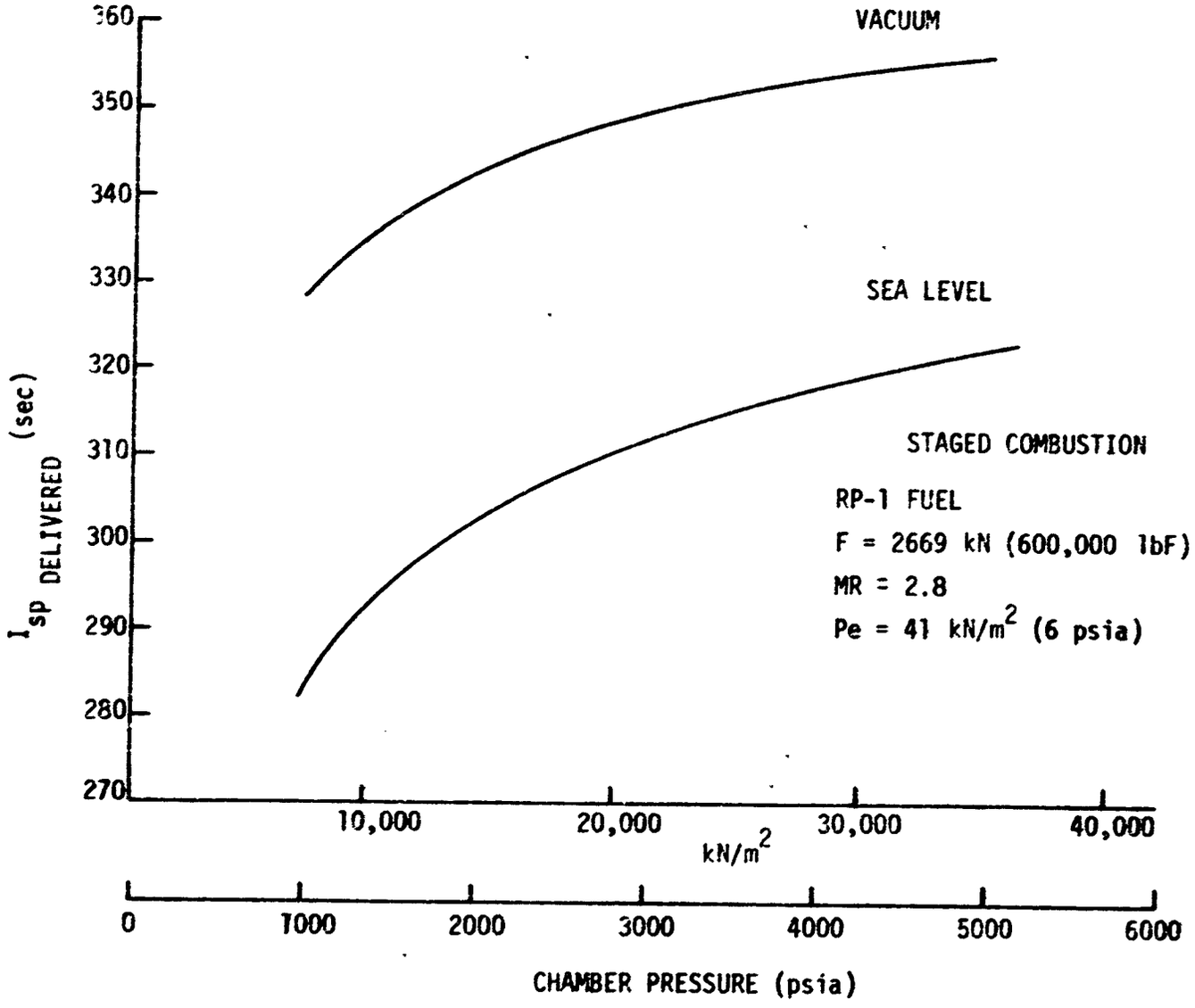

Figure 53. Delivered LOX/RP-1 Engine Performance Versus Chamber Pressure

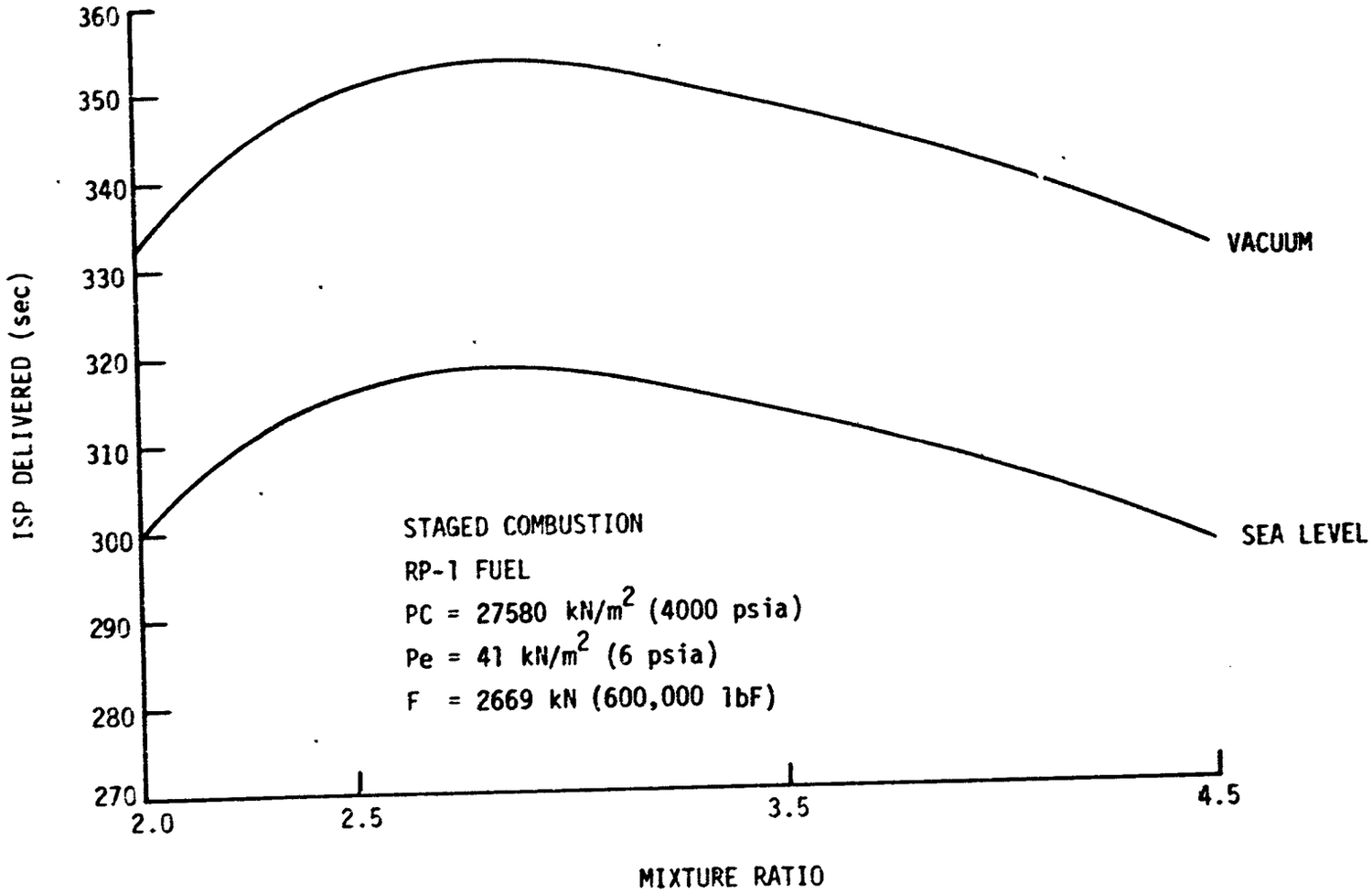

Figure 54. Delivered LOX/RP-1 Engine Performance Versus Mixture Ratio

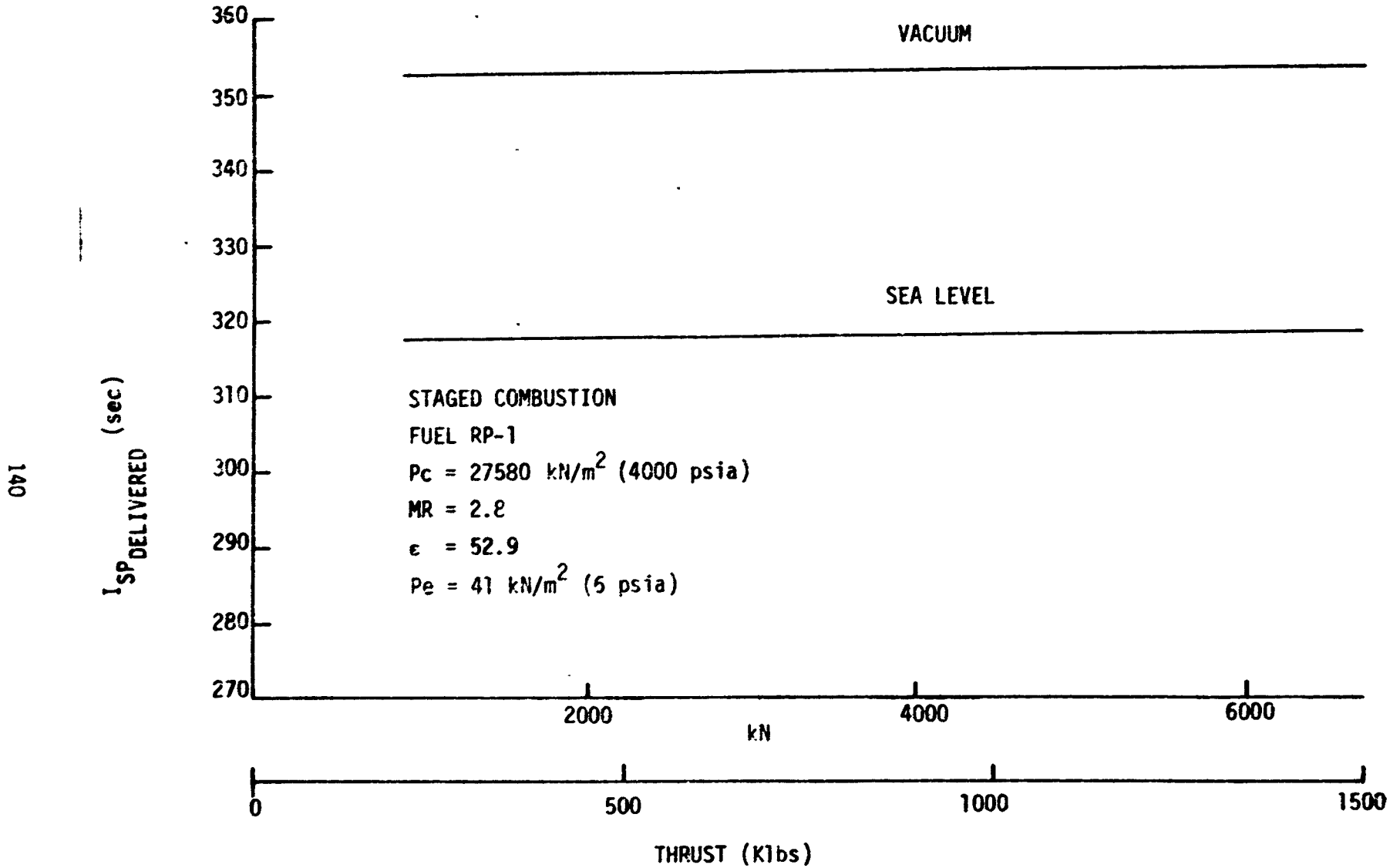

Figure 55. Delivered LOX/RP-1 Engine Performance Versus Thrust

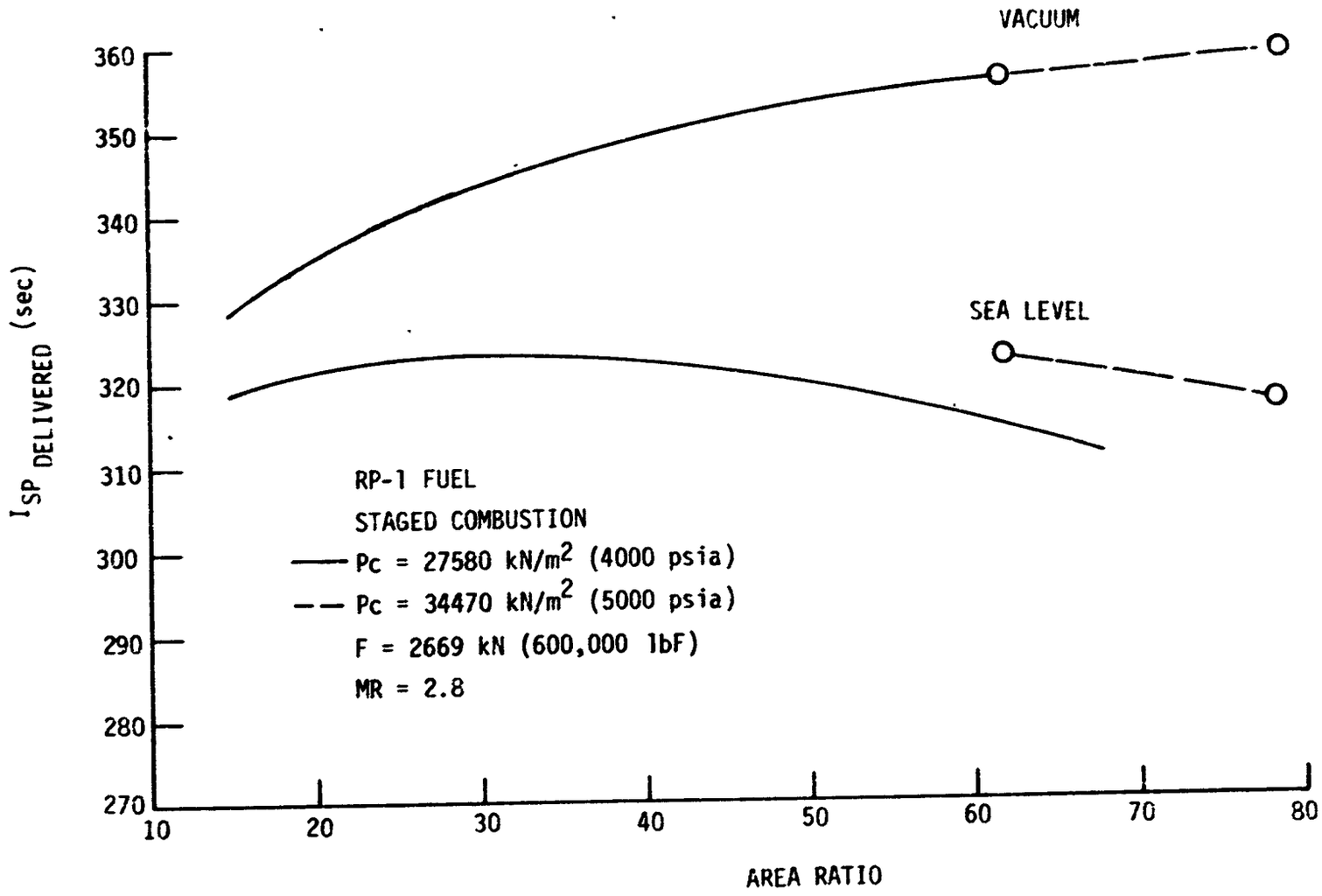

Figure 56. Delivered LOX/RP-1 Engine Performance Versus Area Ratio

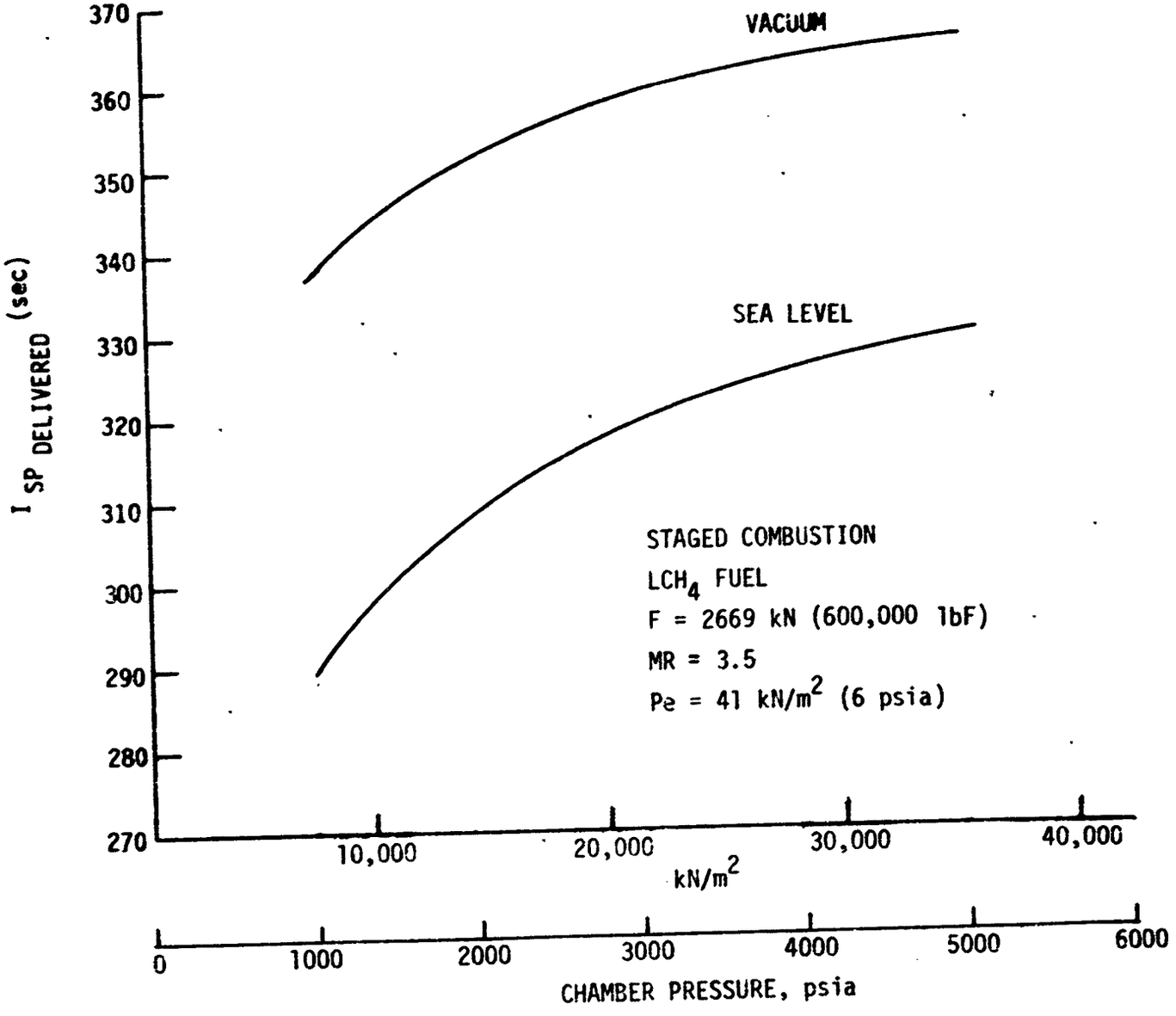

Figure 57. Delivered LOX/CH_4 Engine Performance Versus Chamber Pressure

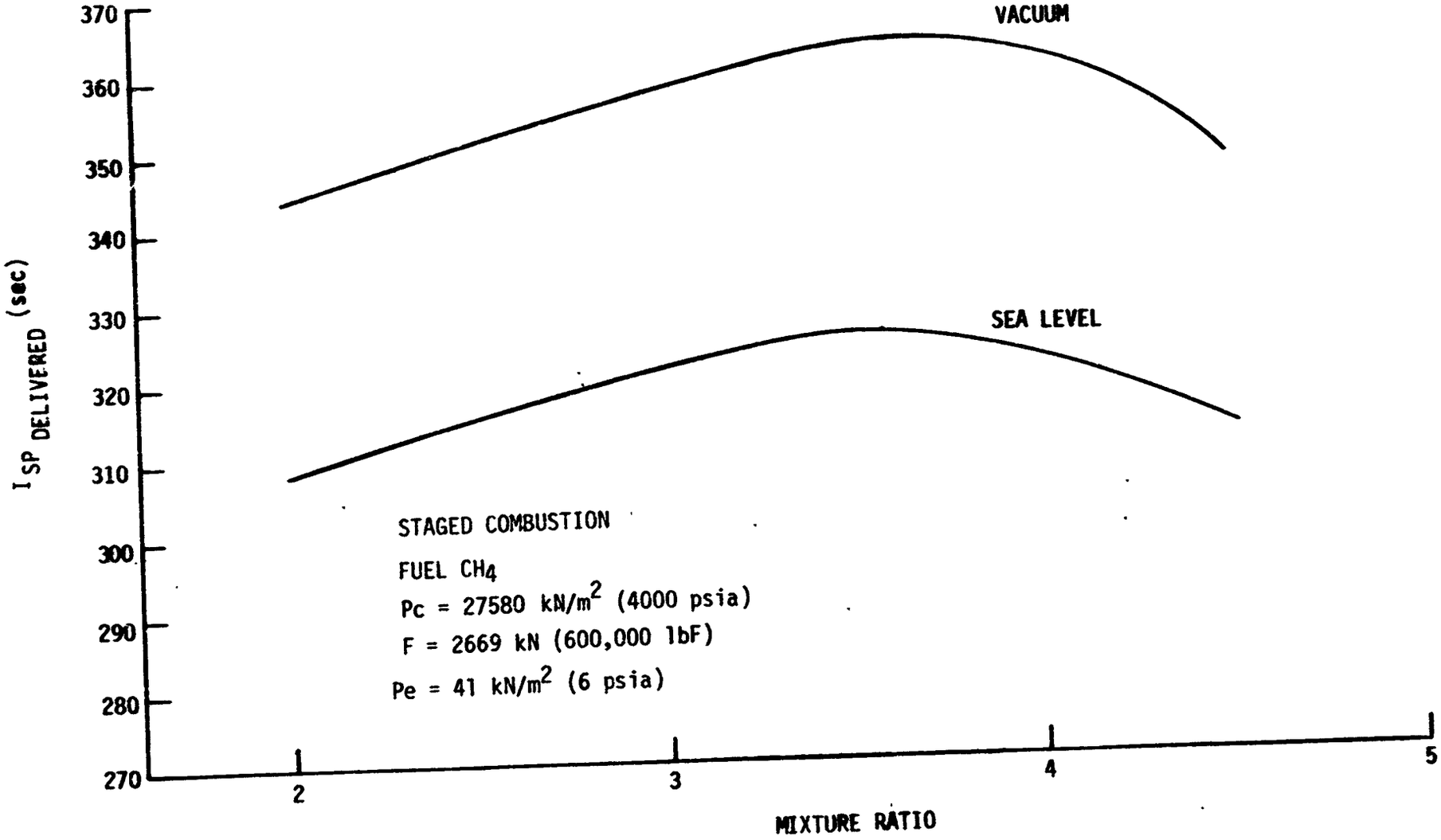

Figure 58. Delivered LOX/CH_4 Engine Performance Versus Mixture Ratio

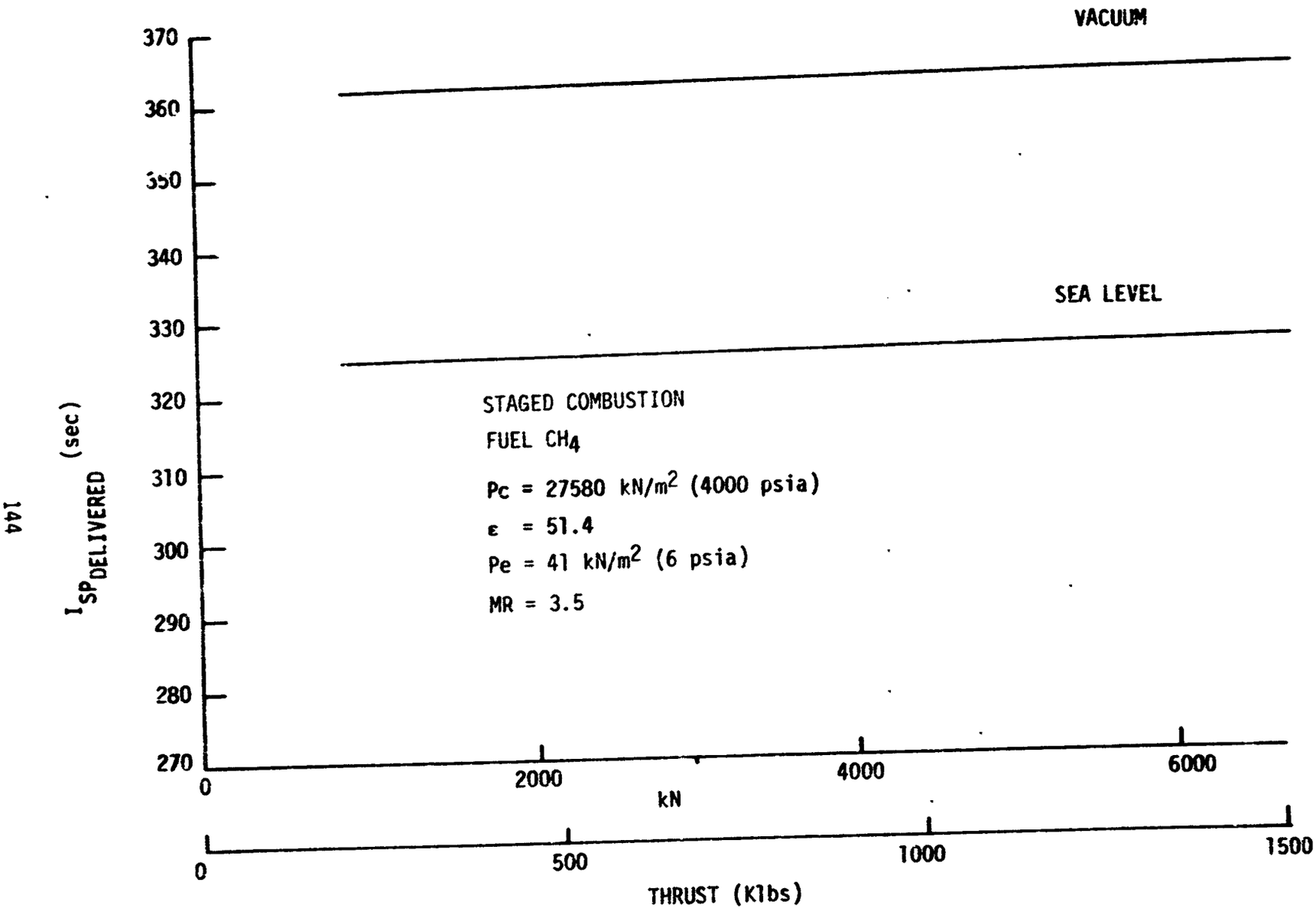

Figure 59. Delivered LOX/CH_4 Engine Performance Versus Thrust

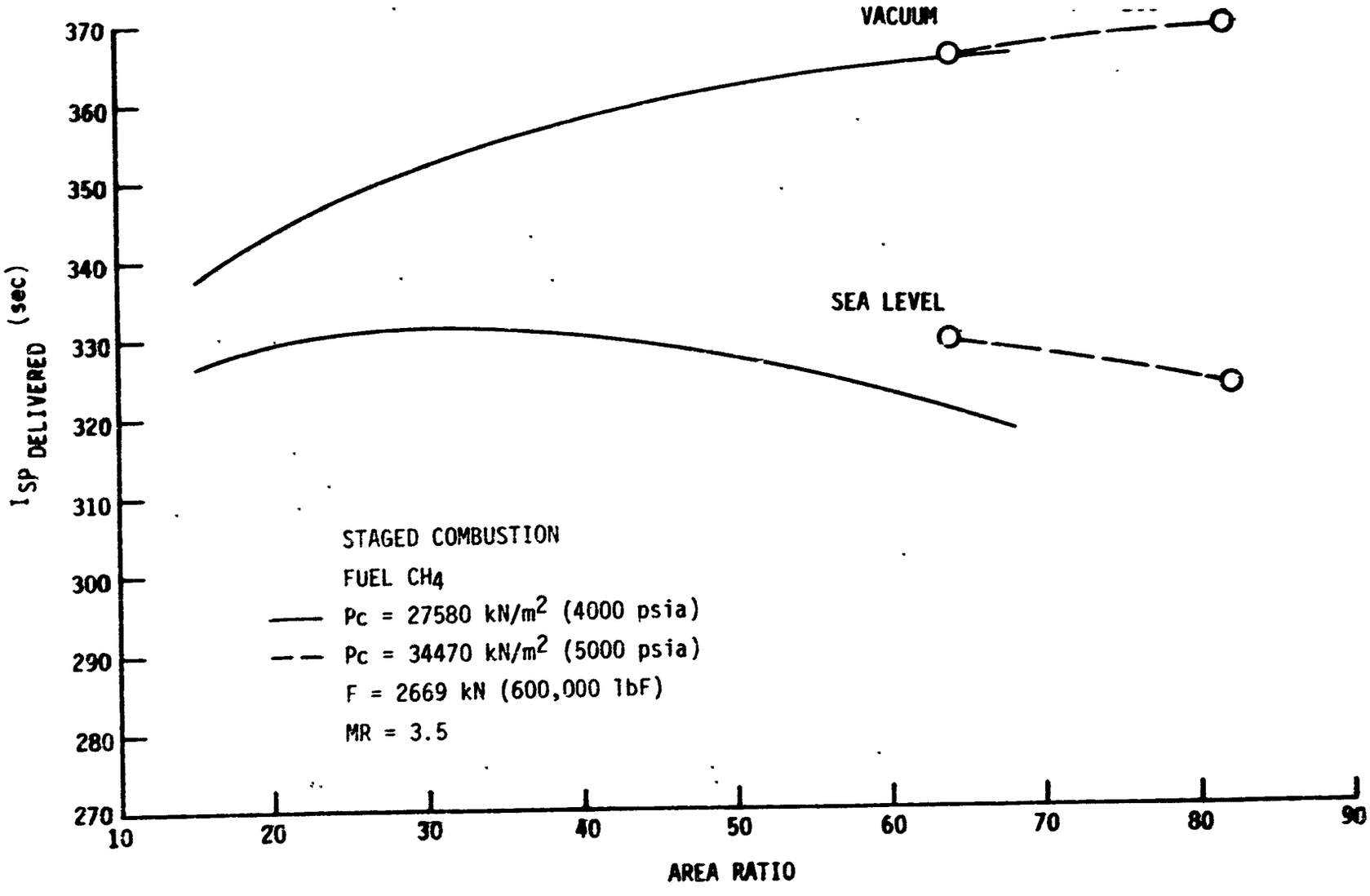

Figure 60. Delivered LOX/CH_4 Engine Performance Versus Area Ratio

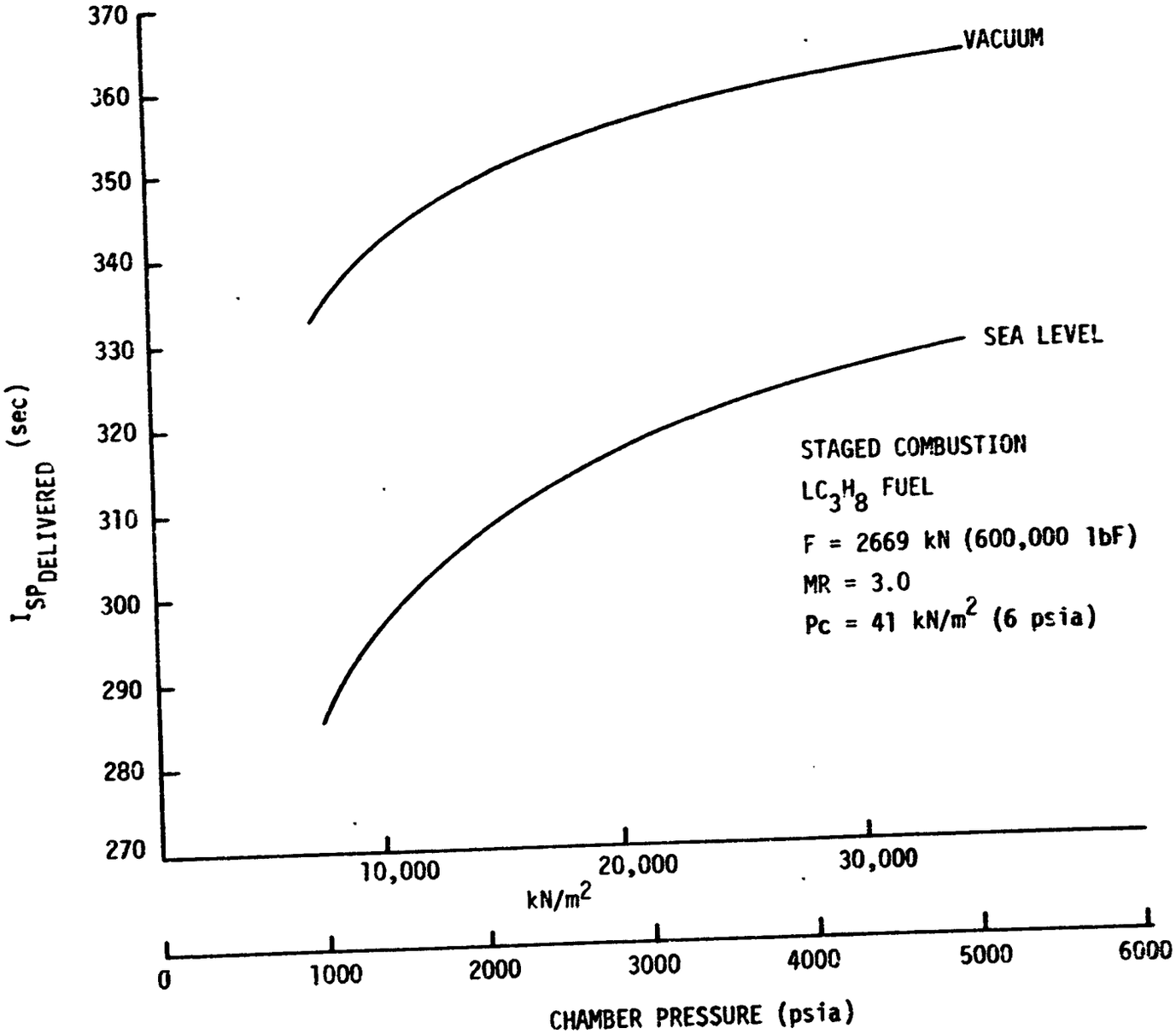

Figure 61. Delivered LOX/C_3H_8 Engine Performance Versus Chamber Pressure

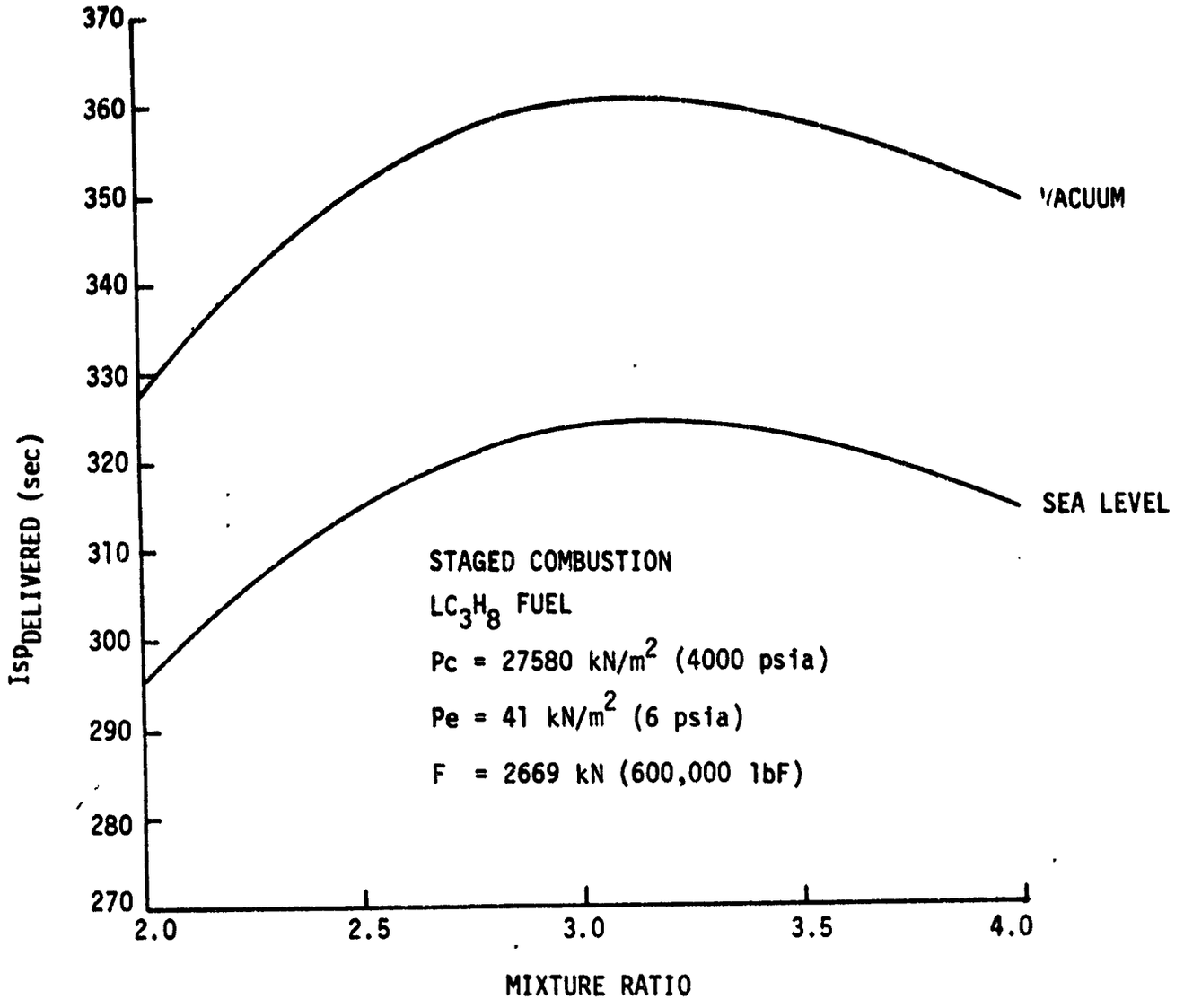

Figure 62. Delivered LOX/C_3H_8 Engine Performance Versus Mixture Ratio

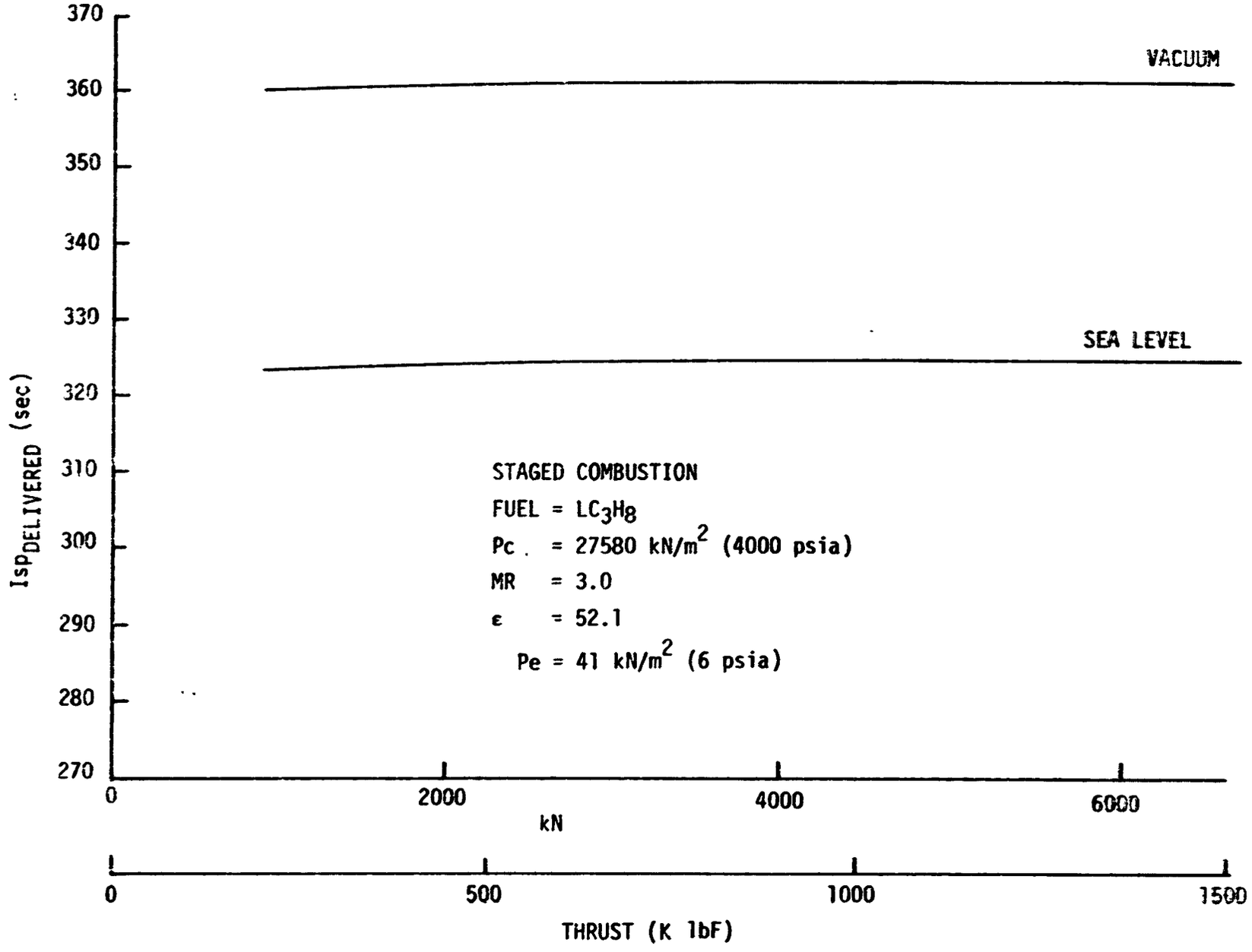

Figure 63. Delivered LOX/C_3H_8 Engine Performance Versus Thrust

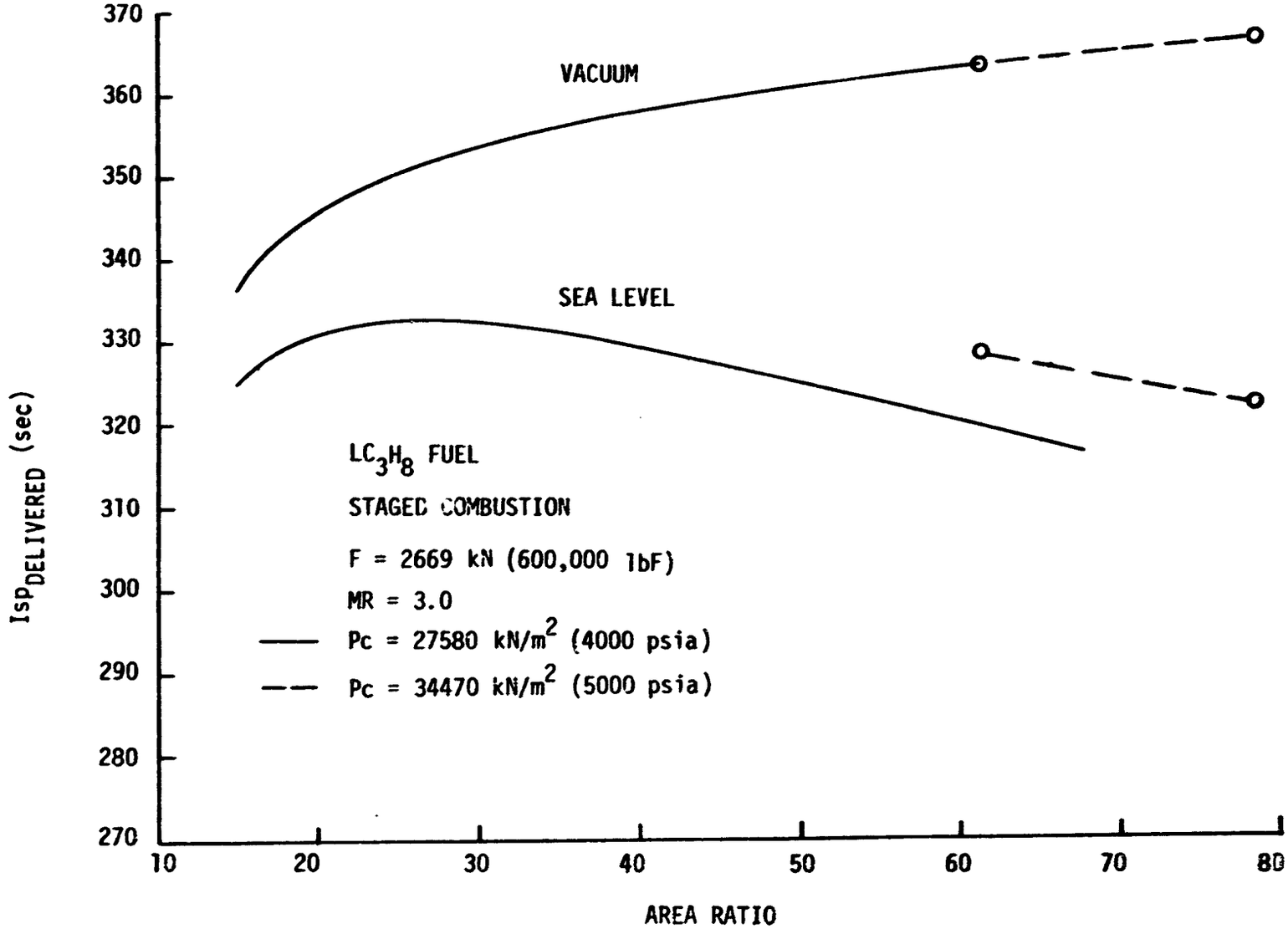

Figure 64. Delivered LOX/C_3H_8 Engine Performance Versus Area Ratio

The effect of area ratio on specific impulse is shown in Figures 56, 60, and 64 for the three fuels, respectively. The vacuum specific impulse increases with increasing area ratio for any chamber pressure. The sea level specific impulse, however, is maximized when the exit pressure is equal to the ambient pressure 101 kN/m^2 (14.7 psia). For each fuel, this point is reached at an area ratio of approximately 26:1 at a chamber pressure of 27580 kN/m^2 (4000 psia). Below this value, the combustion gases are underexpanded with respect to the ambient pressure, and thus performance increases with increasing area ratio. Conversely, above this value, the combustion gases are overexpanded with respect to the ambient pressure, and thus performance decreases with increasing area ratio. The area ratio for optimum sea level is, of course, a direct function of the chamber pressure and will increase with increasing Pc.

2. Dual-Throat Engine Performance

The previous analysis was for a conventional engine system. Engine performance was also predicted for the dual-throat engine configuration using LOX-methane in both the primary and secondary circuits. ALRC's Dual Throat Engine Performance and Geometry Program (FD 0169) was used to calculate engine performance. The program output is shown in Figure 65. During Mode I, the engine is similar to a conventional engine, thus its performance can be calculated by using the JANNAF simplified methodology. The Mode II performance was initially calculated by using the simplified methodology for a conventional nozzle and then modified as described in Reference 10.

The calculations shown in Figure 65 were made for an assumed chamber pressure of 19310 kN/m^2 (2800 psia) during Mode I (Boost Phase) and 27580 kN/m^2 (4000 psia) during Mode II (Sustainer Phase). The secondary area ratio (Mode I Effective Area Ratio) was fixed at 40:1 to provide an exit

AEROJET LIQUID ROCKET COMPANY

• • • DUAL THROAT ENGINE PERFORMANCE MODEL • • •

	MODE 1 - PARALLEL				MODE 2 (CONVENTIONAL NOZZLE)
	PRIMARY CHAMBER	SECONDARY CHAMBER			
	STREAM TUBE		MASS AVERAGED		
PROPELLANTS	C2/CH4	O2/CH4			O2/CH4
THRUST (SEA LEVEL), LBF	183166.3	416833.6	TOTAL =	600000.0	
THRUST (VACUUM), LBF	205822.7	468264.3	TOTAL =	674087.0	7854.6
PER CENT THRUST	30.5	69.5			
PC, PSIA	2798.5 EFFECTIVE	2800.0			4000.0
C/F	3.500	3.500			3.570
GAMMA	1.192	1.194			1.192
NOZZLE EXIT PRESSURE, PSIA	6.000	6.000			
NOZZLE AREA RATIO	40.11	39.93		39.98	166.75
CDE ISP (SEA LEVEL), SEC	330.9	331.1		331.0	
CDE ISP (VACUUM), SEC	370.8	370.7		370.7	385.3
DIVERGENCE EFFICIENCY	.9939	.9939			.9968
KINETICS EFFICIENCY	.9971	.9978			.9966
ENERGY RELEASE EFFICIENCY	.9850	.9850			.9850
BOUNDARY LAYER LOSS, SEC		1.3			2.0
DELIVERED ISP (SEA LEVEL), SEC	322.1	321.2		321.5	319.9*
DELIVERED ISP (VACUUM), SEC	361.9	360.8		361.2	
ISP EFFICIENCY (SEA LEVEL)	.9733	.9702		.9711	
ISP EFFICIENCY (VACUUM)	.9762	.9733		.9742	.9735
C-STAR, FT/SEC	6083.4	6083.4			6186.6
FUEL FLOW RATE, LBM/SEC	126.4	288.4			116.9
OXIDIZER FLOW RATE, LBM/SEC	442.3	1009.4			442.3
TOTAL FLOW RATE, LBM/SEC	568.7	1297.8		1866.5	558.7
THROAT RADIUS, IN	3.50	9.28		6.33	3.93
THROAT AREA, IN2	38.43	87.63		126.06	26.99
PER CENT BELL				90.0	93.7
R/RT				17.9	44.3
NOZZLE LENGTH, IN				113.3	129.8

MODE 1 TO MODE 2 THRUST SPLIT = 3.000
PRIMARY NOZZLE AREA RATIO = 2.595
SECONDARY NOZZLE CONVERGENCE LENGTH = 9.869
SECONDARY CONTRACTION RATIO = 2.554

*NOTE: Excluded additional bleed flow and two-dimensional flow losses associated with Mode II Operation

Figure 65. Dual-Throat Engine Performance

pressure of 41 kN/m^2 (6 psia). This resulted in an area ratio during Mode II operation of approximately 187:1. The following table shows the specific impulse values calculated for the dual-mode engine and compares them to the previously discussed conventional engine results.

	Dual-Mode Engine		Conventional Engine
	Mode I	Mode II	
Sea Level Specific Impulse, sec	331	N/A	331
Vacuum Specific, Impulse, sec	361	379	361

As seen, the dual-mode engine does offer a performance advantage under high-altitude operating conditions.

C. ENGINE WEIGHT

For the purpose of the parametric study, it was necessary to establish the elements of engine weight statements. Table XXVII lists the engine components included in the parametric analyses. Those items not included are also listed.

It was also necessary to establish preliminary baseline weight statements for a typical staged-combustion cycle and for a typical gas-generator cycle engine. These are presented in Table XXVIII for both LO_2/RP-1 and for LO_2/LCH_4 engines. The component weights were based on scaling of historical weights of similar components and/or estimates obtained from conceptual designs such as those given in References 9 and 10.

TABLE XXVII

ENGINE WEIGHT DEFINITION

Included	Not Included
Regeneratively Cooled Combustion Chamber	Gimbal Actuators and Actuation
Regeneratively Cooled Thrust Chamber Nozzle(s)	Pre-Valves
Thrust Chamber Nozzle Extension	Contingency (a total contingency is normally included in the vehicle weight statement)
Main Injector	
Main Turbopumps	
Boost Pumps	
Preburners (or Gas Generator)	
Propellant Valves and Actuation	
Gimbal	
Hot-Gas Manifold (if required)	
Propellant Lines	
Ignition System	
Miscellaneous (Electrical Harness, Instrumentation, Brackets, Auxiliary Lines and Controls)	
Engine Controller	
Tank Pressurant Heat Exchangers and Associated Equipment	

TABLE XXVIII

LOX/HC BASELINE ENGINE WEIGHT BREAKDOWN

	LOX/RP-1		LOX/CH_4	
	STAGED COMBUSTION	GAS GENERATOR	STAGED COMBUSTION	GAS GENERATOR
F_B (Thrust, lb)	600,000	600,000	600,000	600,000
P_{C_B} (Chamber Pressure, psia)	4000	4000	4000	4000
ϵ_B (Area Ratio)	50:1	50:1	50:1	50:1
ϵ_{ATTB} (Attached Area Ratio)	8:1	8:1	8:1	8:1
A_{TB} (Throat Area, $in.^2$)	85.66	85.66	86.14	86.14
(All Weights in lbs)				
WGR (Gimbal	207	207	207	207
WMISCB (Miscellaneous)	296	296	296	296
WINJB (Injector)	656	656	656	656
WTCNB (Nozzle)	420	420	422	422
WCCB (Thrust Chamber)	226	226	227	227
WPBOB (Ox-Rich Preburner)	224	-	224	-
WPBFB (Fuel-Rich Preburner)	181	50	181	51
WVOB (Oxidizer Valves & Actuators)	325	325	331	331
WVFB (Fuel Valves & Actuators)	82	82	131	131
WBPOB (Oxidizer Boost Pump)	307	307	313	313
WBPFB (Fuel Boost Pump)	52	52	83	83
WMPOB (Main Oxidizer Pump)	862	623	878	638
WMPFB (Main Fuel Pump)	327	366	521	567
WLPLB (Low-Pressure Lines)	201	201	243	243
WHPLB (High-Pressure Lines)	268	268	324	324
WPSSB (Pressurization System)	133	133	133	133
WHGMB (Hot-Gas Manifold)	207	207	207	207
WIGNB (Igniters)	60	60	60	60
WCNTRB (Controller)	130	130	130	130
TOTAL	5164	4609	5567	5019

IV, C, Engine Weight (cont.)

With the preliminary baseline engine weight statements established, engine component weight scaling relationships were derived as functions of thrust, chamber pressure, and nozzle are ratio. These scaling relationships, used to calculate the weights over the parametric ranges of interest, are similar to those given in Reference 10. The scaling equations were established through geometry considerations and empirical data fits of historical data. The engine weights derived from the equations represent 1979 state-of-the-art technology, as indicated in Figure 66. The highest thrust-to-weight engine (141 at 600K lbF) shown in the figure is for a LO_2/RP-1 gas-generator cycle engine. This compares well with the 1960's technology Titan I and Atlas booster (1st-stage) engines.

The lowest thrust-to-weight engine (108 at 600K lbF) derived from this study represents the dual-throat engine cycle K. As can be seen by examining Figure 66, the band of (AOHRES) engines from this study follows the trend of the historical engines, and, if anything, is too conservative for 1979 technology.

Scaling relationships based on volumetric flowrates and pump discharge pressures were used to obtain an estimate of the variation in engine weight with power cycle. This evaluation primarily involved turbopumps and preburners (gas generators). The resultant variation in engine weight with power cycle is shown in Figure 67. The lightest-weight engine is seen to be the LOX-cooled gas-generator cycle B, and the heaviest engine is seen to be the dual-throat engine cycle K.

1. 1979 State-of-the-Art Engine Weight Parametrics

Because most of the cycles studied are similar, as are the weight trends with chamber pressure, thrust, etc., parametric data are presented only for a typical gas-generator cycle engine. A sample computer output for this engine (an LO_2/RP-1, fuel-rich gas-generator, RP-1-cooled,

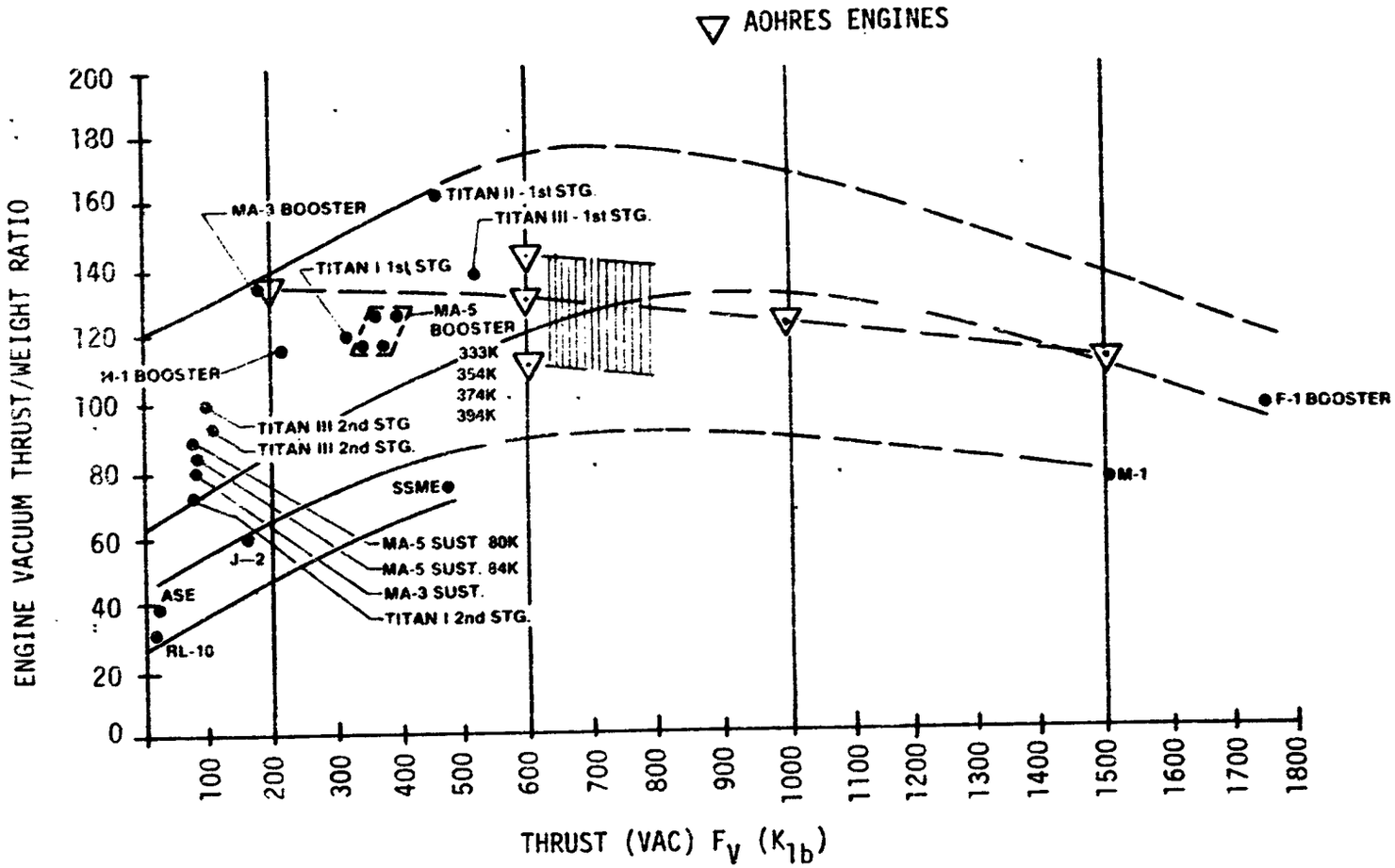

Figure 66. Engine Weight Comparison with Historical Data

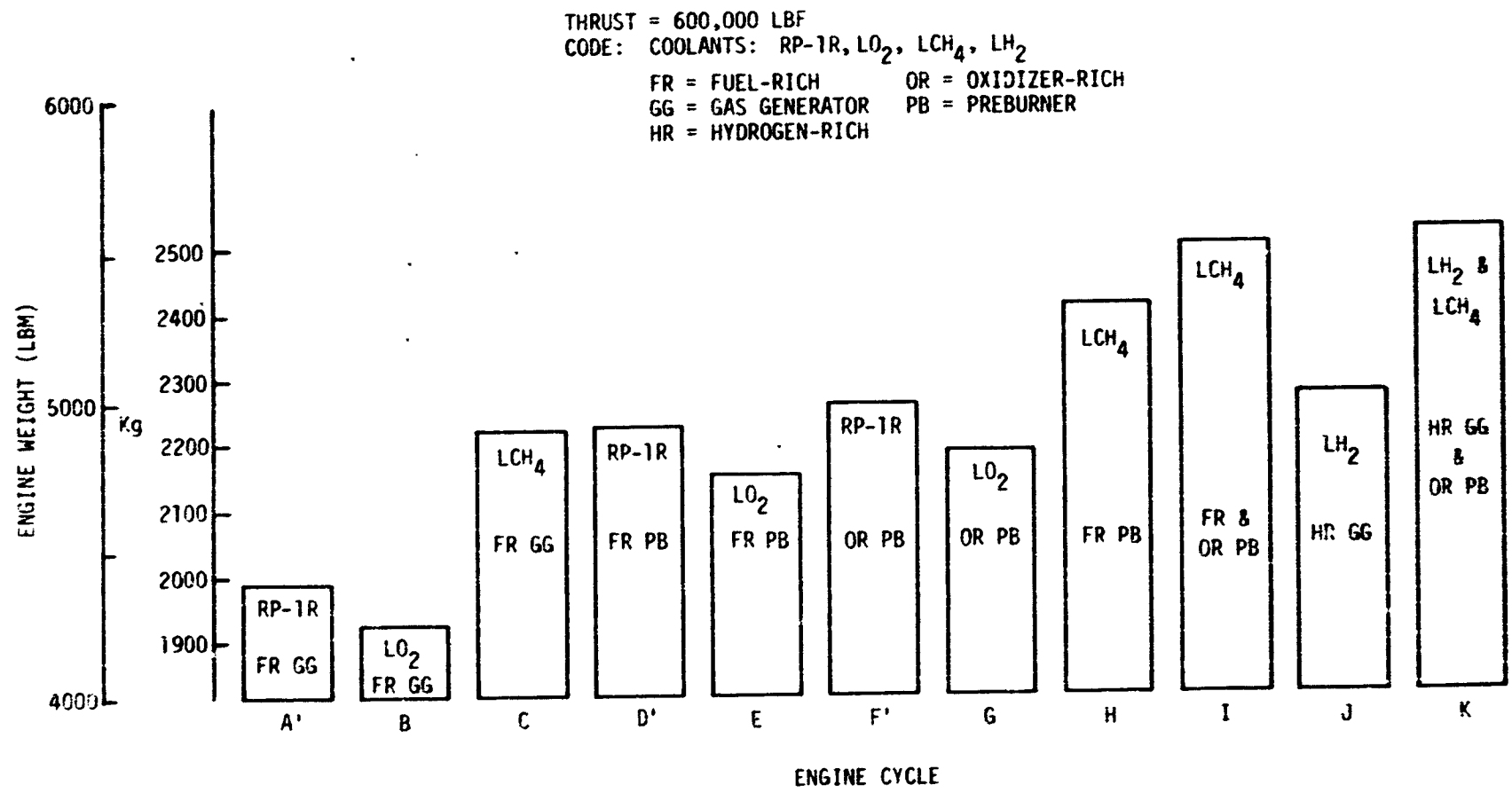

Figure 67. Preliminary Weight Ranking of LO_2/HC Engine Cycles

cycle A engine) is illustrated in Figure 68. The parametric engine weight data are summarized in Figures 69 through 77.

Engine weight data for the corresponding LO_2/LCH_4 gas-generator cycle C engine are presented in Figures 78 through 86.

2. Selected Cycle Engine Weight Statements

Three engine cycles were selected for preliminary design analysis in Task IV. These cycles are C, G, and I. In addition, the LO_2/LC_3H_8 propellant combination was included in the Task IV studies. This section summarizes the baseline engine weights established for these six engine cycles.

The nominal point design engine weight breakdown for each of the LO_2/LCH_4 cycle C, the LO_2/RP-1 cycle G, and the LO_2/LCH_4 cycle I engines is given in Table XXIX. The corresponding weight breakdown for the LO_2/LC_3H_8 engine cycles C',G', and I' is given in Table XXX. Parametric weight data for the LO_2/LC_3H_8 engine cycles are depicted in Figures 87 and 88. It is seen in Figure 87 that the engine weight is at a minimum at about 13790 kN/m^2 (2000 psia) chamber pressure. A similar result was seen with methane at a low area ratio in Figure 78. The more dense fuel RP-1 has its minimum weight at a slightly higher chamber pressure, as seen in Figure 69.

The engine weights given in Tables XXIX and XXX reflect more accurate component weights than those used in the preliminary weight analysis given in Table XXVIII. The engine weights, however, still fall inside the band of AOHRES engine weights illustrated in Figure 66.

ADVANCED OXYGEN HYDROCARBON BOOSTER ENGINE WEIGHT AND ENVELOPE

THRUST	(LBF)	[illegible]0000.00	(NEWTONS)	2668800.00
CHAMBER PRESSURE	(PSIA)	4000.00	(NEWTONS/M**2)	27580000.00
AREA RATIO				53.00

PROPELLANT COMBINATION 1
1=LO2/RP-1. 2=LO2/CH4.

COOLANT TYPE 1
- ICOOL=1 RP-1 COOLED
- ICOOL=2 LH2 COOLED
- ICOOL=3 LO2 COOLED
- ICOOL=4 CH4 COOLED

CYCLE TYPE 1
- ICYCLE=1 FUEL RICH GAS GENERATOR (RP-1 OR CH4)
- ICYCLE=2 FUEL RICH GAS GENERATOR (LH2)
- ICYCLE=3 FUEL RICH STAGED COMBUSTION
- ICYCLE=4 OXIDIZER RICH STAGED COMBUSTION
- ICYCLE=5 EXPANDER BLEED
- ICYCLE=6 MIXED - OX RICH-FUEL RICH PREBURNERS
- ICYCLE=7 STAGED COMBUSTION - 1 PREBURNER
- ICYCLE=8 STAGED COMBUSTION - 2 PREBURNERS
- ICYCLE=9 STAGED COMBUSTION - 3 PREBURNERS
- ICYCLE=10 STAGED COMBUSTION /EXPANDER BLEED

	(LB)	(KG)
GIMBAL	[illegible]	93.9
INJECTOR	[illegible]	297.6
COMBUSTION CHAMBER	[illegible]	102.4
THRUST CHAMBER NOZZLE	[illegible]	190.5
CONTROLLER	[illegible]	59.0
OX RICH PREBURNER	.0	.0
FUEL RICH PREBURNER	[illegible]	22.7
OX VALVE	[illegible]	147.4
FUEL VALVE	[illegible]	37.2
FUEL BOOST PUMP	[illegible]	23.5
OXIDIZER BOOST PUMP	[illegible]	139.3
FUEL MAIN PUMP	[illegible]	166.0
OX MAIN PUMP	[illegible]	282.6
LOW PRESSURE LINE	[illegible]	91.?
HIGH PRESSURE LINE	[illegible]	121.5
IGNITER	[illegible]	27.2
HOT GAS MANIFOLD	[illegible]	93.9
MISCELLANEOUS WEIGHTS	[illegible]	134.3
PRESSURE SYSTEM	[illegible]	60.?
TOTAL ENGINE WEIGHT	[illegible]	2090.?

ENGINE THRUST TO WEIGHT RATIO 1?0.?

	(INCHES)	(METERS)
NOZZLE LENGTH	[illegible]	2.7
GIMBAL LENGTH	[illegible]	.3
CHAMBER LENGTH	[illegible]	.2
INJECTOR LENGTH	[illegible]	.2
IGNITER LENGTH	4.0	.1
TOTAL ENGINE LENGTH	[illegible]	3.?
NOZZLE EXIT DIAMETER	[illegible]	1.9

Figure 68. Typical AOHCWT Weight and Envelope Computer Program Printout

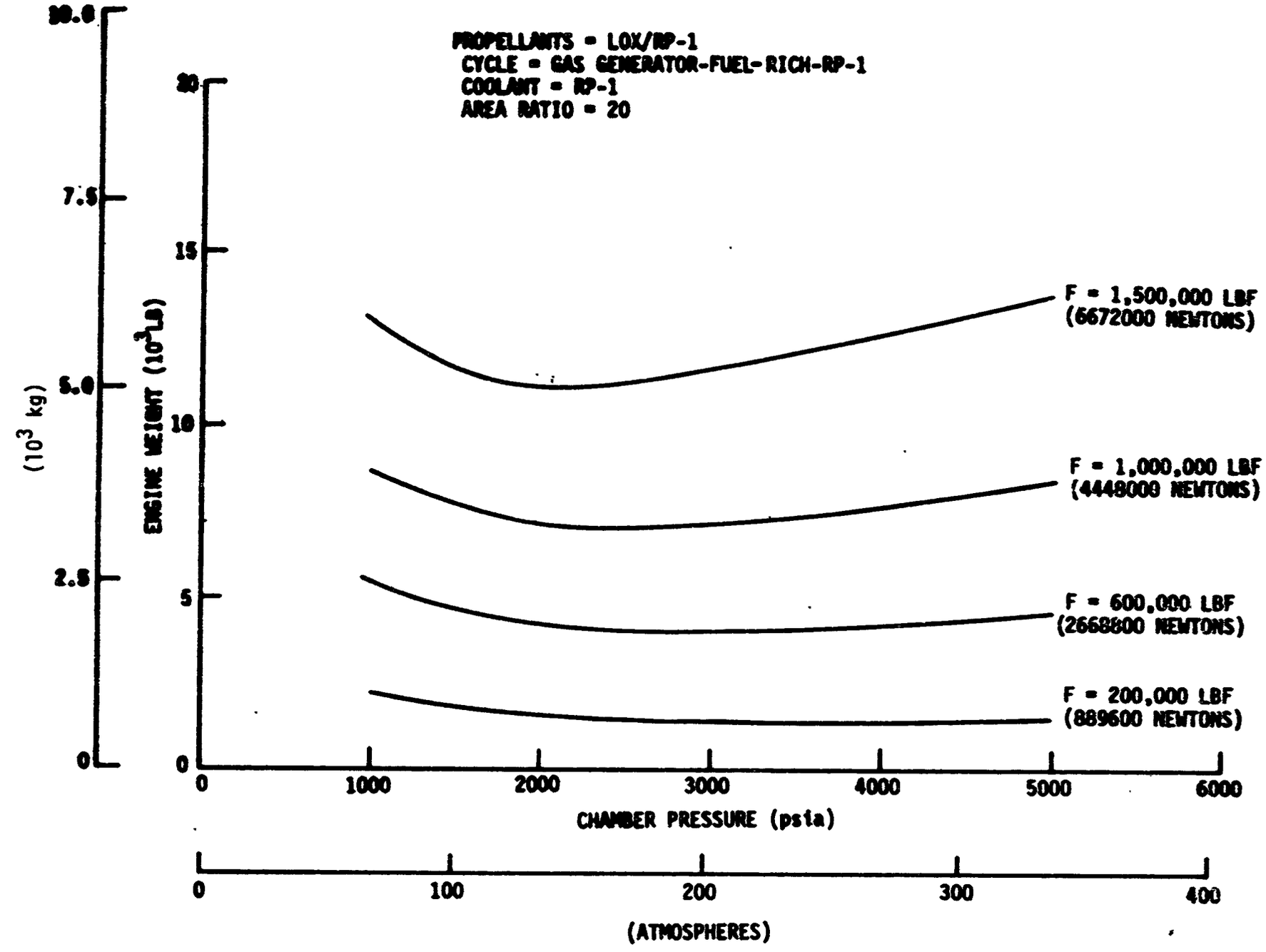

Figure 69. LOX/RP-1 Engine Weight Versus Chamber Pressure (ϵ = 20)

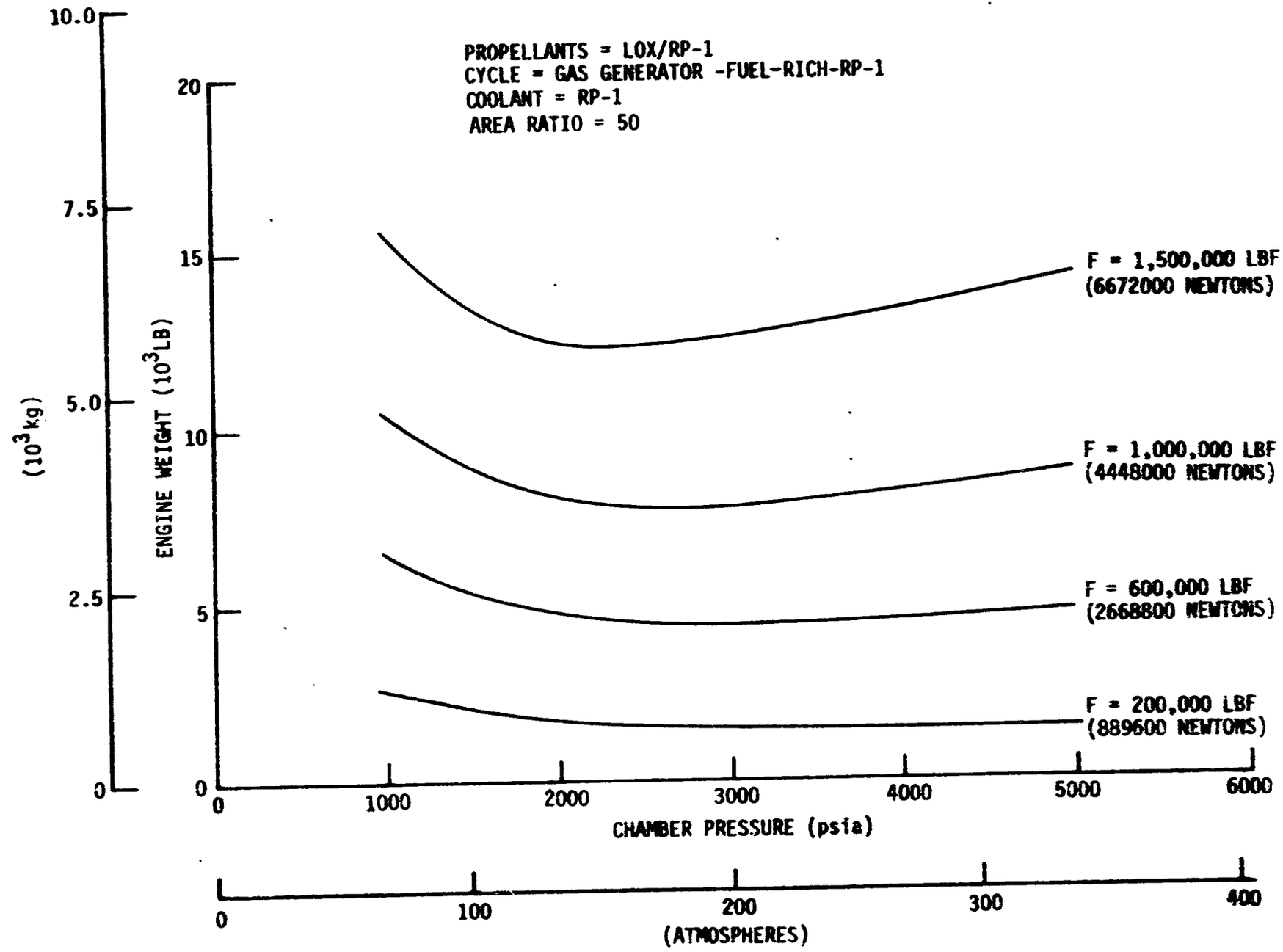

Figure 70. LOX/RP-1 Engine Weight Versus Chamber Pressure (ϵ = 50)

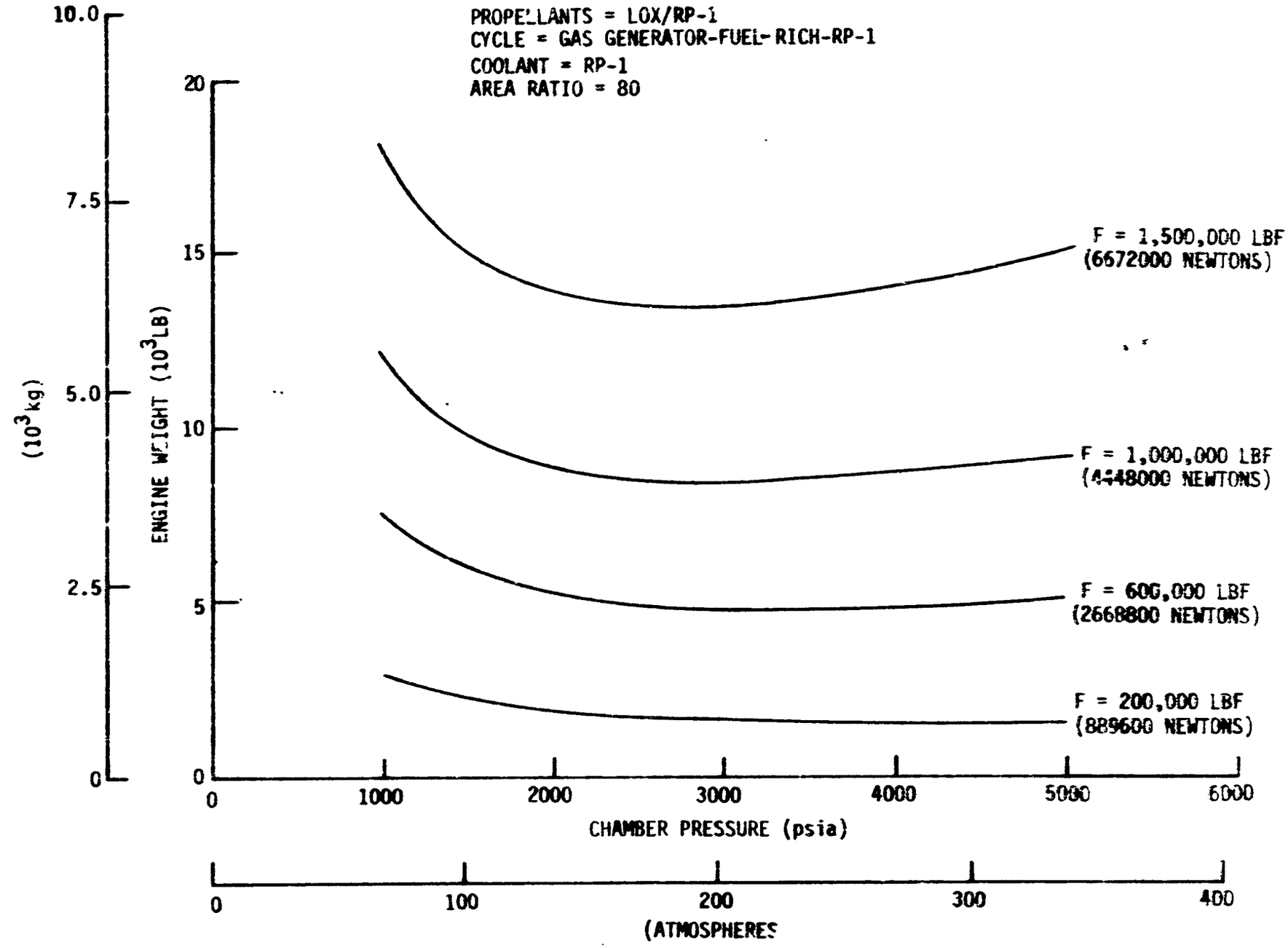

Figure 71. LOX/RP-1 Engine Weight Versus Chamber Pressure (ε = 80)

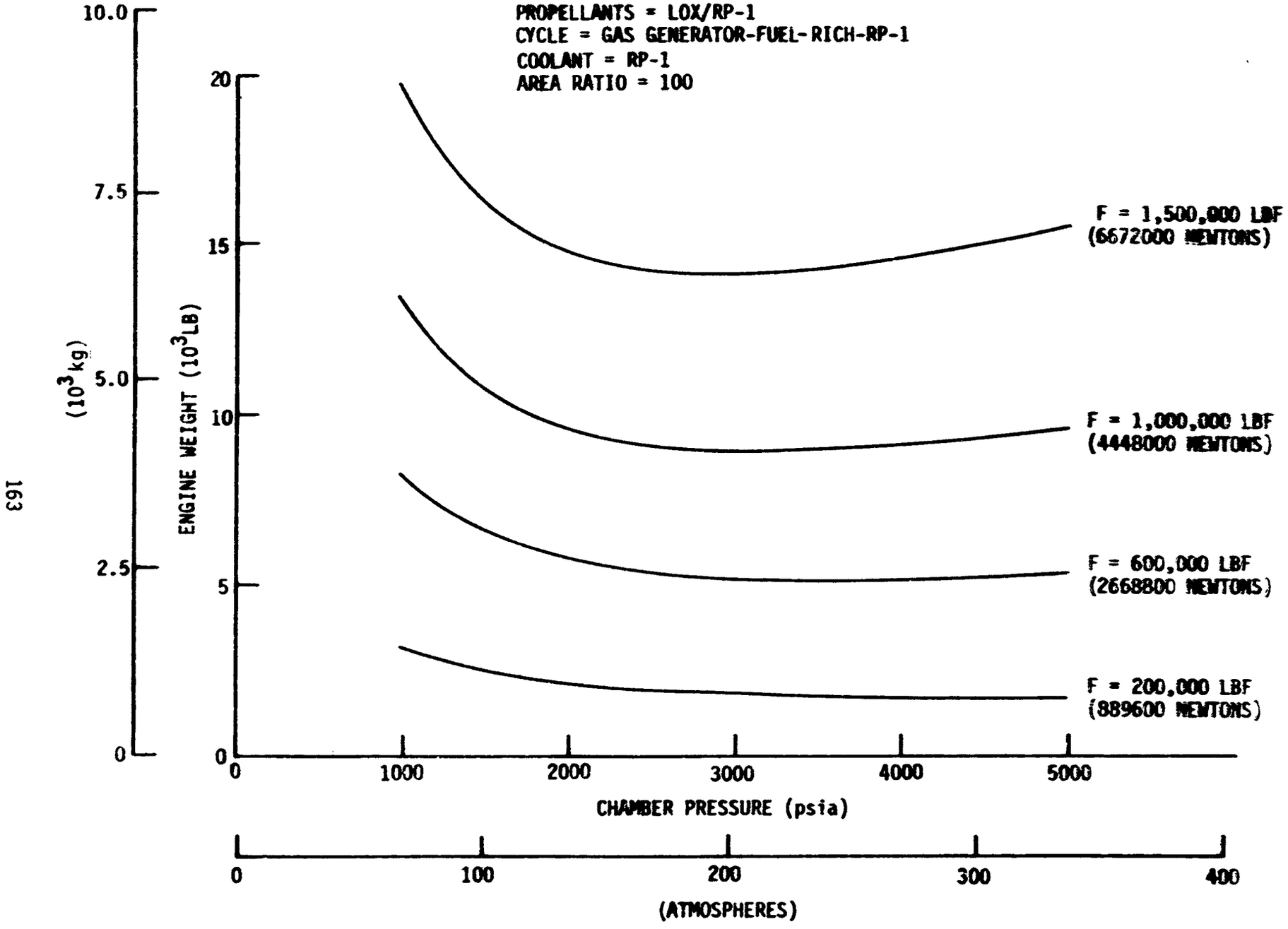

Figure 72. LOX/RP-1 Engine Weight Versus Chamber Pressure (ε = 100)

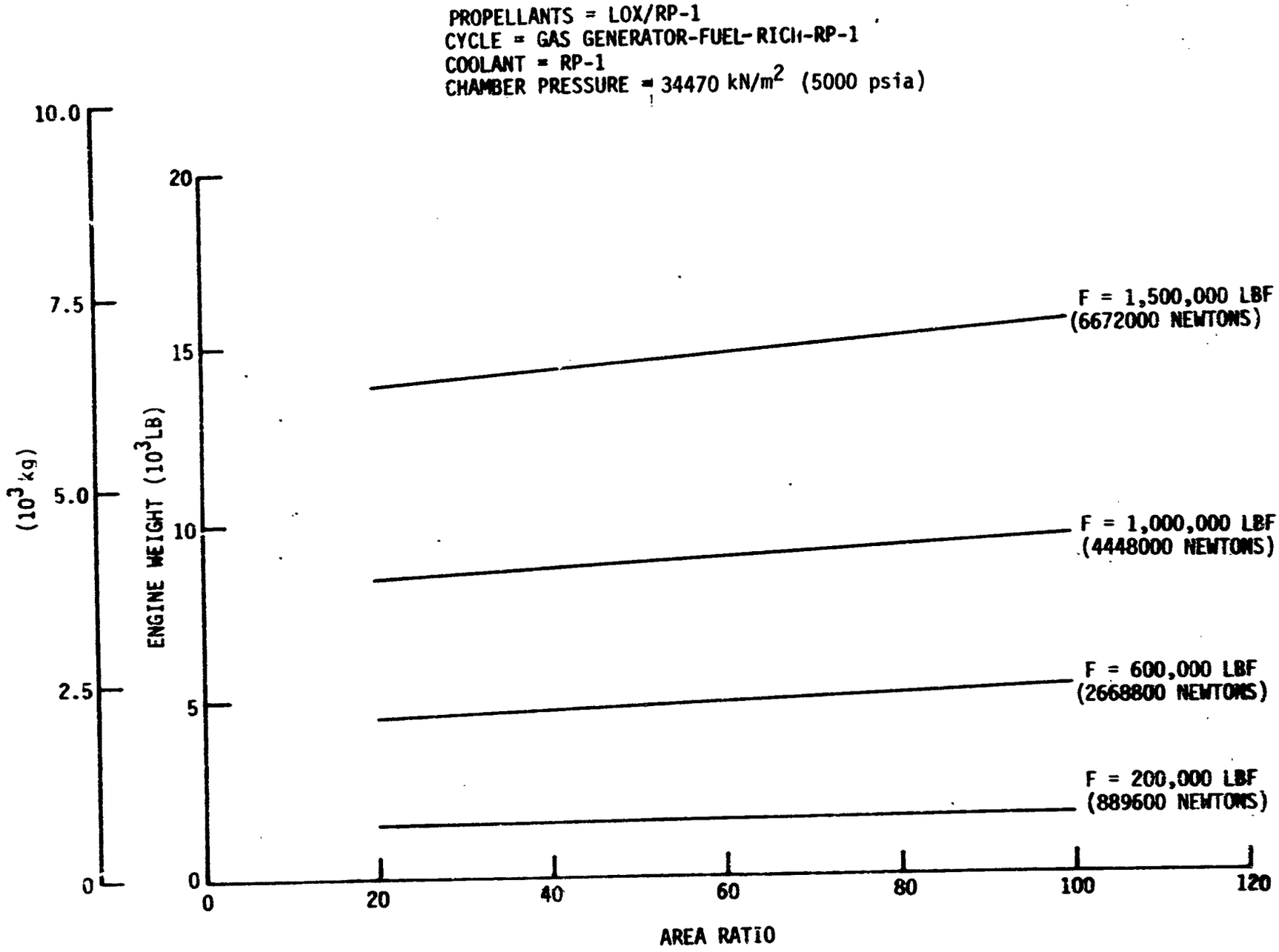

Figure 73. LOX/RP-1 Engine Weight Versus Area Ratio (Pc = 5000)

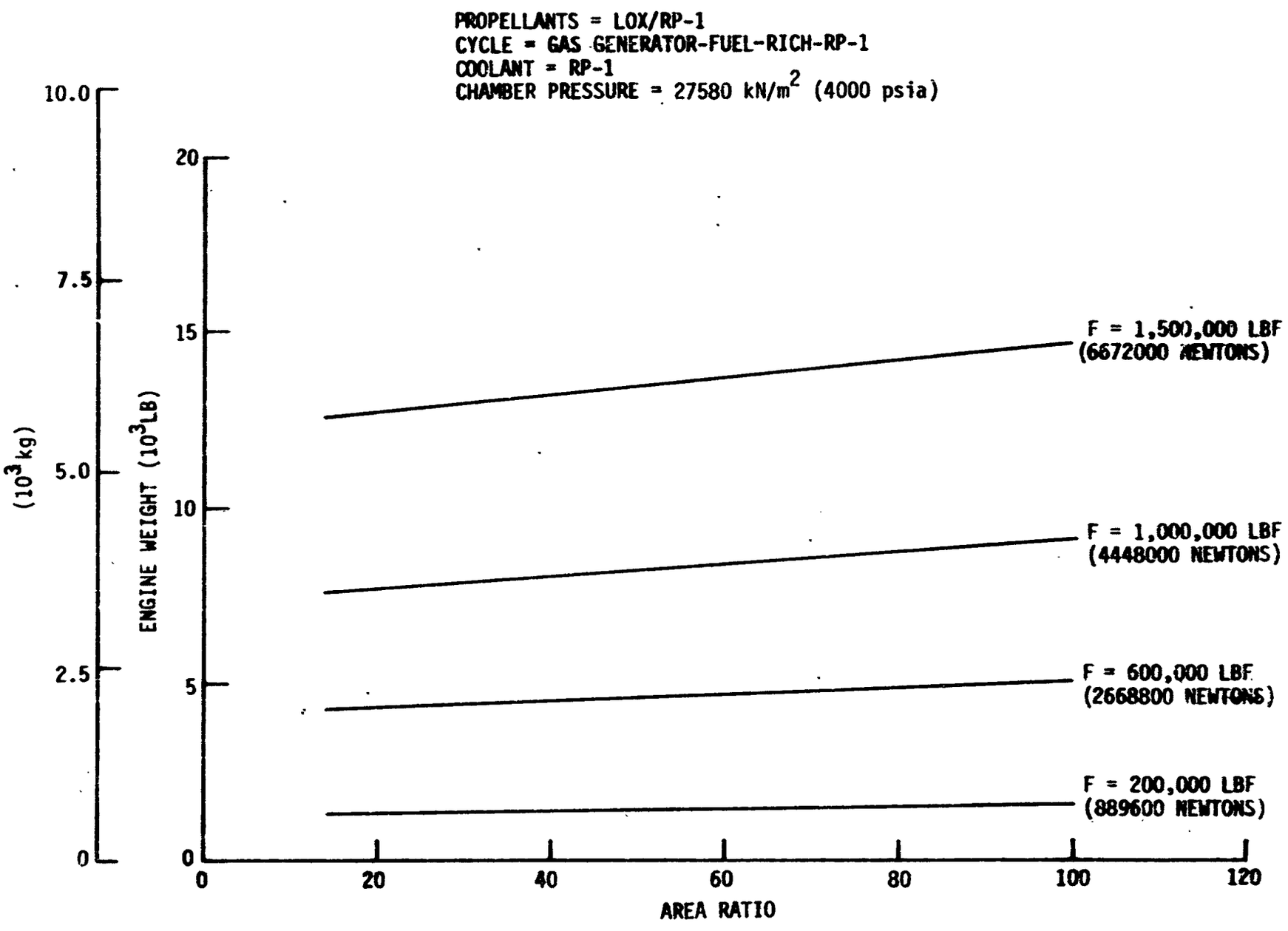

Figure 74. LOX/RP-1 Engine Weight Versus Area Ratio (Pc = 4000)

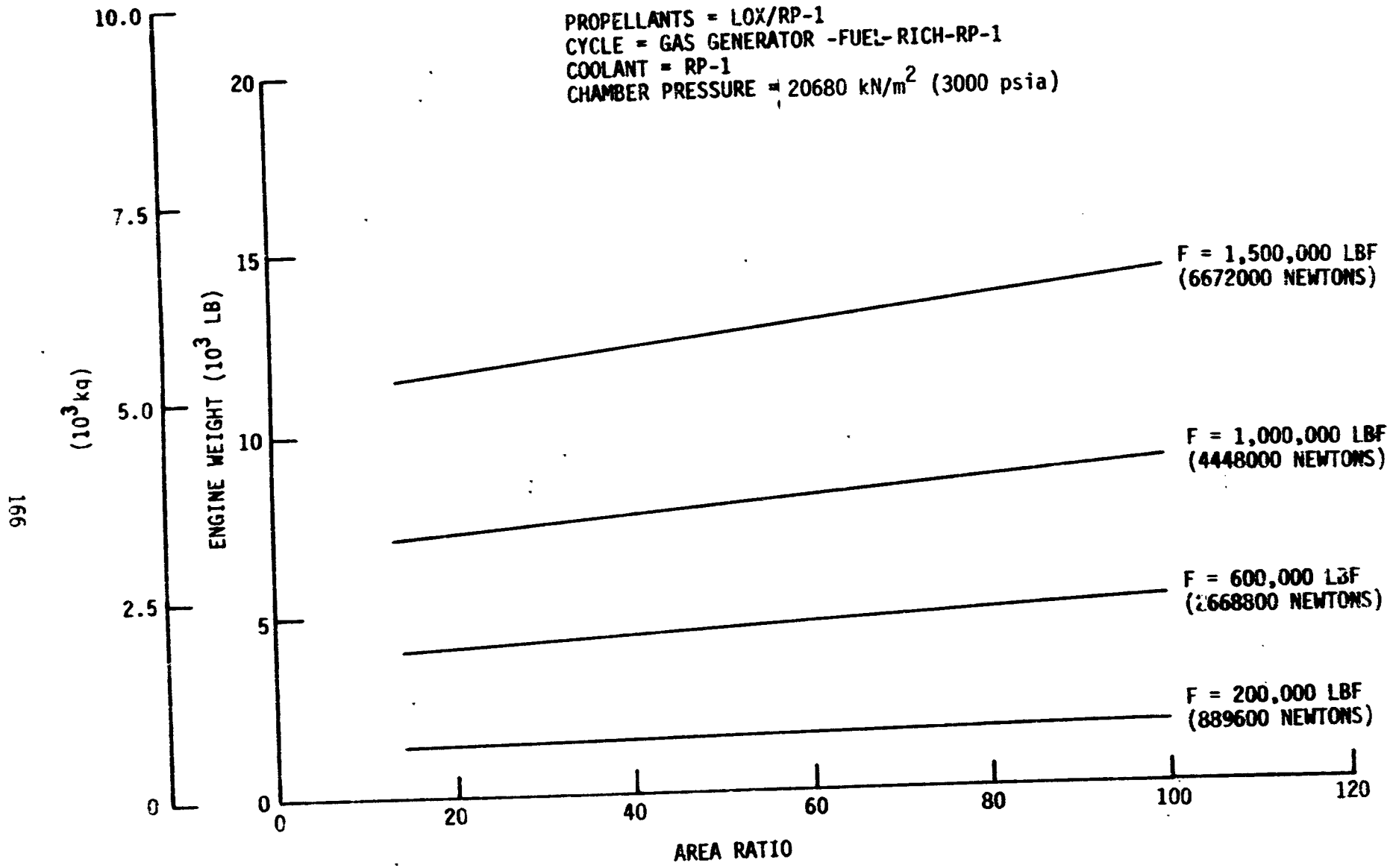

Figure 75. LOX/RP-1 Engine Weight Versus Area Ratio (Pc = 3000)

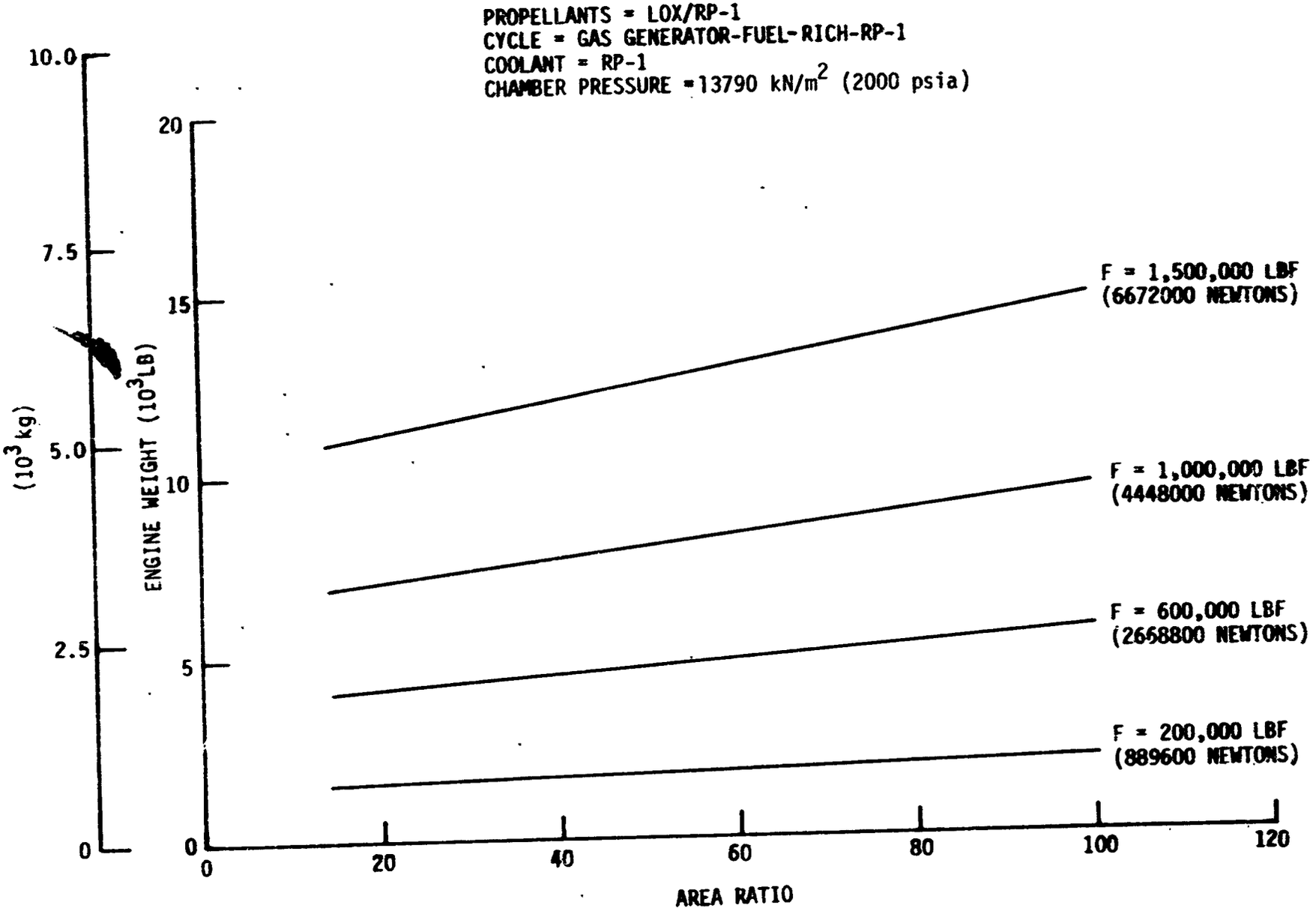

Figure 76. LOX/RP-1 Engine Weight Versus Area Ratio (Pc = 2000)

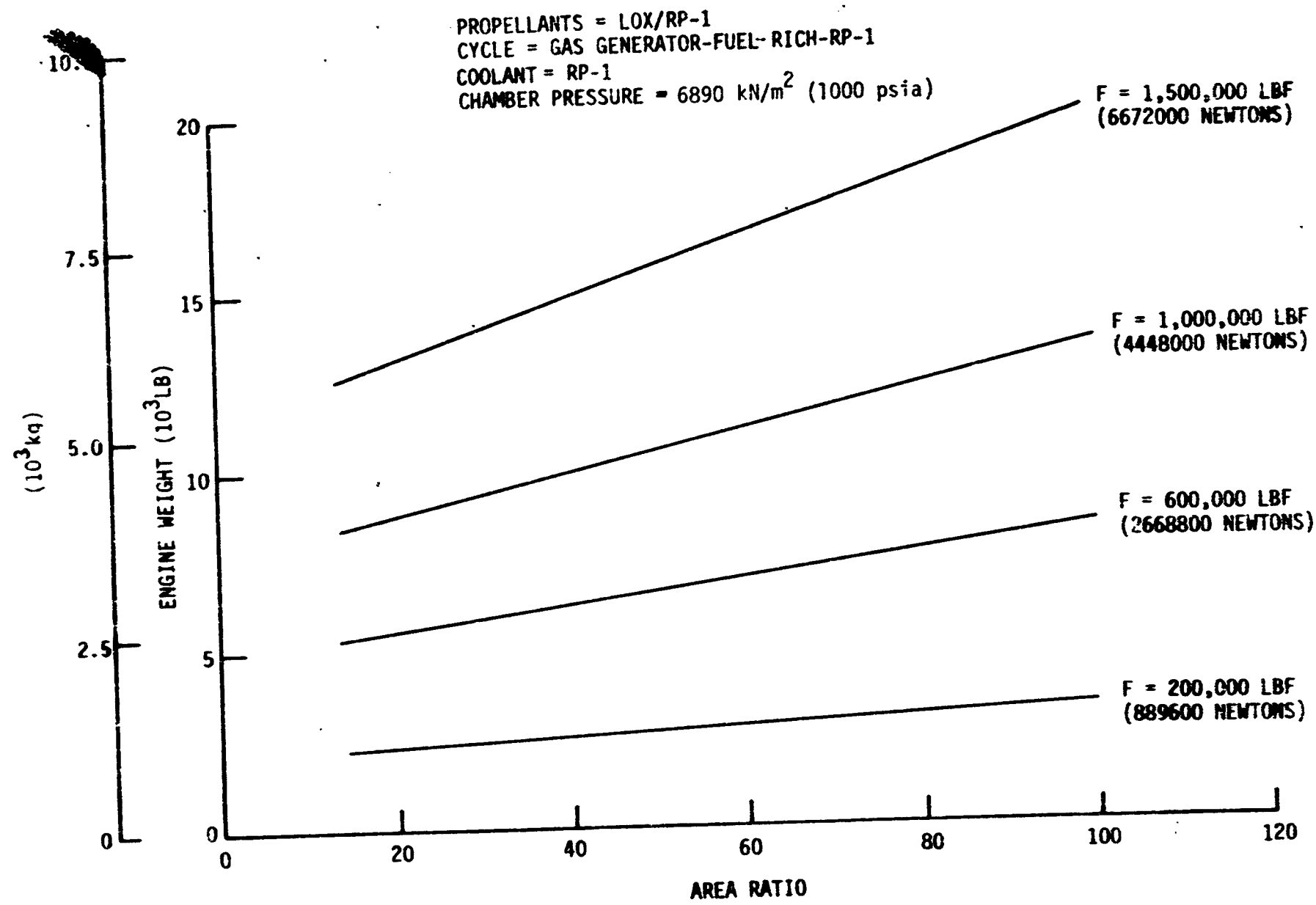

Figure 77. LOX/RP-1 Engine Weight Versus Area Ratio (Pc = 1000)

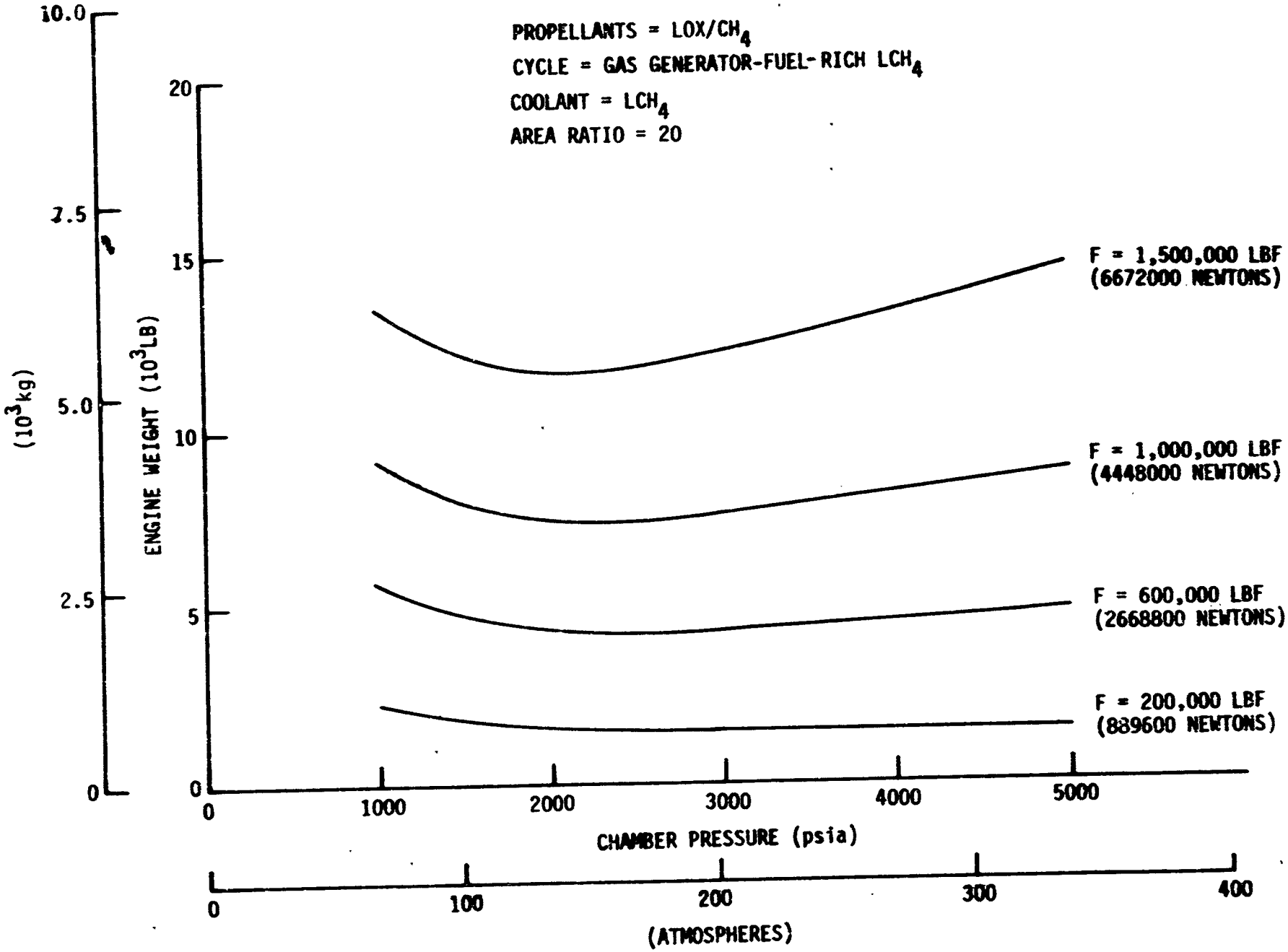

Figure 78. LOX/CH_4 Engine Weight Versus Chamber Pressure (ε = 20)

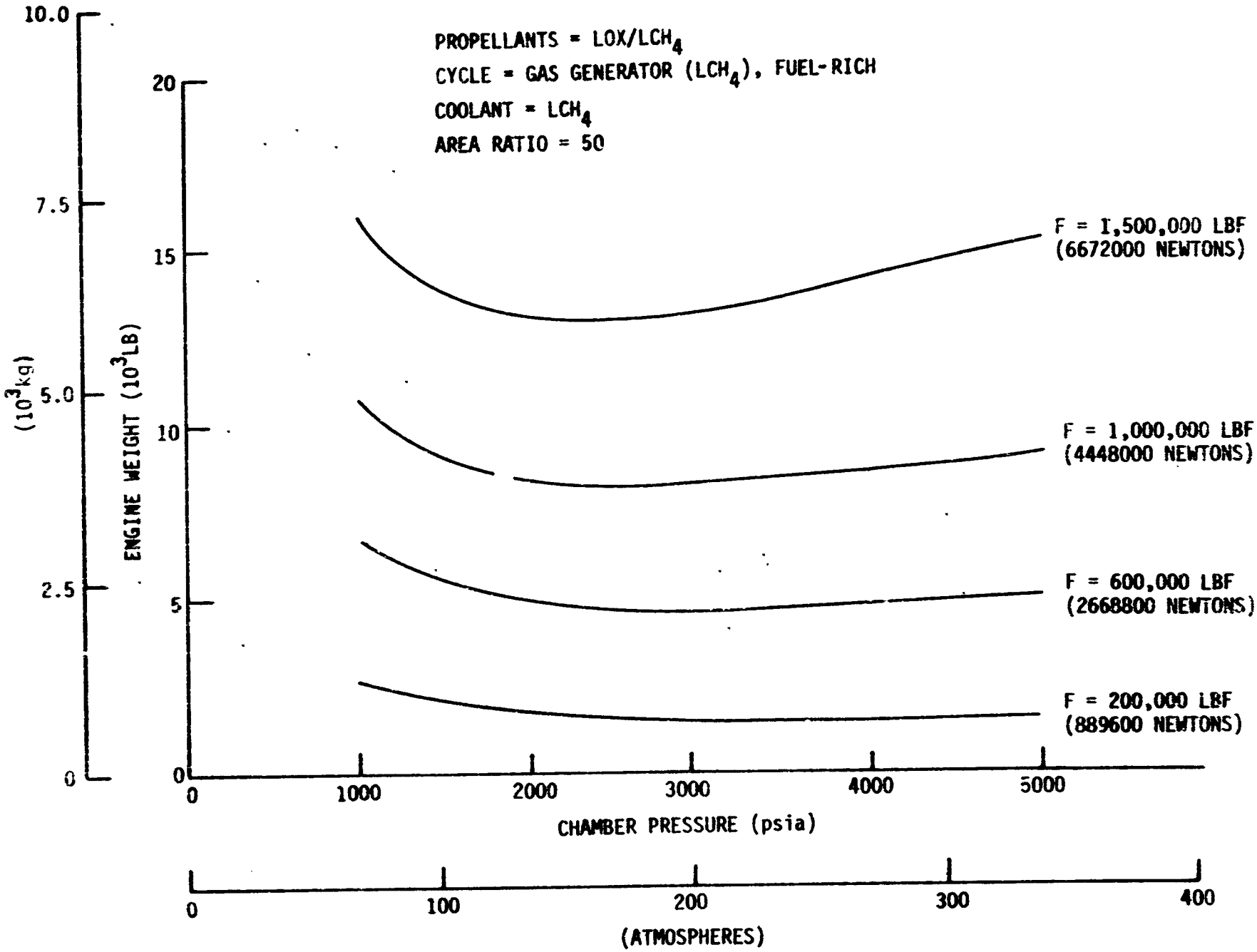

Figure 79. LOX/CH_4 Engine Weight Versus Chamber Pressure (ε = 50)

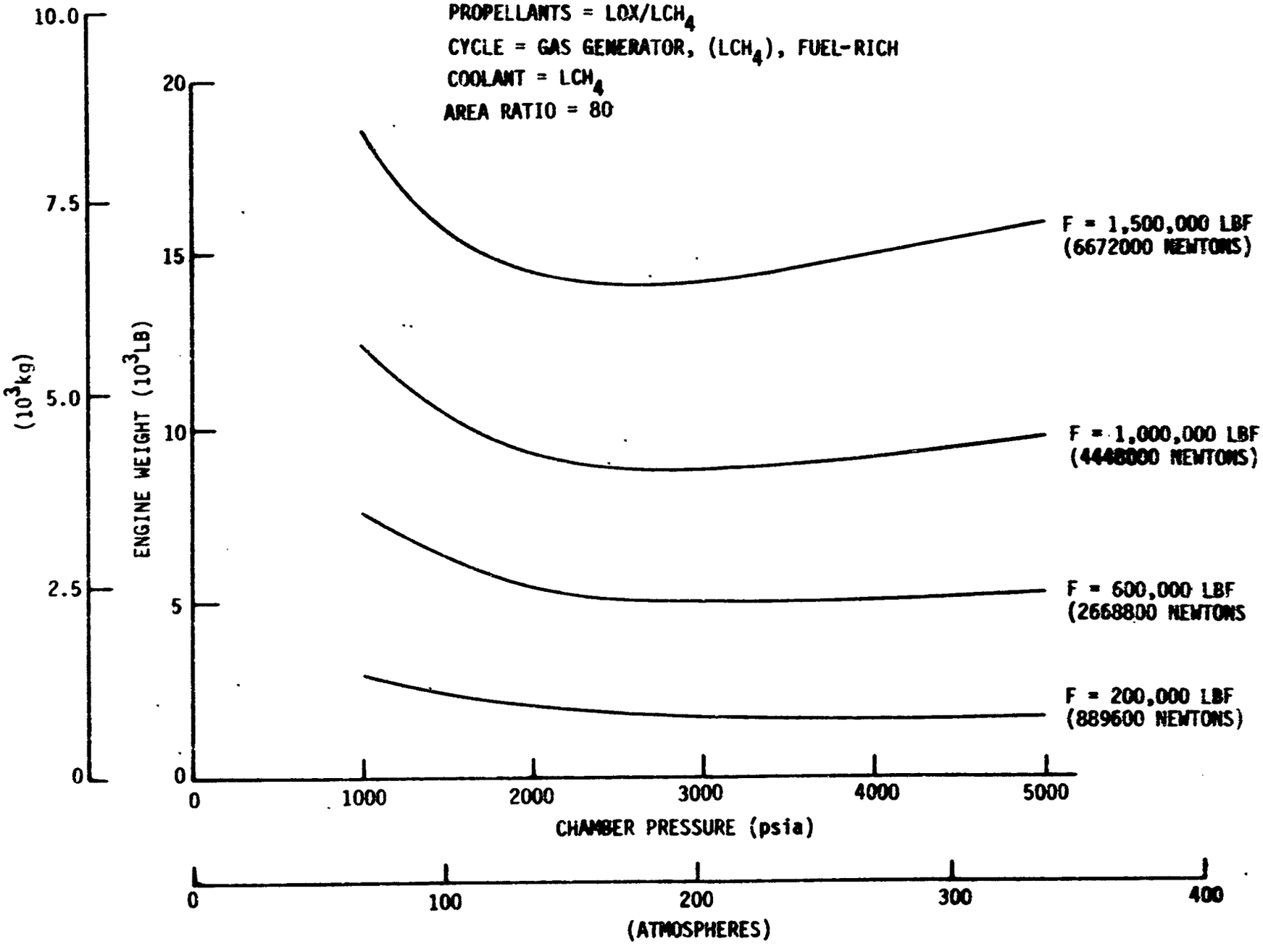

Figure 80. LOX/CH_4 Engine Weight Versus Chamber Pressure (ε = 8

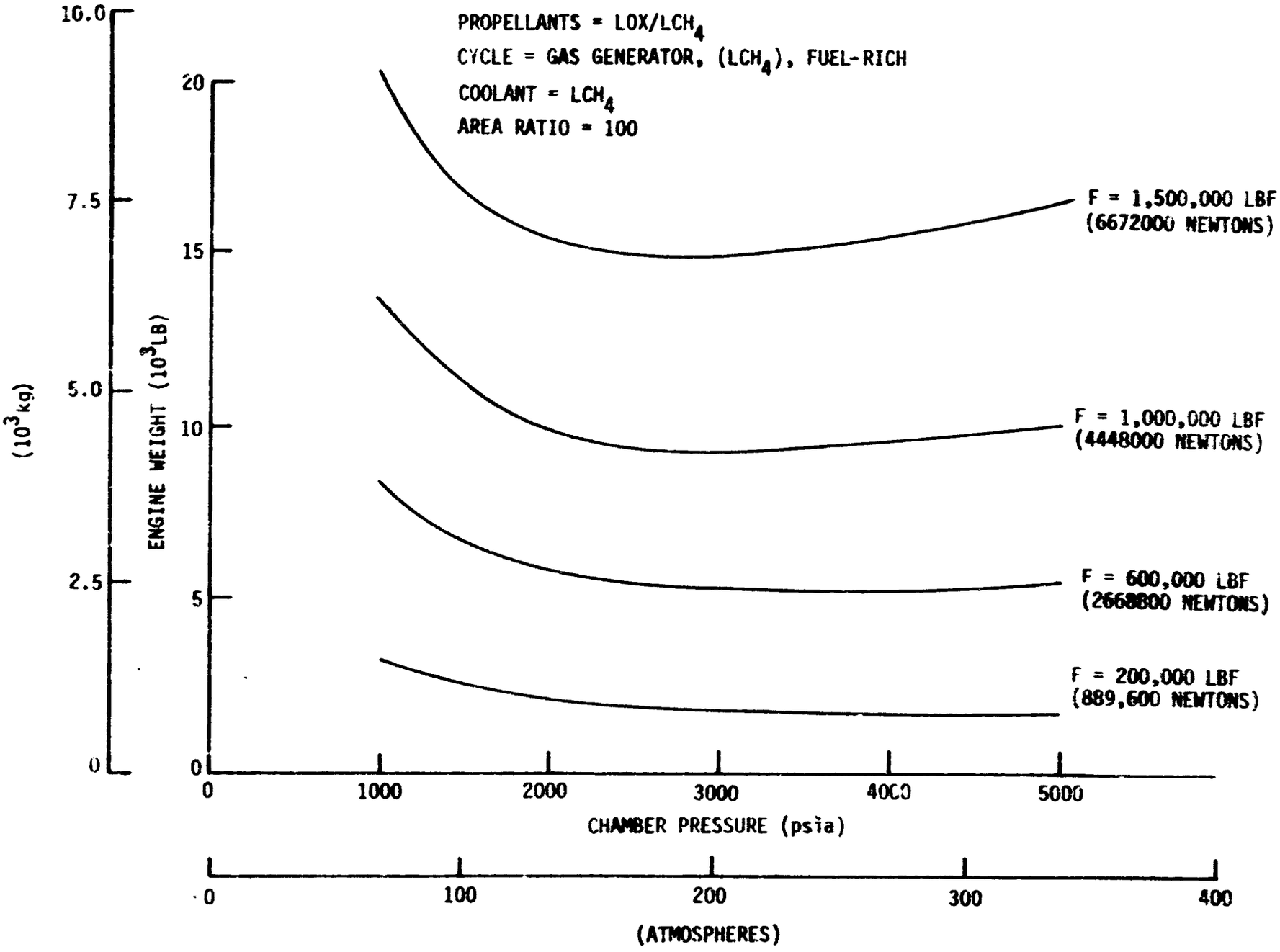

Figure 81. LOX/CH_4 Engine Weight Versus Chamber Pressure (ε = 100)

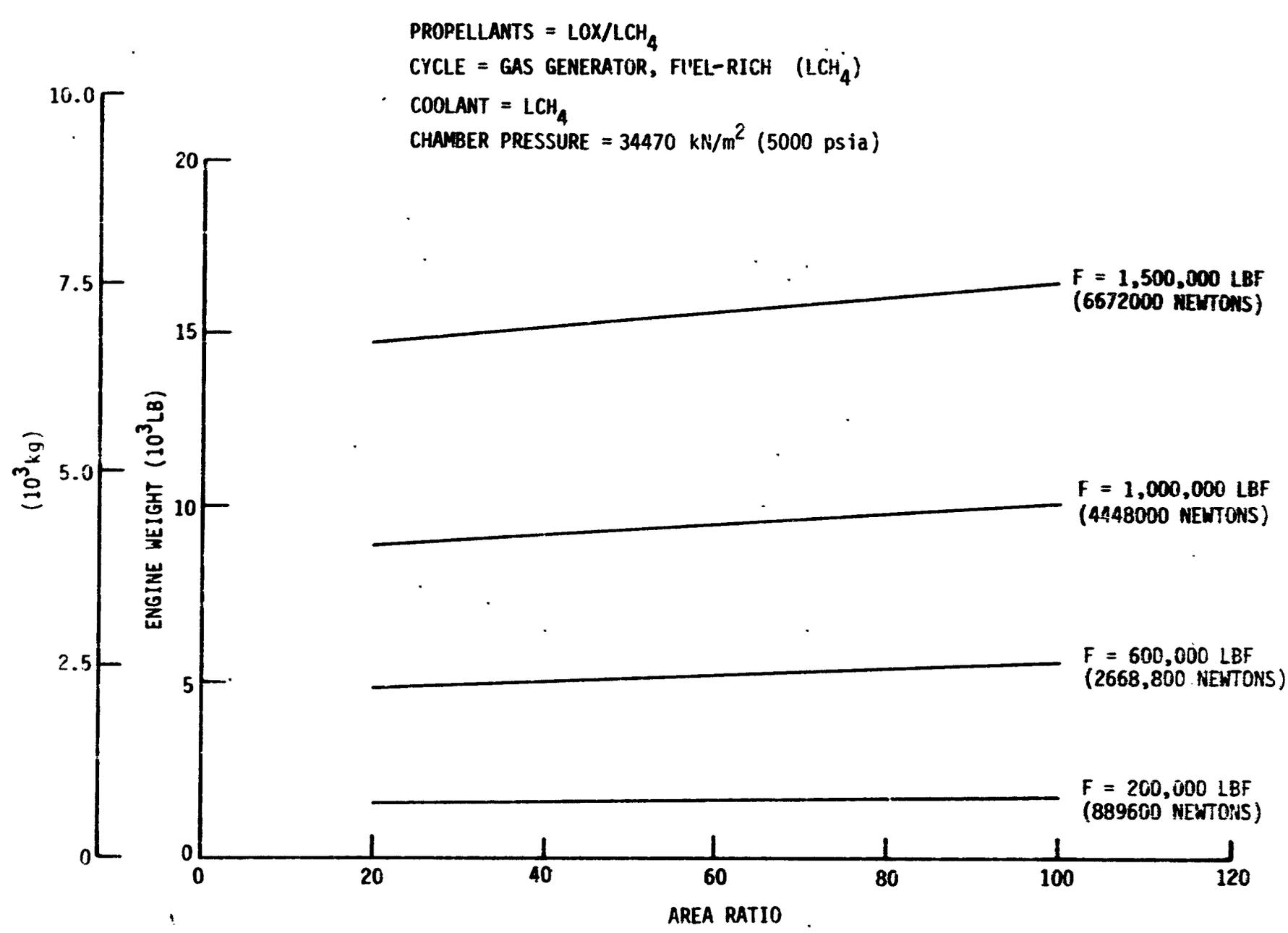

Figure 82. LOX/CH_4 Engine Weight Versus Area Ratio (Pc = 5000)

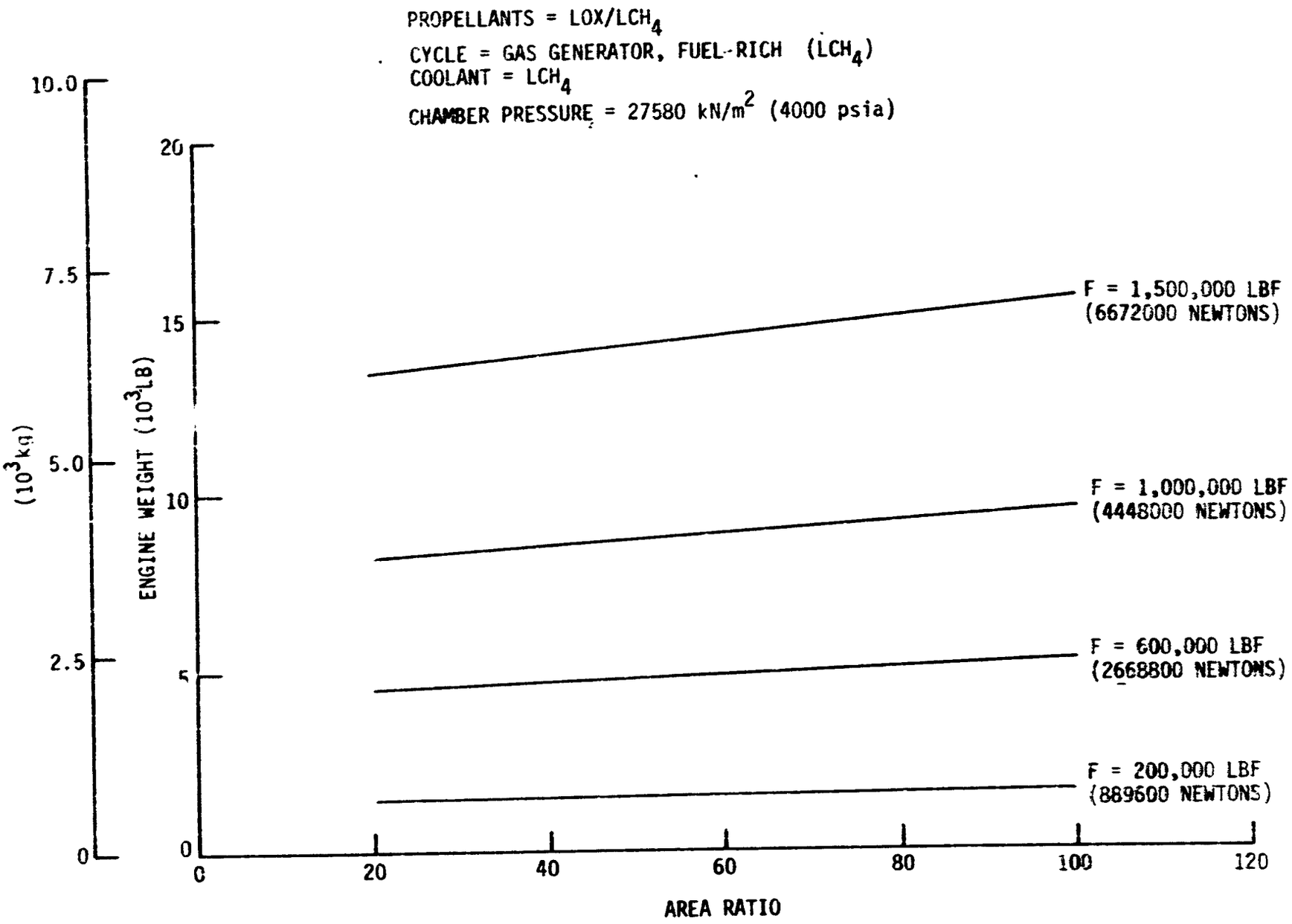

Figure 83. LOX/CH_4 Engine Weight Versus Area Ratio (Pc = 4000)

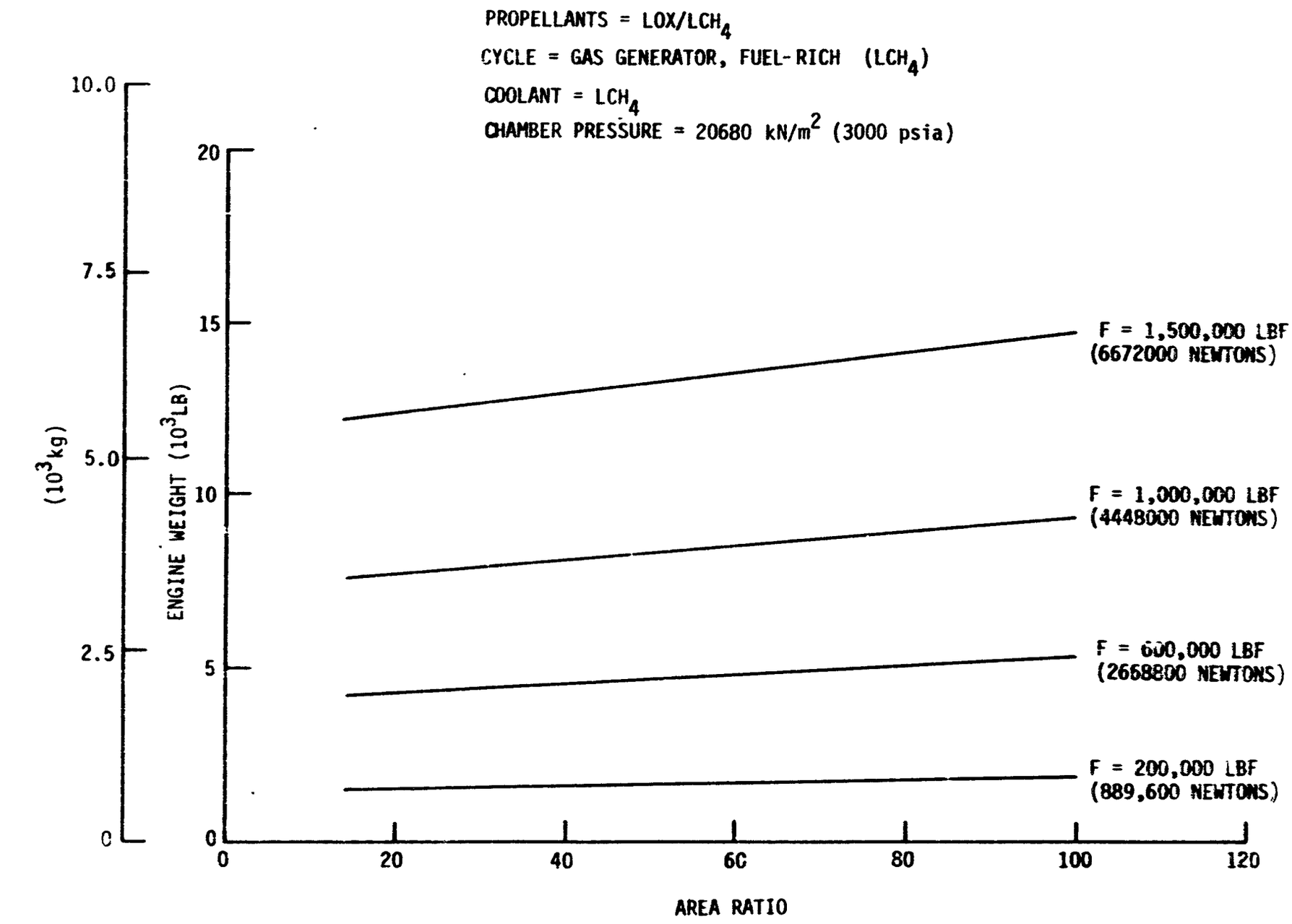

Figure 84. LOX/CH_4 Engine Weight Versus Area Ratio (Pc = 3000)

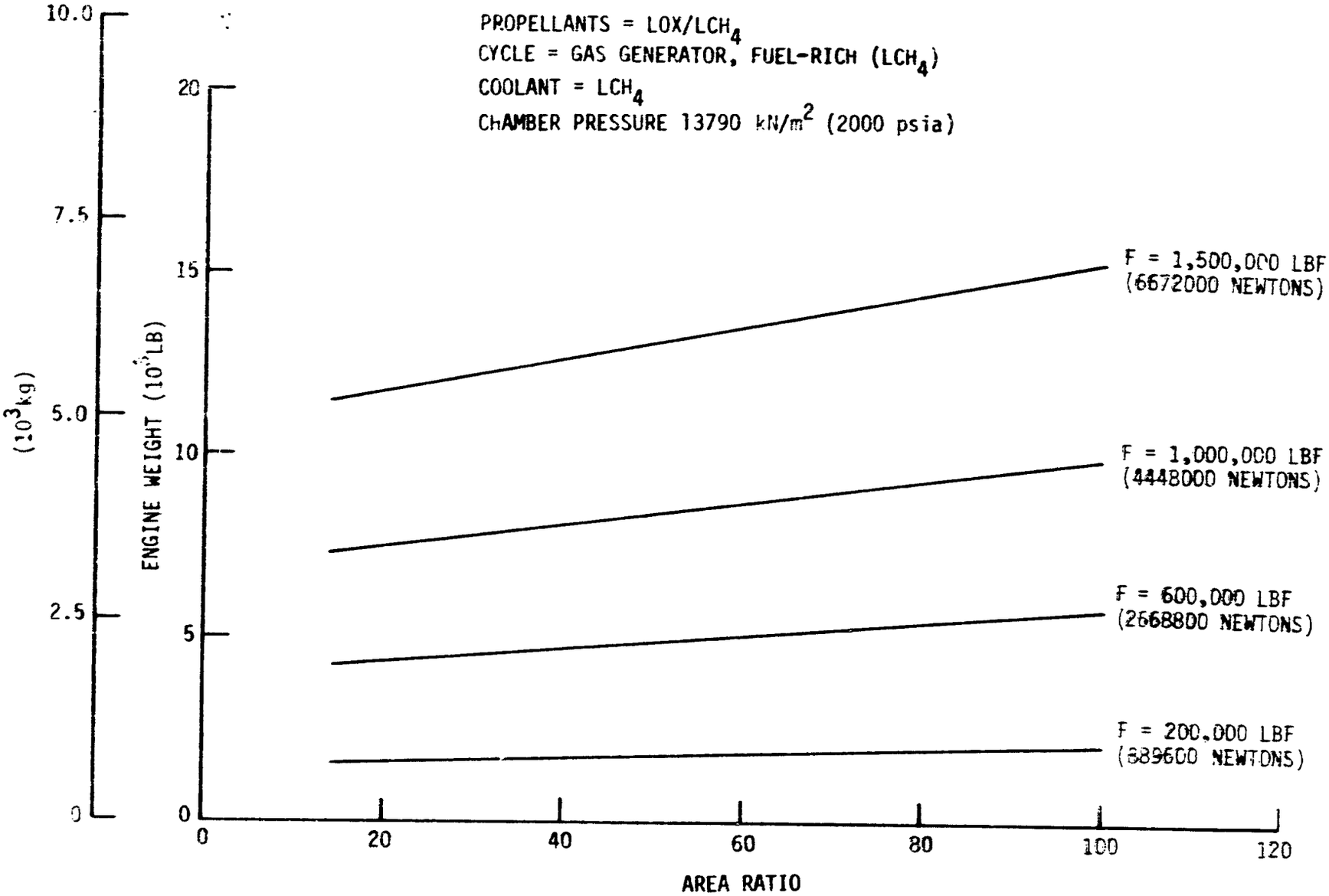

Figure 85. LOX/CH_4 Engine Weight Versus Area Ratio (Pc = 2000)

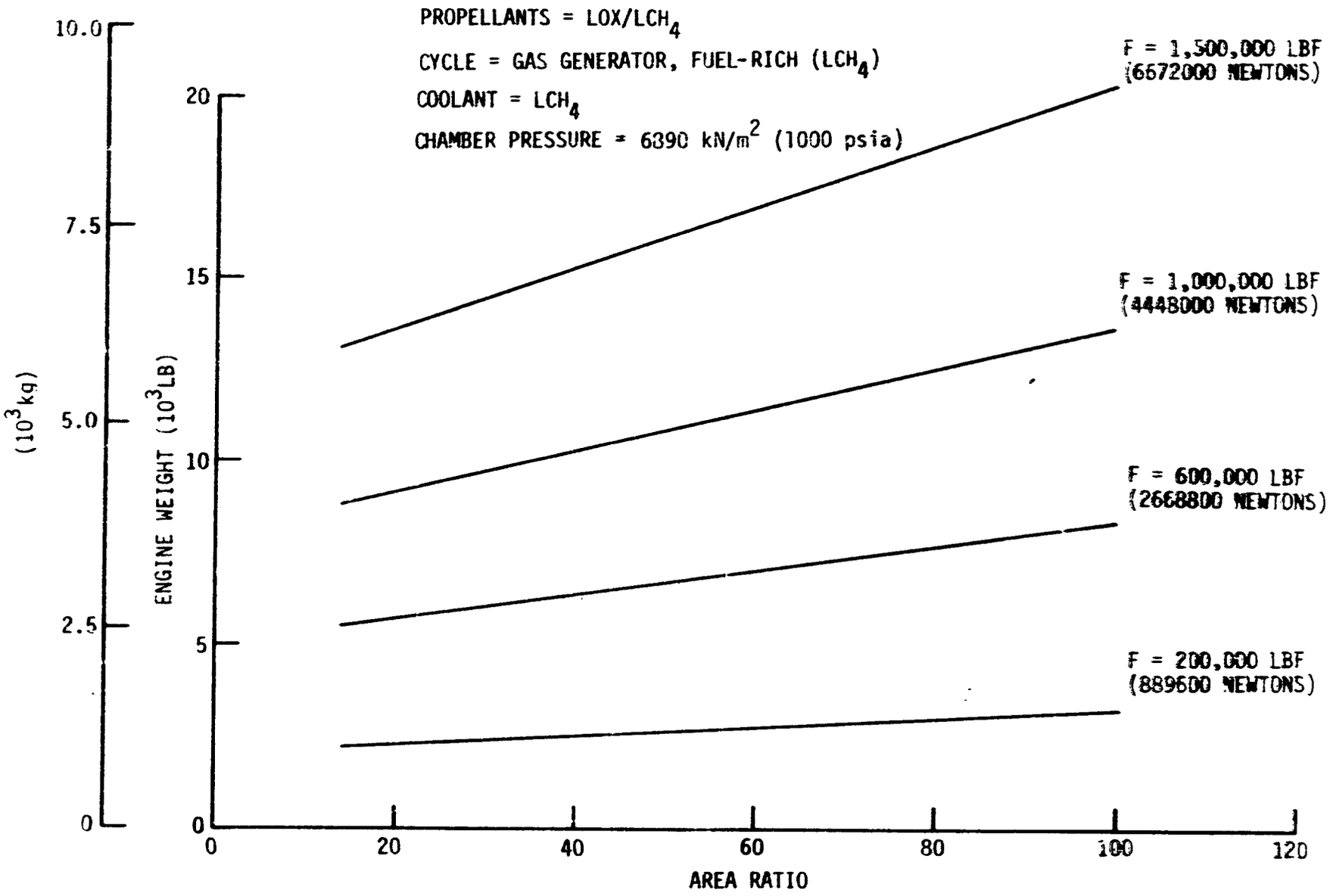

Figure 86. LOX/CH_4 Engine Weight Versus Area Ratio (Pc = 1000)

TABLE XXIX

DESIGN ENGINE WEIGHT BREAKDOWN FOR CYCLES C, G, AND I

COMPONENT	O_2/LCH_4 CYCLE C F = 2669 kN (600K lbF) Pc = 29650 kN/m^2 (4300 psia)		$LO_2/RP\text{-}1$ CYCLE G F = 2699 kN (600K lbF) Pc = 21370 kN/m^2 (3100 psia)		LO_2/LCH_4 CYCLE I F = 2669 kN (600K lbF) Pc = 24130 kN/m^2 (3500 psia)	
	kg	lb	kg	lb	kg	lb
Gimbal	94	207	94	207	94	207
Injector	277	611	352	775	328	723
Combustion Chamber	165	364	198	437	185	407
Nozzle	149	328	155	342	158	349
Fuel Preburner	-	-	-	-	79	174
Oxidizer Preburner	-	-	93	205	98	215
Gas Generator	34	76	-	-	-	-
Fuel Valves	60	133	27	60	79	175
Oxidizer Valves	70	155	94	208	103	228
Oxidizer Boost Pump	141	311	122	268	132	291
Fuel Boost Pump	47	103	21	47	35	77
Oxidizer Main Pump	406	895	317	698	356	785
Fuel Main Pump	300	661	124	274	212	467
Hot-Gas Manifold	10	23	70	155	97	213
Low-Pressure Lines	115	253	92	202	108	238
High-Pressure Lines	174	383	123	271	158	349
Ignition Systems	18	40	18	40	27	60
Miscellaneous	79	174	79	174	79	174
Controller	59	130	59	130	59	130
Pressurization System	63	138	45	100	51	113
Interpropellant Seal	41	90	32	70	0	0
Engine Weight	2302	5075	2115	4663	2438	5375
Sea Level Thrust/Weight Ratio		118.2		128.7		111.6

C-3

TABLE XXX

NOMINAL POINT DESIGN ENGINE WEIGHT BREAKDOWN FOR CYCLES C', G', AND I'

COMPONENT	LO_2/LC_3H_8 CYCLE C' F = 2669 kN (600K lbF) Pc = 31030 kN/m^2 (4500 psia)		LO_2/LC_3H_8 CYCLE G' F = 2669 kN (600K lbF) Pc = 22060 kN/m^2 (3200 psia)		LO_2/LC_3H_8 CYCLE I' F = 2669 kN (600K lbF) Pc = 24820 kN/m^2 (3600 psia)	
	kg	lb	kg	lb	kg	lb
Gimbal	94	207	94	207	94	207
Injector	275	607	349	769	328	722
Combustion Chamber	161	354	197	435	190	419
Nozzle	152	334	160	353	160	352
Fuel Preburner	-	-	-	-	84	186
Oxidizer Preburner	-	-	95	210	98	217
Gas Generator	32	71	-	-	-	-
Fuel Valves	39	85	28	61	52	114
Oxidizer Valves	71	156	97	213	103	227
Oxidizer Boost Pump	141	310	124	274	130	287
Fuel Boost Pump	30	66	21	47	23	50
Oxidizer Main Pump	411	907	327	720	354	781
Fuel Main Pump	194	428	127	280	138	305
Hot-Gas Manifold	10	22	73	161	100	221
Low-Pressure Lines	93	204	92	203	90	198
High-Pressure Lines	146	322	127	281	135	297
Ignition Systems	18	40	18	40	27	60
Miscellaneous	79	174	79	174	79	174
Controller	59	130	59	130	59	130
Pressurization System	70	154	48	106	60	133
Interpropellant Seal	41	91	33	72	—	—
Engine Weight	2115	4662	2148	4736	2304	5080
Sea Level Thrust/Weight Ratio		128.7		126.7		118.1

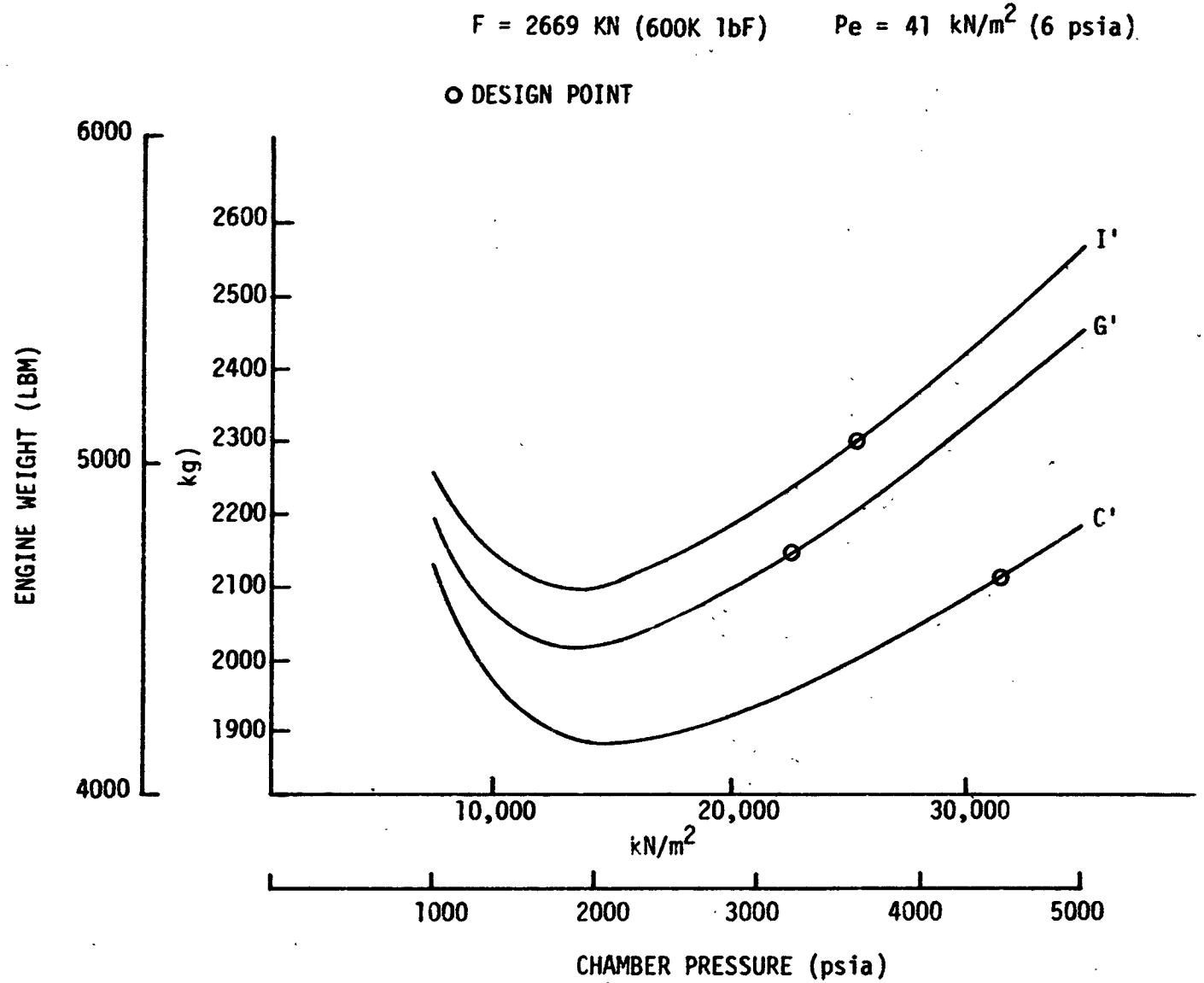

Figure 87. LOX/LC_3H_8 Engine Weight Versus Chamber Pressure

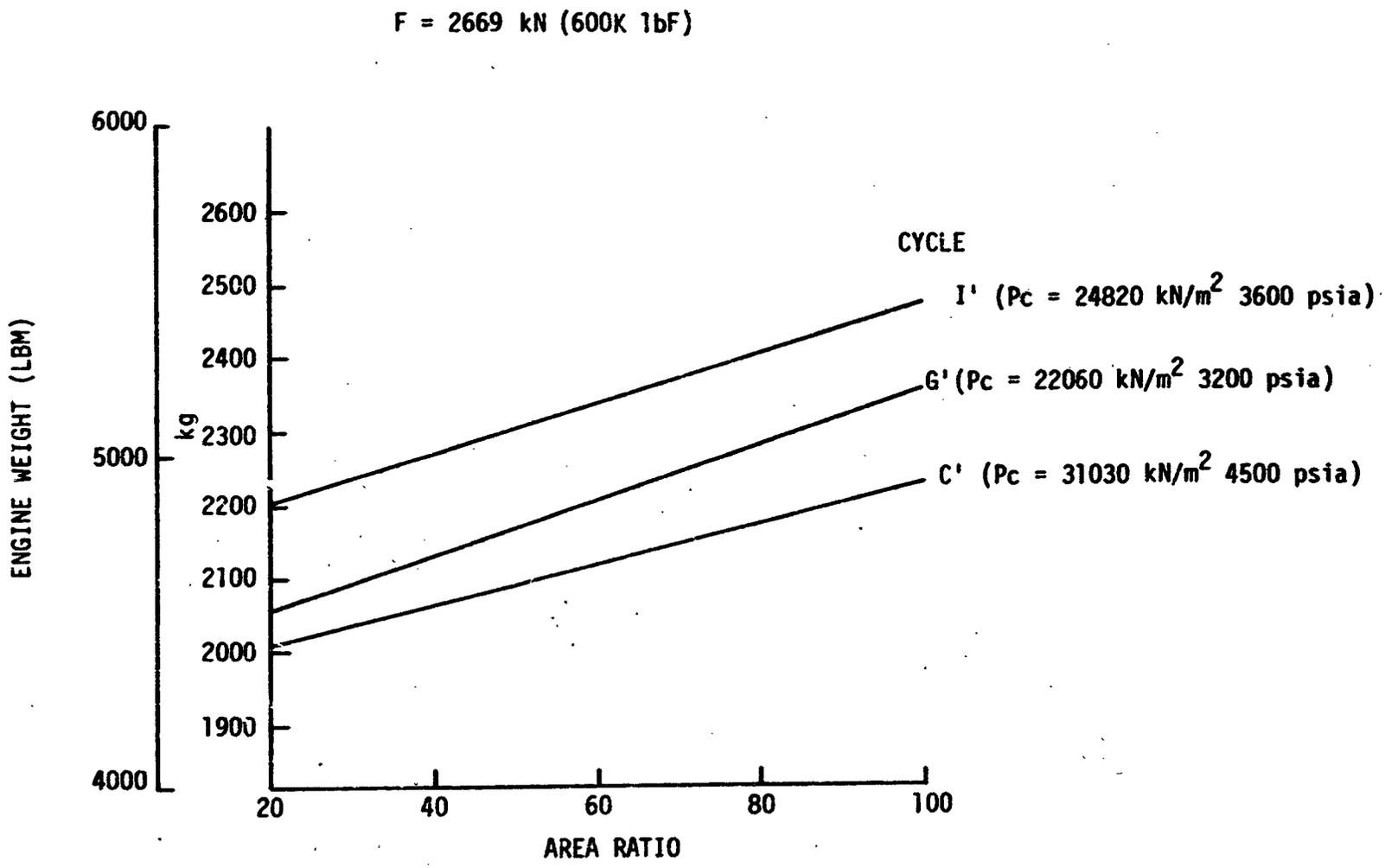

Figure 88. LOX/LC_3H_8 Engine Weight Versus Area Ratio

3. Weight Improvement Through the Year 2000

The potential for weight improvement and increased component maximum temperature for advanced LOX/HC engines lies in the application of advanced materials. In order to place the advanced materials in proper perspective, a listing of 1979 state-of-the-art engine materials is given in Table XXXI. The selections are based on the usual criteria for material strength under the operational environments and fabricability. Since material strength requirements and detail designs were out of scope for this program, selections were based on, and are very similar to, those of previous rocket technology programs.

Advanced materials were studied to determine the feasibility of their application to liquid rocket engine design and to assess the potential for performance improvement associated with their use. The materials of construction, design parameters, and engine component weights for the preliminary design engines of this study were used as a baseline to establish overall weight reductions and increased service temperature capabilities of the engine hot-gas system. The status and the prospects of materials development and their manufacturing technology development were used to make these assessments on a near-term (1980-1985) as well as long-term (1985-2000) basis.

a. Background for Advanced Materials Application

Aerospace application of advanced materials, mainly fiber-reinforced composites, has been previously limited to reinforcement panels and frames in airframe structures. The application of these composites to aircraft turbojet engines, which are similar in many respects to liquid rocket engines, has been underway for at least a decade. One of the problems that is being overcome is the use of these materials at elevated temperatures. This problem, along with the unknowns concerning the applicability of the

TABLE XXXI (1 of 3)

TYPICAL 1979 STATE-OF-THE-ART MATERIALS SELECTION

Component	
1. Low-Speed LOX TPA	
a. Shaft	Inconel 718 15-5 PH H1150M
b. Impeller & Turbine	7075 T-73 Al Alloy
c. Housing	A356 T6 Al Alloy
d. Bolts	A-286
e. Housing Liner	FEP Teflon Fused Coating
f. Bearings	CRES 440C; Haynes Star J Alloy PM
2. Low-Speed RP-1 TPA	All materials the same as low speed LOX TPA except Teflon coating is not required.
3. Low-Speed LH_2 TPA	All materials the same as low speed LOX TPA except Teflon coating is not required.
4. Low-Speed CH_4 and C_3H_8 TPA	All materials same as low speed LOX TPA except Teflon coating is not required.
5. High-Speed LOX TPA	
a. Shaft	A-286
b. Impeller	Inconel 718
c. High-Pressure Pump & Turbine Housing	ARMCO Nitronic-50
d. Inducer Housing	Inconel 718
e. Turbines	Inconel 718
f. Bolts (pump)	A-286

TABLE XXXI (cont.) (2 of 3)

Component	
5. High-Speed LOX TPA (cont.)	
g. Bolts (turbine)	Waspaloy
h. Bearings	CRES 440C or Alternate
6. High-Speed RP-1 TPA	
a. Inducer Housing	5Al-2.5 SnELI Titanium Alloy All other materials the same as high speed LOX TPA.
7. High-Speed CH_4 and C_3H_8 TPA	5Al-2.5 SnELI Titanium Alloy All other materials the same as high speed LOX TPA.
8. High-Speed LH_2 TPA	
a. Inducer Housing	5Al-2.5 SnELI Titanium Alloy
b. High-Pressure Pump Housing	5Al-2.5 SnELI Titanium Alloy
c. Turbine	Inconel 718
d. Impeller	A-286
e. Turbine Housing	ARMCO Nitronic-50
f. Shaft	A-286
g. Bolts (pump)	A-286
h. Bolts (turbine)	Waspaloy
i. Bearings	CRES 440C
9. LOX/RP-1 Ox-Rich Preburner	
a. Injector Body	ARMCO Nitronic-50
b. Chamber	Inconel 625

TABLE XXXI (cont.) (3 of 3)

Component	
10. LOX/CH_4 and LOX/C_3H_8 Ox-Rich Preburner	
a. Injector	ARMCO Nitronic-50
b. Chamber	Inconel 625
11. LOX/CH_4 and LOX/C_3H_8 Fuel-Rich Preburner or Gas Generator	
a. Injector Body	ARMCO Nitronic-50
b. Chamber	Inconel 625
12. Thrust Chamber Injector	
a. Body	Inconel 625 or ARMCO Nitronic-50
b. Manifolds	CRES 347 or ARMCO Nitronic-50
c. Injector Face	Inconel 625
13. Combustion Chamber	Zirconium Copper
14. Tubes	Nitronic-40 or A-286
15. Nozzle Extension	Columbium Alloy
16. Hot-Gas Manifold	Inconel 625

polymer matrix composites at cryogenic temperatures and with LOX compatible systems, requires further investigation before major applications can be made to high- and low-temperature rocket engine components. The more benign environment of the RP-1 propellant system provides the most straightforward application of advanced materials to rocket engine design.

There are many potential applications for reinforced plastic composites (RPC) in liquid rocket engines. The amount of RPC substitution in these applications varies with each engine component. It is estimated, for example, that about 80% of the Titan III engine frame and 60% of the Titan valve body are candidates for RPC substitution. The effect of substituting RPC for metals can result in a significant weight savings because of the higher specific strength and specific modulus properties of RPC (see Figure 89, Ref. 21). The General Electric Company is currently developing an advanced composite engine frame and inner cowl for engines (Ref. 21). The remaining turbojet engine lightweight composite application found in the literature search and review of this study is the replacement of stainless steel and titanium with a boron/aluminum fiber composite as the material of construction for turbofan blades. Although liquid rocket engines do not possess a component equivalent to a fan, this technology, as well as RPC technology, could be utilized in the design of turbines. The metal matrix composites with the superalloy-refractory metal fibers, the directionally solidified refractory oxide eutectics, and improved ceramics that are being developed to increase turbine operating temperatures are directly applicable to rocket engines. As an example, the improvement in temperature capability with time for the various advanced materials for turbine blades is shown in Figure 90 (Ref. 22).

Advances in materials science affecting RPC are expected to ease the manufacturing of parts and slightly increase the temperature capability. These effects will not change the weight of the engine as much as the cost of manufacture. These improvements should be in place in 10 to 15 years.

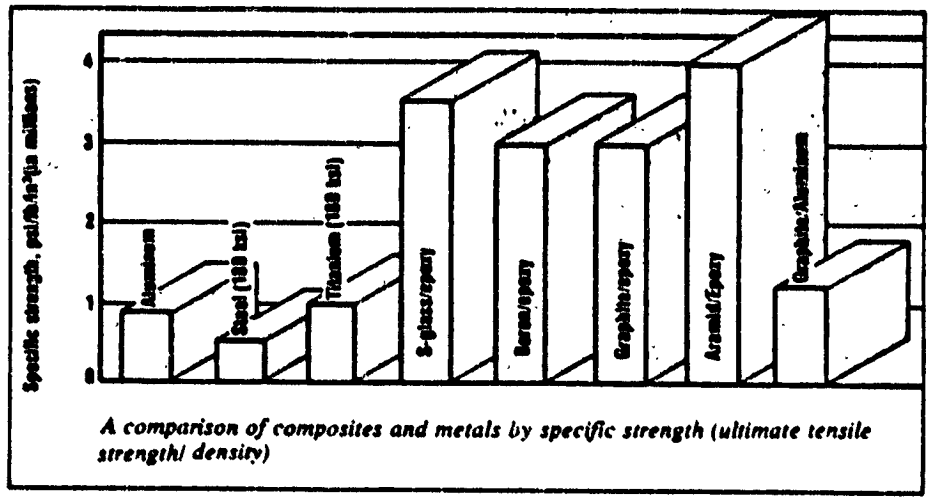

A comparison of composites and metals by specific strength (ultimate tensile strength/ density)

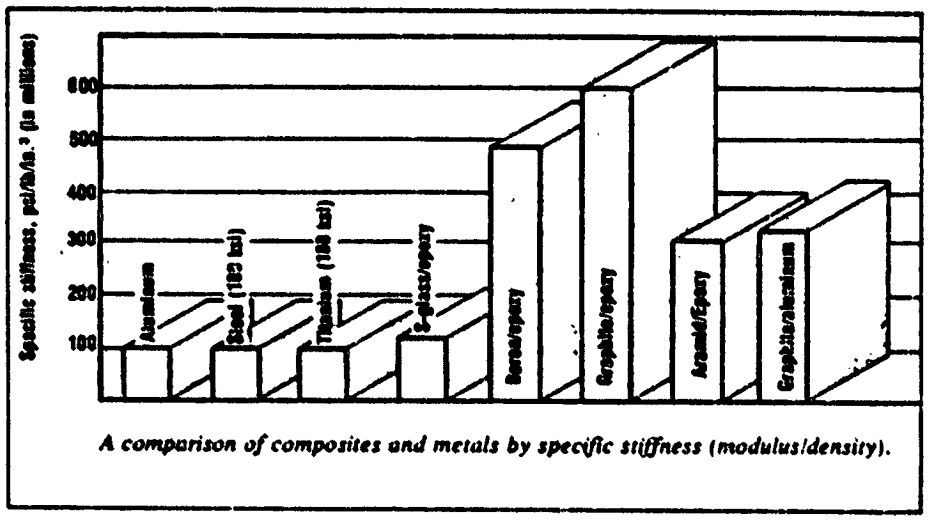

A comparison of composites and metals by specific stiffness (modulus/density).

Composite data shown are for 0° unidirectional laminates. Source: Advanced Composite Design Guide. Air Force Flight Dynamics Laboratory, Wright Patterson Air Force Base. Aramid is Du Pont's Kevlar 49.

Figure 89. Comparison of Structural Properties of Composites and Other Aircraft Materials

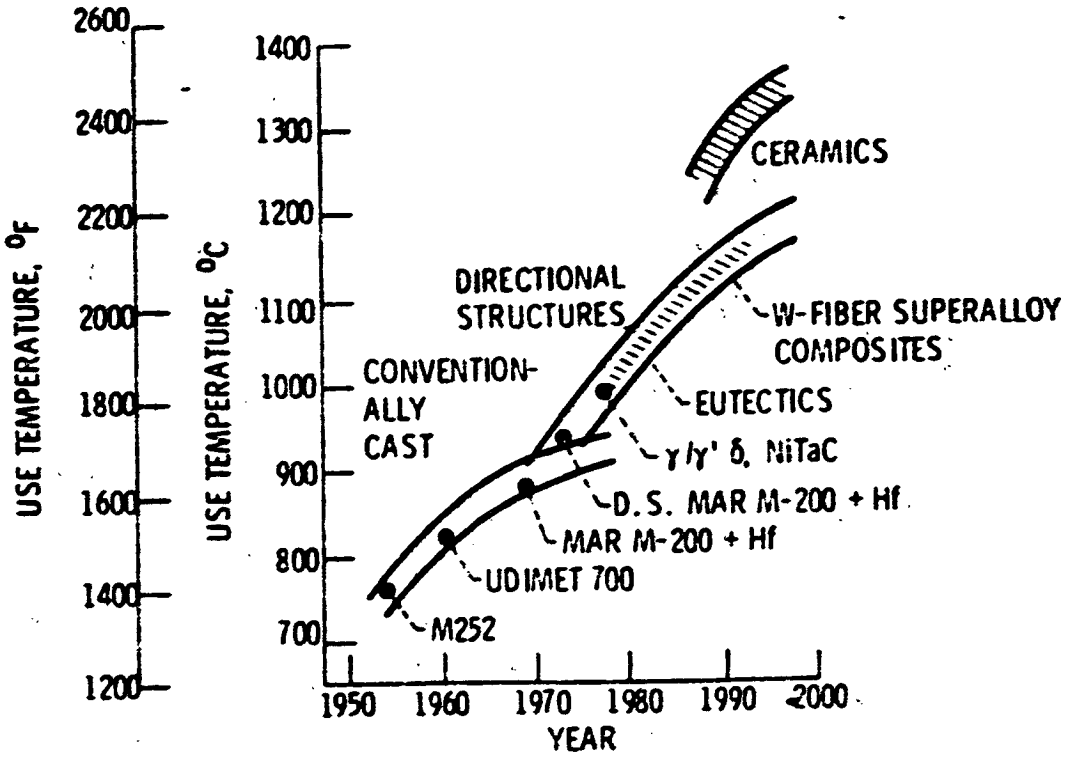

Figure 90. Increased Use Temperature Projected for Directional Structures for High-Stress, High-Temperature Applications

b. Application of RPC to a Baseline Oxygen-Hydrocarbon Engine

Individual engine components have been studied to estimate weight savings that could be realized by the substitution of RPC materials. Each component configuration and service environment was evaluated with regard to the materials, their development status, and the design concepts identified in this study. In some instances, RPC provided a complete material substitution. In components where either elevated temperatures or component configuration restricted their use, RPCs were applied only to portions of the assembly or not at all. The results of this study are shown in Table XXXII, which lists the baseline engine weight by component and compares them with the weights obtained by the use of RPCs on a near- and long-term basis. A 40% weight savings was identified (939 kg/2071 lbs). The individual RPC applications are as follows:

GIMBAL

94 kg (207 lb.) baseline engine
27 kg (60 lb) 85% RPC substitution
24 lb PI-carbon
36 lb aramid-epoxy

Bearing surfaces of the gimbal bearing assembly can be replaced with polyimide-bonded carbon fabric. It is estimated that 55% of the Ti-alloy can be replaced with molded fabric composite and still retain the attachment and rigidity characteristics of the original bearing assembly.

Other design refinements in which portions of the remaining shell are replaced with High Strength (HS), High Modulus (HM) epoxy matrix composite are possible. In these designs, a laminate of titanium and

TABLE XXXII

ADVANCED LOX/HYDROCARBON BASELINE ENGINE
WEIGHT SAVINGS BREAKDOWN

Engine Component	Baseline lbs.	RPC Substitution 1980-1985 lbs.	RPC Substitution 1985-2000 lbs.
Gimbal	207	60	60
Miscellaneous (Frame, Fasteners)	437	251	251
Injector	656	425	265
Nozzle	420	420	420
Thrust Chamber	226	152	152
Preburners (Ox-and Fuel Rich)	405	370	370
Valve Bodies (Ox and Fuel)	407	379	268
Boost Pumps (Ox and Fuel)	359	340	227
Main Pump (Ox and Fuel)	1189	1031	614
Low-Pressure Lines	201	95	95
High-Pressure Lines	268	126	
Pressurization System	133	68	68
Hot-Gas Manifold	207	20	207
Igniters	60	60	60
Controller	130	51	51
WEIGHT TOTALS	5305	4035	3234
ENGINE THRUST/WEIGHT	113	149	186

HS/HM composite would be used for the attaching surfaces, and the shell would be replaced on a stiffness and strength basis with HS/HM composite. This material substitution would introduce several additional manufacturing steps: (1) the attaching surface would be laminated, (2) the bearing surfaces would be molded, (3) the attaching surfaces and bearing surfaces would be joined, and (4) the HS/HM composite shell would be wrapped and molded. The configuration of the part would be guided by a detailed structural analysis of the loads on the thrust-mount bearing assembly in service.

The polyimide-carbon (PI-carbon) fabric material for the bearing surfaces has a temperature limit of 603°K (625°F), a compressive strength of 586,000 kN/m^2 (85,000 psi), a flexual strength of 344,700 kN/m^2 (50,000 psi), a density of 1.5 g/cc, a coefficient of thermal expansion of 5×10^{-6} in/°F, and a modulus of 48,260 MN/m^2 (7×10^6 psi).

A hybrid composite of Kevlar and graphite reinforcement in an expoxy matrix would be used for the shell and attaching surface laminate of the bearing assembly. The composite would have a temperature limit of 422°K (300°F), a modulus ranging from 31,000 to 69,000 MN/m^2 (4.5×10^6 to 10×10^6 psi) at a fiber volume of 55%, and a crossplied strength of 482,600 kN/m^2 (70,000 psi). The hybrid composite would have a density ranging between limits of 1.3 and 1.59 g/cc, depending on the mixture of Kevlar and graphite, respectively.

MISCELLANEOUS (FRAMES, FASTENERS, ETC)

198 kg (437 lb) baseline engine (HSLA steel)
114 kg (251 lb) 52% RPC substitution

The baseline engine frames are constructed of high-strength low-alloy steel tubes welded to forged end fittings. It is estimated that 80% of the miscellaneous weight is frame structure.

IV, C, Engine Weight (cont.)

Wrapped Kevlar-epoxy crossplied composite is suggested as the replacement material for the tubular sections of the frame. Kevlar-epoxy composite has the highest specific strength of the candidate RPC materials. The tubes would be adhesively bonded to the coupling fittings. Material substitution was calculated on a specific strength basis.

A laminate of steel and hybrid composite is suggested for the couplings. The hybrid would be Kevlar and graphite in epoxy matrix. The graphite composite has the highest specific modulus of the candidate materials. The specific configuration of metal, Kevlar, and graphite will depend on the structural requirements of the joint. A 50% substitution of hybrid composite for HSLA steel is considered feasible.

INJECTOR

298 kg (656 lb) baseline engine (stainless steel)
193 kg (425 lb) 57% RPC substitution
120 kg (265 lb) 87% RPC substitution (1990)

The inlet manifolds (LOX and fuel) of the injector can be constructed of HS/HM composite material. Stamped metal liners are required to protect the composite from the corrosive effects of the hot propellant gases and liquid oxygen. These thin liners would be structurally supported with HS/HM plastic matrix composite. The choice of matrix material depends upon the service temperature. Epoxy resin would be used to 422°K (300°F), polysulfone or polyamide-imide would be used to 478°K (400° F), and polyimide resin would be used to 617°K (650°F). Reinforcement would be hybrid selection of crossplied prepregs and chopped fibers of Kevlar, graphite, and fiberglass, depending on local strength and stiffness requirements.

IV, C, Engine Weight (cont.)

The primary and secondary plates of the injector are laminated of metal and HS/HM composite. These structures would have metal faces and HS/HM composite cores. Selection of resin and reinforcement would be based on the same criteria used with the manifold details.

With the exception of the injector face, the injector body can be molded from a potentially LOX-compatible material, a PI-RPC. It is anticipated that this material will be available in ten years or sooner.

THRUST CHAMBER

103 kg (226 lb) baseline engine (nickel/copper)
69 kg (152 lb) 46% RPC substitution

The chamber liner wall is machined copper. Electroformed nickel or copper provide the closeout for coolant channels. The outer surface reinforcement is molded RPC. Epoxy and PI resin matrices will be used, depending on the temperature. Graphite, fiberglass, and Kevlar will be used as reinforcement, depending on structural requirements.

The coolant inlet and outlet flanges, manifold covers, jacket reinforcements, and nozzle attachment flanges are constructed of composite and metal laminate. Thin metal facings will protect the composite from any adverse effects resulting from direct contact with the propellant. Stiffness, strength, and temperature will determine reinforcement and matrix selections in these details. Bearing strength will determine the amount of metal reinforcement needed in the injector attachment flange.

IV, C, Engine Weight (cont.)

PREBURNER (OX- AND FUEL-RICH)

184 kg (405 lb) baseline engine
168 kg (370 lb) 15% substitution

The inlet manifolds appear to be the only feasible application of HS/HM RPC because coolant is not circulated through the structure to limit temperature rise. The proposed manifold is a metal-lined structure externally supported with RPC. The metal liner protects the RPC from any corrosive effects that might result from direct contact with the propellant.

The manifold is fabricated by compression-molding the composite directly to the metal shaped liner. Reinforcement and resin selection will be based upon strength, stiffness, and service temperature.

VALVES AND ACTUATORS (OX AND FUEL)

185 kg (407 lb) baseline engine (aluminum)
172 kg (379 lb) 40% RPC substitution (1980-1990)
122 kg (268 lb) 60% RPC substitution (1990)

Actuation parts and valve body parts can be compression-molded of chopped fiber molding compound. Polysulfone or polyamide-imide thermoplastic resins are capable of molding precision parts that will operate successfully under the demanding conditions required by these sensitive rocket engine control mechanisms. These resins are compatible with RP-1, LH_2, LCH_4, and LC_3H_8 rocket engine fuels. Selection of reinforcements for use with these resins will be based on strength and rigidity requirements.

IV, C, Engine Weight (cont.)

Resins resistant to LOX are anticipated in the next ten years. These resins will be required to design satisfactory valve components for the ox-circuit.

BOOST PUMPS (OX AND FUEL)

163 kg (359 lb) baseline engine (aluminum)
154 kg (340 lb) 10% substitution
103 kg (227 lb) 75% RPC substitution (1990)

Fifteen percent of the pump structure (mostly housing) is estimated to be moldable from chopped fiber molding compound and continuous fiber prepreg. The balance of the housing and the rotating parts (~45%) can be reaction-injection-molded (RIM) by using epoxy resin and hybrid reinforcing fibers.

MAIN PUMP (OX AND FUEL)

539 kg (1189 lb) baseline engine (aluminum)
468 kg (1031 lb) 45% RPC substitution (1980-1990)
279 kg (614 lb) 75% RPC substitution (1990)

This weight estimate was arrived at by substitution of epoxy-Kevlar composite for titanium in the housing. The major internal parts are molded of RFP and substituted for metal on a volumetric basis. Metal-RPC laminate will be used at attachment points, and HS/HM RPC will be used on internal parts requiring a higher level of structural efficiency.

LOW-PRESSURE LINES

91 kg (201 lb) baseline engine (stainless steel)
43 kg (95 lb) 60% RPC substitution

IV, C, Engine Weight (cont.)

The Martin Marietta Corporation has investigated the development of composite propellant lines for cryogenic space vehicles. These lines are lined with metal and overwrapped with fiberglass epoxy for structural support. The weight estimate is based on scaling the weight savings reported in this work which was directed at the space shuttle main engine.

HIGH-PRESSURE LINES

122 kg (268 lb) baseline engine (nickel base alloy)
57 kg (126 lb) 60% RPC substitution

The weight estimate for the high-pressure lines fabricated in composite material is based on scaling described for the low-pressure lines.

CONTROLLER

59 kg (130 lb) baseline engine (aluminum)
23 kg (51 lb) 75% RPC substitution

The controller system box will be molded of fiberglass, epoxy, chopped-fiber material. Microcircuitry applications will further reduce the weight.

PRESSURIZATION SYSTEM

60 kg (133 lb) baseline engine (titanium)
31 kg (68 lb) 37% RPC substitution

The pressure vessel is similar in construction to the high- and low-pressure lines. The tank is lined with metal and overwrapped with fiberglass epoxy for structural support.

c. Conclusions and Recommendations Regarding Advanced Materials Application

The application of advanced metal matrix components, ceramics, carbon-carbon composites, coated refractory metals, and thermal barrier coatings in liquid rocket engine design affords improvements in performance through increased service temperature capability for the hot-gas system.

The application of reinforced plastic composites to liquid rocket engine design affords a potential weight savings of 40% over current designs.

Programs should be initiated to characterize potential advanced materials for rocket engine designs, particularly with regard to their cryogenic mechanical and physical properties and their propellant compatibility behavior.

Advanced materials and processes should be utilized to produce prototype hardware for proof-, cold-, and hot-flow cyclic and destructive testing followed by comprehensive performance analyses.

D. ENGINE ENVELOPE

Envelope scaling equations based upon geometric considerations were formulated as functions of thrust, chamber pressure, and area ratio. Typical geometry variations with chamber pressure and thrust are depicted in Figures 91 and 92 for LOX/RP-1 and LOX/LCH_4 for an area ratio of 50:1. Data for other area ratios are included in Tables XXXIII and XXXIV, respectively. LOX/LC_3H_8 engine envelope parametrics are shown in Figure 93 as a function of chamber pressure for cycles C', G', and I'.

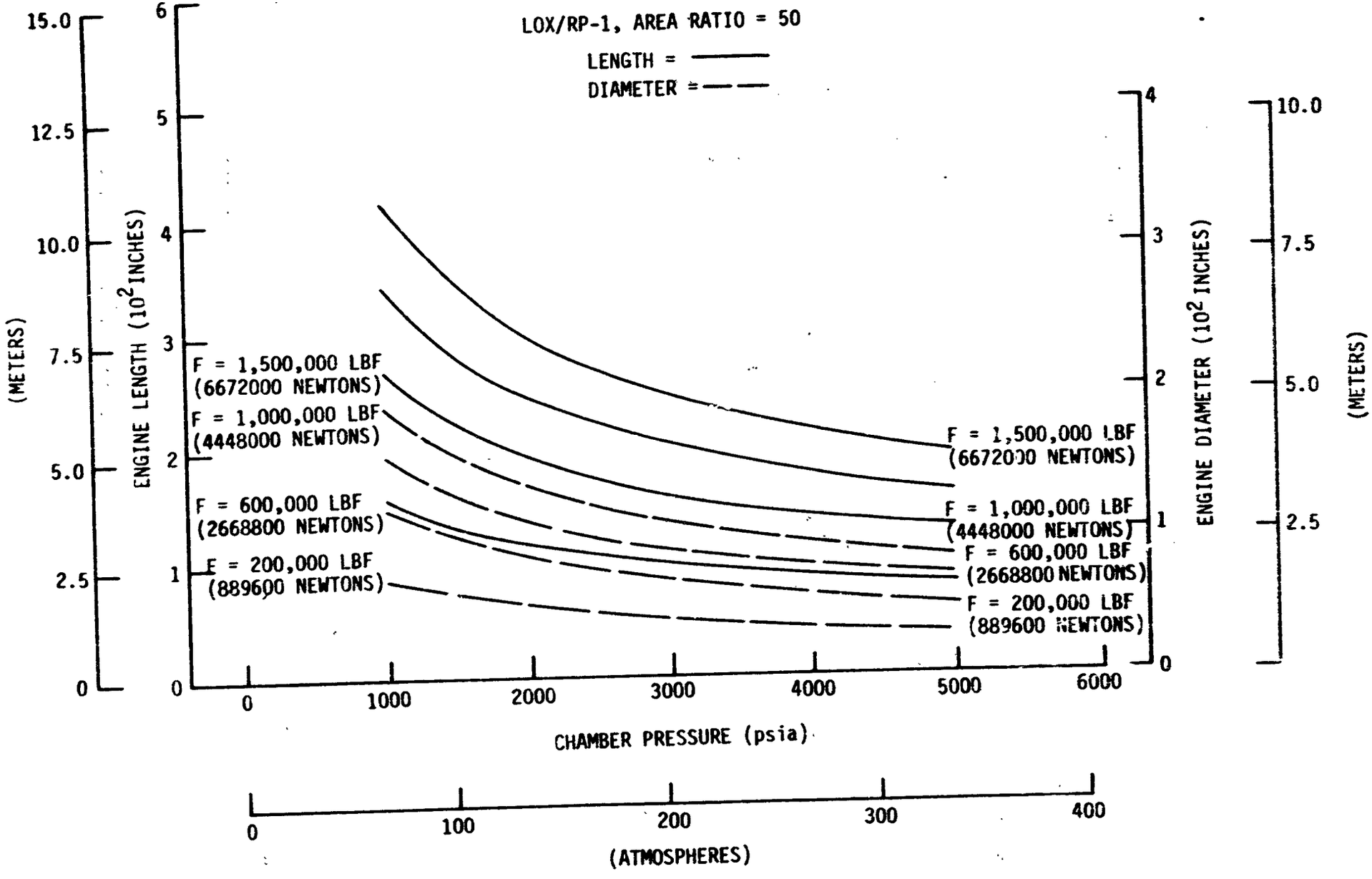

Figure 91. LOX/RP-1 Engine Envelope Parameters Versus Chamber Pressure

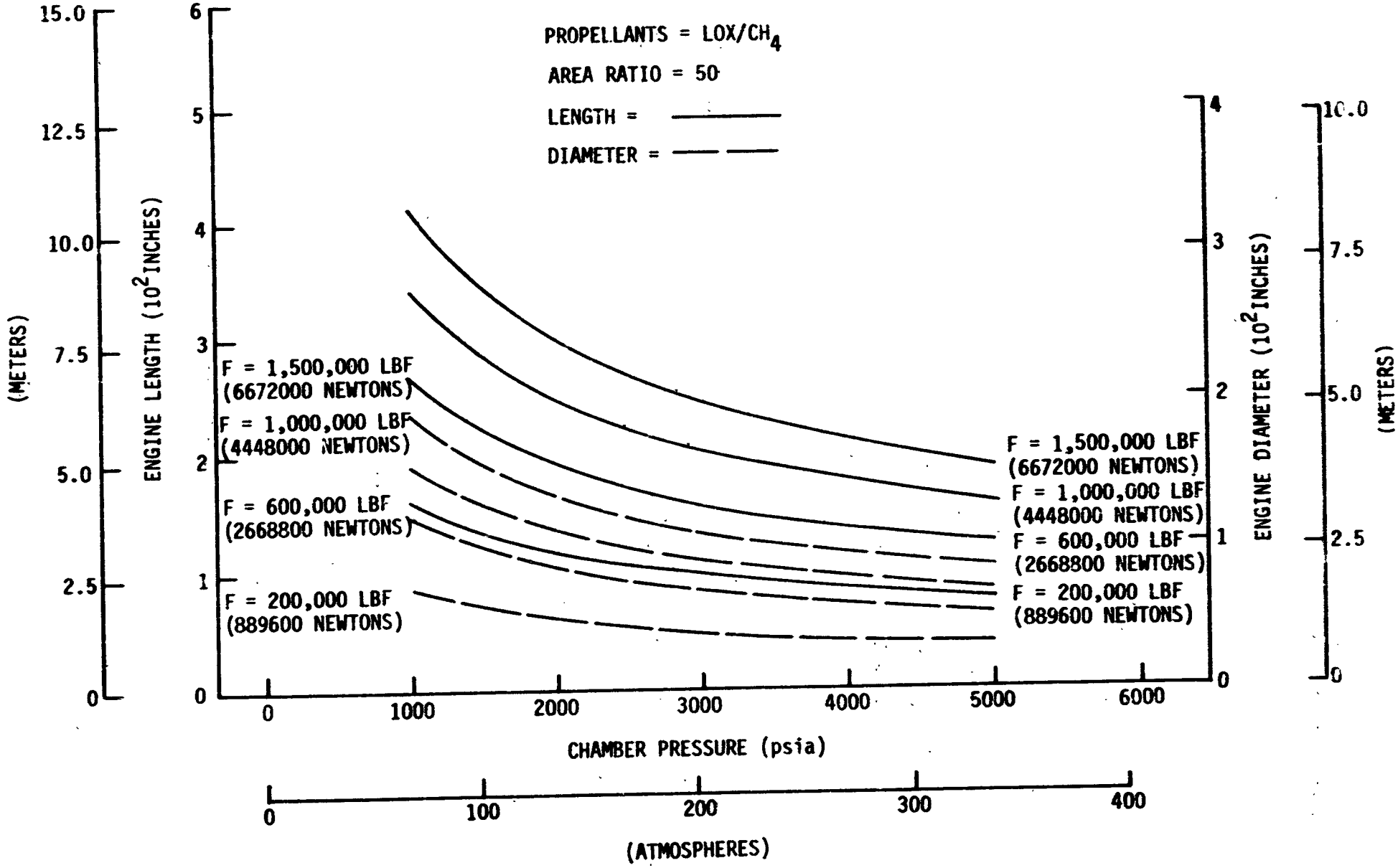

Figure 92. LOX/CH_4 Engine Envelope Parameters Versus Chamber Pressure

TABLE XXXIII

LOX/RP-1 ENGINE ENVELOPE PARAMETRICS

F, lbF (Newtons)	Pc, psia (atm)	ε = 20 L, in. (meters)	ε = 20 D, in. (meters)	ε = 80 L, in. (meters)	ε = 80 D, in. (meters)	ε = 100 L, in. (meters)	ε = 100 D, in. (meters)
200,000 (889600)	1000 (68.03)	107.2 (2.7)	53.9 (1.4)	197.8 (5.0)	107.9 (2.7)	219.2 (5.6)	120.6 (3.1)
	2000 (136.05)	79.6 (2.0)	38.1 (1.0)	143.6 (3.6)	76.3 (1.9)	158.7 (4.0)	85.3 (2.2)
	3000 (204.08)	67.2 (1.7)	31.1 (.8)	119.5 (3.0)	62.3 (1.6)	131.8 (3.3)	69.6 (1.8)
	4000 (272.11)	59.9 (1.5)	27.0 (.7)	105.2 (2.7)	53.9 (1.4)	115.9 (2.9)	60.3 (1.5)
	5000 (340.14)	54.6 (1.4)	24.1 (.6)	95.1 (2.4)	48.2 (1.2)	104.7 (2.7)	53.9 (1.4)
1,000,000 (4448000)	1000 (68.03)	223.2 (5.7)	120.6 (3.1)	425.8(10.8)	241.2 (6.1)	473.6 (12.0)	269.6 (6.8)
	2000 (136.05)	161.6 (4.1)	85.3 (2.2)	304.8 (7.7)	170.5 (4.3)	338.6 (8.6)	190.7 (4.8)
	3000 (204.08)	134.2 (3.4)	69.6 (1.8)	251.1 (6.4)	139.2 (3.5)	278.7 (7.1)	155.7 (4.0)
	4000 (272.11)	117.9 (3.0)	60.3 (1.5)	219.2 (5.6)	120.6 (3.1)	243.1 (6.2)	134.8 (3.4)
	5000 (340.14)	106.5 (2.7)	53.9 (1.4)	197.0 (5.0)	107.9 (2.7)	218.4 (5.5)	120.6 (3.1)
1,500,000	1000 (68.03)	270.4 (6.9)	147.7 (3.8)	518.5(13.2)	295.4 (7.5)	577.0 (14.7)	330.3 (8.4)
	2000 (136.05)	194.9 (5.0)	104.4 (2.7)	370.3 (9.4)	208.9 (5.3)	411.7 (10.4)	233.5 (5.9)
	3000 (204.08)	161.4 (4.1)	85.3 (2.2)	304.6 (7.7)	170.5 (4.3)	338.4 (8.6)	190.7 (4.8)
	4000 (272.11)	141.5 (3.6)	73.8 (1.9)	265.5 (6.7)	147.7 (3.8)	294.8 (7.5)	165.1 (4.2)
	5000 (304.14)	127.6 (3.2)	66.1 (1.7)	238.5 (6.1)	132.1 (3.4)	264.7 (6.7)	147.7 (3.8)

TABLE XXXIV

LOX/LCH_4 ENGINE ENVELOPE PARAMETRICS

F, lbF (Newtons)	Pc, psia (atm)	ε = 20 L, in. (meters)	ε = 20 D, in. (meters)	ε = 80 L, in. (meters)	ε = 80 D, in. (meters)	ε = 100 L, in. (meters)	ε = 100 D, in. (meters)
200,000	1000 (68.03)	107.5 (2.7)	54.1 (1.4)	198.3 (5.0)	108.2 (2.7)	219.8 (5.6)	120.9 (3.1)
(889600)	2000 (136.05)	79.7 (2.0)	38.2 (1.0)	144.0 (3.7)	76.5 (1.9)	159.1 (4.0)	85.5 (2.2)
	3000 (204.08)	67.3 (1.7)	31.2 (.8)	119.8 (3.0)	62.4 (1.6)	132.2 (3.4)	69.8 (1.8)
	4000 (272.11)	60.1 (1.5)	27.0 (.7)	105.5 (2.7)	54.1 (1.4)	116.2 (3.0)	60.5 (1.5)
	5000 (340.14)	54.7 (1.4)	24.2 (.6)	95.3 (2.4)	48.4 (1.2)	104.9 (2.7)	54.1 (1.4)
1,000,000	1000 (68.03)	223.8 (5.7)	120.9 (3.1)	426.9 (10.8)	241.9 (6.1)	474.9 (12.1)	270.4 (6.9)
(4448000)	2000 (136.05)	162.0 (4.1)	85.5 (2.2)	305.6 (7.8)	171.0 (4.3)	339.5 (8.6)	191.2 (4.9)
	3000 (704.08)	134.5 (3.4)	69.8 (1.8)	251.8 (6.4)	139.6 (3.5)	279.4 (7.1)	156.1 (4.0)
	4000 (272.11)	118.2 (3.0)	60.5 (1.5)	219.8 (5.6)	120.9 (3.1)	243.7 (6.2)	135.2 (3.4)
	5000 (340.14)	106.7 (2.7)	54.1 (1.4)	197.6 (5.0)	108.2 (2.7)	219.0 (5.6)	120.9 (3.1)
1,500,000	1000 (68.03)	271.1 (6.9)	148.1 (3.8)	519.9 (13.2)	296.2 (7.5)	578.6 (14.7)	331.2 (8.4)
(6672000)	2000 (136.05)	195.5 (5.0)	104.7 (2.7)	371.3 (9.4)	209.5 (5.3)	412.9 (10.5)	234.2 (5.9)
	3000 (204.08)	161.8 (4.1)	85.5 (2.2)	305.4 (7.8)	171.0 (4.3)	339.3 (8.6)	191.2 (4.9)
	4000 (272.11)	141.9 (3.6)	74.1 (1.9)	266.2 (6.8)	148.1 (3.8)	295.6 (7.5)	165.6 (4.2)
	5000 (340.14)	127.9 (3.2)	66.2 (1.7)	239.1 (6.1)	132.5 (3.4)	265.4 (6.7)	148.1 (3.8)

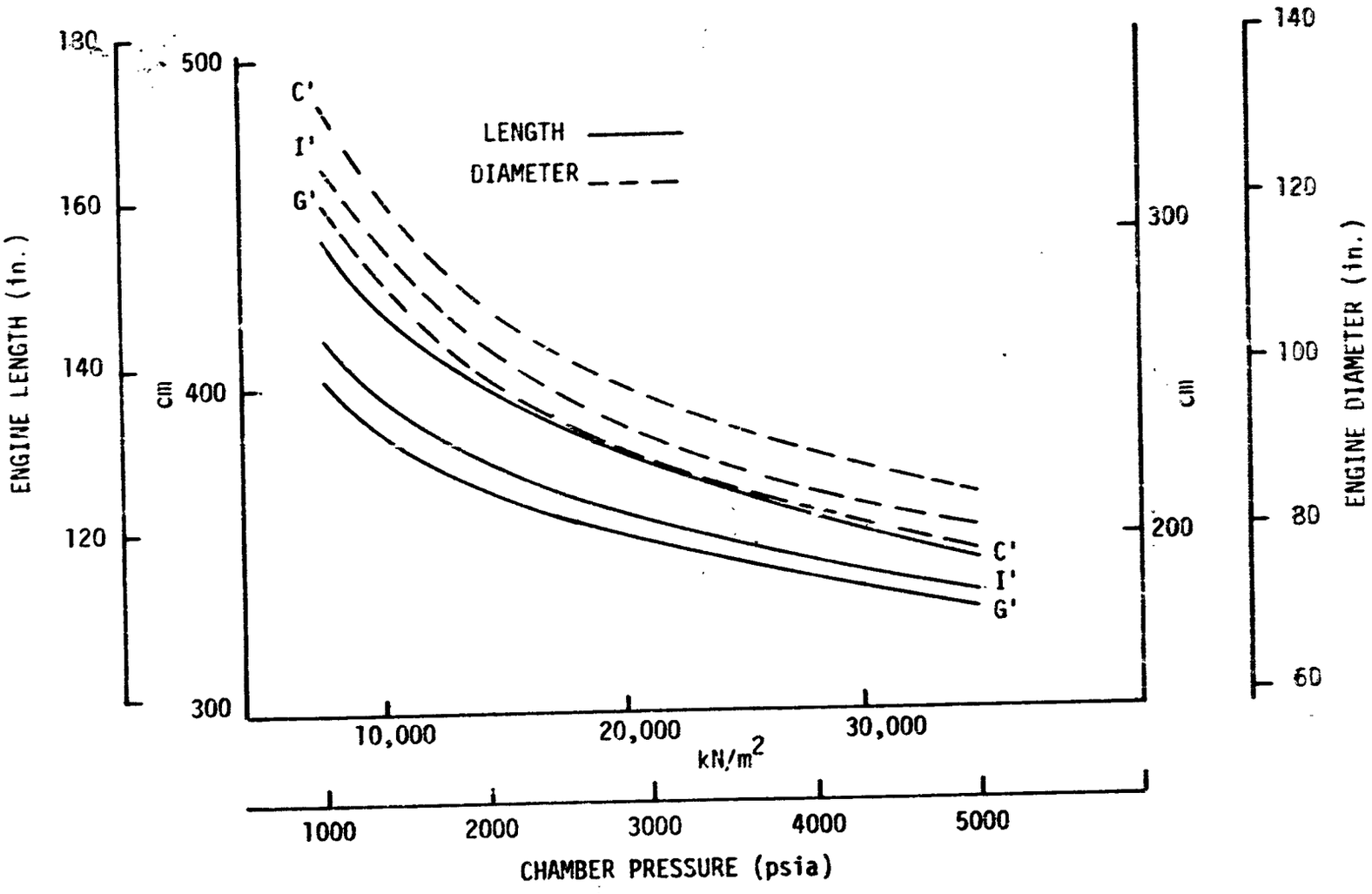

Figure 93. LOX/LC_3H_8 Engine Envelope Parameters Versus Chamber Pressure

IV, D, Engine Envelope (cont.)

The diameter and length parametrics for the engines were calculated by using the envelopes established for similar engines in References 9 and 10. This assumption proved satisfactory when the engine layouts were prepared (see Section VI.I.). The parametrics assume a similar engine packaging arrangement for all power cycles. Diameter parametrics include an estimation of the powerhead diameter (pump envelope) to establish whether the nozzle exit or this envelope is greater. In essentially all cases the nozzle diameter exceeds the powerhead diameter.

V. VEHICLE ANALYSES FOR ENGINE ASSESSMENT

A. OBJECTIVES AND GUIDELINES

Ascent trajectory calculations and vehicle design analyses were employed in order to produce a preliminary comparison of the more promising of the selected engine cycles derived in Task I. The specific application was designated to be a heavy-payload, two-stage-to-orbit vehicle. The simplified vehicle/study results were used to provide a preliminary engine ranking based on vehicle payload capability, weight, size, and new technology requirements criteria. More detailed trajectory analysis with several vehicle concepts is required before a final engine ranking can be made.

B. VEHICLE CHARACTERISTICS

A tandem-mounted heavy-lift launch vehicle (HLLV) was selected over parallel-mounted vehicles that utilized propellant cross-feeding. This selection simplified the trajectory calculations and led to a straightforward evaluation of the engine cycles. The smaller of two NASA/Johnson Space Center (JSC) vehicles cited in Reference 23 was selected for this analysis. The basic characteristics of the two-stage vehicle are given in Figure 94 for both a LOX/RP-1 and a LOX/propane propellant combination. The LOX/RP-1 booster from the figure delivers a 454 metric ton (1,000,900 lbm) payload into a 90 x 500 km orbit. Both stages of the vehicle return ballistically for water recovery.

Since the sole purpose of this analysis was to rank the various LOX/HC engine cycles, it was considered satisfactory to assume typical characteristics regarding the JSC vehicle. The Stage I LOX/RP-1 vacuum specific impulse used was 350 seconds, and the Stage II LOX/LH_2 vacuum specific impulse used was 464 seconds. The Stage I thrust-to-weight ratio was 1.3, and the Stage II thrust-to-weight ratio used was 1.0. The ideal velocity increments calculated for the two stages from the data in Figure 94 are 3036 to

REF. DOE/ER-0023 OCT. 1978

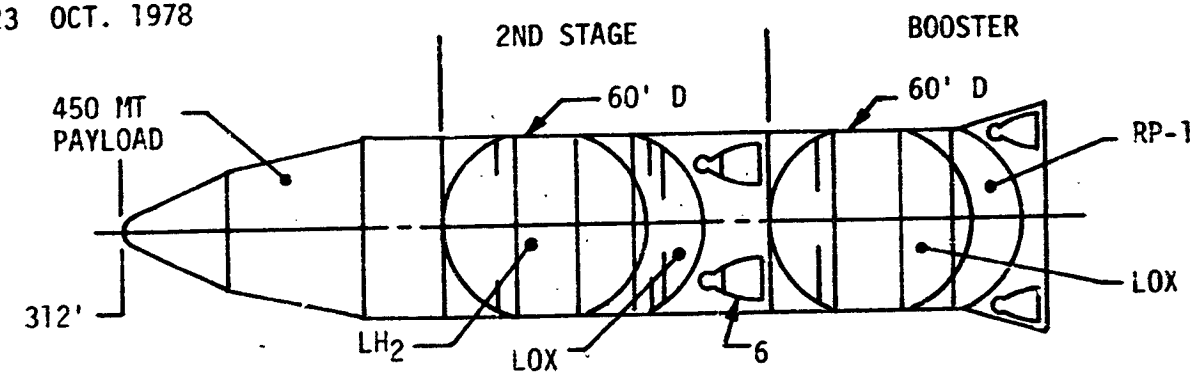

	O_2/RP-1 BOOSTER	O_2/PROPANE BOOSTER
PAYLOAD, TONS, 90 x 500 km	454	454
STAGE 1 INERT, TONS	500	485
STAGE 1 PROPELLANT, TONS	4441	4410
STAGE 2 INERT, TONS	233	245
STAGE 2 PROPELLANT, TONS	1937	2056
GROSS LIFT-OFF WEIGHT, TONS	7565	7659
NUMBER OF ENGINES, STAGE 1	12	12
NUMBER OF ENGINES, STAGE 2	6	6
STAGING ALTITUDE, km	43.4	41.3
STAGING VELOCITY (REL), km/sec	1.84	1.70
BOOSTER MAXIMUM DOWN RANGE	381	346

Figure 94. JSC Two-Stage Ballistic Launch Vehicle

6096 m/s (9,960 and 20,000 ft/sec), respectively, for Stage I and Stage II. An averaged specific impulse (to account for altitude compensation) was utilized for Stage I to simulate integrated trajectory results, modifying the above ideal velocity values for each fuel.

C. VEHICLE RESULTS

Vehicle parametric performance data were generated for both LOX/RP-1 and LOX/CH_4 engines assuming a constant gross liftoff weight (GLOW) and constant conditions for Stage II. The basic number of LOX/HC engines used in Stage I was thirty-six in order to keep the engine thrust consistent with the nominal value of this study (2669 kN or 600K lbF). The tanks were resized as required to accommodate the propellant volume changes in Stage I. Tank weight was assumed to vary linearly with volume as derived from previous SSTO studies. The number of Stage I engines and/or their thrust level was also varied to provide the required liftoff thrust. The payload results for LOX/RP-1 and LOX/LCH_4 engines are summarized in Figure 95. Similar data were generated for LOX/C_3H_8 engines.

Given the Stage I engine cycle performance and engine thrust-to-weight ratio data from Sections IV.B. and IV.C., the relative payload ranking of each cycle can be obtained from the figure. The payload data for the various cycles over the pressure ranges indicated are summarized in Figure 96.

Observations from this analysis are as follows: (1) vehicle performance depends heavily on Stage I specific impulse and is relatively insensitive to engine weight; (2) the payload gains for CH_4 are considered real, but may be altered downward when a detailed vehicle design analysis is performed; and (3) dual-throat nozzles appear to offer orbital payload gains of about 3%, but this gain may be reduced slightly when optimized integrated trajectories are used to fully account for the gravity losses with thrust reduction.

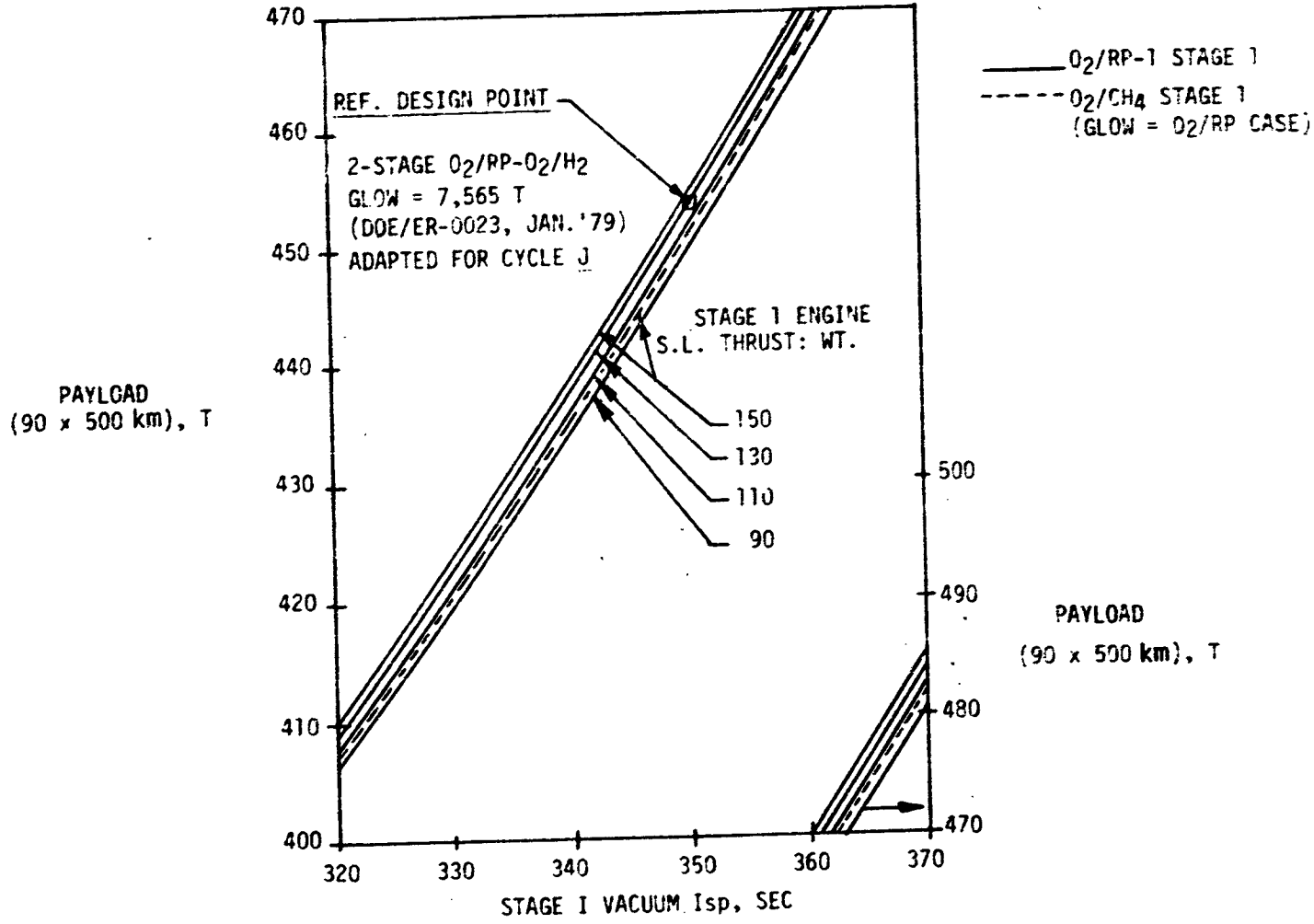

Figure 95. Orbital Payload vs Stage 1 Vacuum Isp

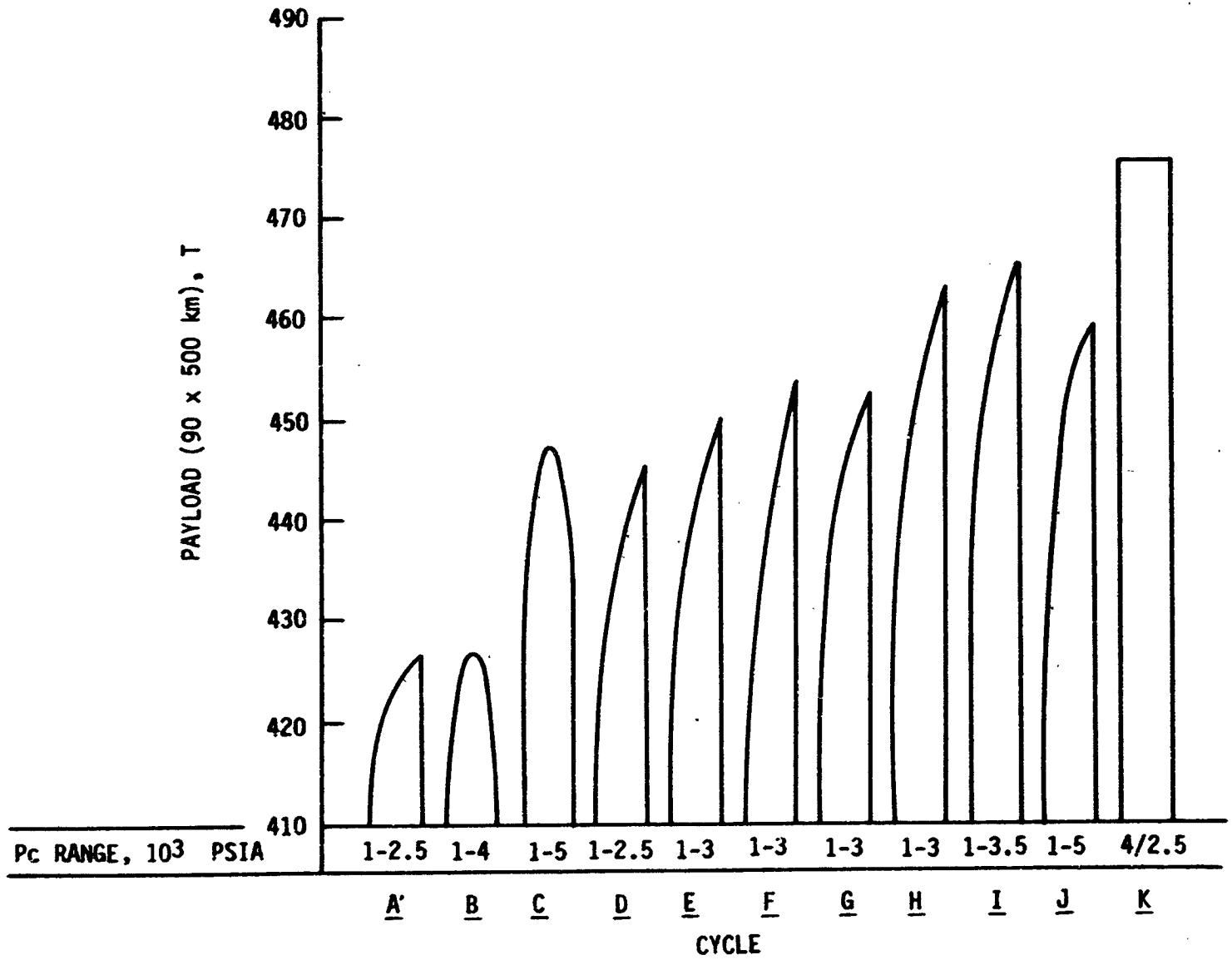

Figure 96. Orbital Payload vs Chamber Pressure for Cycles A Through K

V, Vehicle Analyses for Engine Assessment (cont.)

D. ENGINE CYCLE RANKING

The preliminary orbital payload ranking of the LOX/HC engine cycles is summarized in Figure 97 for each cycle, including the LOX/C_3H_8 engines. Only the optimum chamber pressure points are included in the figure. It can be seen that cycle K offers the highest payload capability because of its altitude compensation (variable performance) feature. Cycles I (and I') and C are the best staged-combustion and gas-generator cycles, respectively. If CH_4 is substituted for RP-1 fuel in Cycle J, this cycle will be closely competitive with Cycle I.

Table XXXV summarizes the engine cycle rating based on the criteria established in Section III.E (Figure 49) and the results of the vehicle applications analysis. It is seen that the preliminary cycle rating in Table XXXV closely follows the orbital payload ranking of Figure 97 because of the emphasis on payload performance in the rating.

From these results, the conclusions of Figure 98 can be made:

(1) Cycles that perform poorly are A, A', B, D and F;
(2) Acceptable performing cycles are D', E, F', G, C and C';
(3) Good performing cycles are G', H, I, I', J, (J', J") and K.

Cycles C, G, and I were jointly selected by NASA and Aerojet for continued analysis in Task IV of the study, as these cycles are representative of typical engines that might be required for advanced launch vehicles.

ASSUMPTIONS

TWO STAGE BALLISTIC LAUNCH VEHICLE

TURBINE TEMP: FR 1860°R; OR 1660°R

ENGINES OPTIMIZED FOR EITHER:

POWER LIMIT ($P_D \leq 8000$ PSIA)

PEAK Is (GG CYCLES)

RP-1 COKING TEMP.

CODE: COOLANTS: RP-1, RP-1R*, LO_2, LCH_4, LH_2, LC_3H_8

FR = FUEL-RICH OR = OXIDIZER-RICH

GG = GAS GENERATOR PB = PREBURNER

HR = HYDROGEN-RICH *REFINED RP-1

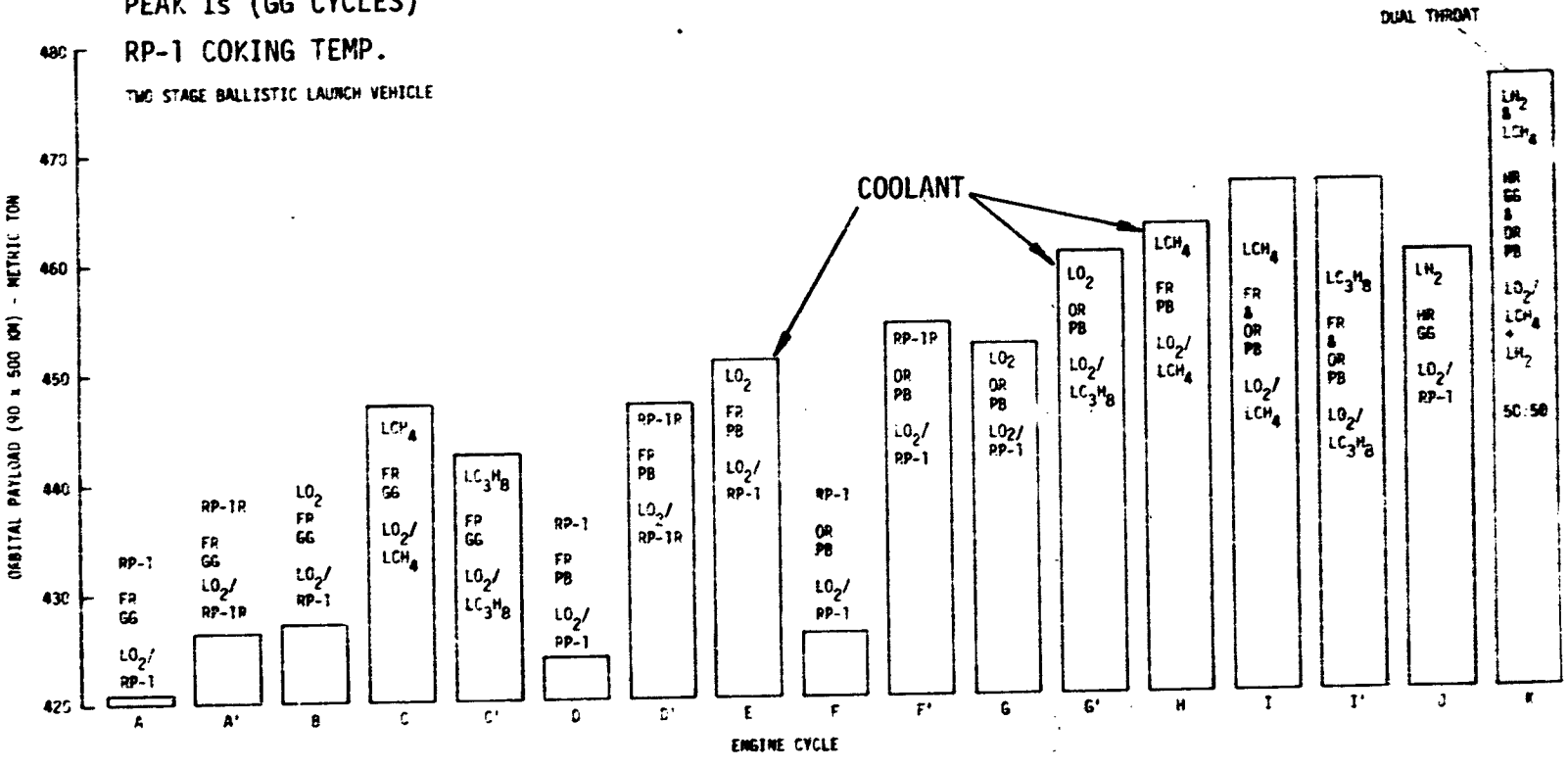

Figure 97. Orbital Payload Ranking of LO_2/HC Engine Cycles (At Optimum Chamber Pressure)

TABLE XXXV

LO_2/HC ENGINE CYCLE RATING

	Cycle	Fuel	Vacuum Performance (Isp)	(Rating)	Engine Weight lbm	(Rating)	Pressure Chamber psia	(Rating)	Hydrocarbon Coking**	(Rating)	Inter-Propellant Seals	(Rating)	Mixture Ratio	(Rating)	Coolant Capability	(Rating)	Pump Discha. Pressure psia	(Rating)	Rating (Maximum Of 30)	Ranking Order
A	FC/FR/GG	RP-1	328	(7)	4720	(0.6)	1300	(2.9)	Yes	(0)	Yes	(0)	2.55	(.6)	Poor	(0)	4500	(2)	7.1	17
A'	FC/FR/GG	RP-1B*	331	(2.1)	4380	(0.9)	2500	(2.1)	Yes	(0)	Yes	(0)	2.40	(.4)	Fair	(1)	5100	(1.7)	8.2	15
B	OF/FR/GG	RP-1	332	(2.4)	4250	(1.2)	2500	(2.1)	Yes	(0)	Yes	(0)	2.43	(.4)	Good	(2)	3900	(2.4)	10.3	14
C	FC/FR/GG	LCH_4	348	(8.2)	4905	(0.5)	3000	(1.7)	?	(2.5)	Yes	(0)	3.07	(.4)	Good	(2)	4500	(2)	17.3	8
C'	FC/FR/GG	LC_2H_2	344	(6.7)	4845	(0.6)	3000	(1.7)	?	(2)	Yes	(0)	2.71	(.4)	Good	(2)	4200	(2.2)	15.6	10
D	FC/FR/GG	RP-1	332	(2.4)	5560	(0)	1200	(3)	Yes	(0)	Yes	(0)	2.80	(1)	Poor	(0)	5530	(1.5)	7.9	16
D'	FC/FR/GG	RP-1B*	347	(7.8)	4915	(0.5)	2500	(2.1)	Yes	(0)	Yes	(0)	2.80	(1)	Fair	(1)	4300	(2)	12.4	12
E	OF/FR/GG	RP-1	343	(6.5)	4760	(0.6)	2900	(2.8)	Yes	(0)	Yes	(0)	2.80	(1)	Good	(2)	3600	(2.8)	14.1	11
F	FC/GR/GG	RP-1	334	(3.2)	5560	(0)	1300	(2.9)	No	(3)	Yes	(0)	2.80	(1)	Poor	(0)	6100	(1.3)	11.3	13
F'	FC/GR/GG	RP-1B*	351	(9.3)	5040	(0.4)	3250	(1.6)	No	(3)	Yes	(0)	2.80	(1)	Fair	(1)	8000	(0.2)	16.5	9
G	OF/GR/GG	RP-1	350	(8.9)	4830	(0.6)	3100	(1.7)	No	(3)	Yes	(0)	2.80	(1)	Good	(2)	4700	(2.3)	17.5	7
G'	OF/GR/GG	LC_2H_2	357	(11.6)	4840	(0.5)	3200	(1.6)	No	(3)	Yes	(0)	3.10	(1)	Good	(2)	8000	(0.2)	19.7	4
H	FC/FR/GG	LCH_4	358	(11.8)	5310	(0.2)	3000	(1.7)	?	(2.5)	Yes	(0)	3.50	(1)	Good	(2)	9600	(0.2)	19.4	5
I	FC/HR/GG	LCH_4	361	(12.9)	5520	(0)	3500	(1.4)	?	(2.7)	No	(2)	3.50	(1)	Good	(2)	8100	(1.1)	22.1	2
I'	FC/HR/GG	LC_2H_2	359	(12.3)	5560	(0)	3600	(1.3)	?	(2.5)	No	(2)	3.10	(1)	Good	(2)	7900	(0.9)	21.1	3
J	HC/HR/GG	RP-1	357	(11.4)	5080	(0.4)	5500	(0)	No	(3)	Yes	(0)	(2.68)	(.8)	Excel.	(3)	7600	(0.8)	19.0	6***
K	HC/HR/HC	LCH_4	356 380	(15)	5570	(0)	2800 4000	(1.5)	?	(2.7)	No	(2)	(3.35)	(.8)	Good	(2.5)	7430	(0.5)	25.0	1
Ref. Maximum Values			367	(15)	4250	(1)	1200	(3)	No	(3)	No	(2)	SC	(1)	Excel	(3)	4500	(2)	30	

*Refined RP-1 Required.

**High Turbine Temperatures May Alleviate Problem.

***Normalized to CH_4 Fuel Would Change Ranking Order to 3.

CYCLE	COMMENT
• LOX/RP-1, GAS GENERATOR CYCLES A, A' & B	POOR PERFORMERS
• LOX/RP-1, RP-1 COOLED, STAGED COMBUSTION CYCLES D AND F	POOR PERFORMERS
• LOX/RP-1, STAGED COMBUSTION CYCLES D', E, F' & G	ACCEPTABLE PERFORMERS
• LOX/CH_4 OR C_3H_8, GAS GENERATOR CYCLES C & C'	ACCEPTABLE PERFORMERS
• LOX/CH_4 OR C_3H_8, STAGED COMBUSTION CYCLES G', H, I & I'	GOOD PERFORMERS
• LOX/RP-1 (OR CH_4 OR C_3H_8) LH_2 GAS GENERATOR CYCLES J (J' & J'')	GOOD PERFORMERS
• DUAL THROAT CYCLE K	GOOD PERFORMER

Figure 98. Recommended Cycles

VI. BASELINE ENGINE SYSTEM DEFINITION

A. OBJECTIVES AND GUIDELINES

The objective is to conduct a preliminary design analysis of the major components and subsystems of the baseline engines selected from the results of Tasks I through III. The analysis is to include engine heat transfer, combustion stability, and structural analyses. The primary control points of the engine are to be defined, including startup and cutoff sequences. The major technology requirements to implementing the engine designs are to be indicated.

Detailed parametric and sensitivity analyses of the selected baseline engine concepts are to be carried out to include a complete power cycle balance for every data point. The sensitivity of engine performance and weight to mixture ratio, thrust, chamber pressure, and area ratio are to be examined. In addition, the effects of increasing maximum allowable turbine inlet temperature is to be investigated to determine the potential of fuel-cooled turbine blading or the use of higher temperature materials. The effects of increasing the number of usable start/shutdown cycles (from the minimum 100 to 200 and 300) on engine performance and weight are to be examined.

The following parametric and sensitivity analysis ranges were selected for guiding this effort:

VI, A, Objectives and Guidelines (cont.)

Parameters	Range
Specific impulse and engine weight as a function of:	
Mixture ratio	Nominal ± 10%
Thrust	600,000 and 1,000,000 lbf
Chamber Pressure	Nominal ± 500 psia
Area Ratio	Nominal, Opt. sea level, @ 10 psia
Turbine Inlet Temperature	
Fuel-Rich	1660°, 1860°, 2260°, and 2960°R
Oxidizer-Rich	1660° and 2600°R
Cycles	100, 200, and 300

B. PARAMETRIC AND SENSITIVITY ANALYSES

Detailed parametric and sensitivity analyses of the selected baseline engine concepts (Figures 99-101) were conducted, including a power balance for each data point. The power balance/engine specifications are given in Tables XXXVI, XXXVII, and XXXVIII. The engine weight breakdown for each nominal engine cycle design point is given in Section IV,C (Table XXIX).

Data for the engine sensitivity analysis are summarized in Table XXXIX. The variation in sea level and vacuum engine performance and the variation in engine weight with the various sensitivity parameters are shown. At one million pounds thrust level, each engine cycle exhibits a very slight performance gain (0.3-0.5 sec), but there is a reduction in the engine thrust-to-weight value. The increase in weight is about 80% compared to a thrust increase of 67%, primarily because of the increase in wall thickness required for the larger diameter components.

Variations in mixture ratio of -10% and +10% from the nominal design point are seen to result in a loss in performance (-1 to -3 sec for

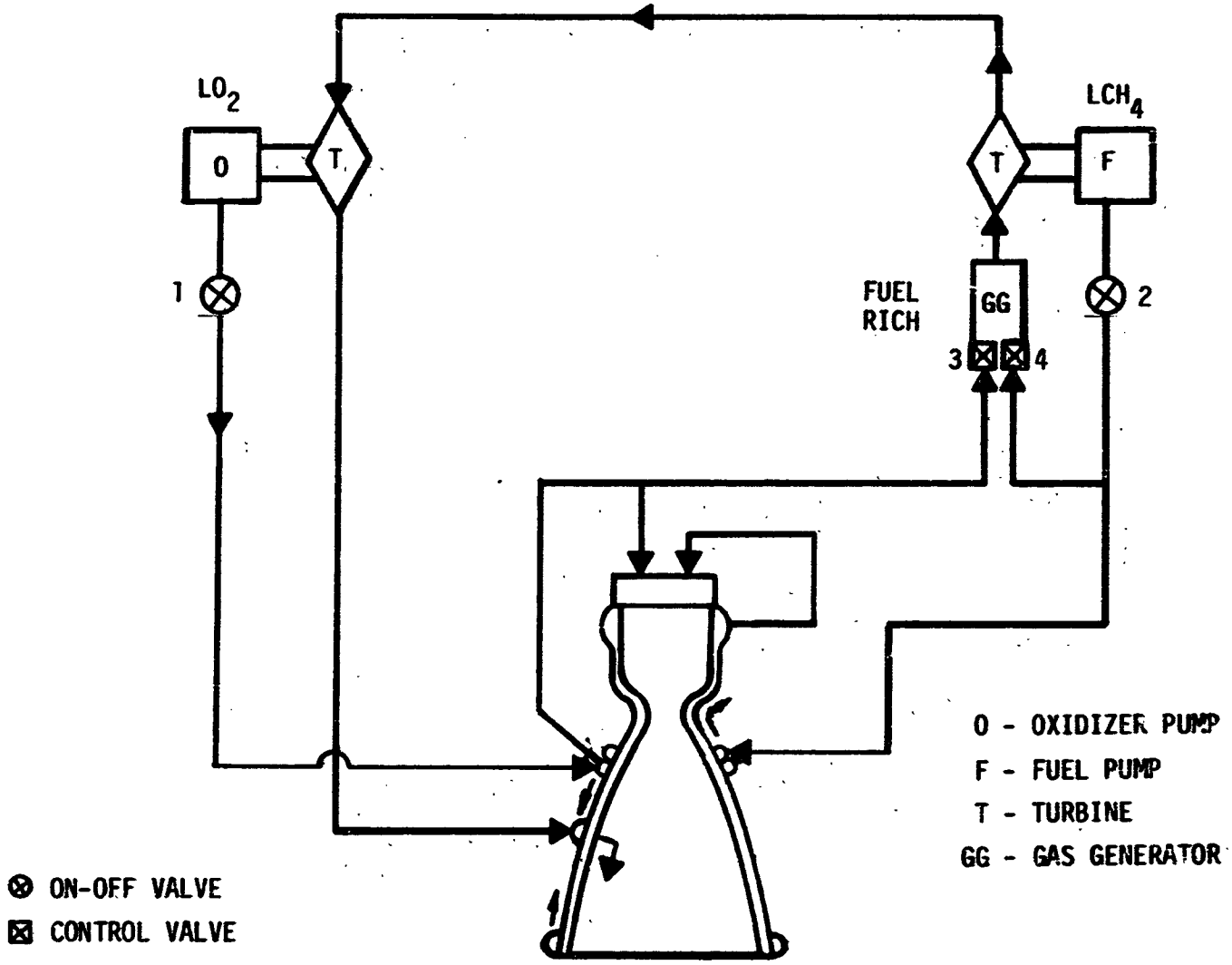

Figure 99. LCH_4 Fuel-Rich Gas-Generator Cycle (C) LCH_4-Cooled

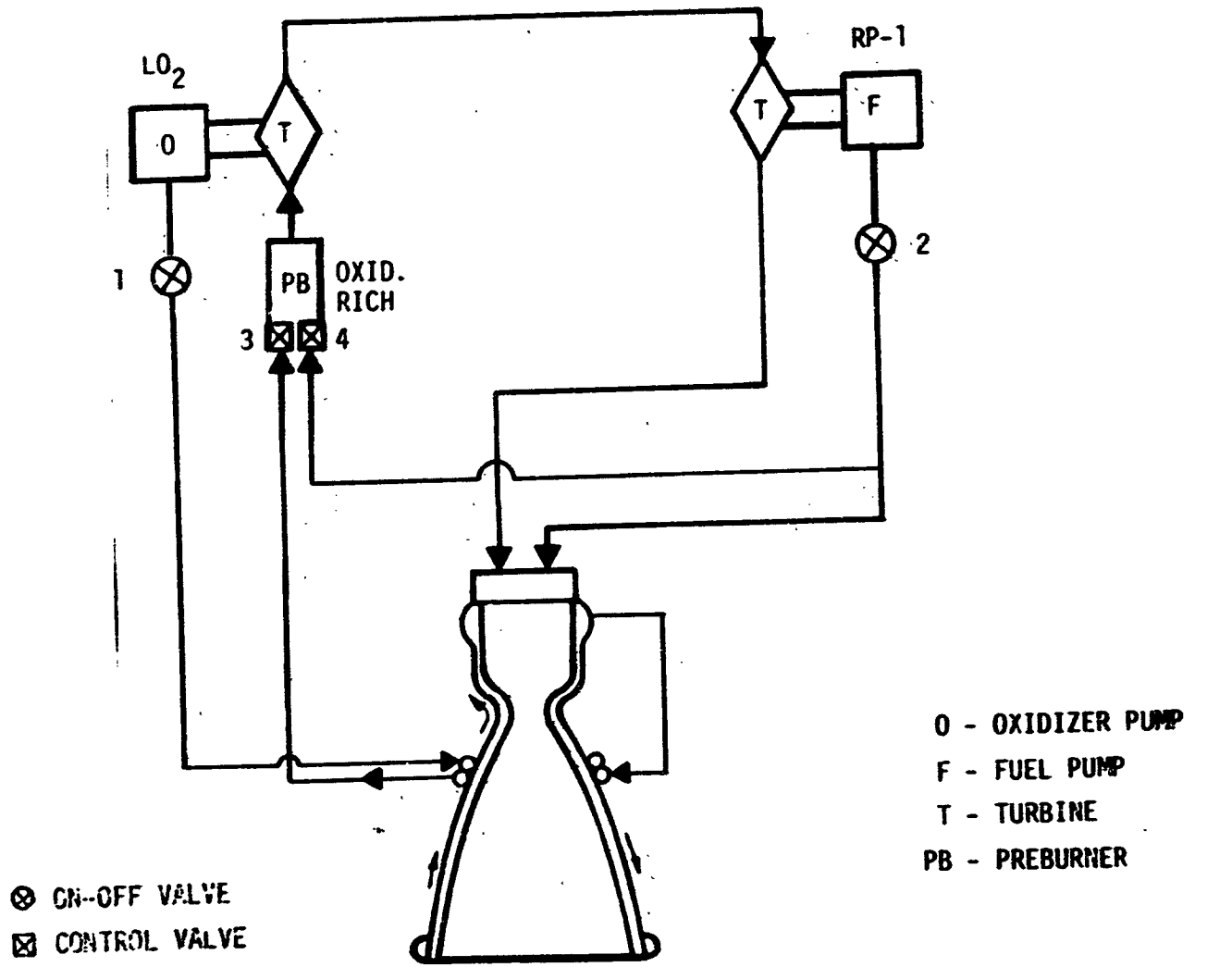

Figure 100. LO_2/RP-1 Oxidizer-Rich Preburner Staged-Combustion Cycle (G) LO_2-Cooled

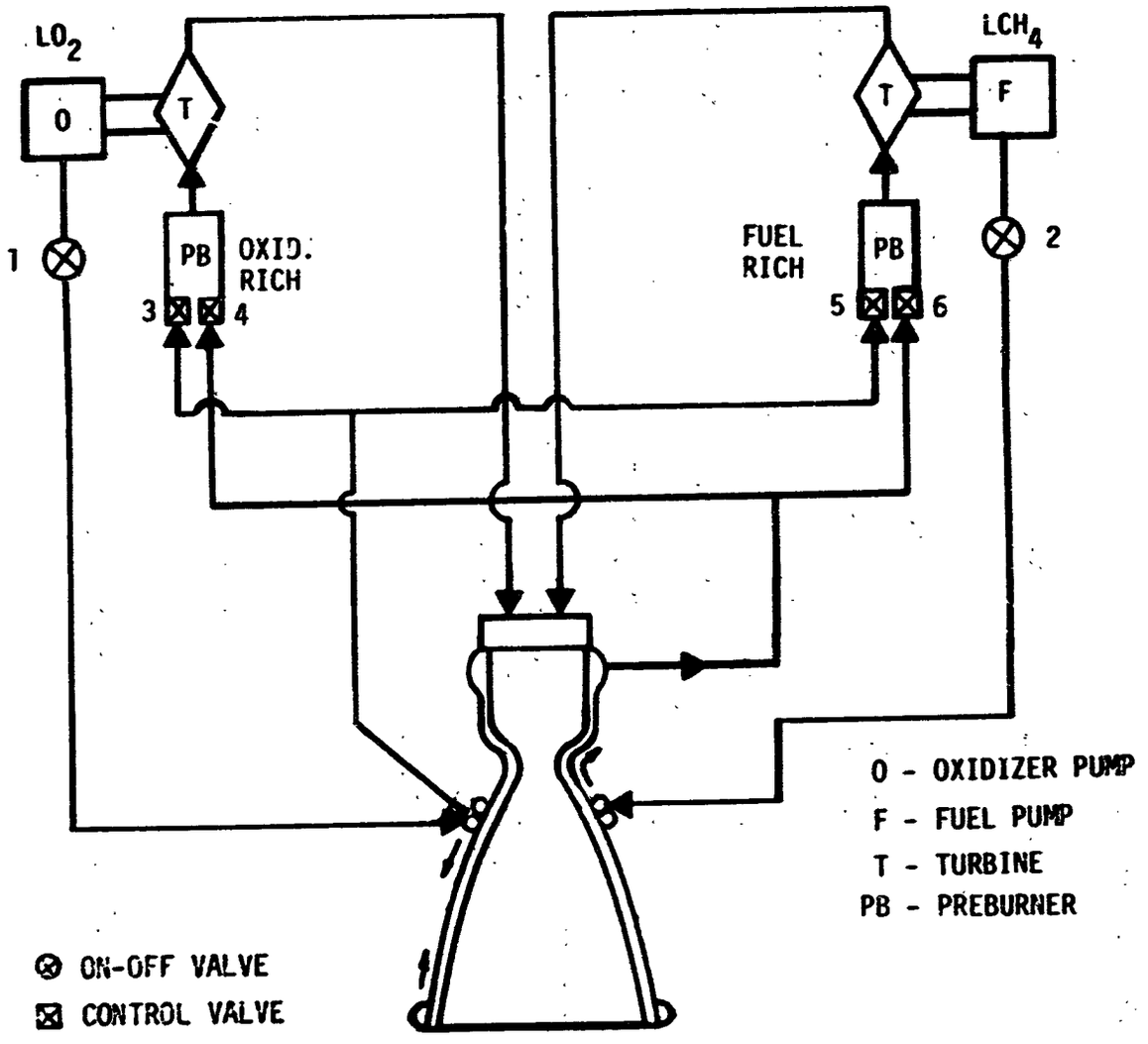

Figure 101. LCH_4 Mixed Preburner Staged-Combustion Cycle (I) LCH_4-Cooled

TABLE XXXVI

LO4/LCH$_4$ ENGINE CYCLE C SPECIFICATIONS

PARAMETER	600K NOMINAL DESIGN POINT	IM DESIGN POINT	600K MP VAR (-10%)	600K MR VAR (+10%)	600K Pc VAR (-500)	600K Pc VAR (+500)	600K ε VAR SL JET	600K ε VAR Pe = 10	600K NOMINAL DESIGN POINT	600K CYCLE ΔP 300	600K CYCLE ΔP 300	500K T_{TI} VAR 1550°R	500K T_{TI} VAR 2250°R	500K T_{TI} VAR 2960°R
Chamber Pressure, Psia	4,300	4,300	4,300	4,300	3,800	4,800	4,300	4,300	4,300	3,800	3,800	4,300	4,300	4,300
S.L. Engine Thrust, lbF	600,000	1,000,000	600,000	600,000	600,000	600,000	600,000	600,000	600,000	600,000	600,000	600,000	600,000	600,000
Vac Engine Thrust, lbF	671,239	1,119,339	672,509	671,893	673,039	670,608	638,877	681,583	671,239	673,685	676,323	671,849	670,330	673,367
Mixture Ratio	2.82	2.81	2.57	3.06	2.91	2.71	2.82	2.82	2.82	2.85	3.08	2.55	3.08	3.34
Area Ratio	56.5	56.5	55.6	56.7	51.1	61.9	28.1	38.2	56.5	51.2	55.0	56.5	56.5	56.5
TCA ODE S.L. Is, Sec	340.2	340.2	337.4	337.7	337.9	342.3	344.7	344.1	340.2	337.9	338.2	340.2	340.2	340.2
TCA ODE Vac, Is, Sec	376.5	376.5	374.1	374.2	374.8	378.1	363.1	369.2	376.5	374.8	374.7	376.5	376.5	376.5
Is Efficiency, % (-)	.918	.919	.922	924	.927	.910	.919	.920	.918	.922	.922	.907	.958	.946
Gel. S.L. Is, Sec	309.1	309.2	307.8	308.8	309.7	307.6	313.3	312.9	309.1	307.8	308.7	304.3	314.3	317.3
Gel. Vac Is, Sec	345.8	346.1	345.0	345.8	347.4	343.9	333.6	339.8	345.8	345.6	345.7	341.2	351.7	356.1
Flowrate, lb/sec	1941.12	3434.15	1949.3	1943.01	1937.36	1950.59	1916.10	1917.65	1941.12	1949.32	1959.12	1968.62	1905.97	1890.95
LO_2 Flowrate, lb/sec	1432.70	2385.29	1403.28	1464.14	1441.87	1424.82	1413.76	1415.67	1433	1443.07	1451.48	1428.85	1439.95	1354.92
CH_4 Flowrate, lb/sec	508.43	848.86	546.02	478.87	495.49	525.77	501.34	501.98	508.43	506.25	507.64	540.06	467.02	436.02
C*, Ft/Sec	6,111	6,111	6,174	6,007	6,104	6,117	6,111	6,111	6,111	6,109	6,098	6,111	6,111	6,111
Throat Area, In.^{2}	76.6	127.7	77.7	75.9	88.2	67.8	75.6	75.8	76.6	87.7	95.9	76.3	77.6	79.1
Exit Area, In.^{2}	4,349	7,214	4,319	4,402	4,598	4,196	2,122	2,894	4,342	4,492	5,600	4,315	4,325	4,473
Exit ODE Pressure, Psia	6.0	6.0	5.0	6.0	6.0	6.0	14.7	10.0	6.0	6.0	6.0	6.0	6.0	6.0
TCA LO_2 Flowrate, lb/sec	1387.95	2307.42	1357.09	1421.60	1404.81	1377.96	1369.43	1387.93	1387.95	1400.65	1410.77	1383.58	1394.34	1409.15
TCA CH_4 Flowrate, lb/sec	396.56	659.26	430.82	369.25	401.37	391.99	391.27	391.71	396.56	400.19	403.28	416.31	398.38	402.61
TCA S.L. Thrust, lbF	583,712	972,184	583,215	584,176	586,230	579,995	583,494	583 275	583,712	585,092	586,052	581,705	586,099	592,628
TCA Vac Thrust, lbF	648,668	1,080,171	649,010	649,721	654,020	648,145	618,884	630,343	648,668	652,283	654,797	646,614	651,644	658,576
TCA S.L. Is, Sec	327.1	327.1	326.2	326.2	324.9	328.8	331.4	330.9	327.1	324.9	325.1	327.1	327.1	327.1
TCA Vac Is, Sec	363.5	364.1	363.0	362.8	362.1	364.6	361.5	357.6	363.5	362.2	361.0	363.5	363.5	363.5
TCA Mixture Ratio	3.5	3.5	3.15	3.85	3.5	3.5	3.5	3.5	3.5	3.5	3.5	3.5	3.5	3.5
GG Mixture Ratio	0.40	0.40	0.40	0.40	0.40	0.40	0.40	0.40	0.40	0.40	0.40	0.31	0.48	1.37
GG S.L. Thrust, lbF	16,288	27,816	16,785	15,824	13,170	20,005	16,596	16,724	16,288	14,909	17,848	18,127	13,601.35	7,372
GG Vac Thrust, lbF	22,928	39,156	23,628	22,278	18,902	27,694	19,993	21,201	22,922	21,084	24,147	47,608	30,592	21,322
GG S.L. Is, Sec	104.0	104.0	104.0	104.0	100.4	107.2	106.9	108.0	104.0	100.4	97.9	95.6	120.1	93.1
GG Vac Is, Sec	146.4	146.4	146.4	146.4	144.1	146.4	128.9	138.9	146.4	144.7	139.6	124.4	137.1	139.3
GG Flowrate, lb/sec	156.61	267.66	161.39	152.16	131.17	186.62	154.41	154.85	156.61	139.36	140.47	179.52	110.25	79.19
GG LO_2 Flowrate lb/sec	44.75	76.42	46.11	43.97	37.48	53.32	44.19	44.26	44.75	42.40	40.71	54.37	44.61	45.77
GG CH_4 Flowrate, lb/sec	111.87	191.04	115.28	108.68	93.69	133.30	110.22	110.61	111.87	106.96	100.76	123.77	89.64	34.41
Coolant Flowrate, lb/sec	396.56	659.26	430.82	369.25	401.37	391.99	391.27	391.27	396.56	400.19	403.24	416.31	394.19	402.61
Coolant ΔP, Psi	2,750	5,127	2,750	2,750	1,827	4,191	3,750	3,750	2,750	2,687	2,755	2,750	2,750	2,750
Coolant ΔT, °R	154	138	154	154	152	156	154	154	154	152	159	153	154	154
Turbine Inlet Temp °R	1,860	1,860	1,860	1,860	1,860	1,860	1,860	1,860	1,860	1,860	1,860	1,860	1,860	2,960
Fuel Pump Discha P., Psia	7,953	8,336	7,954	7,953	6,409	9,924	7,953	7,953	7,973	8,058	8,003	7,960	7,953	7,953
LO_2 Pump Discha. P., Psia	5,262	5,262	5,262	5,262	4,626	5,909	5,262	5,262	5,262	4,626	4,085	5,262	5,262	5,262
Engine Weight, lbs	5,075	9,111	5,138	5,004	4,902	5,177	4,840	4,911	5,075	4,836	4,784	5,151	4,978	4,957

TABLE XXXVII

LOX/RP-1 ENGINE CYCLE G SPECIFICATIONS

PARAMETER	600K NOMINAL DESIGN POINT	IM DESIGN POINT	600K MR VAR. (-10%)	600K MR VAR. (+10%)	600K Pc VAR. (-500)	600K Pc VAR. (+500)	600K ε VAR. S.L. OPT.	600K ε VAR. Pe = 10
Chamber Pressure, Psia	3,100	3,100	3,100	3,100	2,600	3,600	3,100	3,100
S.L. Engine Thrust, lbF	600,000	1,000,000	600,000	600,000	600,000	600,000	600,000	600,000
Vac. Engine Thrust, lbF	670,832	1,117,816	670,579	671,939	675,316	669,582	635,176	647,002
Mixture Ratio	2.8	2.8	2.52	3.08	2.8	2.8	2.8	2.8
Area Ratio	42.5	42.5	41.4	43.0	37.0	47.5	20.9	28.3
ODE S.L. Is, Sec	325.9	325.9	322.7	325.3	321.4	329.0	329.6	329.4
ODE Vac. Is, Sec	362.8	362.8	359.3	362.3	359.6	364.9	348.2	354.1
Is Efficiency, % (V)	0.964	0.965	0.966	0.957	0.965	0.965	0.965	0.965
Del. S.L. Is, Sec	312.8	313.2	310.5	309.7	308.3	315.6	317.4	316.9
Del. Vac. Is, Sec	349.7	350.1	347.1	346.7	347.0	352.2	336.0	341.7
Flowrate, LB/Sec	1918.31	3192.85	1932.37	1937.36	1946.16	1901.14	1890.33	1893.44
LO_2 Flowrate, LB/Sec	1413.49	2352.62	1383.40	1462.52	1434.01	1400.84	1392.88	1395.17
HC Flowrate, LB/Sec	504.82	840.22	548.97	474.84	512.15	500.30	497.46	498.27
C*, Ft/Sec	5,927	5,927	5,988	5,853	5,914	5,938	5,927	5,927
Throat Area, IN^2	114.0	189.7	116.0	113.7	137.6	97.5	112.3	112.5
Exit Area, IN^2	4,845	8,064	4,803	4,889	5,091	4,630	2,348	3,184
Exit ODE Pressure, Psia	6.0	6.0	6.0	6.0	6.0	6.0	14.7	10
PB Mixture Ratio	45	45	45	45	45	45	45	45
PB LO_2 Flowrate, LB/Sec	1413.49	2352.62	1383.40	1462.52	1434.01	1400.84	1392.88	1395.17
PB HC Flowrate, LB/Sec	31.41	52.28	30.74	32.50	31.87	31.13	30.95	31.00
Coolant Flowrate, LB/Sec	1413.49	2352.62	1383.40	1462.52	1434.01	1400.84	1392.88	1395.17
Coolant ΔP, Psi	1,281	1,532	1,281	1,281	805	2,085	1,281	1,281
Coolant ΔT, °R	77	69	77	77	75	78	77	77
Turbine Inlet Temp. °R	1,660	1,660	1,660	1,660	1,660	1,660	1,660	1,660
Fuel Pump Dischg. P., Psia	3,702	3,702	3,702	3,702	3,105	4,299	3,702	3,702
Fuel (PB) Pump Dischg. P., Psia	6,400	6,504	6,486	6,333	4,836	8,691	6,400	6,400
LO_2 Pump Dischg. P., Psia	7,733	8,091	7,819	7,665	5,678	10,851	7,733	7,733
Engine Weight, lb_M	4,663	8,379	4,684	4,690	4,584	4,780	4,432	4,496

TABLE XXXVII (cont.)

LOX/RP-1 ENGINE CYCLE G SPECIFICATIONS

PARAMETER	600K NOMINAL DESIGN POINT	600K CYCLE VAR. 200	600K CYCLE VAR. 300	600K TTI VAR. 2600°R
Chamber Pressure, Psia	3,100	2,920	2,780	3,500
S.L. Engine Thrust, lbF	600,000	600,000	600,000	600,000
Vac. Engine Thrust, lbF	670,832	672,039	672,634	670,073
Mixture Ratio	2.8	2.8	2.8	2.8
Area Ratio	42.5	40.5	39.0	46.6
ODE S.L. Is, Sec	325.9	324.2	323.3	328.6
ODE Vac. Is, Sec	362.8	361.8	361.0	364.6
Is Efficiency, % (V)	0.964	0.964	0.964	0.965
Del. S.L. Is, Sec	312.8	311.5	310.6	315.1
Del. Vac. Is, Sec	349.7	348.9	348.2	351.9
Flowrate, LB/Sec	1918.31	1926.16	1931.75	1904.16
LO_2 Flowrate, LB/Sec	1413.49	1419.28	1423.39	1403.06
HC Flowrate, LB/Sec	504.82	506.89	508.35	501.09
C*, Ft/Sec	5,927	5,922	5,919	5,936
Throat Area, IN^2	114.0	121.42	127.83	100.37
Exit Area, IN^2	4,845	4,917	4,986	4,677
Exit ODE Pressure, Psia	6.0	6.0	6.0	6.0
PB Mixture Ratio	45	45	45	25
PB LO_2 Flowrate, LB/Sec	1413.49	1419.28	1423.39	1403.06
PB HC Flowrate, LB/Sec	31.41	31.54	31.63	56.12
Coolant Flowrate, LB/Sec	1413.49	1419.28	1423.39	1403.06
Coolant ΔP, Psi	1,281	1,897	2,176	1,908
Coolant ΔT, °R	77	76	75	78
Turbine Inlet Temp. °R	1,660	1,660	1,660	2,600
Fuel Pump Dischg. P., Psia	3,702	3,487	3,320	4,180
Fuel (PB) Pump Dischg. P., Psia	6,400	6,079	5,754	6,306
LO_2 Pump Dischg. P., Psia	7,733	8,035	7,992	8,275
Engine Weight, lb_M	4,663	4,627	4,599	4,779

TABLE XXXVIII

LOX/LCH_4 ENGINE CYCLE I SPECIFICATIONS

PARAMETER	600K NOMINAL DESIGN POINT	1M DESIGN POINT	600K MP VAR. (-10%)	600K MR VAR. (+10%)	600K PC VAR. (-500)	600K PC VAR. (+500)	600K ε VAR. sl OPT.	600K ε VAR. Pe = 10
Chamber Pressure, Psia	3,500	3,500	3,500	3,500	3,000	4,000	3,500	3,500
S.L. Engine Thrust, lbF	600,000	1,000,000	600,000	600,000	600,000	600,000	600,000	600,000
Vac. Engine Thrust, lbF	670,381	1,117,417	670,528	670,426	673,553	668,416	634,164	646,216
Mixture Ratio	3.5	3.5	3.15	3.85	3.5	3.5	3.5	3.5
Area Ratio	48.0	48.0	47.1	48.2	42.2	53.2	23.6	31.9
ODE S.L. Is, Sec	336.2	336.2	333.2	333.5	332.4	338.3	340.8	340.5
ODE Vac, Is, Sec	374.1	374.1	371.1	371.2	371.6	375.4	359.6	365.9
Is Efficiency, % (V)	.965	.966	.970	.969	.965	.966	.970	.971
Del. S.L. Is, Sec	323.1	323.4	322.1	322.1	319.4	325.4	330.0	329.9
Del. Vac. Is, Sec	361.0	361.4	360.0	359.8	358.5	362.5	348.8	355.3
Flowrate, LB/Sec	1857.01	3091.91	1862.78	1862.78	1878.52	1843.88	1818.18	1818.73
LO_2 Flowrate, LB/Sec	1444.34	2404.82	1413.91	1478.70	1461.07	1434.13	1414.14	1414.57
HC Flowrate, LB/Sec	412.67	687.09	448.86	384.08	417.45	409.75	404.04	404.16
C*, Ft/Sec	6,098	6,098	6,166	5,996	6,088	6,107	6,098	6,098
Throat Area, IN^2	100.6	167.4	102.0	99.19	118.5	87.5	98.5	98.5
Exit Area, IN^2	4,827	8,037	4,804	4,781	5,000	4,655	2,324	3,142
Exit ODE Pressure, Psia	6.0	6.0	6.0	6.0	6.0	6.0	14.7	10.0
PB Mixture Ratio	0.39/44.5	0.39/44.5	0.39/44.5	0.39/44.5	0.39/44.5	0.39/44.5	0.39/44.5	0.39/44.5
PB LO_2 Flowrate, LB/Sec	149.59/1294.75	247.69/2157.13	164.10/1249.81	138.04/1340.66	151.33/1309.74	148.54/1285.59	146.44/1267.70	146.51/1268.06
PB HC Flowrate, LB/Sec	383.58/29.10	635.11/51.98	420.77/28.09	353.95/30.13	388.02/29.43	380.86/28.89	375.49/28.55	375.66/28.50
Coolant Flowrate, LB/Sec	383.58	635.11	420.77	393.95	388.02	380.86	375.49	375.66
Coolant ΔP, Psi	1,370	1,535	1,370	1,370	833	2,088	1,370	1,370
Coolant ΔT, °R	150	134	150	150	147	153	150	150
Turbine Inlet Temp. °R	1860/1660	1860/1660	1860/1660	1860/1660	1860/1660	1860/1660	1860/1660	1860/1660
Fuel Pump Dischg. P., Psia	8,272	8,523	8,252	8,296	6,253	10,959	8,272	8,272
LO_2 (FPB) Pump Disch. P., Psia	6,847	6,930	6,827	6,871	5,381	8,795	6,847	6,847
LO_2 Pump Disch. P., Psia	6,654	6,651	6,694	6,622	5,282	8,101	6,654	6,654
Fuel (OPB) Pump Disch. P., Psia	6,504	6,501	6,544	6,472	5,227	7,983	6,504	6,504
Engine Weight, lbm	5,375	9,595	5,453	5,322	5,186	5,592	5,104	5,165

TABLE XXXVIII (cont.)

LOX/LCH$_4$ ENGINE CYCLE I SPECIFICATIONS

PARAMETER	600K NOMINAL DESIGN POINT	600K CYCLE VAR. 200~	600K CYCLE VAR. 300~	600K T_{TIF} VAR. 1660°R	600K T_{TIF} VAR. 2260°R	600K T_{TIF} VAR. 2960°R	600K T_{TIF}/T_{TI_D} VAR. 2960/2600
Chamber Pressure, Psia	3,500	3,200	3,000	3,200	3,700	3,700	4,000
S.L. Engine Thrust, lbF	600,000	600,000	600,000	600,000	600,000	600,000	600,000
Vac. Engine Thrust, lbF	670,381	670,962	673,553	670,962	669,195	669,195	668,416
Mixture Ratio	3.5	3.5	3.5	3.5	3.5	3.5	3.5
Area Ratio	48.0	44.7	42.2	44.7	50.0	50.0	53.2
ODE S.L. Is, Sec	336.2	334.2	332.4	334.2	337.3	337.3	338.3
ODE Vac, Is, Sec	374.1	372.1	371.6	372.1	374.3	374.3	375.4
Is Efficiency, % (V)	.965	.965	.965	.965	.966	.966	.966
Del. S.L. Is, Sec	323.1	321.3	319.4	321.3	324.3	324.3	325.4
Del. Vac. Is, Sec	361.0	359.3	358.5	359.3	361.7	361.7	362.5
Flowrate, LB/Sec	1857.01	1867.41	1878.52	1867.41	1850.14	1850.14	1843.88
LO_2 Flowrate, LB/Sec	1444.34	1452.43	1461.07	1452.43	1439.00	1439.00	1434.13
HC Flowrate, LB/Sec	412.67	414.98	417.45	414.98	411.14	411.14	409.75
C*, Ft/Sec	6,098	6,093	6,088	6,093	6,102	6,102	6,107
Throat APea, IN^2	100.6	110.5	118.5	110.5	94.8	94.8	87.5
Exit Area, IN^2	4,827	4,940	5,000	4,940	4,742	4,742	4,655
Exit ODE Pressure, Psia	6.0	6.0	6.0	6.0	6.0	6.0	6.0
PB Mixture Ratio	.39/44.5	.39/44.5	.39/44.5	.31/44.5	.65/44.5	1.37/44.5	1.37/29.2
PB LO_2 Flowrate, LB/Sec	149.59/1294.75	150.49/1302.00	151.33/1309.74	119.36/1333.07	249.87/1189.13	535.44/903.56	518.39/915.74
PB HC Flowrate, LB/Sec	383.58/29.10	385.72/29.26	388.02/29.43	385.02/29.96	384.42/26.72	390.84/20.31	378.39/31.36
Coolant Flowrate, LB/Sec	383.58	385.72	388.02	385.02	384.42	390.84	378.39
Coolant ΔP, Psi	1,370	1,907	2,121	1,001	1,582	1,582	2,088
Coolant ΔT, °R	150	148	147	148	151	151	153
Turbine Inlet Temp. °R	1860/1660	1860/1660	1860/1660	1660/1660	2260/1660	2960/1660	2960/2600
Fuel Pump Disch. P., Psia	8,272	8,193	7,951	7,681	7,893	7,168	8,217
LO_2 (FPB) Pump Disch. P., Psia	6,847	6,226	5,769	6,632	6,256	5,534	6,067
LO_2 Pump Disch. P., Psia	6,654	5,888	5,293	5,740	7,325	8,314	7,309
Fuel (OPB) Pump Disch.P., Psia	6,504	5,742	5,239	5,676	7.234	8,218	7,195
Engine Weight, lbm	5,375	5,253	5,186	5,245	5,486	5,572	5,708

TABLE XXXIX

ENGINE SENSITIVITY ANALYSIS SUMMARY

DESIGN POINT	CYCLE C LO_2/LCH_4 GG (CH_4-Cooled) Pc = 4300 F = 500K MR = 3.5 Life = 100~ ε = 56.5 T_{T_I} = 1860°R (Fuel-Rich) Wt = 5075			CYCLE G LO_2/RP-1 SC (LO_2-Cooled) Pc = 3100 F = 600K MR = 2.8 Life = 100~ ε = 42.5 T_{T_I} = 1660°R (OX-Rich) Wt = 4663			CYCLE I LO_2/LCH_4 SC (CH_4-Cooled) Pc = 3500 F = 600K MR = 3.5 Life = 100~ ε = 48.0 T_{T_I}(FR) = 1860 T_{T_I}(OR) = 1660°R Wt = 5375		
SENSITIVITY PARAMETER	ΔIs(SL)	ΔIs(V)	ΔWt %	ΔIs(SL)	ΔIs(V)	ΔWt %	ΔIs(SL)	ΔIs(V)	ΔWt %
THRUST F = 1M	+0.1	+0.3	81.5	+0.4	+0.4	79.7	+0.3	+0.4	78.5
MIXTURE RATIO -10%	-1.3	-0.8	+1.24	-2.3	-2.6	+0.45	-1.0	-1.0	+1.45
+10%	-0.3	-0.0	-1.40	-3.1	-3.0	+0.58	-1.0	-1.2	-0.99
CHAMBER PRESSURE -500	+0.6	+1.6	-3.41	-4.5	-2.7	-1.69	-3.7	-2.5	-3.52
+500	-1.5	-1.9	+2.01	+2.8	+2.5*	+2.51	+2.3	+1.5*	+4.04
APEA RATIO ε @ Pe = 14.7	+4.2	-12.2	-4.63	+4.6	-13.7	-4.95	+6.9	-12.2	-5.04
ε @ Pe = 10.0	+3.8	-6.0	-3.23	+4.1	-8.0	-3.58	+6.8	-5.7	-3.91
CYCLE LIFE 200	-1.3	-0.2	-3.55	-1.3	-0.8	-0.77	-1.8	-1.7	-2.27
300	-2.4	-0.7	-5.54	-2.2	-1.5	-1.37	-3.7	-2.5	-3.52
TURBINE TEMP. 1660°R (FR)	-4.3	-4.5	+1.50	-	-	-	-1.8	-1.7	-2.42
2260°R (FR)	+5.7	+5.9	-1.71	-	-	-	+1.2	+0.7	+2.07
2600°R (OR)	-	-	-	+2.3	+2.2	+2.49	-	-	-
2960°R (FR)	+8.2	+10.3	-2.33	-	-	-	+1.2	+0.7	+3.67
2600/2960 (OR/FR)	-	-	-	-	-	-	+2.3	+1.5	+6.20

*Pump Discharge Pressure >8000 psia

staged combustion cycles G and I, and -0.2 to -0.6 sec for the gas-generator cycle C) and a slight change in engine weight depending upon the volumetric flowrate (propellant density) change.

A decrease in chamber pressure of 500 psia from the nominal design value is seen to cause about 1% loss (2.5-4.5 sec) in specific impulse for the staged-combustion cycles G and I. The chamber pressure decrease for the gas-generator cycle C results in a slight performance gain (+0.4 sec) because of the reduction in gas generator flow required by the turbines. In all cases, there is a decrease in engine weight corresponding to the reduction in pressure level in the engine components.

An increase in chamber pressure of 3450 kN/m^2 (500 psia) is listed in Table XXXIX. The sensitivity values, however, are not consistent with the approximately 55160 kN/m^2 (8000 psia) pump discharge pressure limit that is used throughout the study as representing 1980 state of the art. The +500 psia chamber pressure calculations require a pump discharge pressure between 68950 and 75840 kN/m^2 (10,000 and 11,000 psia) for the cycles analyzed.

Variations in area ratio are based upon variations in nozzle exit pressure from the nominal 41 kN/m^2 (6 psia) value to 69 kN/m^2 (10 psia) and to the optimum sea level value of 101 kN/m^2 (14.7 psia). In all cases, the sea level performance improves significantly at the expense of vacuum performance when the area ratio is reduced. There is a corresponding weight reduction with a reduction in engine area ratio (nozzle size), as shown in the table.

The effects of increasing the number of usable start/shutdown cycles (from the minimum 100 to 200 and 300) on engine performance and weight

are given in Table XXXIX. In all cases, there is a slight reduction in engine performance resulting from a reduction in engine chamber pressure to limit the pump discharge pressure to about 55160 kN/m^2 (8000 psia). A corresponding weight reduction follows the reduction in chamber pressure.

The effects of increasing maximum allowable turbine inlet temperature was investigated to determine the potential of fuel-cooled turbine blading or the use of higher temperature materials. The nominal fuel-rich turbine inlet temperature utilized in the study is 1033°K (1860°R) and the oxidizer-rich turbine inlet temperature is 922°K (1660°R). The data for gas-generator cycle C are summarized in Table XXXIX and Figure 102.

The increase (see Figure 102) in turbine inlet temperature from 922 to 1256°K (1660 to 2260°R) is seen to result in an increase in vacuum specific impulse of about 10 sec. The increase results from the requirement of less turbine drive fluid which must be dumped into the nozzle at a low specific impulse. The benefit from increasing turbine temperature beyond 1256°K (2260°R) is seen to be much less (about 4 sec of vacuum specific impulse).

As shown in Figure 102, the maximum sea level specific impulse is achieved at a turbine inlet temperature of about 1556°K (2800°R).

Figure 103(A) and Figure 103(B) present the results of increasing the turbine inlet temperature for staged-combustion cycles I and H, respectively. The gain in specific impulse for the staged-combustion cycle I is much less between the temperatures of 922 to 1256°K (1660° and 2260°R). The gain is seen to be 2.2 sec in vacuum specific impulse, with very little gain above 1256°K (2260°R).

The sea level specific impulse gain for the staged-combustion cycle I is larger than the vacuum gain shown in Figure 103(A). This results

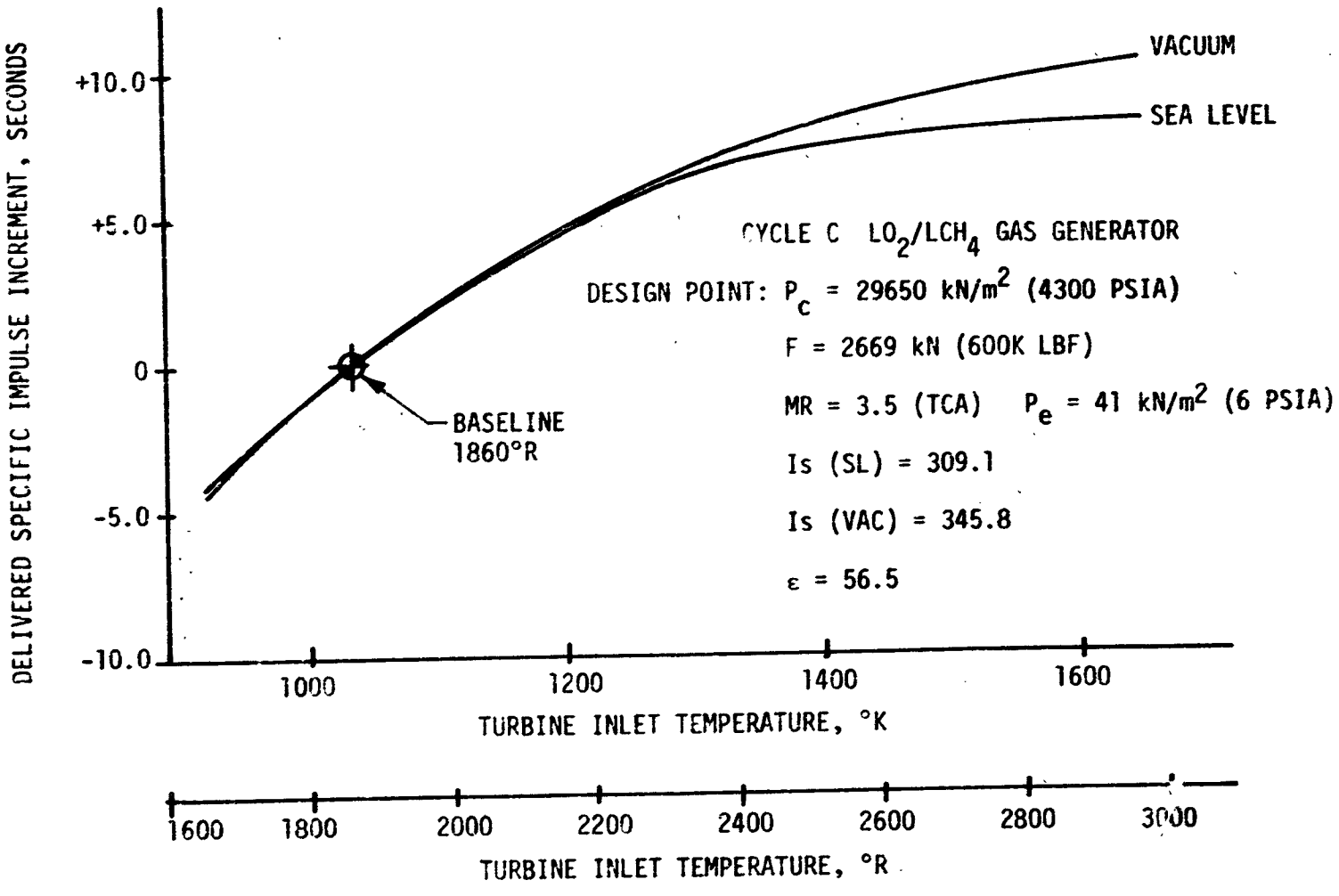

Figure 102. Cycle C Turbine Inlet Temperature Sensitivity Analysis

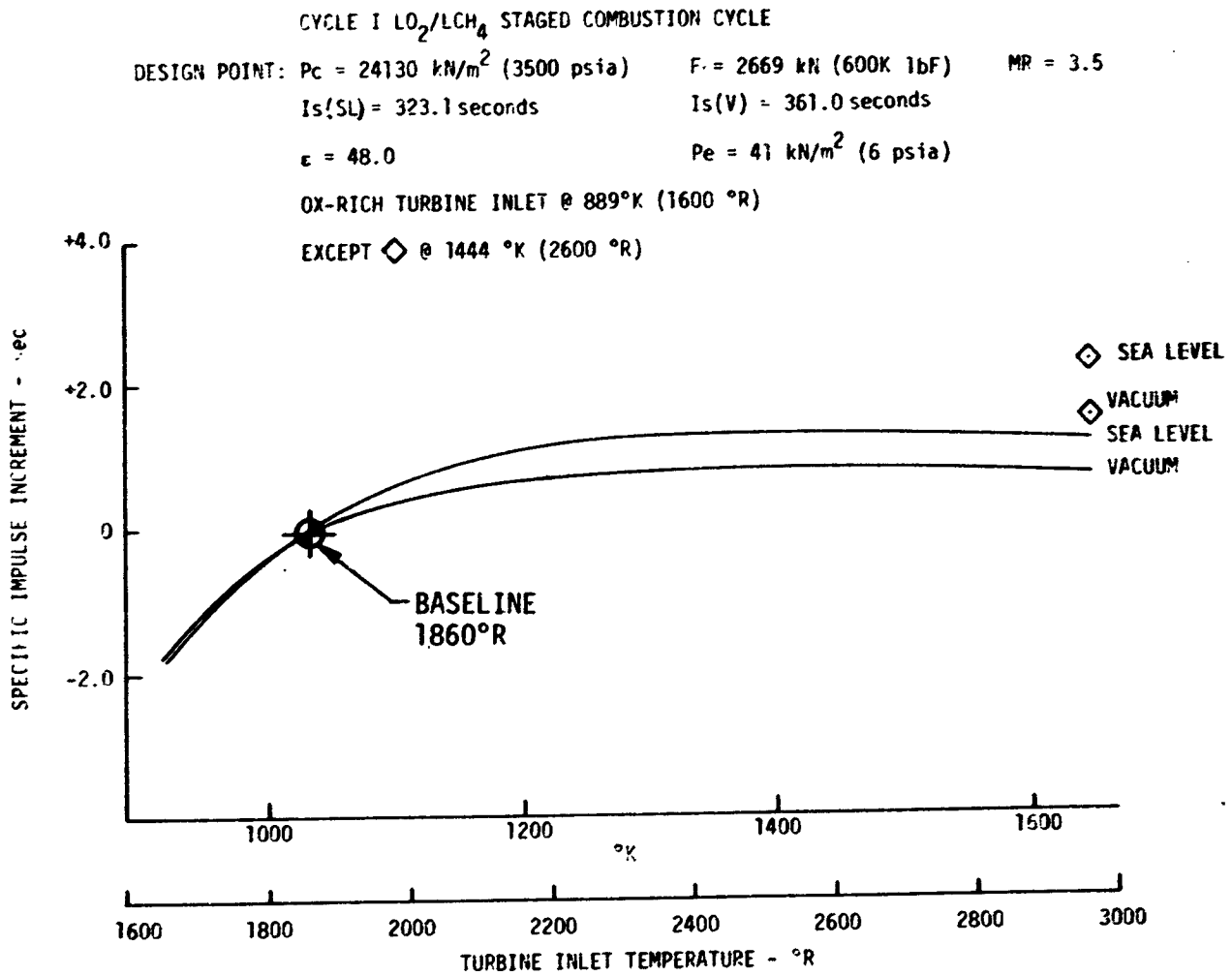

Figure 103A. Cycle I Turbine Inlet Temperature Sensitivity Analysis

CYCLE H: LO_2/LCH_4 STAGED COMBUSTION CYCLE
DESIGN POINT: Pc = 3000 PSIA F = 600K LBF
MR = 3.5 Is(SL) = 319.4 Is(V) = 358.5 ϵ = 42.2
FUEL-RICH PREBURNER ONLY

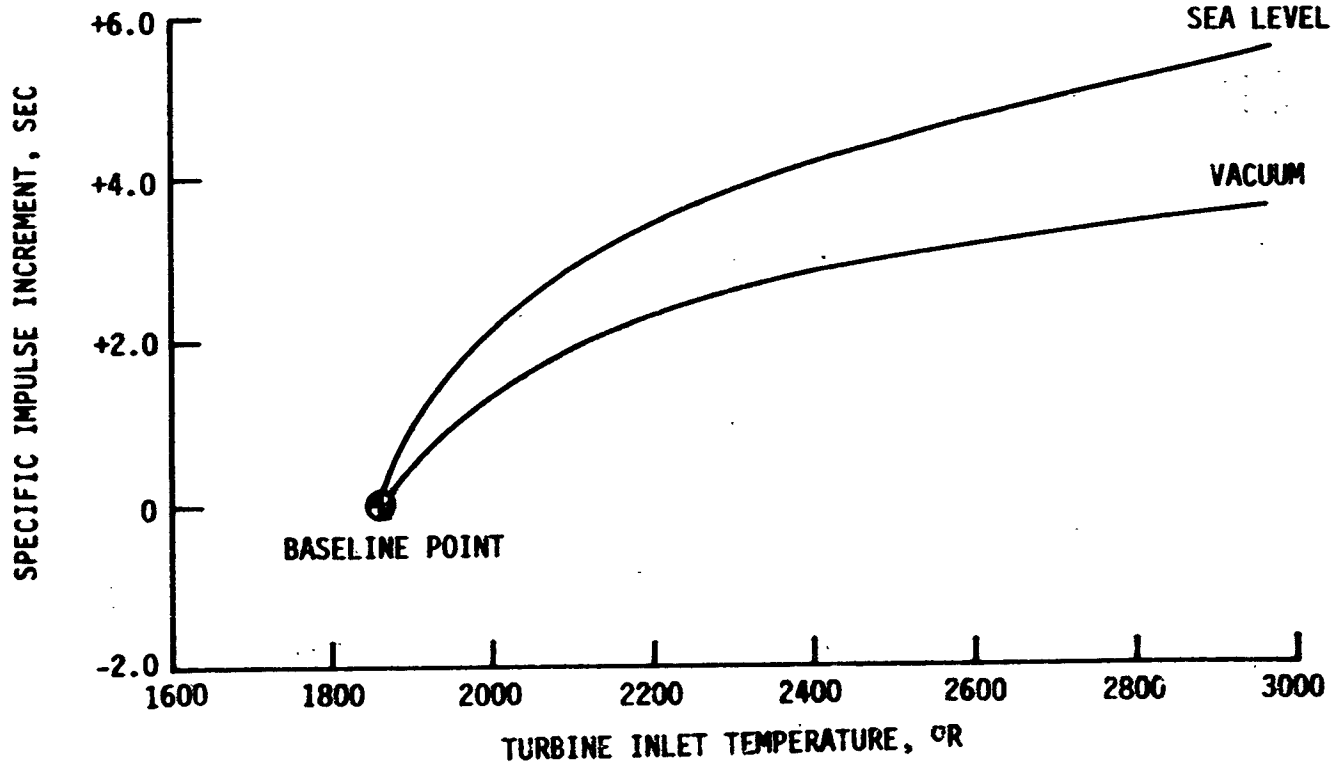

Figure 103(B). Cycle H Turbine Inlet Temperature Sensitivity Analysis

from the power balance state-of-the-art guideline (given in Table XXXVIII) limiting the pump discharge pressure to 55160 kN/m^2 (8000 psia). The sea level performance is much more sensitive to an increase in chamber pressure from 22060 to 25510 kN/m^2 (3200 to 3700 psia) allowed by an increase in turbine inlet temperature from 922 to 1644°K (1660° to 2960°R).

Another factor influences the results of the power balance data for cycle I. Since two preburners are utilized (fuel-rich and oxidizer-rich), both fuel and oxidizer pump discharge pressure limits must be considered. At a turbine inlet temperature of 1256°K (2260°R), the fuel pump discharge pressure of 54420 kN/m^2 (7893 psia) (see Table XXXVIII) limits the chamber pressure to 25510 kN/m^2 (3700 psia). Because of the shift in mixture ratio (and resulting oxidizer-rich flowrate to the oxidizer turbine), the fuel-rich turbine inlet temperature design point at 1644°K (2960°R) is also limited to a chamber pressure of 25510 kN/m^2 (3700 psia). This is due to the oxidizer pump discharge pressure reaching about 55160 kN/m^2 (8000 psia) (8314 psia in Table XXXVIII). A solution to this problem is to increase the oxidizer-rich turbine inlet temperature to achieve a higher chamber pressure and resultant higher engine performance (see Figure 103 and Table XXXVIII). In other words, with both fuel-rich and oxidizer-rich preburners, increases in turbine inlet temperature for both preburners should be pursued.

The magnitude of the change in specific impulse with turbine inlet temperature increase is dependent upon the baseline chamber pressure for staged combustion cycles. This is illustrated by comparing cycle H (single fuel-rich preburner) with cycle I (mixed preburners). As shown in Figure 103(B), 5.5 seconds (sea level) and 3.6 seconds (vacuum) improvement in specific impulse are achieved with cycle H, compared with the smaller improvement shown in Figure 103(A) for cycle I. The reason for the larger improvement with cycle H is that the imposed pump discharge pressure limit of

approximately 55160 kN/m^2 (8000 psia) is reached at a chamber pressure of 20685 kN/m^2 (3000 psia) in cycle H and at a chamber pressure of 24130 kN/m^2 (3500 psia) in cycle I. Cycle H does not utilize the chemical energy of both propellants to obtain power, and, therefore, can benefit more from a temperature increase.

Increasing the turbine inlet temperature of cycle H from 1033°K (1860°R) to 1256°K (2260°R) allows a chamber pressure increase of 3450 kN/m^2 (500 psia). The corresponding temperature increase for cycle I allows only a 1380 kN/m^2 (200 psia) increase in chamber pressure. An increase in turbine inlet temperature from 1256 to 1644°K (2260 to 2960°R) allows a chamber pressure increase for cycle H of 2070 kN/m^2 (300 psia), but no increase for cycle I, as previously cited.

To summarize, the specific impulse benefit for increasing turbine inlet temperature for staged combustion cycles is dependent upon the cycle and the baseline chamber pressure attainable with an 1033°K (1860°R) turbine inlet temperature. In all cases examined, it is lower than the benefit achievable for gas generator cycles.

Cycle G utilizes an oxidizer-rich turbine at the nominal temperature of 922°K (1660°R). One additional turbine inlet temperature is shown in Table XXXIX to indicate the benefit of raising the oxidizer-rich turbine inlet temperature. A vacuum performance increase of 2.2 sec can be achieved with this cycle through the use of a 1444°K (2600°R) turbine-drive gas. This improvement corresponds to that for fuel-rich staged-combustion systems, as shown in Table XXXIX.

The major conclusion to be drawn from the sensitivity analysis is that high-pressure gas-generator cycle engines can approach the performance of

high-pressure staged-combustion cycle engines through an increase in turbine inlet temperature. Another important conclusion is that oxidizer-rich turbine inlet temperatures as well as fuel-rich turbine inlet temperatures can beneficially be increased. These two conclusions offer the engine designer a great deal of potential to improve future engines with technology advancements.

C. HEAT TRANSFER DESIGN ANALYSIS

Parametric heat transfer data were previously reported in Section III,C. Task IV studies extend the chamber cooling analyses as follows: (1) Definition of the selected baseline designs for an oxygen-cooled LOX/RP-1 chamber (cycle G) and for a fuel-cooled LOX/methane chamber (cycle I); (2) Determination of the design sensitivity to the cycle life requirements; and (3) Investigation of coolant channel fabrication feasibility.

Channel design procedures for the effort are consistent with those previously used. None of these results consider gas-side carbon deposition, which has been shown to reduce the coolant requirement in Section III,C.

1. Baseline LOX/RP-1 and LOX/CH_4 Designs

The coolant pressure drop and temperature rise data for the baseline designs are given in Table XL. Results at the 2669 kN (600K lbF) thrust level were obtained by interpolation of the Section III,C pressure drop data using $\ln \Delta P$ versus chamber pressure plots. Since thrust interpolation is difficult, computer runs were made for the one million lb thrust designs using the channel layout models of Section III,C.

TABLE XL

BASELINE DESIGN HEAT TRANSFER DATA

Cycle	G	I
Propellants	LOX/RP-1	LOX/CH_4
Coolant	LOX	CH_4
Coolant Flow Fraction	1.0	1.0
Chamber Pressure, kN/m^2 (psia)	21370 (3100)	24130 (3500)
Pressure Drop, kN/m^2 (psia)		
F = 600K	8620 (1250)	9310 (1350)
F = 1M	10560 (1532)	10580 (1535)
Bulk Rise, °K (°F)		
F = 600K	298 (76)	339 (150)
F = 1M	294 (69)	330 (134)

VI, C, Heat Transfer Design Analysis (cont.)

2. Cycle Life Sensitivity

A 2669 kN (600K lbF) thrust oxygen-cooled LOX/RP-1 chamber at 20680 kN/m^2 (3000 psia) chamber pressure was selected for the cycle life sensitivity study. This operating point is very close to one of the baseline designs of Table XL and is one of the cases which was optimized in detail in Section III,C for a life (N_f/4) of 100 cycles. The number of allowable cycles, N_f includes a scatter factor of 4. Additional designs were developed for 204 (nominally 200) and 300 cycles using the wall temperature criteria from a previous study (Ref. 10). In each case, the channel layout was optimized in a two-step procedure:

(a) The throat channel width was varied to obtain the minimum pressure drop with the interface between the constant channel width section and the straddle-milled section fixed at the area ratio defined by the optimum design for 100 cycles.

(b) The barrel land width was varied for the throat channel width determined in (a) to minimize coolant pressure drop.

In the 300 cycle case, the resultant pressure drop for an assumed inlet pressure of 41370 kN/m^2 (6000 psia) was so large that the coolant outlet pressure was less than the desired chamber pressure. Therefore, additional inlet pressures were considered using the same channel layout. The results are given in Table XLI. Figure 104 shows the required coolant pressure drop as a function of cycle life, with the outlet pressure for 300 cycles consistent with that for 200 cycles. It is seen that the pressure drop is approximately directly proportional to the specified cycle life for this cooling system.

These results indicate that increased-life design requirements will result in reduced chamber pressure at a given pump discharge

TABLE XLI

CYCLE LIFE SENSITIVITY STUDY LOX/RP-1
CYCLE G WITH LOX COOLING

F = 600K lbF

Pc = 3000 psia

Cycle Life ($N_f/4$)	P_{inlet} psia	Throat Channel Width, in.	Barrel Land Width, in.	ΔP psi
100	6000	.100	.100	1128
204	6000	.085	.100	2102
300	6000	.075	.092	3018
300	7000	.075	.092	3045
300	8000	.075	.092	3289

OXYGEN COOLING LOX/RP-1

F = 2669 kN (600K lbF) Pc = 20680 kN/m^2 (3000 psia)

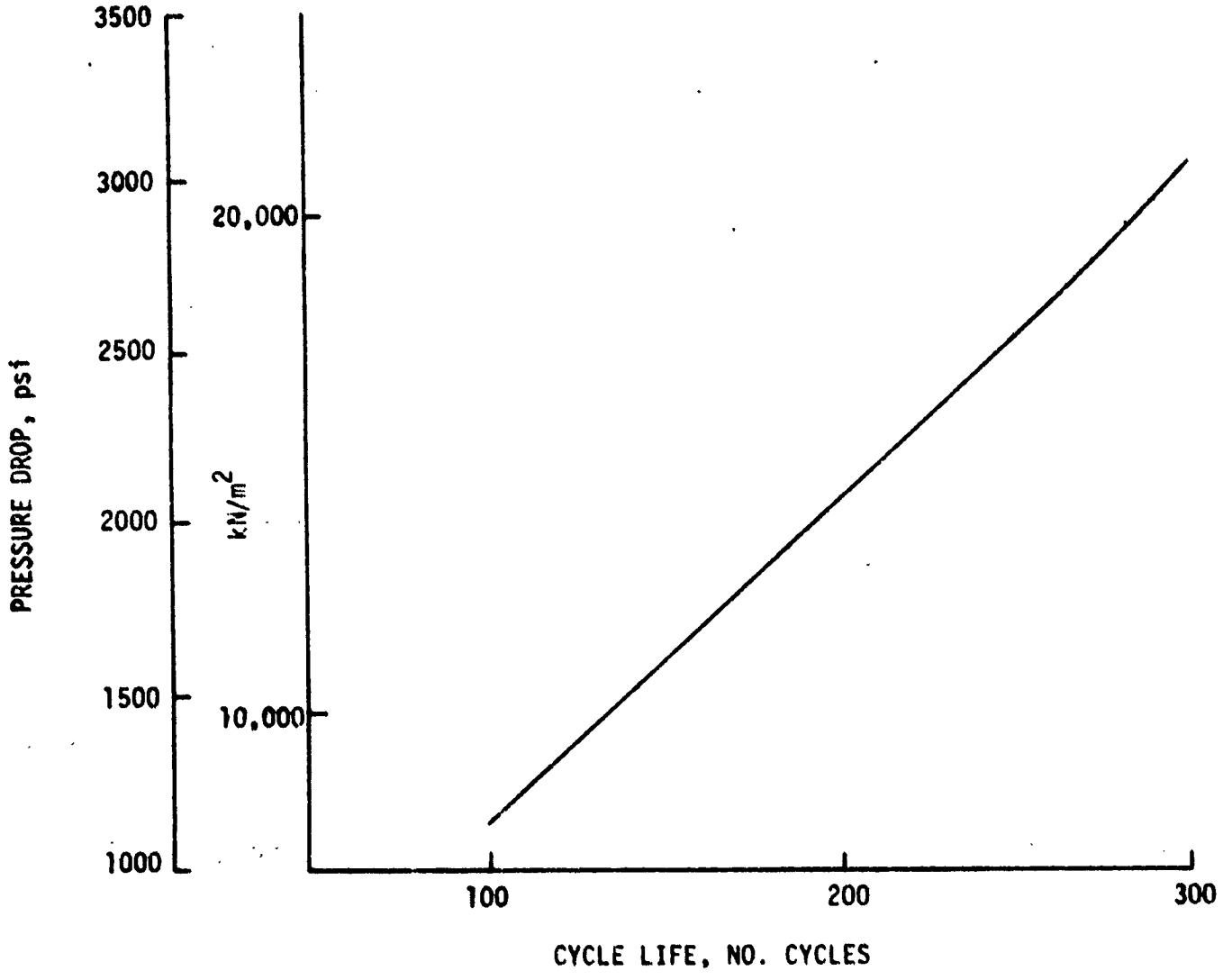

Figure 104. Effect of Cycle Life on Chamber Pressure Drop

pressure or will require increased pump discharge pressure. Further study is required to determine the optimum design life for a particular application.

3. Investigation of Coolant Channel Fabrication Feasibility

Preliminary design analysis of the heat transfer subsystem was performed to establish major technology requirements. Chamber coolant slot layouts for two LO_2/RP-1 engines were prepared. The engines are of a 2669 kN (600K lbF) thrust level, utilize RP-1R or LO_2 cooling, and operate at either 20680 or 27580 kN/m^2 (3000 or 4000 psia) chamber pressure. Figure 105 illustrates typical sections of the slot layout for the 27580 kN/m^2 (4000 psia) LOX-cooled chamber.

Coolant channel fabrication feasibility was checked by considering state-of-the-art approaches as well as advanced manufacturing processes. The design can be manufactured conventionally, i.e., with a slotted zirconium copper chamber with an electroformed nickel closure similar to that of the Space Shuttle Orbit Maneuvering System (OMS) chamber. However, the cost of the slotting operation of the chamber will not only be proportionately greater than the OMS because of the size difference, but also because of two significant channel parameter differences. The greatest cost impact is the 1.68 cm (0.66 in.) maximum depth of channel as compared to the 0.41 cm (0.16 in.) on the OMS chamber. Not only will a greater diameter slitting saw be required, but, at the two chamber extremes, where coolant enters and leaves the chamber, the slots will also have to be deepened locally. This is required because the larger radius cut leaves a greater chamber wall thickness. Deepening the channels locally will probably have to be performed with the more expensive Electrical Discharge Machining (EDM) process.

The second cost impact is the very narrow but constant channel wall land width of 0.10 cm (.04 in.) from the throat to the aft end of

THRUST 600,000 lbF
CHAMBER PRESSURE 4,000 psia
COOLANT LO_2

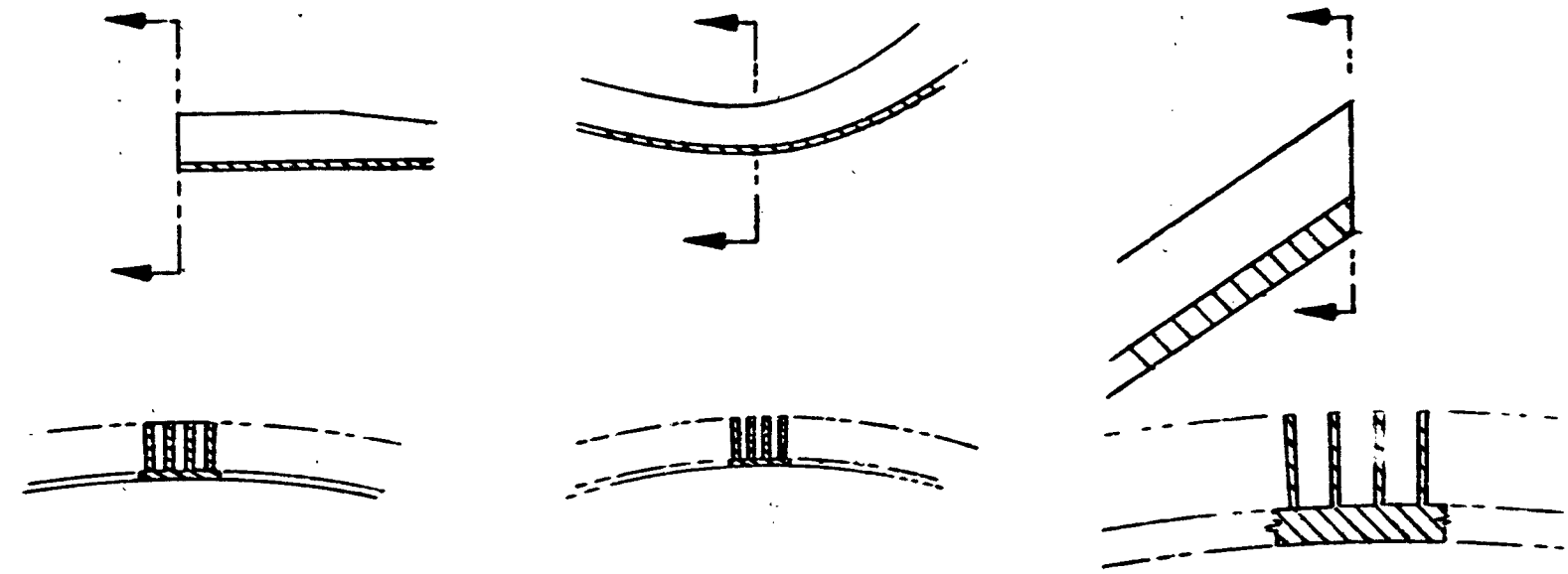

D_c = 40.8 cm (16.048 in.)

CHAMBER SECTION

D_t = 26.8 cm (10.553 in.)

THROAT SECTION

D_e = 76.2 cm (30.003 in.)

NOZZLE EXIT SECTION

Figure 105. Sections of Coolant Channel Layout for LO_2/RP-1 Engine

the chamber. It is possible to redesign the aft end of the chamber to avoid this narrow land, but optimization of the design was beyond the scope of the study. Constant width wall lands are normally machined by straddle milling, but it is doubtful that a 0.10 cm (0.04 in.) wall can be machined to a depth of over 1.52 cm (0.6 in.). For this reason, it is more likely that every other channel will be cut and then filled with Rigidax prior to machining the remaining channels.

Alternate fabrication concepts considered for these advanced engine cooling system designs are shown in Figures 106 through 109. The first concept, shown in Figure 106, shows the cross section of an all-electroformed chamber configuration. In this concept, individual tubes are first electroformed around a wax preform simulating the flow channel. These tubes are then assembled onto a mandrel, forming every other coolant passage. The vacant spaces between the tubes are then filled with wax, permitting a closeout shell of electroformed nickel to be formed. The chamber mandrel is then removed, permitting the copper liner to be electroformed to the inside, thus completing the all-electroformed assembly.

A second concept is shown in Figure 107. In this concept, preformed U-tubes are brazed to the copper liner forming every other coolant passage. The vacant spaces between the U-tubes are filled with wax prior to electroforming the nickel closeout structure.

The third alternate fabrication concept is shown in Figure 108. Individual copper ribs are manufactured by either the investment casting process or by swedge forming to produce an optimum heat transfer configuration fin. These preformed copper ribs are then assembled on a mandrel to form the coolant channel circuit as shown. The electroformed nickel closure is then deposited, followed by electroforming the copper liner.

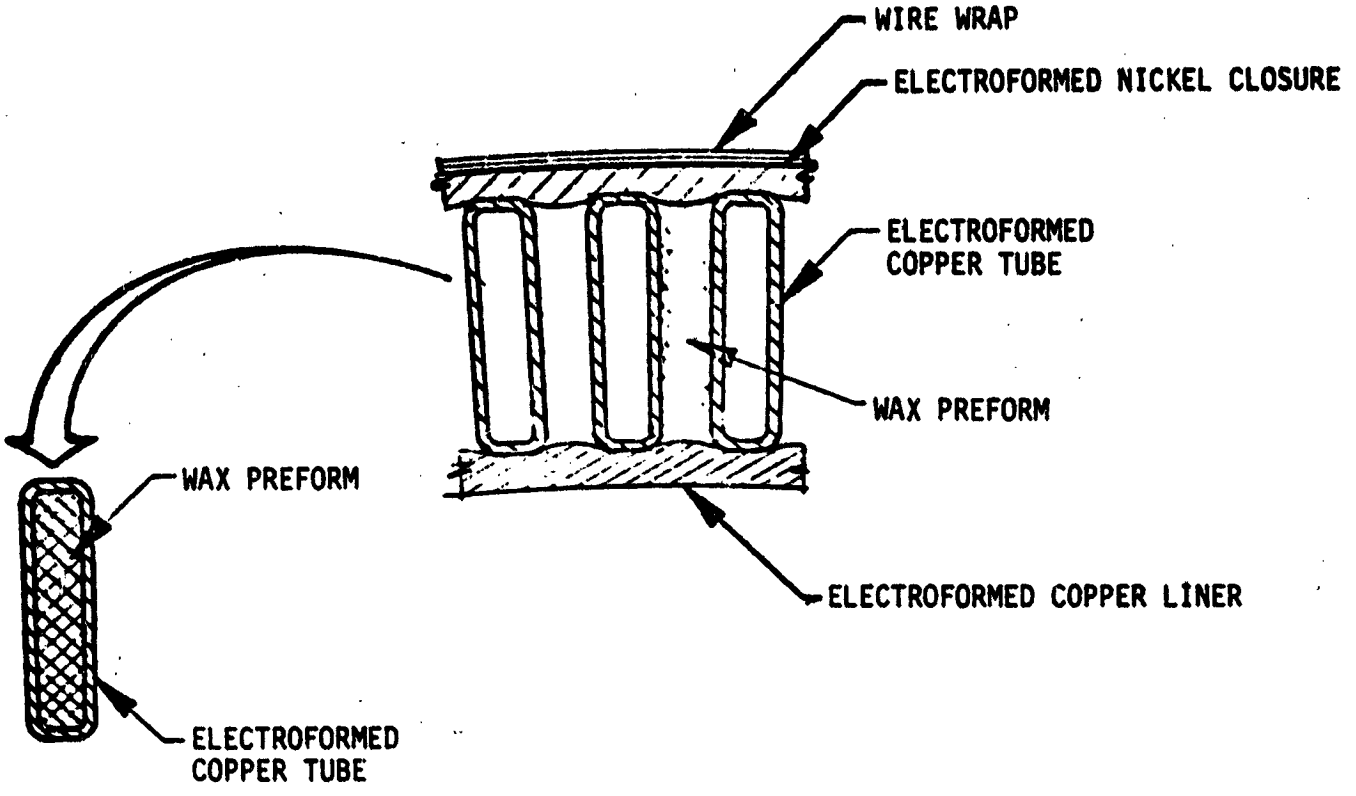

Figure 106. Conceptual Electroformed Coolant Channel Design

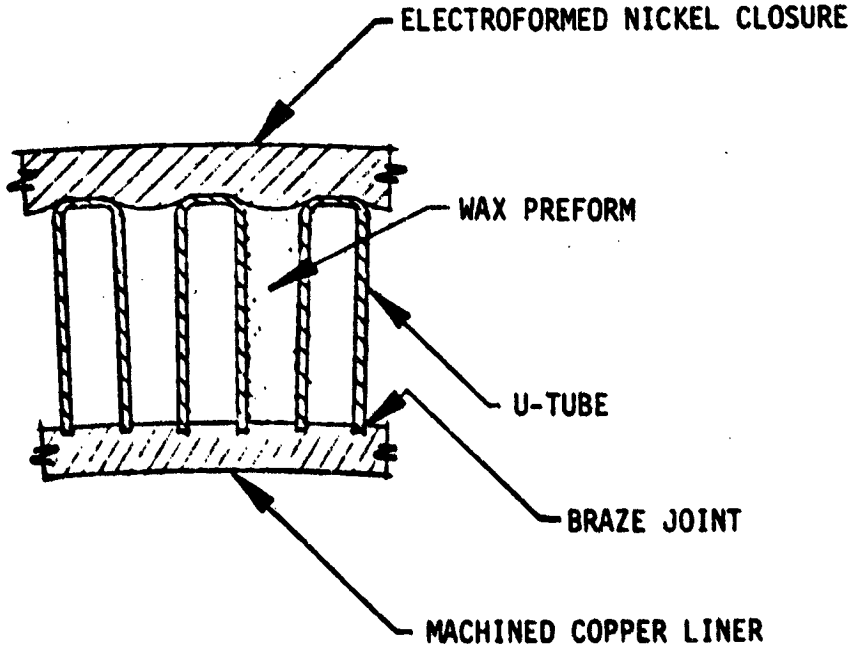

Figure 107. Conceptual Brazed Coolant Channel Design

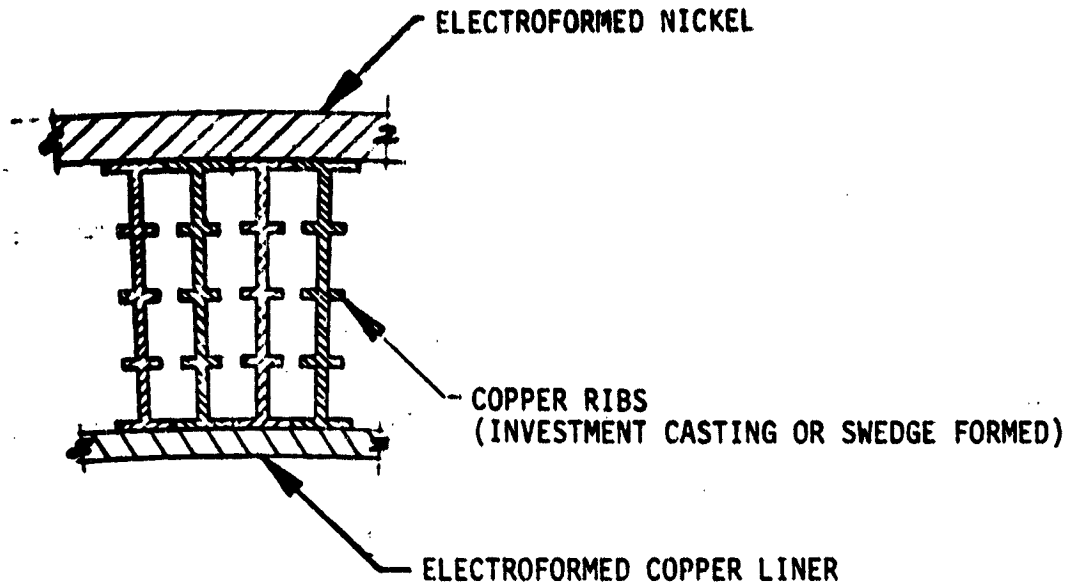

Figure 108. Conceptual Investment Casting Coolant Channel Design

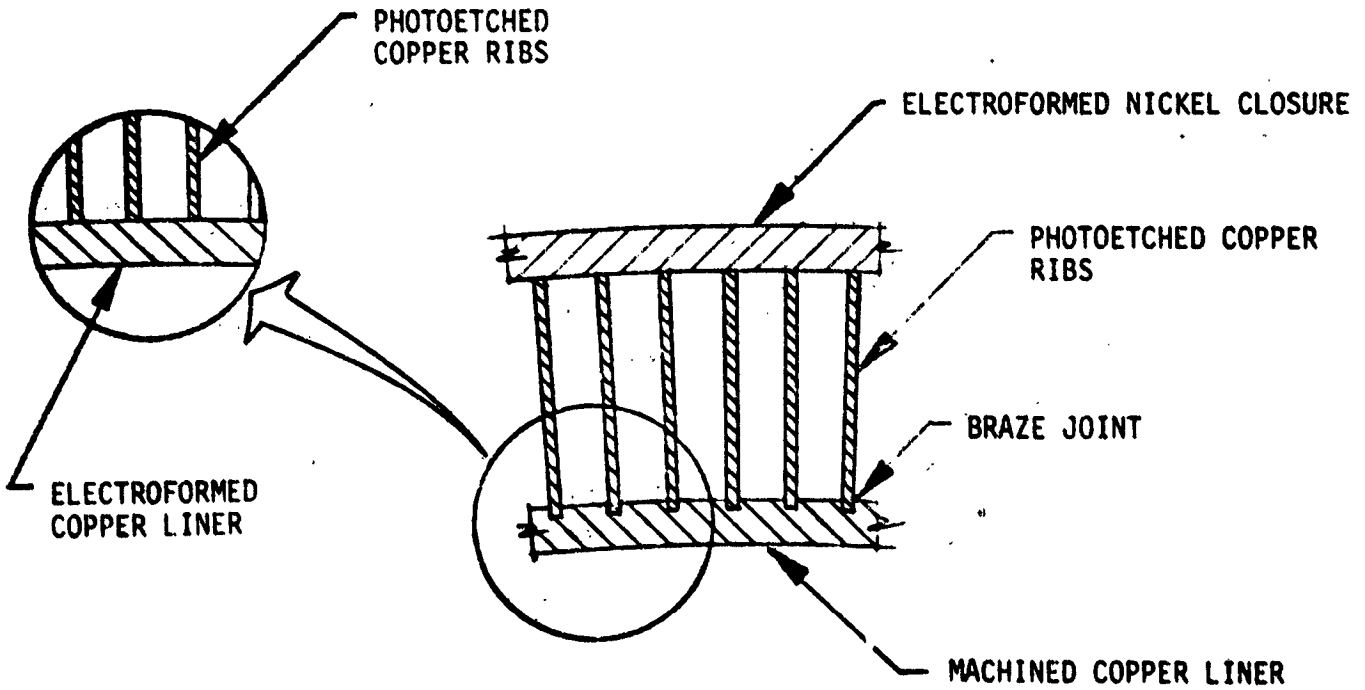

Figure 109. Conceptual Photoetch Coolant Channel Design

The fourth alternate fabrication concept is shown in Figure 109. In this concept, the chamber ribs are fabricated by the photoetch process. The 0.04-in.-thick, through-etched rib edges are squared off on a drum sander and assembled into the forward and aft flange which serves as the fixture to achieve proper radial and circumferential alignment. The vacant spaces or flow passages between the ribs are filled with wax, permitting both the closure wall and liner wall to be electroformed. The photoetched ribs could also be brazed into a premachined copper liner, requiring only the closure wall to be electroformed.

Before a final design can be recommended and selected, the overall chamber cooling concept configuration must be analyzed in more depth. For instance, a feature which may eliminate excessive channel depth is to put the inlet torus just downstream of the throat, i.e., at an Ae/At = 2. This would also increase the rib width from 0.10 cm (0.04 in.) to a more acceptable width, required not only for ease of manufacturing but also for structural adequacy. Another approach to be considered would be to segment the coolant circuit of the chamber into four or more axial sections, each having its own inlet and outlet torus and each flowing only a portion of the available cooling. This scheme would reduce the required coolant channel cross-sectional area (reduced channel depth) and would be structurally superior because of the increased number of tori which would act as hoop bands around the high-pressure chamber.

D. TURBOMACHINERY DESIGN ANALYSIS

The turbomachinery designs for the three engine cycles C, G, and I are similar. Each cycle utilizes hydraulically driven boost pumps effectively to obtain higher main turbopump speed. The primary difference stems from the cycle I turbomachinery which eliminates the need for an interpropellant shaft seal through the use of both an oxidizer-rich and a fuel-rich preburner.

VI, D, Turbomachinery Design Analysis (cont.)

The hydraulic turbines are multistaged and drive single-stage boost pumps. The main turbopumps have single-stage gas turbines that drive multistaged pumps.

1. Cycle C Turbomachinery

The fuel and oxidizer boost pumps are single-stage, driven by four staged turbines. The multistaged turbines were selected to provide good rotor blade heights and efficiency. The design parameters are given in Table XLII.

The high-pressure liquid methane turbopump assembly utilizes five stages: an inducer stage, three identical stages to achieve the gas--generator pressure level, and an additional stage to generate the pressure for the main flow used to cool the thrust chamber. The design parameters are given in Table XLIII.

The high-pressure liquid oxygen turbopump assembly (Table XLIII) utilizes one inducer stage and one additional stage. The oxidizer requires fewer stages than the fuel (for the same discharge pressure) mainly due to the higher density of the oxidizer.

Both high-pressure turbopump assemblies are driven by single-stage, series-flow turbines.

2. Cycle G Turbomachinery

The design operating specifications for cycle G turbomachnery are given in Tables XLIV and XLV. The turbomachinery is similar to that for cycle C except for the following differences: (1) the high-pressure oxidizer pump utilizes three stages, with the additional stage required to meet the

TABLE XLII

CYCLE C BOOST PUMP DESIGN PARAMETERS

PUMPS	DIMENSIONS	FUEL	OXIDIZER
Stages		1	1
Propellant		CH_4	O_2
Propellant Temperature	°F	-253.5	-293.6
Propellant Density	lb/ft^3	26.2	70.6
Shaft Speed	rpm	5322	4080
Total Discharge Pressure	psia	135	231
Total Suction Pressure	psia	24	15
Total Pressure Rise	psi	111	216
Total Head Rise (Stage)	ft	609	440
Weight Flow	lb/sec	495.4	1396.5
Capacity	gpm	8490	8882
Specific Speed (Based on Stage Head)	$\frac{rpm \times gpm^{1/2}}{ft^{3/4}}$	4000	4000
Efficiency	%	77	77
Fluid Horsepower	h.p.	549	1117
Shaft Horsepower	h.p.	712	1451
Net Positive Suction Head	ft	31	30
Suction Specific Speed	$\frac{rpm \times gpm^{1/2}}{ft^{3/4}}$	37,500	30,000
Vapor Pressure	psia	18.5	18.5
Diameter	in.	12.2	13.5
TURBINE			
Stages		4	4
Liquid		CH_4	O_2
Shaft Power	h.p.	734	1494
Weight Flow/Percent Engine	lb/sec	99/20	215/15.3
Pressure Drop	psi/ft	989/5436	2499/5079
Static Back Pressure	psia	135	231
Shaft Speed	rpm	5322	4080
Efficiency	%	75	75
Inlet Total Pressure	psia	1124	2730
Diameter	in.	6.9	7.0

TABLE XLIII

CYCLE C MAIN PUMP DESIGN PARAMETERS

PUMPS	DIMENSIONS	CHAMBER FUEL	INDUCER FUEL	MAIN FUEL	INDUCER OXIDIZER	MAIN OXIDIZER
Stages		1	1	3	1	1
Propellant		CH_4	CH_4	CH_4	O_2	O_2
Propellant Temperature	°F		-253.5		-293.6	
Propellant Density	lb/ft^3	26.2	26.2	26.2	70.6	70.6
Shaft Speed	rpm	25212	25212	25212	19942	19942
Total Discharge Pressure	psia	7953	1249	5262	3033	5262
Total Suction Pressure	psia	5262	135	1249	231	3033
Total Pressure Rise	psi	2691	1114	4013	2802	2229
Total Head Rise (Stage)	ft	14790	6123	22056 (7352)	5715	4546
Weight Flow	lb/sec	407.7	594.5	495.4	1611	1396.5
Capacity	gpm	6988	10188	8490	10249	8882
Specific Speed (Based on Stage Head)	$\frac{rpm \times gpm^{1/2}}{ft^{3/4}}$	1571	3676	2926	3071	3395
Efficiency	%	76	77	77	77	77
Fluid Horsepower	h.p.	10965	6618	19866	16740	11543
Shaft Horsepower	h.p.	14427	8595	25802	21740	14991
Net Positive Suction Head	ft		640		470	
Suction Specific Speed	$\frac{rpm \times gpm^{1/2}}{ft^{3/4}}$		20000		20000	
Diameter Impeller	in.	9.4	7.8	7.7	8.7	8.1

TURBINE			
Gas		O_2/CH_4 @ 0.65 M.R.	
Shaft Power	h.p.	50,289	37,833
Gas Weight Flow	lb/sec	115.8	115.8
Gas Inlet Total Temperature	°F/°R	1800/2260	1568/2028
Pressure Ratio		3.2	3.4
Static Back Pressure	psia	1308	363
Shaft Speed	rpm	25,212	19,942
Efficiency	%	70	80
Gas Inlet Total Pressure	psia	4186	1233
Exhaust Temperature	°F/°R	1568/2028	1319/1779
Specific Heat	Btu/lb°R	0.926	0.926
Specific Heat Ratio		1.158	1.158
Gas Constant	ft/°R	98.4	98.4
Diameter Rotor	in.	12	21.7

TABLE XLIV

CYCLE G BOOST PUMP DESIGN PARAMETERS

PUMPS	DIMENSIONS	FUEL	OXIDIZER
Stages		1	1
Propellant		RP-1	O_2
Propellant Temperature	°F	60	-293.6
Propellant Density	lb/ft^3	50.6	70.6
Shaft Speed	rpm	6061	4067
Total Discharge Pressure	psia	181	250
Total Suction Pressure	psia	14.7	33.6
Total Pressure Rise	psi	166	216.7
Total Head Rise (Stage)	ft	473	442
Weight Flow	lb/sec	504.8	1413.5
Capacity	gpm	4479	8989
Specific Speed (Based on Stage Head)	$\frac{rpm \times gpm^{1/2}}{ft^{3/4}}$	4000	4000
Efficiency	%	77	77
Fluid Horsepower	h.p.	434	1136
Shaft Horsepower	h.p.	564	1623
Net Positive Suction Head	ft	39	31
Suction Specific Speed	$\frac{rpm \times gpm^{1/2}}{ft^{3/4}}$	26000	30000
Vapor Pressure	psia	1.0	18.5
Diameter	in.	8.9	13.6
TURBINE			
Stages		4	4
Liquid		RP-1	O_2
Shaft Power	h.p.	581	1671
Weight Flow/Percent Engine	lb/sec/%	101/20	320/22.6
Gas Inlet Total Temperature	°F/°R	1567/4459	1760/3590
Pressure Drop	psi/ft	181	250
Static Back Pressure	psia	6061	4067
Shaft Speed	rpm	71	80
Efficiency	%	1748	2010
Inlet Total Pressure	psia	3.1	9.3
Diameter	in.		

TABLE XLV

CYCLE G MAIN PUMP DESIGN PARAMETERS

PUMPS	DIMENSIONS	PREBURNER FUEL	INDUCER FUEL	MAIN FUEL	INDUCER OXIDIZER	MAIN OXIDIZER
Stages		1	1	1	1	2
Propellant		RP-1	RP-1	O_2	O_2	O_2
Propellant Temperature	°F	60	60	60	-293.6	-293.6
Propellant Density	lb/ft^3	50.6	50.6	50.6	70.6	70.6
Shaft Speed	rpm	29357	29357	29357	19322	19322
Total Discharge Pressure	psia	6400	1942	3703	2233	7733
Total Suction Pressure	psia	3333	181	1942	250	2233
Total Pressure Rise	psi	3067	1761	1761	1983	5500
Total Head Rise (Stage)	ft	8728	5012	5012	4045	11218(5609)
Weight Flow	lb/sec	31.4	606	504.8	1733	1413.5
Capacity	gpm	279	5377	4479	11021	8989
Specific Speed (Based on Stage Head)	$\frac{rpm \times gpm^{1/2}}{ft^{3/4}}$	543	3614	3298	4000	2826
Efficiency	%	57	77	77	77	77
Fluid Horsepower	h.p.	498	5522	4600	12745	28830
Shaft Horsepower	h.p.	874	7172	5974	16552	37442
Net Positive Suction Head	ft		512		473	
Suction Specific Speed	$\frac{rpm \times gpm^{1/2}}{ft^{3/4}}$		20000		20000	
Diameter	in.	5.8	5.9	5.7	8.2	10.5
TURBINE						
Gas			O_2/RP-1 @ 45 M.R.		O_2/RP-1 @ 45 M.R.	
Shaft Power	h.p.		14,441		55,614	
Gas Weight Flow	lb/sec		1445		1445	
Gas Inlet Total Temperature	°F/°R		1096/1556		1200/1660	
Pressure Ratio			1.1034		1.4088	
Static Back Pressure	psia		3243		3614	
Shaft Speed	rpm		29,357		19,322	
Efficiency	%		75		80	
Gas Inlet Total Pressure	psia		3578		5091	
Exhaust Temperature	°F/°R					
Specific Heat	BTU/lb°R		0.263		0.263	
Specific Heat Ratio			1.31		1.31	
Gas Constant	ft/°R		48.4		48.4	

coolant jacket pressure drop, and (2) the higher density of the RP-1 fuel, plus no use of RP-1 as a coolant, allows the use of only three pump stages compared to five for the liquid methane pump. Series-flow turbines are utilized.

3. Cycle I Turbomachinery

Tables XLVI and XLVII provide the design parameters for the boost pump and main (high-pressure) pumps for cycle I. All components reach maximum potential desigr efficiencies because of the parallel flow arrangement. The pumps are similar to those utilized for cycle C, except that the liquid oxygen boost pump turbine is a three-stage design and the liquid methane main pump incorporates six stages.

E. COMBUSTION STABILITY DESIGN ANALYSIS

The combustion stability that may be expected with large advanced LO_2/hydrocarbon rocket engines was evaluated. Anticipated stability problems are defined, and stability damping devices and design practices that would ensure stable operation are recommended. The evaluation was made for the two staged-combustion cycle engines, cycle G and cycle I (Figures 100 and 101). The gas-generator cycle C (Figure 99) may require similar stability design features in the main combustion chamber.

The results of the study show that the high-frequency transverse modes could be effectively damped with multiple-tune quarterwave-tube acoustic resonators. The possibility of chug instability exists within the preburner combustors with turbopump feedback. Precautions will have to be taken to design the preburner injectors to provide adequate pressure drop and to tailor the combustion time lags to prevent coupling with the feed system.

TABLE XLVI

CYCLE I BOOST PUMP DESIGN PARAMETERS

PUMPS	DIMENSIONS	FUEL	OXIDIZER
Stages		1	1
Propellant		Methane	Oxygen
Propellant Temperature	°F	-253.5	-293.6
Propellant Density	lb/ft^3	26.2	70.6
Shaft Speed	rpm	4198	4172
Total Discharge Pressure	psia	94	261
Total Suction Pressure	psia	72	34
Total Pressure Rise (Stage)	psi	22	227
Total Head Rise (Stage)	ft	393	464
Weight Flow	lb/sec	412.67	1444.34
Capacity	gpm	7072	9186
Specific Speed (Based on Stage Head)	$\frac{rpm \times gpm^{1/2}}{ft^{3/4}}$	4000	4000
Efficiency	%	77	77
Fluid Horsepower	h.p.	295	1218
Shaft Horsepower	h.p.	383	1582
Net Positive Suction Head	ft/psi	20/3.6	32/15.5
Suction Specific Speed	$\frac{rpm \times gpm^{1/2}}{ft^{3/4}}$	37,500	30,000
Vapor Pressure	psia	18.5	18.5
Diameter	in.	11.7	12.8
TURBINE			
Stages		4	3
Liquid		Methane	Oxygen
Shaft Power	h.p.	394	1630
Weight Flow/Percent Engine	lb/sec	82.6/20	289/20
Pressure Drop	psi/ft	628/3452	1909/3878
Static Back Pressure	psia	94	261
Shaft Speed	rpm	4198	4172
Efficiency	%	76	80
Gas Inlet Total Pressure	psia	722	2170
Diameter	in.	8.8	7.5

TABLE XLVII

CYCLE I MAIN PUMP DESIGN PARAMETERS

PUMPS	DIMENSIONS	PRE-BURNER FUEL	INDUCER FUEL	MAIN FUEL	INDUCER OXIDIZER	MAIN OXIDIZE
Stages		1	1	4	1	1
Propellant		CH_4	CH_4	CH_4	O_2	O_2
Propellant Temperature	°F					
Propellant Density	lb/ft^3	26.2	26.2	26.2	70.6	70.6
Shaft Speed	rpm	19888	19888	19888	20023	20023
Total Discharge Pressure	psia	8272	898	6504	2121	6847
Total Suction Pressure	psia	6504	94	898	261	2121
Total Pressure Rise	psi	1768	804	5606	1860	4726
Total Head Rise (Stage)	ft	9717	4419	30812 (7703)	3794	9639
Weight Flow	lb/sec	383.58	495.3	412.67	1733	1444.
Capacity	gpm	6574	8488	7072	11021	9186
Specific Speed (Based on Stage Head)	$\frac{rpm \times gpm^{1/2}}{ft^{3/4}}$	1647	3380	2034	4348	1972
Efficiency	%	76	77	77	76	77
Fluid Horsepower	h.p.	6777	3979	23118	11954	25313
Shaft Horsepower	h.p.	8917	5168	30024	15730	32874
Net Positive Suction Head	ft		413		496	
Suction Specific Speed	$\frac{rpm \times gpm^{1/2}}{ft^{3/4}}$		20000		20000	
Diameter	in	10.6	7.8	9.2	7.7	10.1

TURBINE			
Gas		O_2/CH_4 @ 0.39 M.R.	O_2/CH_4 @ 44.5 M.R.
Shaft Power	h.p.	45,432	50,062
Gas Weight Flow	lb/sec	533.17	1323.84
Gas Inlet Total Temperature	°F/°R	1400/1860	1200/1660
Pressure Ratio		1.444	1.39
Static Back Pressure	psia	3771	3722
Shaft Speed	rpm	19,888	20,023
Efficiency	%	80	80
Gas Inlet Total Pressure	psia	5446	5173
Exhaust Temperature	°F/°R	1331/1791	1102/1562
Specific Heat	BTU/lb°R	0.875	0.273
Specific Heat Ratio		1.148	1.303
Gas Constant	ft/°R	87.8	49.4
Diameter	in.	13.4	14.4

VI, E, Combustion Stability Design Analysis (cont.)

1. Combustion Instability

Combustion instability is a consequence of coupling of the combustion process with the propellant injection process (low frequency) or with the chamber acoustic modes (high frequency). The propensity for combustion process coupling is determined by the combustion time lags associated with the various combustion processes.

As shown in Figure 110, the characteristic combustion time lags for liquid propellant combustion include 1) propellant flight time, 2) atomization time, 3) vaporization time, 4) mixing time, and 5) chemical reaction time. Methods for analytically predicting these combustion delay times in terms of the injector design and propellant properties are available for specific injector designs. A qualitative evaluation of the importance of each of these time lags for the two staged-combustion cycles is given in Table XLVIII.

2. Low-Frequency Stability

The possible modes of system-coupled instability for systems G and I are outlined in Figures 111 and 112. The forward perturbation flowrate and pressure relationships between the various components are indicated by the wide arrows. For example, the chamber pressure influences the fuel turbine and oxidizer turbine outlet pressure which, in turn, influences the fuel and ox pump outlet pressures which, in turn, influence the oxidizer-rich preburner. Feedback occurs in terms of pressure and flowrate oscillations indicated by the narrow arrows. Both cycle G and cycle I are sensitive to coupling of preburner pressure oscillations with the turbopumps. Therefore, it is imperative that the preburners be designed to avoid low-frequency instability.

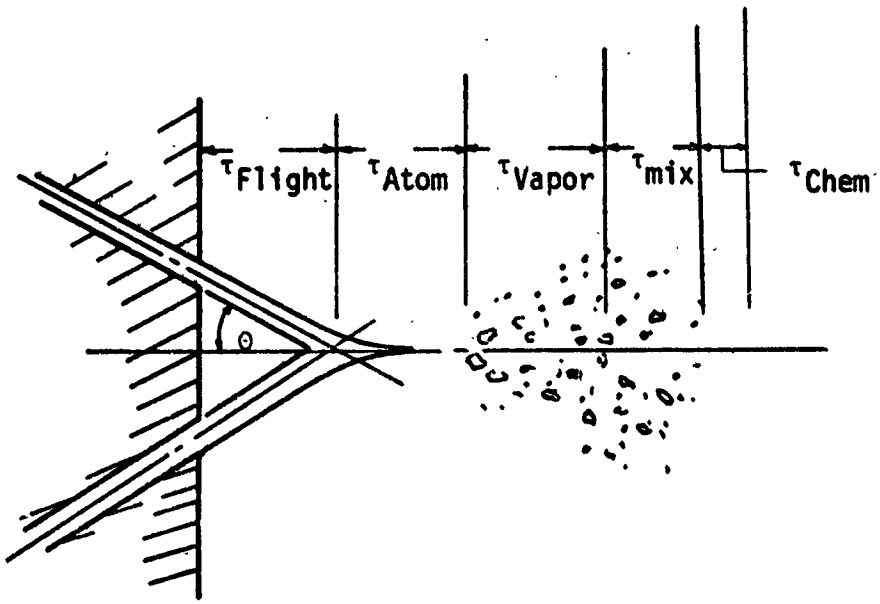

Figure 110. Characteristic Combustion Time Lags

TABLE XLVIII

CONTROLLING COMBUSTION TIME LAG

		Flight	Atom.	Vapor	Mixing	Chem.
Main Chamber	Cycle G	N/A	N/A	Fuel	N/A	N/A
	Cycle I	N/A	N/A	N/A	Fuel/Ox	N/A
Preburner Chamber	Cycle G	Fuel	Fuel	Fuel	N/A	N/A
	Cycle I	Ox	Ox	Ox	N/A	N/A

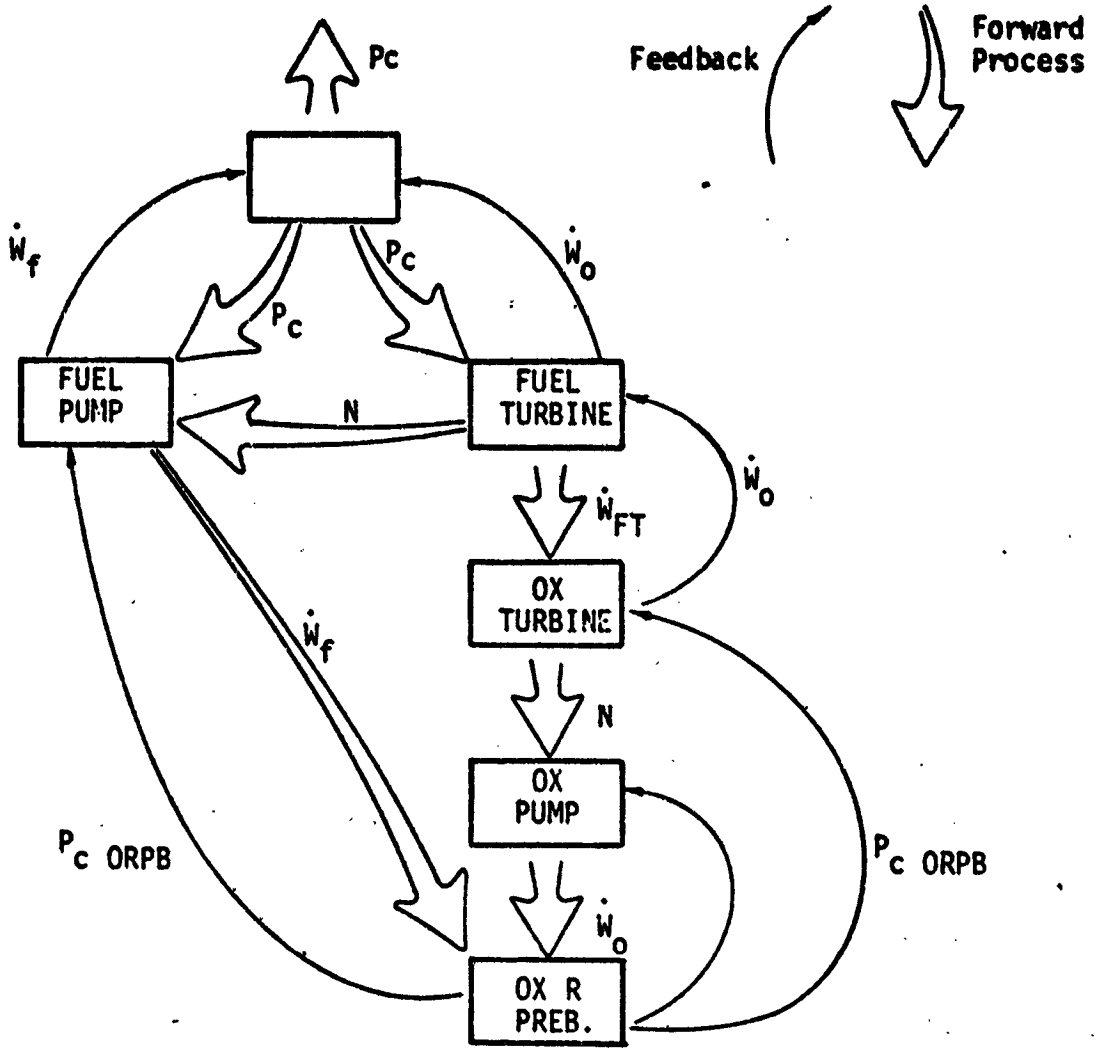

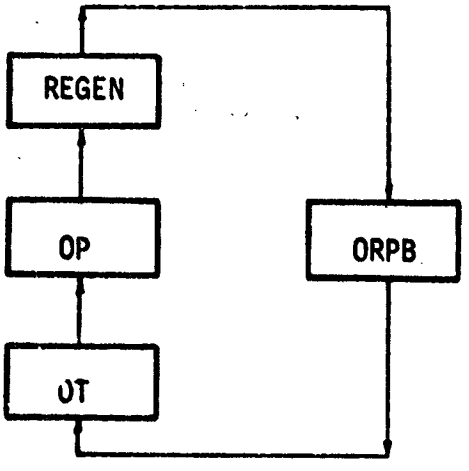

Forward
Closed-Loop
Coupling of
Preburner-
Rich Propellant

Figure 111. System Low-Frequency Coupling - Cycle G

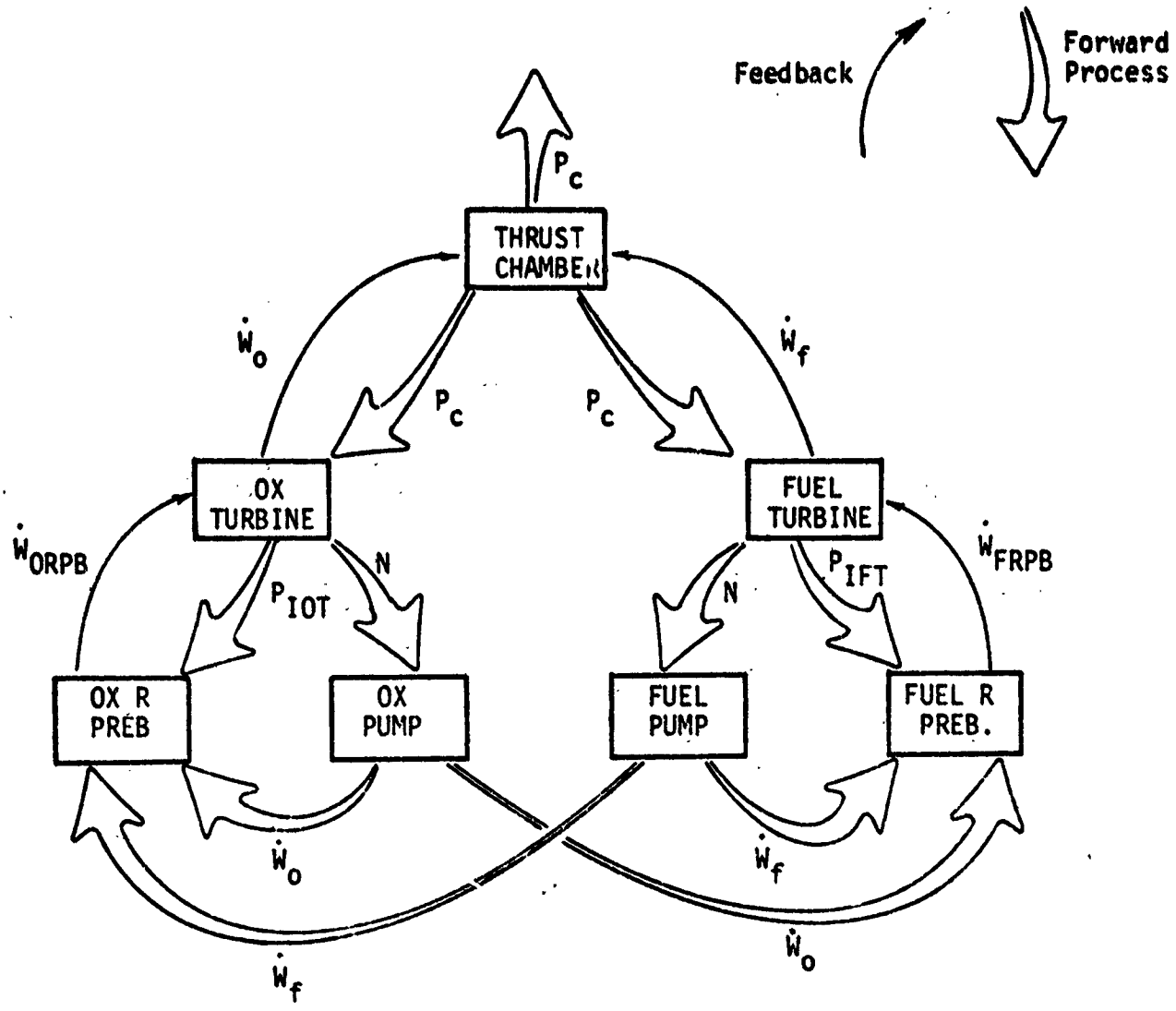

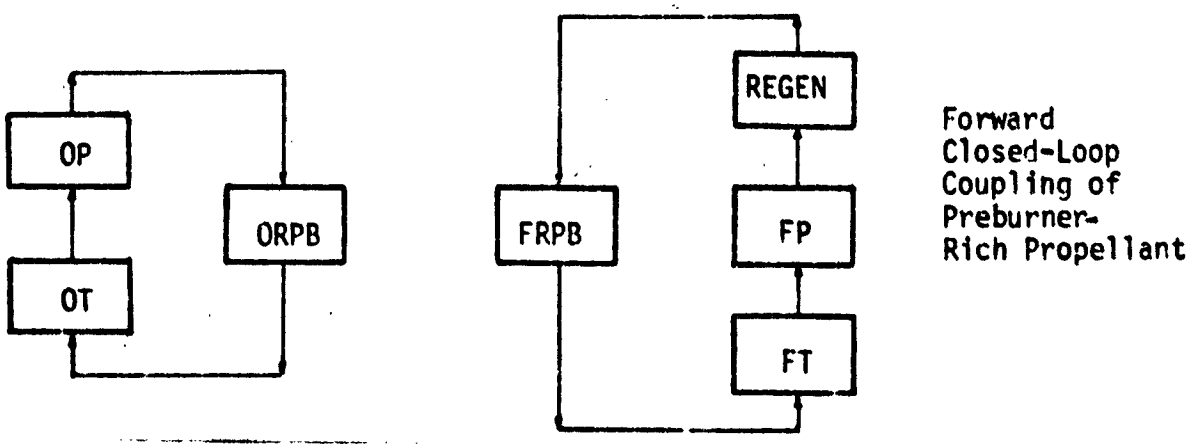

Figure 112. System Low-Frequency Coupling - Cycle I

VI, E, Combustion Stability Design Analysis (cont.)

Stable preburner operation is achieved by providing adequate pressure drops across the preburner injector to achieve isolation from the injection process. Pressure drops are generally normalized to the chamber pressure ($\Delta P_J/P_c$) for the purpose of specifying low-frequency stability. Experience has shown that the $\Delta P/P_c$ ratio required is generally on the order of 10-20%, depending on propellants and injector design. Generally, gas injection elements are stabilized with as little as 10%, whereas liquid injectors require 15-20%.

3. High-Frequency Stability

The high-frequency stability damping requirements are estimated by evaluating the undamped acoustic mode frequencies and by comparing these to estimated combustion time lag sensitive frequencies. The estimated chamber resonant frequencies are shown in Figure 113. The assumed chamber diameter and combustion gas properties are also included in the figure.

The transverse mode frequencies range from about 1400 Hz to 5000 Hz, representing a wide range of potential coupling. Stabilizing engines is accomplished by either (1) damping the acoustic mode, (2) shifting the acoustic mode frequency away from the injector response, or (3) shifting the injector response away from the acoustic mode. Acoustic resonators and baffles accomplish both (1) and (2) and are therefore ideal solutions to the problem. Item (3) is accomplished with injector design changes and is limited in applicability.

Acoustic resonators are preferred since they do not protrude into the combustion field and hence are easier to cool. Design of an acoustic resonator to damp all of the possible modes expected in advanced LO_2/hydrocarbon engines may require demonstration of a multiple-tune resonator,

CHAMBER PARAMETERS

Chamber Pressure = 20680 kN/m^2 (3000 psia)
Chamber Diameter = 51 cm (20 inches)
Combustion Gas Molecular wt. = 20
Combustion Gas Sound Speed = 1189 m/S (3900 ft/sec)

	CYCLE G		CYCLE I			
Cycle Propellants	LO_2	RP-1	LO_2	LCH_4	LO_2	LC_3H_8
Main Chamber Propellants	ORPB Gases	RP-1	ORPB Gases	FRPB Gases	ORPB Gases	FRPB Gases
Propellant Injection State	Gas	Liquid	Gas	Gas	Gas	Gas

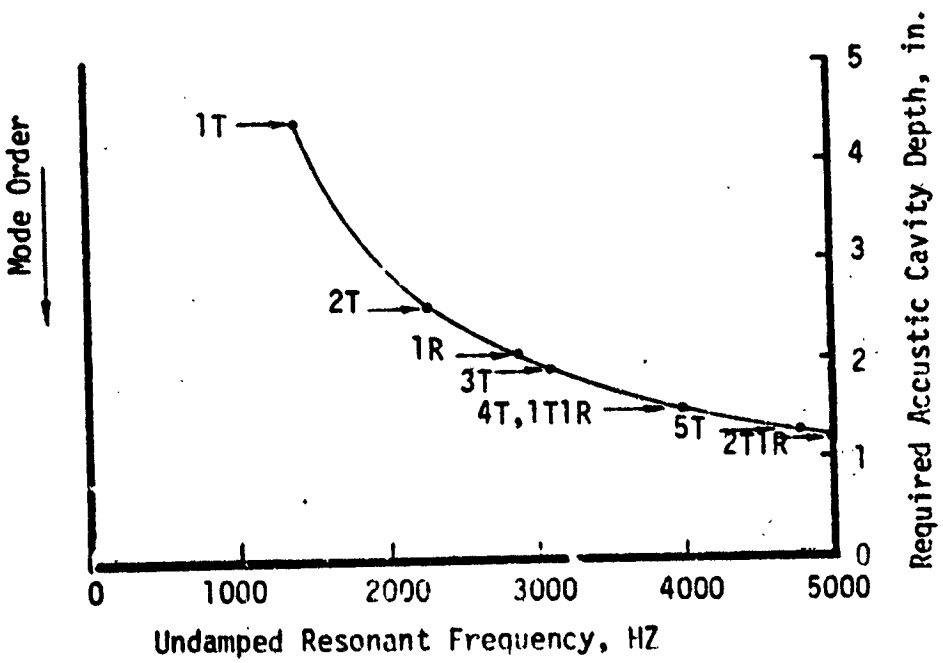

Figure 113. Updamped Resonant Frequencies for a Large LO_2/HC Engine

as shown in Figure 114. Analytically, a multiple-tune resonator will provide the necessary damping. However, resonators having more than two tune depths have not been experimentally demonstrated.

The primary mode to be damped will depend on the injector design and the propellant combustion time lags. In general, cycle I, having gas/gas injection into the main chamber, will have significantly shorter sensitive time lags than cycle G which has liquid RP-1 injection. Consequently, the suspectible modes of the cycle I injector will favor the higher frequencies, whereas the cycle G injector will favor lower frequencies. Cycle G is expected to be more difficult to stabilize than cycle I.

4. Required Stability Technology

Development of new large-thrust advanced LO_2-hydrocarbon engines may require the demonstration of multitune acoustic resonators for damping wide frequency ranges in large-diameter engines. Earlier large-diameter engines have resorted to injector face baffles to provide the required damping. Our analysis would indicate that multitune acoustic resonators would provide equally effective damping and avoid baffle cooling problems. The largest engine to incorporate only acoustic resonators is the ALRC ITIP engine. It is 30.5 cm (12 in.) in diameter. It has been demonstrated to be dynamically stable per the CPIA #247 stability test requirements. The engine stability is man-rated.

Another area requiring demonstration is resonator cooling techniques. Current acoustic resonators are regeneratively fuel-cooled. It would be desirable from a design and fabrication standpoint to film-cool the resonator by bleeding gaseous oxygen or gaseous fuel into the cavities. This technique needs to be demonstrated.

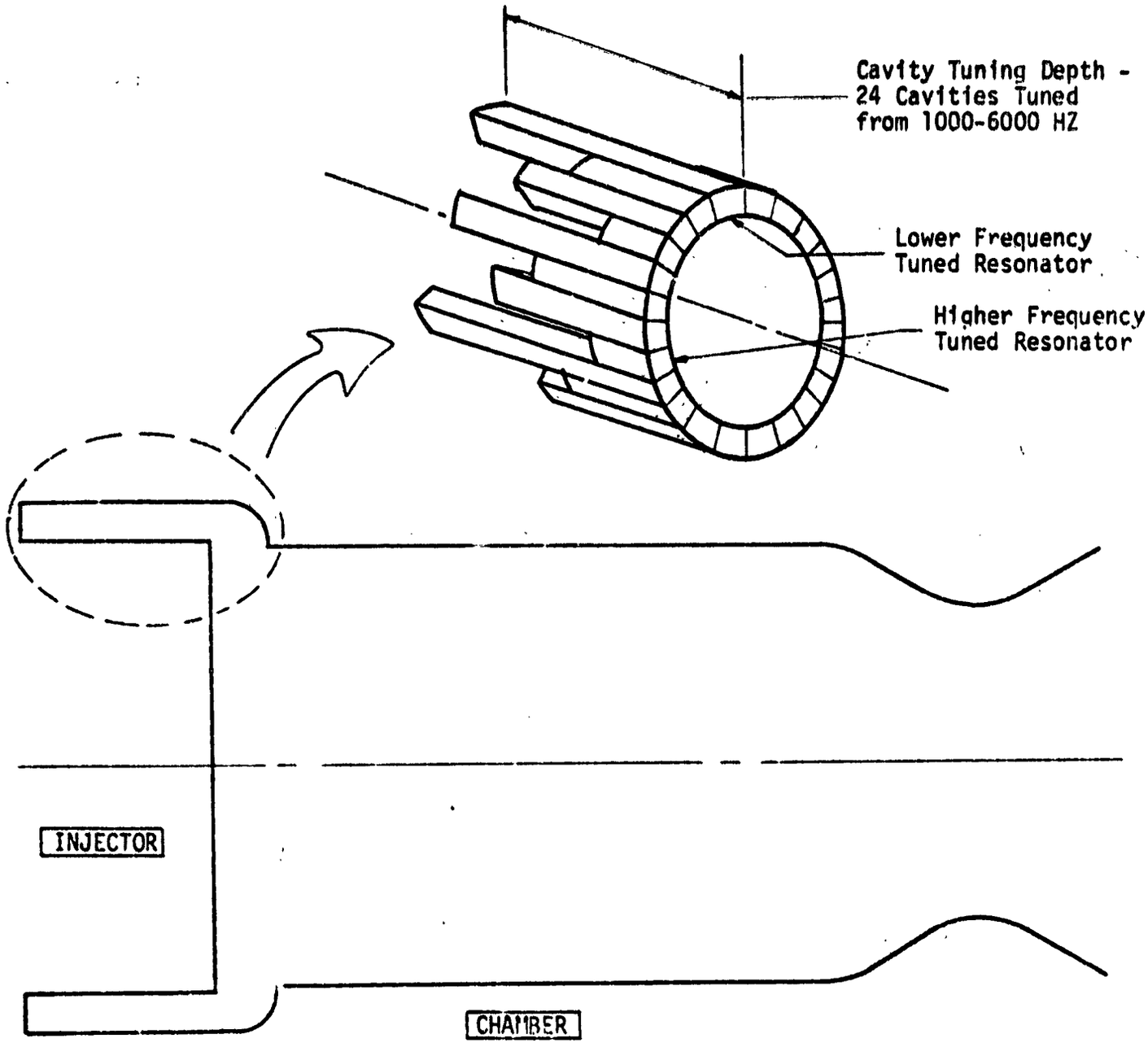

Figure 114. Multiple Tune Resonator for Large-Scale Engine

Finally, methods for accurately predicting combustion time lags for high-pressure LO_2/hydrocarbon injectors need to be developed. Analytical methods now exist for storable propellants. These methods need to be modified and verified for LO_2/hdyrocarbon propellants.

F. STRUCTURES DESIGN ANALYSIS

Stress and low-cycle fatigue analyses were conducted for the baseline LOX/HC thrust chamber design. The stress analysis results indicate that the chamber will require an electroformed nickel thickness greater than 1.5 cm (0.6 in.) in the cylindrical region to sustain the predicted pressure regime. Consideration should, therefore, be given to some form of wrapping (boron, glass, or steel filaments) to reduce the amount of nickel for weight savings.

The low-cycle fatigue (LCF) analyses indicate that a maximum strain range equal to 2.5% is predicted for the zirconium copper liner. This maximum strain occurs in the throat section liner directly beneath a web (land). The number of allowable cycles (Nf) corresponding to this strain range is 100 cycles, and this number includes a scatter factor of 4 and is based on 756°K (900°F) 10-hour hold time data.

1. Method of Analysis

The initial step in the analysis procedure consists of establishing the minimum thickness of electroformed nickel (EFNi) closeout required to sustain the hoop membrane forces due to thrust chamber pressure and coolant pressures, as illustrated in Figure 115. F_J and F_C are the yield strengths of the jacket and liner material, respectively. For the extreme case, when the liner is hot and yields, the jacket must take all of the load. Therefore, the minimum required wall thickness is based on the assumption that

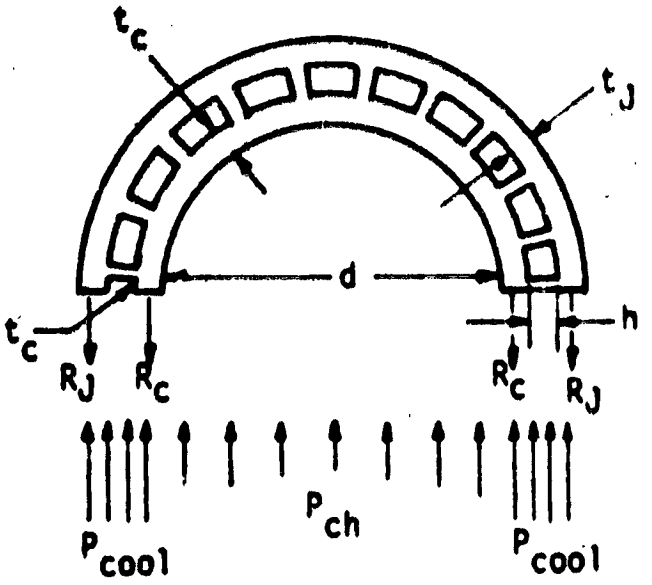

$$P_{ch}\, d + 2\, P_{cool}\, h = 2\,(R_J + R_c)$$

$$d/2 = r$$

$$\therefore\ R_J + R_c = P_{ch}\, r + P_{cool}\, h$$

Proportioned according to stiffness

i.e., $$\frac{R_J}{(Et)_J} = \frac{R_c}{(Et)_c} \qquad \therefore R_J = \frac{(Et)_J}{(Et)_c}\, R_c$$

& $$\left(1 + \frac{(Et)_J}{(Et)_c}\right) R_J = P_{ch}\, r + P_{cool}\, h$$

$$\therefore\ R_J = \frac{(Et)_J}{(Et)_J + (Et)_c}\,(P_{ch}\, r + P_{cool}\, h)$$

& $$R_c = \frac{(Et)_c}{(Et)_J + (Et)_c}\,(P_{ch}\, r + P_{cool}\, h)$$

$$\therefore\ \sigma_J = \frac{R_J}{t_J} = \frac{E_J}{(Et)_J + (Et)_c}\,(P_{ch}\, r + P_{cool}\, h) \le F_J$$

& $$\sigma_c = \frac{R_c}{t_c} = \frac{E_c}{(Et)_J + (Et)_c}\,(P_{ch}\, r + P_{cool}\, h) \le F_c$$

Figure 115. Preliminary Sizing of Required Jacket Thickness

the hoop membrane pressure loads are carried entirely by the nickel structure. The minimum thickness also includes a design safety factor to account for proof pressure loads. These minimum thicknesses are utilized in the finite-element model for the throat and cylindrical regions of the chamber.

Preliminary sizing of the required land width is illustrated in Figure 116. This sizing is checked for a prefiring condition at ambient temperature and also at steady-state temperatures, assuming the coolant flow is maintained after firing.

With the basic model geometry defined, a detailed elastic/plastic plane strain analysis is performed for thermal plus pressure, and thermal and pressure alone loading conditions. A sufficient number of iterations is made to ensure a convergent solution. The principal analytical tool used for this phase of the analysis is the AB5U finite-element computer program which utilizes a bilinear stress strain procedure for the elastic/plastic solution.

The program output includes effective stress and effective strain for each element centroid for each iteration. These data are utilized for plotting the curves shown in Figures 117 and 118.

2. Finite-Element Model

Finite-element model representations of the chamber throat and cylindrical wall sections are depicted in Figures 119 and 120, respectively. The model contains 110 quadrilateral elements and 141 nodal points. The orientation is chosen so that one boundary coincides with a mid-land radial and the other boundary coincides with a mid-channel radial. The included angle between the boundaries is defined as $\theta = 360°/2N$, where N is the number of coolant channels. The temperature distribution determined for the throat and cylindrical sections is given in Figures 121 and 122.

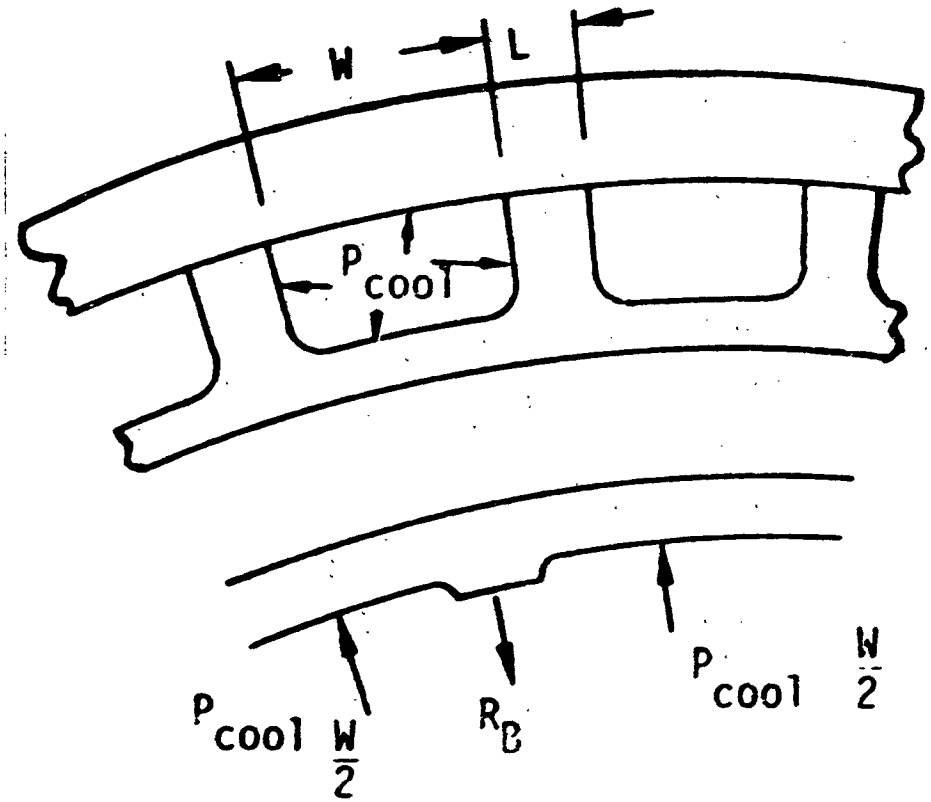

$$R_B = P_{cool}\ W$$

$$\therefore\ \sigma_B = \frac{R_B}{L} = \frac{P_{cool}\ W}{L} \leq F_B + \text{BOND STRENGTH}$$

$$\text{OR}\quad L \geq \frac{P_{cool}\ W}{F_B}$$

Figure 116. Preliminary Sizing of Required Land Width, L

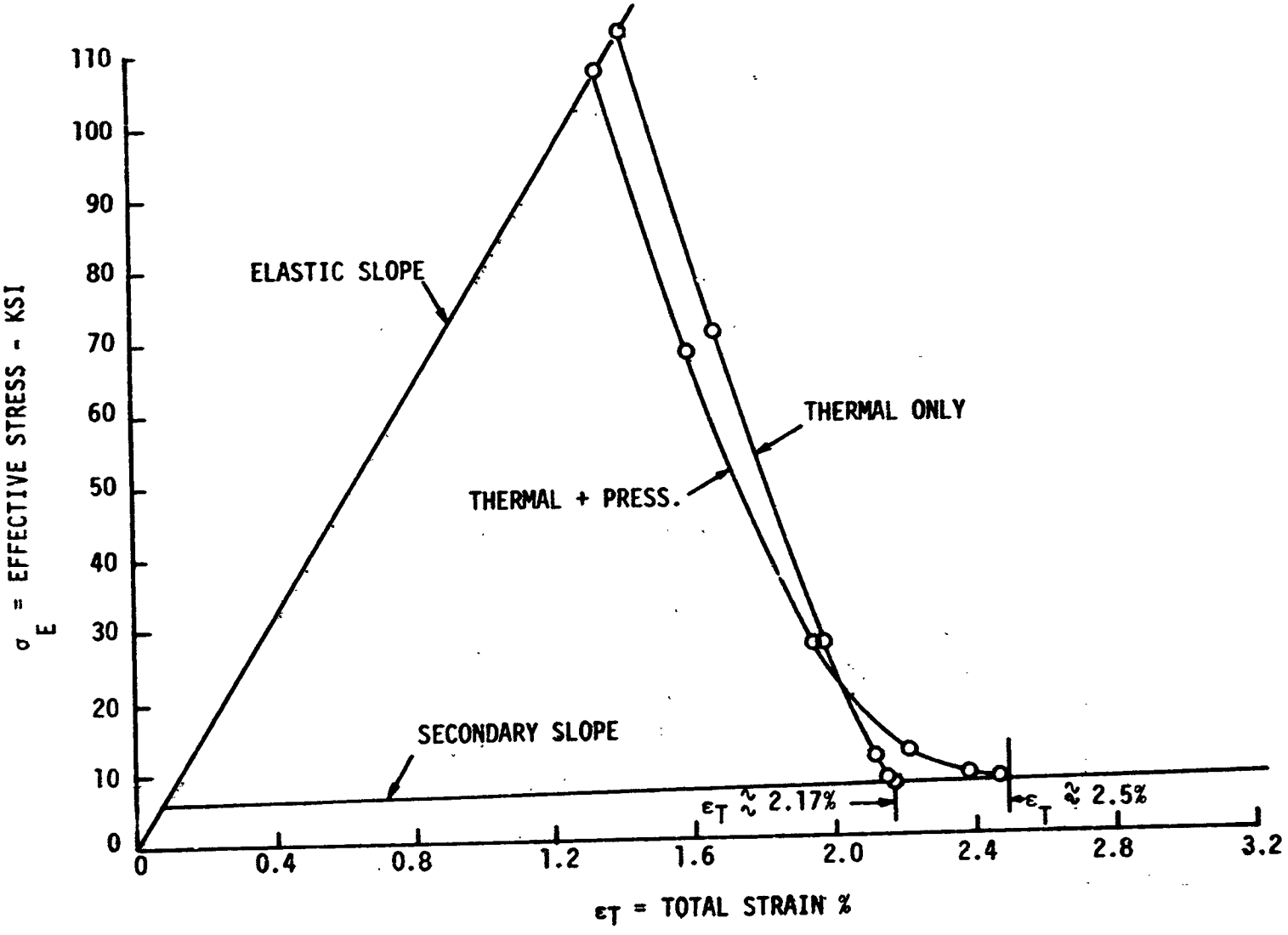

Figure 117. Predicted Strain Range for the Throat Section

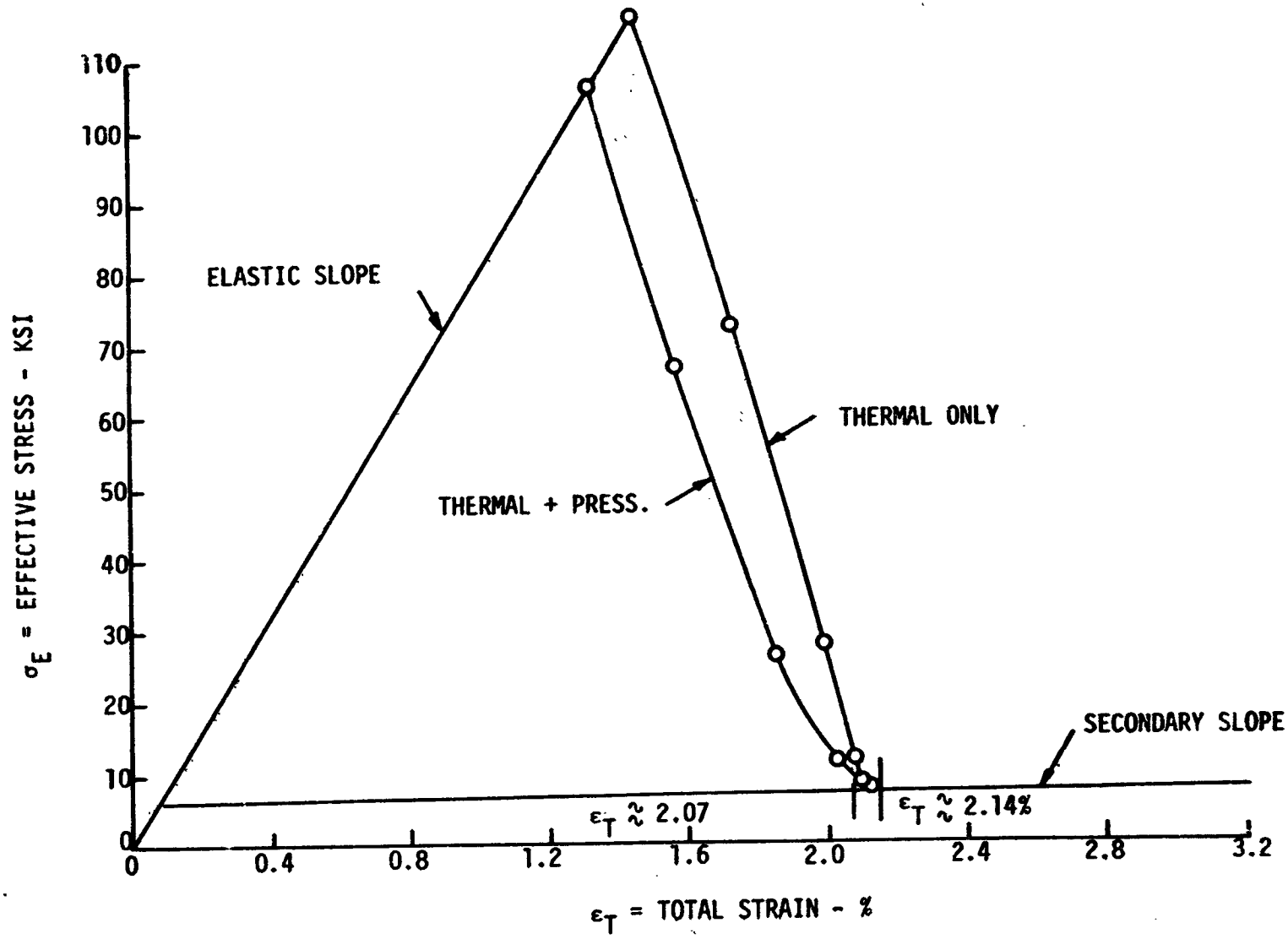

Figure 118. Predicted Strain Range for the Cyclindrical Section

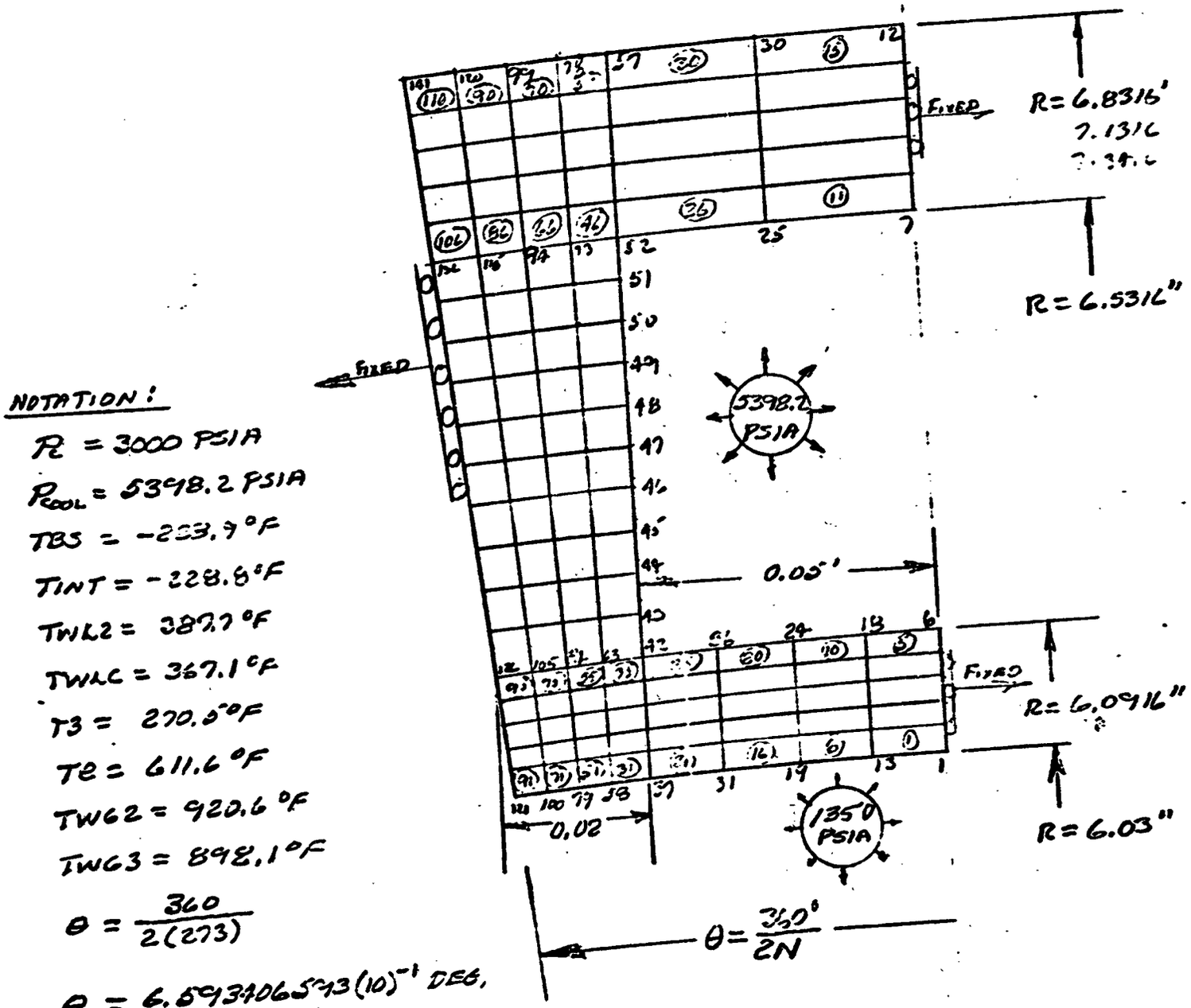

NOTATION:

$R = 3000$ PSIA

$P_{COOL} = 5398.2$ PSIA

$TBS = -233.9\,^{\circ}F$

$TINT = -228.8\,^{\circ}F$

$TWL2 = 387.7\,^{\circ}F$

$TWLC = 367.1\,^{\circ}F$

$T3 = 270.5\,^{\circ}F$

$Te = 611.6\,^{\circ}F$

$TWG2 = 920.6\,^{\circ}F$

$TWG3 = 898.1\,^{\circ}F$

$\theta = \frac{360}{2(273)}$

$\theta = 6.593406593(10)^{-1}$ DEG,

Figure 119. Throat Section Finite-Element Model

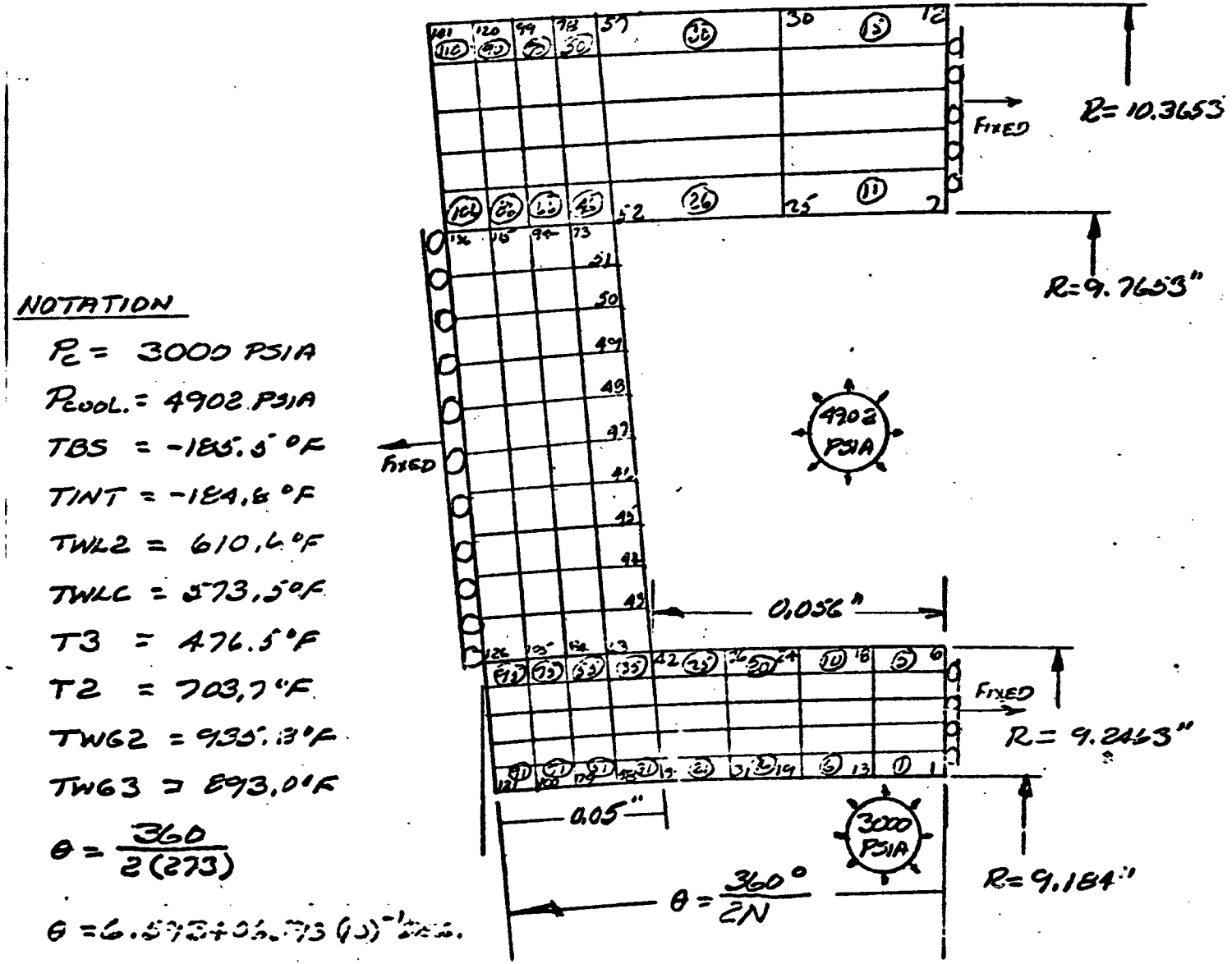

Figure 120. Cyclindrical Section Finite-Element Model

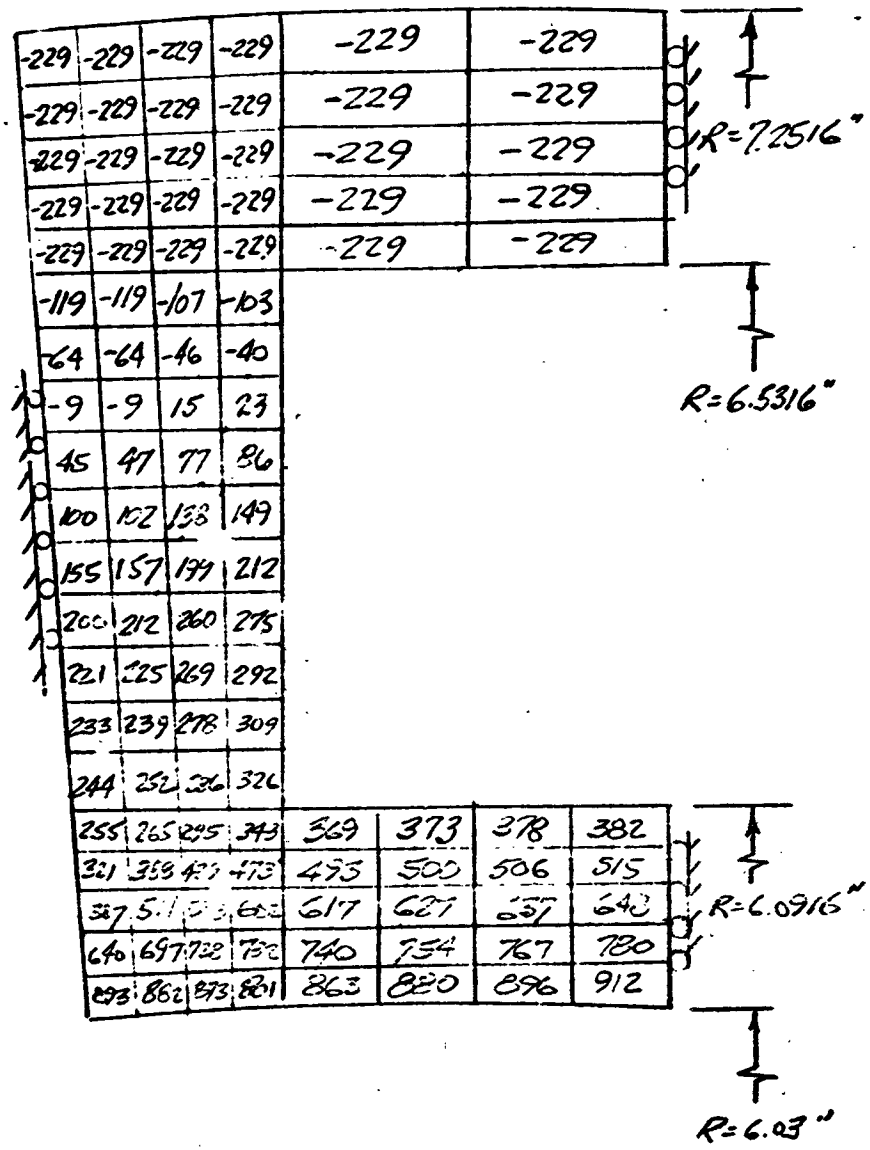

Figure 121. Finite-Element Model Temperatures at Throat Section

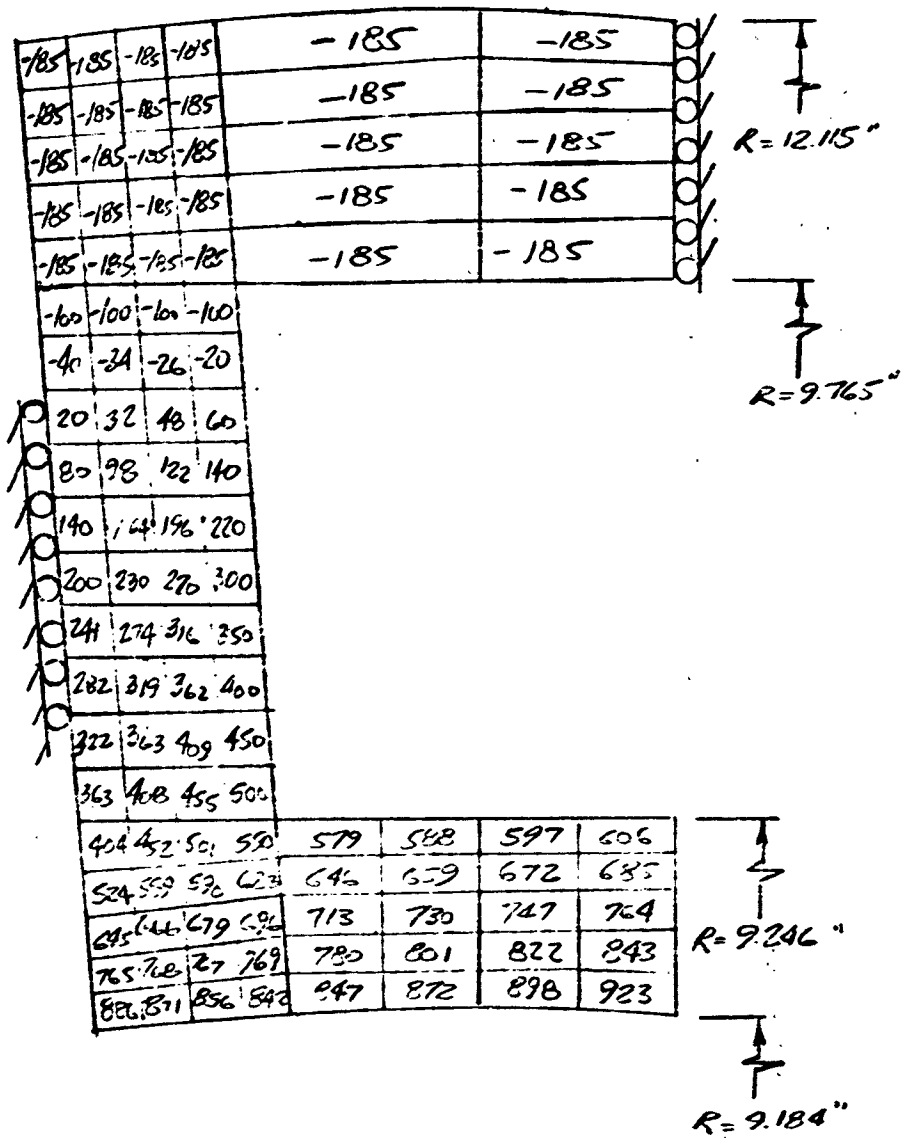

Figure 122. Finite-Element Model Temperatures at Cyclindrical Section

Boundary conditions along the two radials are designed to permit only radial deformation. Out-of-plane forces (Poisson Effect) are accounted for by adjusting the out-of-plane strain (EPST) magnitude until the normal forces are essentially zero.

3. Summary of Results

The minimum wall thickness values determined for the mechanical (pressure) loading are as follows:

	Location	
	Throat cm (in.)	Cylinder cm (in.)
t_{EFNi}	0.8 (0.3)	1.5 (0.6)
t_{Zr-Cu}	0.16 (0.0616)	0.16 (0.0623)

The values above are adequate to meet the anticipated proof pressure regimes.

Component low-cycle fatigue life is predicted on the basis of computerized plane strain results and appropriate fatigue and creep rupture data for the material being considered. Service life (Nf) is found by utilizing the maximum effective strain, ε_E, from Figures 117 and 118, together with the lesser of (1) the Nf from a 10-hour hold time data divided by a scatter factor of 4 or (2) the Nf from zero hold time data divided by 10. The following table presents the findings:

VI, F, Structures Design Analysis (cont.)

	TGS °F	TBS °F	t EFNi	ϵ_T %	N_f* (Allowable)	N_f Required
Throat - Mid-Land	893	-220	0.3	2.5	100	100
Cycle - Mid-Land	886	-185	0.6	2.14	130	100

*Includes Factor of 4

The highest operational strain levels were found in the throat section zirconium copper (Zr-Cu) coolant channel geometry, and accordingly, this area has the minimum predicted service life. As expected, the maximum strain occurs at the Zr-Cu liner hot gas-side wall in an area directly below a land and is due to the effects of combined pressure and thermal loading.

The high-pressure regime proposed for the advanced oxygen/hydrocarbon engine design concept dictates the need for a relatively thick-wall electroformed nickel cylinder. Meeting this requirement may be possible by using a lesser thickness of nickel augmented with wrapping (boron, glass, or wire filaments) to carry the predominant pressure hoop membrane forces.

G. CONTROLS DESIGN ANALYSIS

The primary control points of the three engine systems (cycles C, G, and I) are defined, including startup and cutoff sequences. The sequence of operation for these LOX/hydrocarbon engines is patterned after engine experience with the F-1 ("Model Specification 1,500,000 lb Thrust Liquid Oxygen RP-1 Liquid-Propellant Engine," Rocketdyne Model F-1, Rocketdyne Report R-1420cS, 15 January 1963) and the Titan I ("Titan Engines and Applications," Aerojet-General Corporation Report Number CR128, 31 October 1960).

VI, G, Controls Design Analysis (cont.)

1. Cycle C

The engine control requirements for cycle C (Figure 99) are primarily governed by the engine start and shutdown sequences. The start and shutdown sequences are given in Table XLIX.

The sequence of operations listed is assumed to occur after the engine has been bled-in and the methane and oxygen components have been chilled down to the main propellant shutoff valves prior to receipt of the start signal. The thrust, total impulse, and propellant consumptions during operation are summarized in Table L from start to 90% of rated thrust down to shutdown at 5% of rated thrust.

Engine performance at the design thrust level over a mixture ratio range encompassing the design point mixture ratio $\pm$ 10% is summarized on Table LI.

2. Cycle G

The LOX/RP-1 modes of operation for cycle G (Figure 100) are patterned after F-1 and Titan I engine experience. The primary concern with these propellants is to keep contaminants out of the LOX manifolds. Therefore, all LOX/RP-1 combustors are started oxidizer-rich to reduce the chance of RP-1 entering the oxidizer circuits.

The engine start and shutdown sequence is presented in Table LII. The sequence of operations listed is assumed to occur after the vehicle prevalves have been opened and the cryogenic components have been chilled down to the main engine shutoff valves.

TABLE XLIX

SEQUENCE OF OPERATIONS FOR LOX/LCH_4 GAS-GENERATOR CYCLE ENGINE C

Start

1. Purge Gas Generator and Thrust Chamber Oxidizer Lines and Manifold.
2. Energize Spark Igniters.
3. Open Main Ox. Valve (#1)*.
4. Open Gas Generator Igniter Valves.
5. Open Main LCH_4 Valve (#2).
6. Open Gas Generator Ox. Valve (#3).
7. Open Gas Generator Fuel Valve (#4).
8. Open Thrust Chamber Igniter Valves.

Shutdown

1. Cut off Gas Generator Spark Energy.
2. Close Gas Generator Igniter Valves.
3. Close Ox. Gas Generator Valve (#3).
4. Close Main Ox. Valve (#1).
5. Initiate Ox. Purge.
6. Close Gas Generator Fuel Valve (#4).
7. Close Main CH_4 Valve (#2).
8. Close Thrust Chamber Igniter Valves.
9. Cut off Thrust Chamber Spark Energy.

*Numbers refer to the valves in Figure 99.

TABLE L

LOX/LCH$_4$ ENGINE CYCLE C START AND

SHUTDOWN TRANSIENT DATA SUMMARY

Start to 90% F

Time, sec.	0.80	
Total Start Impulse, kg-sec (lb-sec)	68,150	(150,250)
LOX Consumption, kg (lb)	129	(285)
CH_4 Consumption, kg (lb)	124	(273)

Shutdown to 5% F

Time, sec	0.50	
Total Shutdown Impulse, kg-sec (lb-sec)	79,900	(176,150)
LOX Consumption, kg (lb)	163	(358)
CH_4 Consumption, kg (lb)	75	(166)

TABLE LI

LOX/LCH_4 ENGINE CYCLE C DESIGN AND OFF-DESIGN MR PERFORMANCE

ε = 56.5

Engine	Mixture Ratio 2.57	2.82	3.06
Sea Level Thrust, lb	600,000	600,000	600,000
Vacuum Thrust, lb	672,515	671,239	671,891
Sea Level Specific Impulse, sec	307.8	309.1	308.8
Vacuum Specific Impulse, sec	345.0	345.8	345.8
Total Flowrate, lb/sec	1949.3	1941.1	1943.0
Fuel Flowrate, lb/sec	546.0	508.1	478.6
Oxidizer Flowrate, lb/sec	1403.3	1433.0	1464.4
Chamber Pressure, psia	4350	4300	4232

TABLE LII

SEQUENCE OF OPERATIONS FOR LOX/RP-1
ENGINE CYCLE G

Start

1. Purge Oxidizer Lines and Manifolds in Ox.-Rich Preburner.
2. Energize Spark Igniters.
3. Open Main Ox. Valve (#1)*.
4. Open Igniter Valves on Ox.-Rich Preburner.
5. Open Main (RP-1) Fuel Valve (#2).
6. Open Control Valves (#3 and #4) on Ox.-Rich Preburner

Shutdown

1. Close Main Ox. Valve (#1).
2. Initiate Ox. Purge.
3. Close Main (RP-1) Fuel Valve (#2).
4. Close Control Valves on Ox.-Rich Preburner
5. Close Igniter Valves on Ox.-Rich Preburner.
6. Cut off Igniter Spark Energy.

te: Numbers refer to valves on Figure 100.

C-14

The engine start and shutdown transients are also estimated. The staged-combustion cycle engine is assumed to be chilled down and bled-in to the main chamber valves prior to receipt of the fire signal. The engine is then assumed to be started under tank head. The transient estimates are based upon the analytical modeling of similar engine configurations on the ALRC Liquid Engine Transient Simulation (LETS) model.

The start and shutdown transient data are summarized on Table LIII. Start to 90% of rated thrust and shutdown down to 5% of rated thrust are generally specified values to establish transient times.

The design and off-design engine performance at the design thrust level for ± 10% MR excursions are presented in Table LIV. The nominal engine operating mixture ratio is 2.8.

3. Cycle I

The engine control requirements for cycle I are indicated in Figure 101, and the start and shutdown are given in Table LV. As with cycle G, the combustors are started oxidizer-rich. This practice is maintained for the LCH_4 engine, although the gaseous nature (high vapor pressure) of methane reduces the possible accumulation of a liquid and its potential detonation, as in the case of RP-1. The sequence of operations is assumed to occur after the vehicle prevalves have been opened and the cryogenic components have been chilled down to the main engine shutoff valves.

The engine start and shutdown transients are summarized in Table LVI. The engine is assumed to be chilled down and bled-in to the main chamber valves prior to receipt of the fire signal. The engine is assumed to be started under tank head.

TABLE LIII

LOX/RP-1 ENGINE CYCLE G START AND SHUTDOWN TRANSIENT DATA SUMMARY

Start to 90% F		
Time, Sec	2.52	
Total Start Impulse, kg-sec (lb-sec)	68,150	(150,250)
LOX Consumption, kg (lb)	131	(289)
RP-1 Consumption, kg (lb)	126	(278)
Shutdown to 5% F		
Time, Sec	0.50	
Total Shutdown Impulse, kg-sec (lb-sec)	79,900	(176,150)
LOX Consumption, kg (lb)	165	(363)
RP-1 Consumption, kg (lb)	77	(169)

TABLE LIV

LOX/RP-1 ENGINE CYCLE G DESIGN AND OFF-DESIGN MR PERFORMANCE

$\varepsilon = 42.5$

Engine	Mixture Ratio 2.52	2.80	3.08
Sea Level Thrust, lb	600,000	600,000	600,000
Vacuum Thrust, lb	670,700	670,800	671,700
Sea Level Specific Impulse, sec	310.5	312.8	309.7
Vacuum Specific Impulse, sec	347.1	349.7	346.7
Total Flowrate, lb/sec	1932.4	1918.3	1937.4
Fuel Flowrate, lb/sec	549.0	504.8	474.8
Oxidizer Flowrate, lb/sec	1383.4	1413.5	1462.5
Chamber Pressure, psia	3155	3100	3092

TABLE LV

SEQUENCE OF OPERATIONS FOR LOX/LCH_4

ENGINE CYCLE I

Start

1. Purge Oxidizer Lines and Manifolds in Fuel- and Ox.-Rich Preburners.
2. Energize Spark Igniters.
3. Open Main Ox. Valve (#1).*
4. Open Igniter Valves on Fuel-and Ox.-Rich Preburners.
5. Open Main(LCH_4)Fuel Valve (#2).
6. Open Control Valves (#3, #4, #5 and #6) on the Fuel-and Ox.-Rich Preburners.

Shutdown

1. Close Main Ox. Valve (#1).
2. Initiate Ox. Purge.
3. Close Main (CH_4) Fuel Valve (#2).
4. Close Control Valves on Fuel- and Ox.-Rich Preburners.
5. Close Igniter Valves on Fuel- and Ox.-Rich Preburners.
6. Cut off Igniter Spark Energy.

*Note: Numbers refer to valves on Figure 101.

TABLE LVI

LOX/LCH_4 ENGINE CYCLE I START AND SHUTDOWN TRANSIENT DATA SUMMARY

Start to 90% F		
Time, sec	2.52	
Total Start Impulse, kg-sec (lb-sec)	68,150	(150,250)
LOX Consumption, kg (lb)	134	(295)
LCH_4 Consumption, kg (lb)	103	(227)
Shutdown to 5% F		
Time, sec	0.50	
Total Shutdown Impulse, kg-sec (lb-sec)	79,900	(176,150)
LOX Consumption, kg (lb)	168	(371)
LCH_4 Consumption, kg (lb)	63	(138)

VI, G, Controls Design Analysis (cont.)

The design and off-design engine performance at the design thrust level for ± 10% MR excursions are presented on Table LVII. The nominal engine operating mixture ratio is 3.5.

4. Technology Areas

Based upon review of the system schematics, several technology areas related to valves and engine control are briefly described as follows:

a. Shutoff and Dynamic Seals

High cycle life and low leak rates for dynamic seals over a wide temperature range present a significant valve design problem. Seal design is hampered, to some extent, by lack of material properties data needed to predict leak rates and wear life. This is particularly true for temperatures other than normal ambient temperature. A program to obtain needed data for candidate seal materials, followed by a prediction-validation program, would provide a higher confidence level that desired leak rates and cycle life will be achieved without time-consuming development programs.

b. Materials of Construction

Several of the valves required for these systems are fairly large (about 4-5 in. diameter). Potential weight savings may be achieved by evaluation of high-strength, low-weight materials not currently in use for high- pressure engine valves. Valve housings and shutoff elements are two valve components that may provide worthwhile weight savings.

TABLE LVII

LOX/LCH_4 ENGINE CYCLE I DESIGN AND OFF-DESIGN MR PERFORMANCE

$\varepsilon = 48$

	Mixture Ratio		
Engine	3.15	3.50	3.85
Sea Level Thrust, lb	600,000	600,000	600,000
Vacuum Thrust, lb	670,600	670,400	670,200
Sea Level Specific Impulse, sec	322.1	323.1	322.1
Vacuum Specific Impulse, sec	360.0	361.0	359.8
Total Flowrate, lb/sec	1862.8	1857.0	1862.8
Fuel Flowrate, lb/sec	448.9	412.7	384.1
Oxidizer Flowrate, lb/sec	1413.9	1444.3	1478.7
Chamber Pressure, psia	3549	3500	3451

VI, G, Controls Design Analysis (cont.)

c. Engine Controller

Present-day rocket engine flight controllers were designed and developed in a time frame when discrete components or medium-scale integration (MSI) components were used. The rapid advance in electronics during the late 1960's and through the 1970's resulted in large-scale integration (LSI) components -- microprocessors in particular. The reduced size and increased memory density of electronic control elements offers the potential for reduced size, weight, power consumption, and hardware cost of engine controllers. A program to evaluate the applicability of these new electronic components to engine control may provide greater control and diagnostic capability with a smaller, lighter controller.

H. CONCEPTUAL DESIGNS

Preliminary assembly drawings were prepared for each of the three engine cycles C, G, and I. The engine designs feature fixed boost pumps for each propellant circuit clustered around the engine gimbal center. The turbopump assemblies (TPAs) are side-mounted in order to obtain a favorable center of gravity location.

The TCA designs incorporate slotted zirconium copper channels from the injector face to a nozzle area ratio of 8:1. A two-pass Inconel 718 tube bundle is used from an area ratio of 8:1 to the nozzle exit area ratio. The chamber coolant is introduced at an area ratio of 8:1 and flows countercurrent up to the plane of the injector face. The nozzle coolant is introduced at an area ratio of 8:1, cools the nozzle, and then exits the return manifold at the 8:1 area ratio.

The gimballed envelope was evaluated for a 10° square pattern.

1. Cycle C Engine Configuration

The flow schematic for engine cycle C is given in Figure 99 (Section VI,B). The conceptual design layout for this gas-generator cycle engine is depicted in Figures 123 and 124 (Dwg. 1193242). The configuration, as shown, utilizes a LCH_4-cooled chamber and a LOX-cooled nozzle. It was previously shown in Section III,D that LCH_4 can adequately cool the entire engine with only a small penalty in pump discharge pressure. The overall engine dimensions do not change if methane replaces oxygen as the nozzle coolant, and there is only a slight change in the general configuration depicted in the figure.

The engine envelope data are:

Engine Length, cm (in.)	358 (141)
Nozzle Exit Diameter, cm (in.)	194 (76.4)

2. Cycle G Engine Configuration

The LOX/RP-1 cycle G engine utilizes a single-preburner staged-combustion cycle with a LOX-cooled thrust chamber and nozzle, as shown in the schematic of Figure 100. The preliminary assembly drawing of the baseline engine is shown in Figures 125 and 126 (Dwg. 1193240).

The engine envelope data are:

Engine Length, cm (in.)	351 (138.0)
Nozzle Exit Diameter, cm (in.)	210 (82.5)

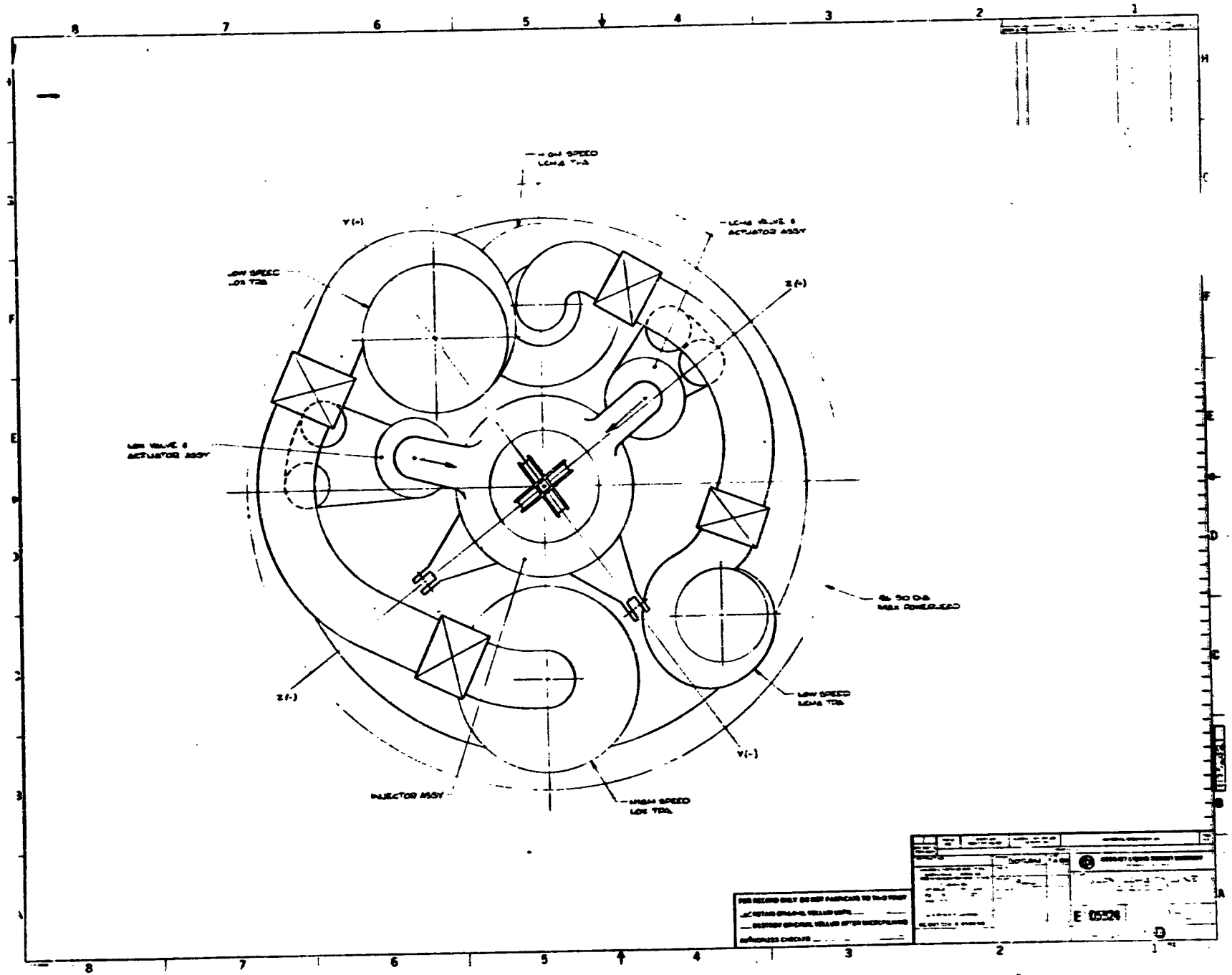

Figure 123. LOX/LCH_4 Engine (Cycle C) Conceptual Design (Top View)

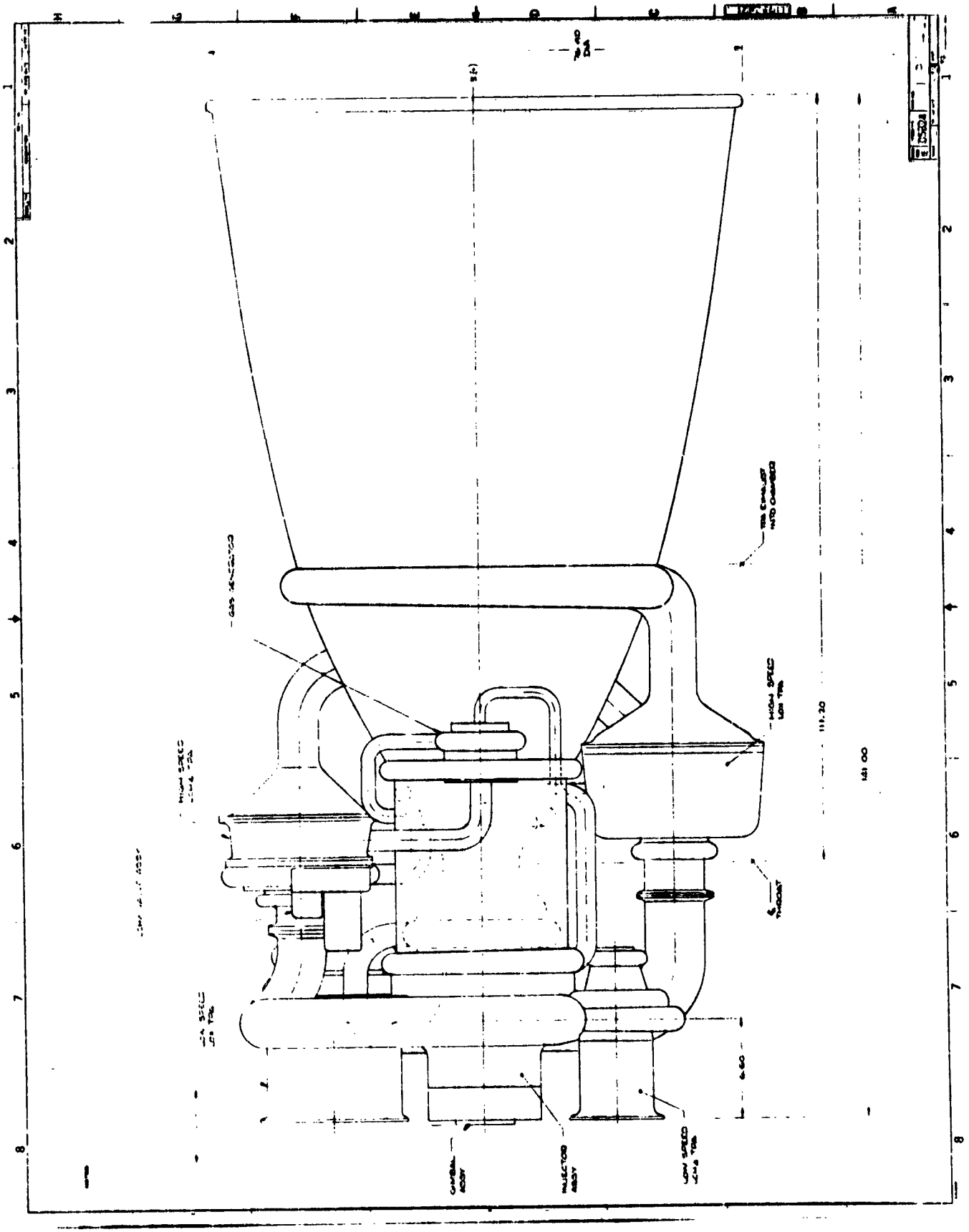

Figure 124. LOX/LCH_4 Engine (Cycle C) Conceptual Design (Side View)

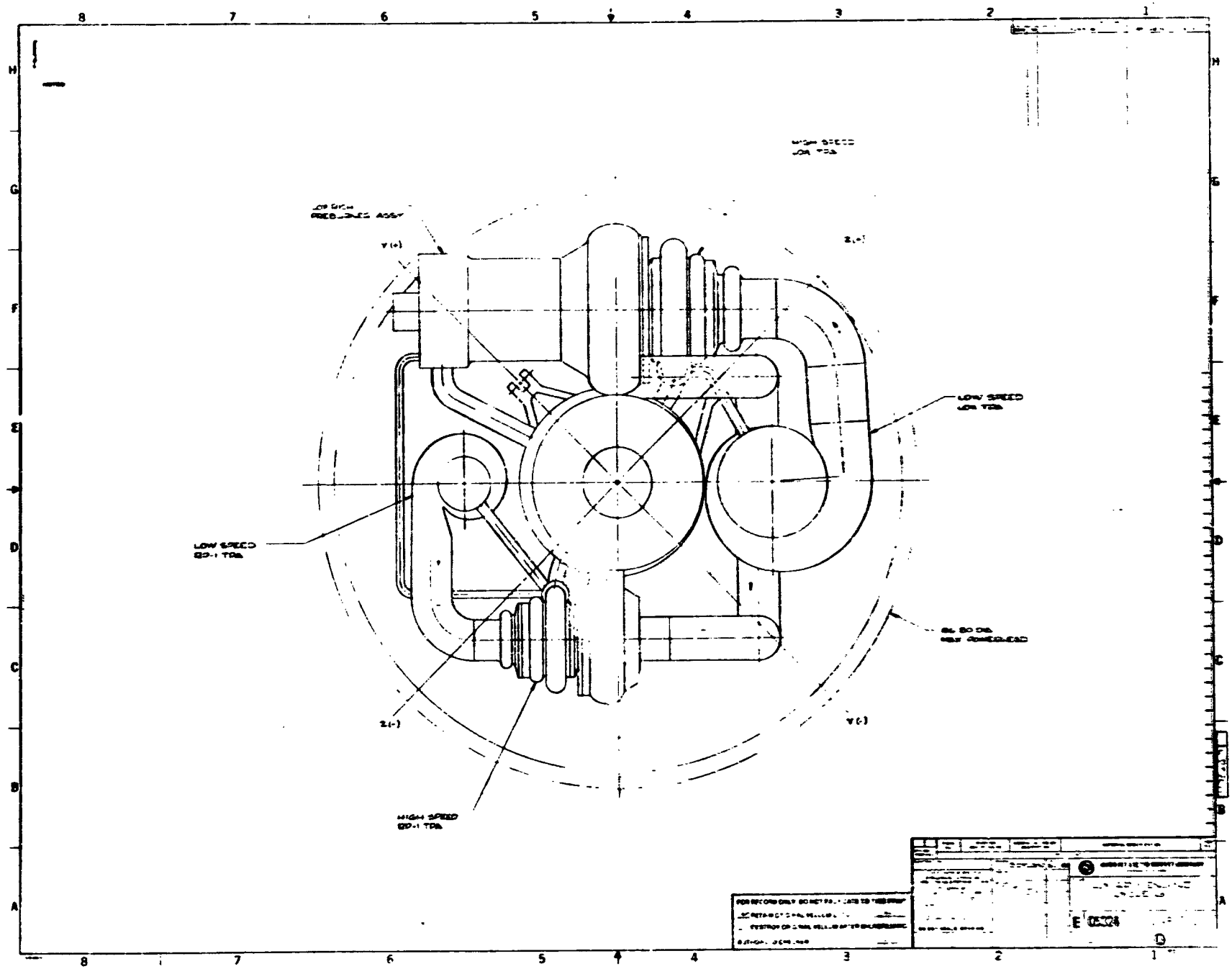

Figure 125. LOX/RP-1 Engine (Cycle G) Conceptual Design (Top View)

3. Cycle I Engine Configuration

The LOX/LCH_4 engine cycle I engine design is a dual-preburner staged-combustion cycle with a LCH_4-cooled chamber. The engine schematic is shown in Figure 101. The preliminary assembly drawing of the engine is given in Figures 127 and 128 (Dwg. 1193241). Hot-gas ducting is minimized through completely integrated TPAs which are mounted to the engine by means of the hot- gas crossover ducts. A LOX-cooled nozzle is shown in the figure in order to reduce the methane pump discharge pressure. Should an all-methane-cooled engine be desired, essentially no dimensional changes would have to be made to the drawing aside from re-routing the nozzle coolant line.

The engine envelope data are:

Engine Length, cm (in.)	351 (138.0)
Nozzle Exit Diameter, cm (in.)	209 (82.4)

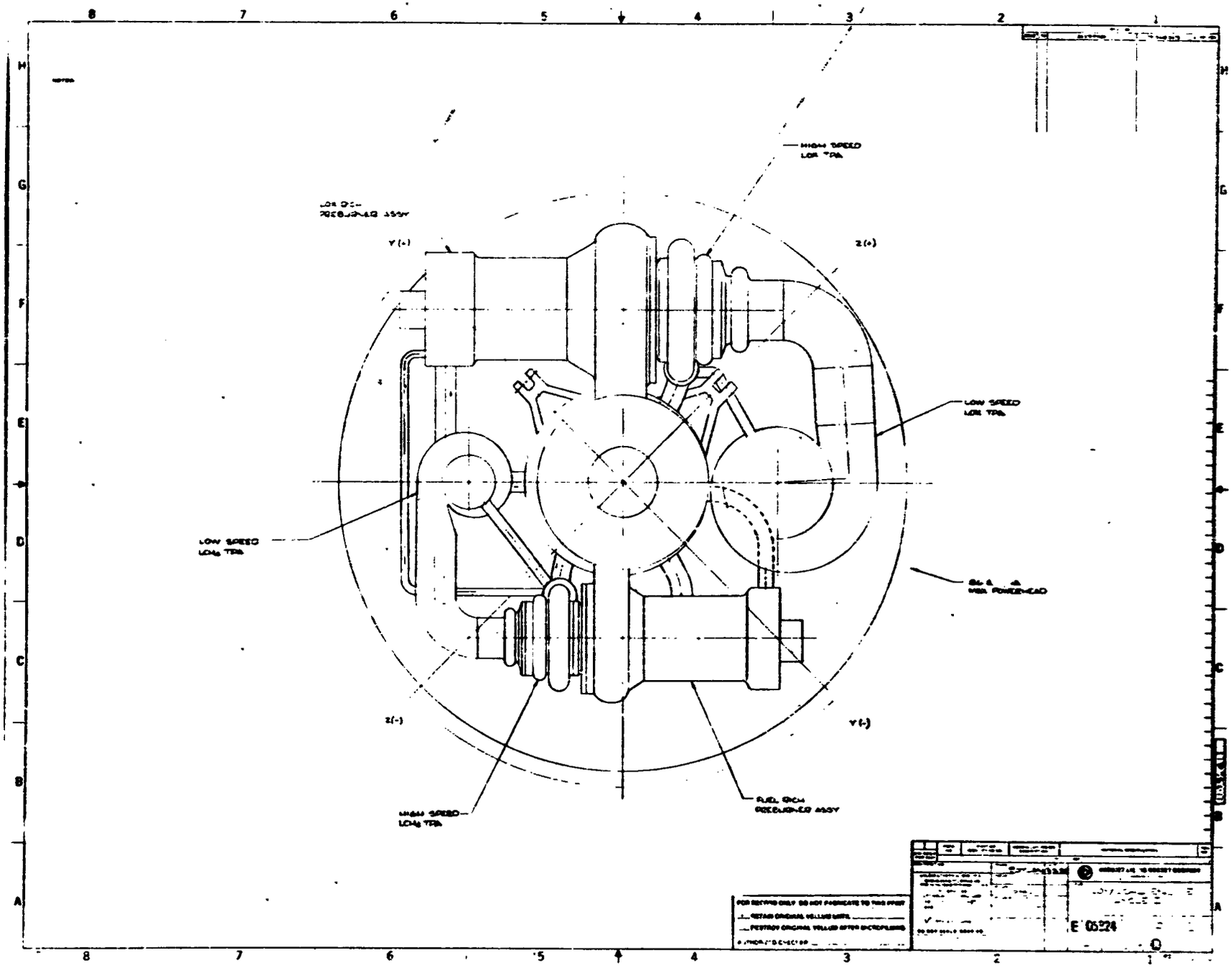

Figure 127. LOX/LCH_4 Engine (Cycle I) Conceptual Design (Top View)

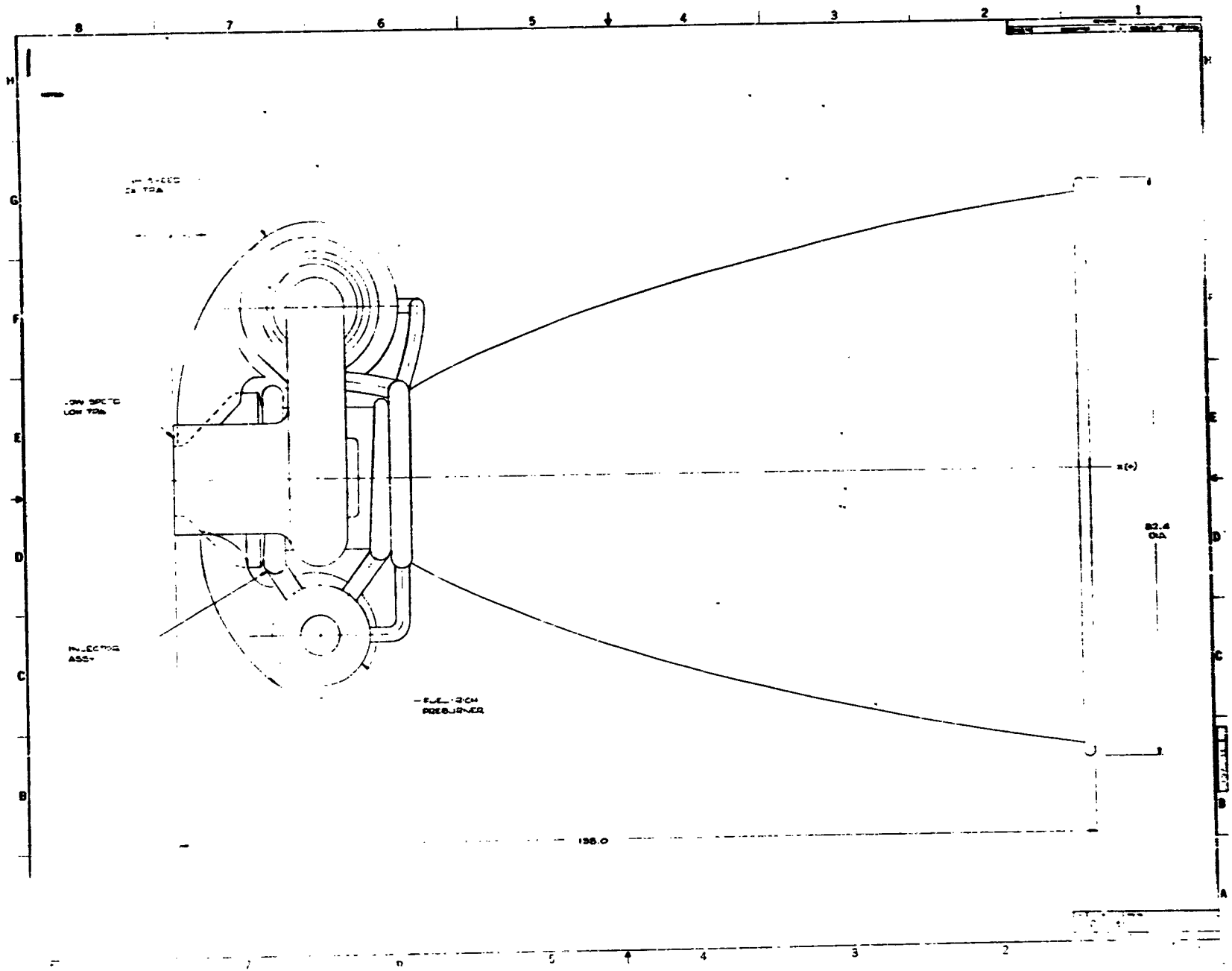

Figure 128. LOX/LCH_4 Engine (Cycle I) Conceptual Design (Side View)

VII. DISCUSSION OF RESULTS

The pertinent findings from this study are placed in perspective in this section. Items to be discussed include cooling, power generation, carbon deposition, power cycles, fuels, etc. While these findings are presented here in a positive and logical manner, it must be remembered that the relative merit of a given cycle or coolant, for example, could possibly change if the ground rules and assumptions were changed. Therefore, the assumptions utilized throughout the study are summarized in Table LVIII.

Reference is made in the following discussion to cooling limit, power limit, etc. where these limits are necessarily a function of the assumptions given in Table LVIII. Since it is the purpose of this study to rank the various cycles, basic ground rules were set to limit the number of variables. It is believed that the relative ranking of the cycles is not biased by these assumptions, except as outlined in the following discussion.

A. CYCLES

Engine cycles for a space transportation system (STS) must be ranked by a number of factors including performance (payload capability), weight and packaging volume, life, reliability, safety margin, and ease of maintenance. Engine cost is not considered a major factor, since the engine will be reusable and the cost amortized. Operational cost is the significant driver for an STS, but this factor is usually considered as part of vehicle studies.

In this study the LOX/HC cycles have been ranked primarily by their specific impulse (see Figure 97) and by features that imply life, reliability and ease of maintenance (see Table XXXV). As might have been expected, the RP-1 cooled engine cycles (A, D, and F) turned out to be the poorest performers (cf. Figure 97). These cycles are poor primarily

TABLE LVIII

BASIC ASSUMPTIONS UTILIZED FOR THE ADVANCED OXYGEN-HYDROCARBON ROCKET ENGINE STUDY

1. Pump discharge limit at approximate 1980 state-of-the-art: 55160 kN/m^2 (800 psia)
2. Chamber life minimum at 100 cycles and 10-hour hold time (see Figure 10, p. 24)
3. Coolant Mach number limit at approximately 3.0
4. Coolant channel dimension limitations (see p. 25)
5. Propane is subcooled to LO_2 NBP in the tank by LO_2 vapor or by submerging the propane tank inside the LOX tank
6. LO_2 cooling correlation utilized for methane (see p. 27)
7. Coking limit for RP-1 in the cooling jacket is 561 °K (550 °F)
8. Coking limit for RP-1R in the cooling jacket is 700 °K (800 °F)
9. Carbon deposition on chamber walls is zero (except as noted)
10. Turbine inlet temperature limit (fuel-rich) at 1033 °K (1860 °R) except as indicated
11. Non-equilibrium fuel-rich properties for LOX/RP-1 determined from kinetic model and extrapolated to high pressure
12. Non-equilibrium fuel-rich properties for LOX/CH_4 and LOX/C_3H_8 modeled from LOX/RP-1 data using equilibrium data for extrapolation
13. High temperature turbine efficiency cooling losses are zero
14. Power cycle optimization uses split flow pumps to minimize horsepower requirement
15. Injector, valve and line pressure drops from Table III, p. 19
16. Vehicle payload assessment used JSC two-stage vehicle and approximate tank scaling relationship for different cycles and fuels

because of the cooling (coking) limit which severely limits the attainable chamber pressure to about 8963 kN/m^2 (1300 psia). Even the assumption of a higher turbine temperature and/or a higher pump discharge pressure limit cannot significantly improve the ranking of the RP-1 cooled engine cycles.

Gas generator cycles A' and B, utlizing a refined RP-1 (RP-1R) as coolant or LOX as coolant, are poor performers when compared with their staged combustion cycle counterparts D', E, F' and G (see Figure 97). Cycles A' and B are not cooling limited (as shown in Figures 22 and 25). These cycles are "performance (specific impulse) limited" by the poor fluid properties of the LOX/RP-1 fuel-rich, gas-driven turbine and the resultant gas generator exhaust performance. The vacuum specific impulse reaches its maximum at a chamber pressure of 15168 kN/m^2 (2200 psia) and 19305 kN/m^2 (2800 psia), respectively, for cycles A' and B.

The effect of increased turbine inlet temperature and/or carbon deposit on these gas generator cycles is to bring their specific impulse levels closer to that for corresponding staged combustion cycles (see Figures 22 and 25).

Unless it can be shown that a carbon deposit can be achieved at the higher mixture ratio and high chamber pressure of this study, or that the high pressure LOX/RP-1 fuel-rich turbine-drive-gas properties are better than those assumed for this study, all of the gas generator cycles involving RP-1 and RP-1R fuels will not be competitive with the other cycles of this study.

The methane-fueled and propane-fueled gas generator cycles C and C' are performance (specific impulse) limited. They show a maximum in vacuum specific impulse versus chamber pressure (see Figures 28 and 30). The delivered payload for these cycles (see Figure 97) is nearly competitive

with the staged combustion cycles using LOX/RP-1, but the payload is quite inferior to the staged combustion cycles utilizing methane or propane fuels. There is a marked improvement in specific impulse for these cycles when a higher temperature turbine is utilized (cf. Figures 102 and 28). It is possible that experimentally gathered fuel-rich LOX/CH_4 and LOX/C_3H_8 turbine-drive-gas data may be superior to the data used in this study. Such data could make these cycles even more competitive.

The families of staged combustion cycles for RP-1 (D', E, F' and G) and for CH_4 and C_3H_8 (G', H, I and I') are good performers, as shown in Figure 97. These cycles are all "power limited" as indicated by Figures 32, 34, 36, 38, 39, 41, 43 and 44. Higher pump discharge pressures than the assumed limit of 55160 kN/m^2 (8000 psia) are seen to be possible. The slope of the P_D vs Pc curve has become so steep, however, that very little is gained by pushing P_D much higher.

The least competitive cycle in the RP-1 family is cycle D', which utilizes the fuel as coolant and as turbine-drive-gas, when partially burned in the preburner. Cycle E splits the work load between the two propellants, allowing the LOX (a better coolant) to act as chamber coolant, and the fuel (as fuel-rich preburner gas) to power the cycle. This usage promotes a payload gain (Figure 97) of about 40 metric tons.

The best LOX/RP-1 cycle is cycle F', which utilizes RP-1R as coolant and the LOX (as oxidizer-rich preburner gas) to power the cycle. Cycle G which requires the LOX to accomplish both the cooling and power drive functions is slightly inferior in payload capability to cycle F' (see Figure 97).

Cycles I and I' offer the highest payload capability of the LOX/HC engine cycles (see Figure 97). Both cycles deliver the same payload

(466 metric tons) despite the higher performance of methane (ΔIs = 2 sec). Because subcooled propane is a better coolant than methane, cycle I' can operate at a slightly higher chamber pressure. The higher chamber pressure and the higher engine thrust-to-weight ratio for cycle I' compensate for its lower performance. Both cycles I and I' make maximum use of the chemical energy in the propellants through oxidizer-rich and fuel-rich preburners.

Cycle H affords lower payload capability than cycle I because it requires the fuel to both cool and power the engine. Cycle G' primarily illustrates the benefit from switching fuels (RP-1 from cycle G to C_3H_8). An improvement in cycle G' would be cycle H' (not shown in Figure 97), which would utilize C_3H_8 for both cooling and engine power.

Cycles J and K are hybrid LOX/HC cycles, which use a small amount (about 11-14 kg/s [25-30 lb/sec]) of liquid hydrogen for cooling and turbine drive fluid (when burned fuel-rich in the gas generator). Cycle J, a gas generator cycle, provides higher payload capability than any "pure" LOX/RP-1 cycle (see Figure 97) because of the higher chamber pressure capability. This cycle has no power limit within the constraints imposed by the assumptions. As indicated in the note in Table XXXV, cycle J with CH_4 or C_3H_8 fuel (termed cycles J' or J") would be ranked in the top three cycles.

Examination of Table XXXV and Figure 97 shows the dual throat engine cycle K with the highest ranking. This ranking results primarily from the high specific impulse achieved at the mode 2 area ratio. A more accurate trajectory integration would be required to properly assess the effect of the thrust reduction of cycle K with mode 2 operation. Liquid hydrogen is used as a partial coolant and as the gas generator fuel component, but not as a fuel in the main combustion chambers.

Only the point design in Table XXV is presented for this cycle. Analyses of other dual-throat engines in Reference 10, however, indicate that the point design may be close to the cooling limit for a fully regeneratively cooled engine. Other cooling options are, of course, available.

Simplifying assumptions were made in assessing the payload potential of all the candidate engines, in particular, the dual throat cycle K. It is, therefore, not practical from the results of this study alone to select the LOX/HC engine cycle for NASA to pursue. Detailed trajectory analysis using the parametric data from this study, and a propulsion system evaluation involving development time/cost/risk, recurring costs, and reliability considerations are required before a cycle can be selected with confidence.

B. FUELS

Fuels were ranked in this study for their cooling capability, their turbine-drive-gas power generation, and their engine performance. Other factors that should be included in the ranking, but were beyond the scope of this study, are availability, cost, safety, operational handling, and engine maintainability.

Methane is an excellent candidate fuel. It is a good coolant, provides high specific impulse, and is probably the best HC turbine-drive-fluid when burned fuel-rich with LOX. Fuel-rich methane is relatively free of coke, when compared to other HC fuels.

Subcooled propane is the best HC coolant. This fuel also provides high engine specific impulse and the estimated fuel-rich properties provide a good turbine-drive fluid. The bulk density of LOX/propane is nearly as high

as that of LOX/RP-1 and is significantly higher than that of LOX/methane. While subcooled propane has not been handled in appreciable quantities outside of the laboratory, tankage design should be straightforward. Propane can be maintained in the subcooled state in the vehicle by at least two approaches. One design incorporates the propane tank within the LOX tank, thus maintaining the fuel at the temperature of the LOX. Another design utilizes a jacket around the propane tank, where the jacket temperature is maintained at the LOX NBP by boiloff from the LOX tank.

As stated in the previous section concerning engine cycles, RP-1 fuel coking in the coolant channels severely limits the achievable chamber pressure. Thus the engine performance and the engine size are unacceptable for the stringent STS mission. The more refined RP-1 is a capable coolant for a fuel-cooled engine. Although more refined RP-1 (e.g., JP-7) is considered an operational fuel for military aircraft, it is not presently available in the quantities required by the STS.

Subcooled propane, with its high density, is the most promising hydrocarbon fuel candidate when compared with the low density methane, assuming all other properties are essentially equivalent.

C. TECHNOLOGY REQUIREMENTS

Areas requiring technological investigation can be separated into two categories: (1) those specifically needed to develop a LOX/HC engine, and (2) those that improve the state of the art of high-pressure engines in general. Those areas critical to the development of LOX/RP-1 and a LOX/LCH_4 engine are described in Figures 129 and 130, respectively. Both categories are summarized in Table LVIX.

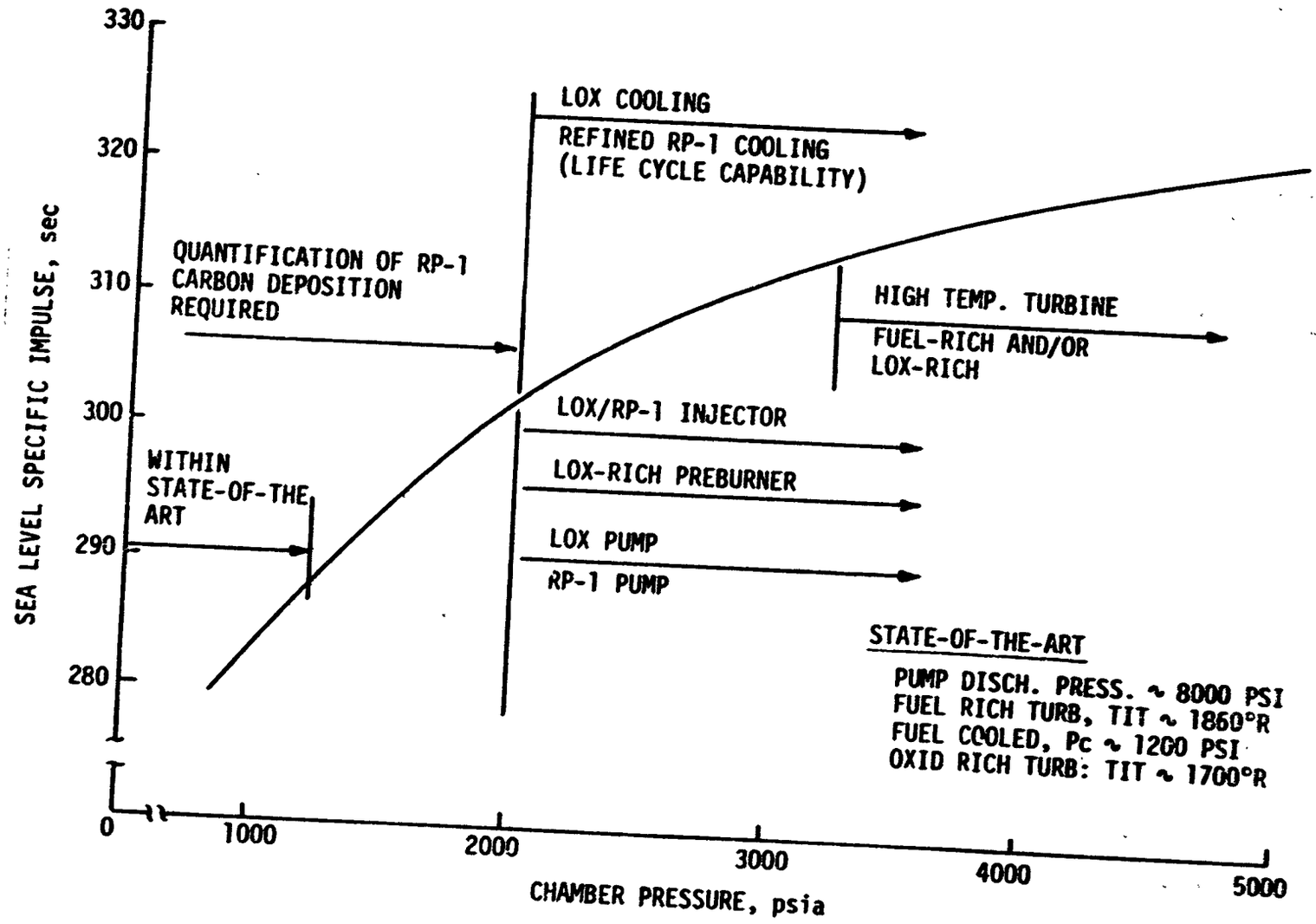

Figure 129. Technology Needs for Oxygen/RP-1 Staged-Combustion Cycle Engine

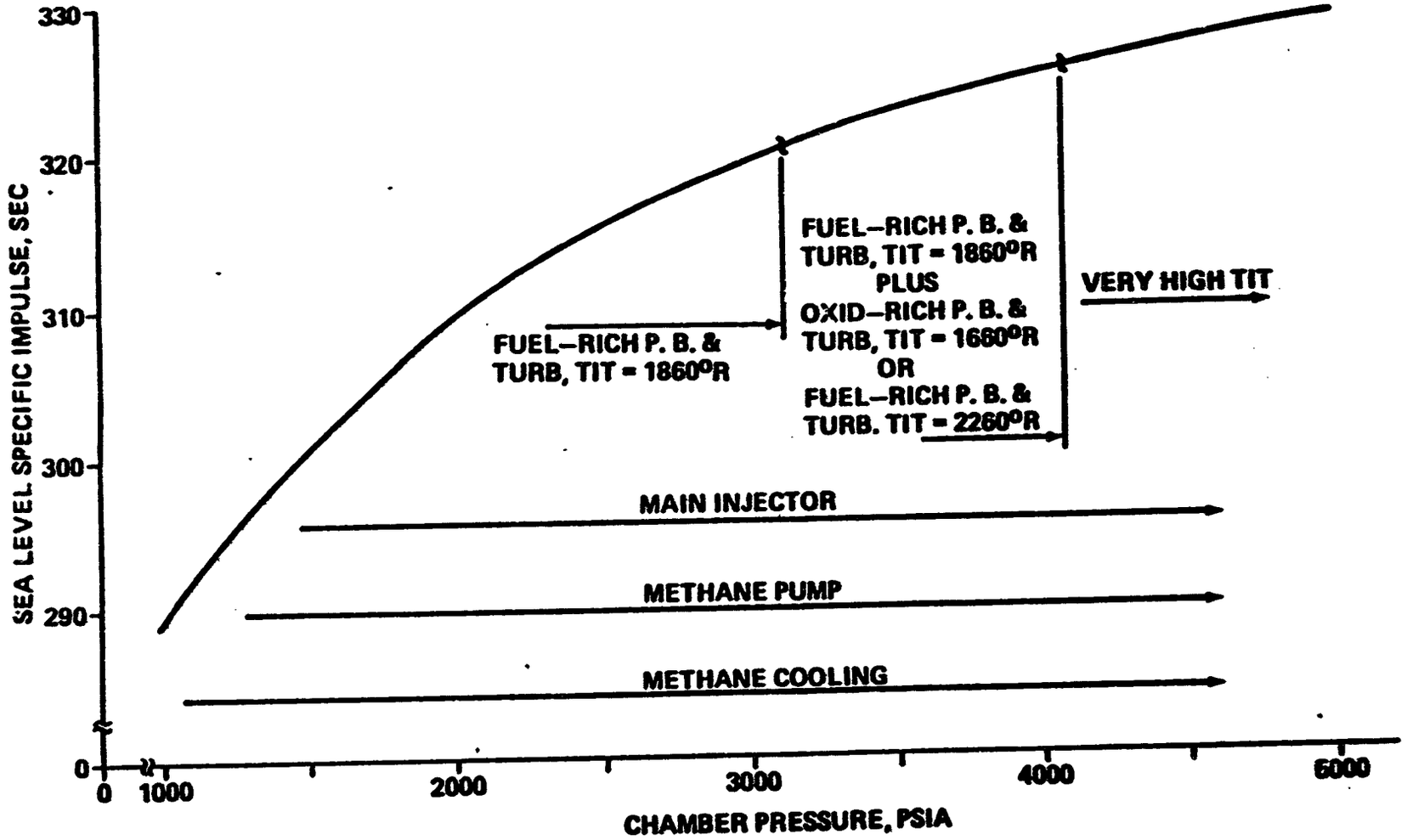

Figure 130. Technology Needs for Oxygen/Methane Staged-Combustion Cycle Engine

TABLE LIX

OXYGEN/HYDROCARBON ROCKET ENGINE REQUIRED TECHNOLOGY

TECHNOLOGY	JUSTIFICATION	TECHNICAL APPROACH
1. Fuel Turbopump RP-1, LCH_4 or LC_3H_8	Design criteria for rocket-type (high-speed) turbopumps are available for low pressures and for 1960s technology. High-pressure technology must be established prior to the development of an advanced LOX/HC engine.	Conduct detailed design study for a typical TPA that meets the design requirements of the engines in this study. Formulate a test program to incorporate 1980s technology, such as hydrostatic bearings, etc.
2. LOX Turbopump (LOX-rich Turbine)	Design criteria exist for high pressure, high-speed LOX TPAs driven by fuel-rich gas. Design criteria must be established for LOX-rich turbine-drive gas to achieve optimum LOX/HC engine.	Conduct detailed design study for typical TPA for cycle G or I from this study. Formulate a test program to demonstrate needed components and assembly.
3. Stoichiometric Preburner	Fuel-rich and oxidizer-rich preburners operate at conditions close to flame-out and on the steep portion of the T-vs-MR curve. A stoichiometric preburner operates at no worse than design condition. That is, the	Generate and evaluate designs in subscale hot-fire tests with LOX/HC fuel-rich and oxidizer-rich working fluids.

TECHNOLOGY	JUSTIFICATION	TECHNICAL APPROACH
3. Stoichiometric Preburner (cont.)	combuster and mixer (to achieve the desired temperature) are designed with transpiration cooling to withstand the highest combustion temperature. Control malfunctions thus lead to less severe operating conditions. Bad (hard) starts for high-pressure engines will be eliminated.	
4. High-Temperature Turbine (Fuel-rich)	High-temperature turbines provide additional horsepower and reduce either pump discharge pressure (SC) or gas turbine flowrate (GG), thus improving cycle efficiency. Turbine losses due to cooling need to be determined to ascertain the actual benefit of high-temperature turbines.	Perform a cooled turbine design analysis. Formulate a test program to demonstrate performance and life capability of cooled, high-temperature turbines.

TABLE LIX (cont.)

TECHNOLOGY	JUSTIFICATION	TECHNICAL APPROACH
5. High-Temperature Turbine (oxidizer-rich)	High-temperature oxidizer-rich turbines offer similar benefits to fuel-rich turbines, but very little technology exists. It is necessary to establish the upper limit that can be safely realized with high-temperature oxidizer-rich turbines.	Perform a cooled turbine design analysis. Formulate a test program to demonstrate the performance, life and temperature limit for oxidizer-rich turbines.
6. LCH_4 Supercritical Heat Transfer Data/ Correlation	Supercritical pressure heat transfer data do not exist for liquid methane. LOX and propane correlations are being used, leaving some uncertainty.	Conduct heated tube tests and correlate the data similar to the methods used for oxygen and propane.
7. Refined RP-1 Supercritical Heat Transfer Data/ Correlation	Supercritical pressure heat transfer data do not exist for refined grades of fuels such as JP-7. Design criteria do not exist for long duration operation with multiple restarts for high pressure RP-1-cooled engines.	Conduct heated tube tests to obtain a heat transfer correlation for supercritical (refined) RP-1 fuel. Conduct tests to determine the design criteria concerning long duration. and multiple restarts of RP-1-cooled high-pressure systems.

TABLE LIX (cont.)

TECHNOLOGY	JUSTIFICATION	TECHNICAL APPROACH
8. Cycle C Injector (LOX/LCH_4 or LC_3H_8)	Liquid-liquid injectors have not been established for high-pressure methane or propane.	Generate detail injector designs for Cycle C. Conduct single-element and subscale testing and analytical model development to establish design criteria.
9. Cylce G Injector Gas-Liquid (LOX/RP-1)	Design criteria for oxidizer-rich hot (1000°F) gas-liquid injectors is limited.	Conduct subscale (20K-40K) tests to evaluate performance, geometry, and heat transfer effects.
10. Cycle I Injector Gas-Gas (LOX/LCH_4 or LC_3H_8)	Design criteria for two 1000°F (oxidizer-rich and fuel-rich) gas streams not available at high chamber pressures.	Generate detail injector designs for Cycle I. Formulate a test program involving single-element and subscale testing and analytical model development.
11. Engine Weight Reduction with Advanced Materials	Reusability of the advanced LOX/HC engine allows the utilization of advanced composite materials to significantly reduce engine weight and to increase engine operating temperature capability.	Design, fabricate and test select subscale components made of advanced composite materials. Determine the weight savings and the life cycle capability.

TABLE LIX (cont.)

TECHNOLOGY	JUSTIFICATION	TECHNICAL APPROACH
12. Carbon Deposit Thrust Chamber Heat Transfer Enhancement	Titan I and Atlas engines formed a soot deposit on the chamber walls during normal operation. Conflicting data exist concerning the benefit of this deposit and whether the deposit will exist at the high pressure and higher mixture ratios utilized for advanced LOX/HC engines.	Conduct long duration tests with a calorimetric chamber, burning LOX/RP-1, LOX/LCH_4 or LC_3H_8 at high chamber pressures. Determine the heat transfer benefit of the carbon deposit buildup.
13. Single-Fuel Dual-Throat Engine	The single-fuel dual-throat thruster appears to offer a significant performance improvement over conventional booster engines because of its altitude compensating performance feature.	Conduct definitive design and trajectory analyses to verify the preliminary results obtained in this study.

VII, C, Technology Requirements (cont.)

The known state of the art of LOX/HC engines in Figure 129 is about 8270 kN/m^2 (1200 psia) chamber pressure. Any engine development much beyond this pressure will require a substantial data base prior to initiation, since high-pressure engine design criteria are markedly different from low-pressure design criteria. The selection of the engine cycle is all-important in reducing the hazards that can occur with marginal cycles.

The technology requirements in Figure 129 include the following:

(1) Quantification of carbon deposition on chamber walls at high pressures and high mixture ratios;

(2) Demonstration of the cooling capability of refined RP-1 and the elimination of coolant coking during engine operation and during the heat soakback on engine shutdown;

(3) Demonstration of LOX cooling in high-pressure LOX/RP-1 engines;

(4) Demonstration of a LOX-rich preburner, such as required for cycles F' and G;

(5) Development of design criteria for a high-speed RP-1 turbopump;

(6) Establishment of design criteria for a high-speed LOX turbopump with LOX-rich turbine-drive fluid;

(7) Evaluation of high-temperature turbines (cooled or uncooled);

(8) Development of high-pressure LOX/RP-1 injector design criteria.

The technology requirements listed in Figure 130 for a LOX/LCH_4 staged-combustion cycle engine are similar to those from Figure 129. Additional items include (1) demonstration of a LOX/LCH_4 gas-gas injector as required for cycle I; (2) development of liquid methane cooling at supercritical pressures; (3) development of LCH_4 turbopump design criteria; (4) demonstration of fuel-rich and oxidizer-rich LOX/LCH_4 preburners; and (5) evaluation of high-temperature turbines.

The above technical requirements for LOX/HC engines are summarized in Table LVIII. The data listed delineate both a justification and a typical program approach for each technology. Three additional technologies that are included in the table are (1) a stoichiometric preburner, (2) advanced materials, and (3) a single-fuel dual-throat engine. The justification for including the advanced materials is described in detail in Section IV,C,3. The justification for including the single-fuel dual-throat engine is described in more detail in Section V,D.

Although the stoichiometric preburner is not discussed elsewhere in this document, it is added here as the outgrowth of Aerojet's experience with high-pressure staged-combustion cycle engines. A similar device is reportedly utilized on the first-stage Ariane engine. Its use on a LOX/HC staged- combustion cycle engine (cycles G or I) should eliminate the potential for hard starts in case a slight malfunction in the start sequence were to occur.

VIII. CONCLUSIONS AND RECOMMENDATIONS

A. CONCLUSIONS

This study presents data on gas generator and staged combustion engine cycles for LOX/RP-1, LOX/refined RP-1, LOX/LCH_4, and LOX/LC_3H_8 propellant combinations, as well as data on hybrid cycles using LH_2 as a coolant and turbine-drive fluid. Since the LOX/HC application will be for a reusable, economic launch vehicle, engine selection should be made after a thorough operational cost evaluation has been conducted. Studies conducted to date by and for NASA (Refs. 4-8 and 24) have emphasized high engine performance and long engine life as major requirements for the propulsion system. These requirements are best met with an engine that makes maximum utilization of all propellants for cooling and for power system drive. Further investigation is required in order to select the optimum hydrocarbon fuel.

The specific conclusions (based on the assumptions given in Table LVIII) derived from this study are as follows:

(1) RP-1-cooled engines are limited to a chamber pressure of about 8960 kN/m^2 (1300 psia) because of fuel coking in the coolant jacket at higher pressures.

(2) RP-1-cooled engines with carbon deposit on the chamber walls are limited to a chamber pressure of about 13790 kN/m^2 (2000 psia) because of coking of the fuel in the cooling jacket.

(3) Refined RP-1 (e.g., JP-7) cooled engines are limited to a chamber pressure of about 17230 kN/m^2 (2500 psia) because of specific impulse (gas generator cycle) and to about 22060 kN/m^2 (3200 psia) because of power limit (staged combustion cycle).

VIII, A, Conclusions (cont.)

(4) Refined RP-1-cooled gas generator cycle engines with carbon deposit on the chamber walls are specific impulse limited to a chamber pressure of about 18610 kN/m^2 (2700 psia).

(5) LOX-cooled engines are specific impulse limited to a chamber pressure of about 17230 kN/m^2 (2500 psia) and 21370 kN/m^2 (3100 psia), respectively, as gas generator and staged combustion cycles.

(6) LOX-cooled gas generator cycle engines with carbon deposit on the chamber walls are specific impulse limited to a chamber pressure of about 18610 kN/m^2 (2700 psia).

(7) LCH_4-cooled engines are specific impulse limited to a chamber pressure of about 20680 kN/m^2 (3000 psia) and 24130 kN/m^2 (3500 psia), respectively, as gas generator and staged combustion cycles.

(8) LC_3H_8-cooled engines are specific impulse limited to a chamber pressure of about 20680 kN/m^2 (3000 psia) and 24820 kN/m^2 (3600 psia), respectively.

(9) LH_2-cooled LOX/HC gas generator cycle engines are power limited to a chamber pressure of about 37920 kN/m^2 (5500 psia).

(10) Increased turbine inlet temperatures (fuel- and oxidizer-rich) offer a large benefit for gas-generator and mixed-cycle engines and a smaller benefit for staged-combustion cycle engines.

(11) Application of reinforced plastic composite materials could result in an engine weight reduction of 30% by the year 1985 and a weight reduction of 40% by the year 2000.

(12) LOX-RP-1 staged-combustion cycle engines with LOX-rich preburner and LOX or refined RP-1 cooling provide the highest specific impulse potential for an RP-1 (or refined RP-1) fueled engine.

(13) The LOX/LCH_4 dual-throat engine with LH_2 cooling and a mixed gas-generator/staged-combustion cycle offers the highest specific impulse potential of the cycles included in this study.

(14) The highest payload capability for the two-stage ballistic recovery vehicle considered was achieved with the dual-throat engine. With conventional nozzles, the highest payload capability was achieved with staged combustion engine cycles incorporating dual-preburners or with gas generator engines using hydrogen-cooling and hydrogen-rich turbine drive.

(15) The LOX/LCH_4 gas-generator cycle engines offer the highest specific impulse for a LOX/HC gas-generator engine.

B. RECOMMENDATIONS

The majority of the technology requirements defined in this study are common to all LOX/HC engines. Because the NASA mission and the engine cycle selection may not be made for several years, and because it requires at least eight years to provide the technology base for the economical development of a LOX/HC engine, it is recommended that the major technology items be demonstrated as early as the budget permits. These include the following:

(1) Fuel and LOX turbopumps
(2) Stoichiometric preburner
(3) High-temperature turbines
(4) LCH_4 supercritical heat transfer data

VIII, B, Recommendations (cont.)

(5) Refined RP-1 supercritical heat transfer data

(6) LOX/HC injectors

(7) Advanced material application to valves, pump housings, lines, etc.

(8) Carbon deposit evaluation

(9) Dual throat evaluation

Vehicle applications analyses similar to those performed by NASA/LaRC (Ref. 4) should be conducted to determine the comparative merit of the LOX/HC engine cycles for several NASA missions.

More definitive engine design studies should be conducted for the more promising cycles in order to establish the design methodology for achieving optimum reusability and ease of maintenance.

REFERENCES

1. Salkeld, R., "Mixed-Mode Propulsion for the Space Shuttle," Astronautics & Aeronautics, Vol. 9, No. 8, pp. 52-58, August 1971.

2. Salkeld, R. and Beichel, R., "Reusable One-Stage-to-Orbit Shuttles: Brightening Prospects," Astronautics & Aeronautics, Vol. 11, No. 6, pp. 48-58, June 1973.

3. Beichel, R., "Propulsion Systems for Single-Stage Shuttles," Astronautics & Aeronautics, Vol. 12, No. 11, pp. 32-39, Nov. 1974.

4. Henry, B.Z. and Eldred, C.H., "Advanced Technology and Future Earth-to-Orbit Transportation Systems," AIAA Paper No. 77-530, presented at the Third Princeton/AIAA Conference on Space Manufacturing Facilities, May 1977.

5. Haefeli, R.C., Littler, E.G., Hurley, J.B., and Winger, M.G., "Technology for Advanced Earth-Orbital Transportation Systems, Dual-Mode Propulsion," Martin Marietta Corporation, Report NASA-CR-2868, Contract NAS 1-13916, October 1977.

6. Hepler, A.K. and Bangsund, E.L., "Technology Requirements for Advanced Earth Orbital Transportation Systems - Dual Mode Propulsion," Boeing Aerospace Company, Report NASA-CR-3037, Contract NAS 1-13944, July 1978.

7. Wilhite, A.W., "Propulsion -- A Key Technology for Advanced Space Transportation," AIAA Paper No. 79-1219, presented at the AIAA/SAE/ASME 15th Joint Propulsion Conference, 18-20 June 1979.

8. Martin, J.A., "Parallel-Burn Options for Dual-Fuel Single-Stage Orbital Transports," Journal of Spacecraft and Rockets, Vol. 15, No. 1, pp. 4-6, January-February, 1978.

9. Luscher, W.P. and Mellish, J.A., "Advanced High Pressure Engine Study for Mixed-Mode Vehicle Applications," Aerojet Liquid Rocket Co. Report NASA-CR-135141, Contract NAS 3-19727, January 1977.

10. O'Brien, C.J., "Dual-Fuel, Dual-Throat Engine Preliminary Analysis," Aerojet Liquid Rocket Company, Report 32967F, Contract NAS 8-32967, August 1979.

11. Taylor, W.F., ed., "Jet Fuel Thermal Stability," NASA/LeRC Workshop November 1978, NASA-TM-79231, 1979.

12. Hess, H.L. and Kunz, H.R., "A Study of Forced Convection Heat Transfer to Supercritical Hydrogen," ASME Paper 63-WA-205, November 1963.

REFERENCES (cont.)

13. Spencer, R.G. and Rousar, D.C., "Supercritical Oxygen Heat Transfer," Report NASA CR-135339, November 1977.

14. Gross, R.S., "Combustion Performance and Heat Transfer Characterization of LOX/Hydrocarbon Propellants, Task I Data Dump," Aerojet Liquid Rocket Company, Contrct NAS 9-15958, August 1980.

15. Hines, W.S., "Turbulent Forced Convection Heat Transfer to Liquids at Very High Heat Fluxes and Flow Rates," Rocketdyne Research Report No. 61-14, 30 November 1961.

16. Romine, W.D., "Investigation of Advanced Cooling Techniques for High-Pressure Hydrocarbon-Fueled Engines," 6th Monthly Report, Contract NAS 3-21381, Rocketdyne Division Report ATU-79-5030, 17 February 1979.

17. Beichel, R., "Advanced Rocket Engine-Storable," Contract AF04(611)-10830, Aerojet-General Corporation Report AFRPL-TR-67-75, August 1967.

18. Kuntz, R.J., Sjogren, R.G., et al., "Advanced Propellant Staged-Combustion Feasibility Program," Aerojet-General Corporation Report AFRPL-TR- 67-204, Contract AF04(611)-10785, September 1967.

19. Nickerson, G.R., Coats, D.E., and Bartz, J.L., "Two-Dimensional Kinetic Reference Computer Program-TDK," Contract NAS 9-12652, December 1973.

20. Pieper, J.L., "ICRPG Liquid Propellant Thrust Chamber Performance Evaluation Manual," Aerojet General Corp., CPIA Publication No. 178, 30 September 1968.

21. Werner, George A., "Aerospace Charts Future for Composite Materials," Iron Age, December 3, 1979.

22. Freche, J.C. and Ault, M.A., "Progress in Advanced High Temperature Turbine Materials, Coatings and Technology," NASA TM X-73628.

23. "Satellite Power System: Concept Development and Evaluation Program, Reference System Report," DOE/ER-0023, NASA TM-79762, January 1979.

24. Caluori, V.A., Conrad, R.T. and Jenkins, J.C., "Technology Requirements for Future Earth-to-Geosynchronous Orbit Transportation Systems," Boeing Aerospace Company, NASA CR 3265, Contract NAS 1-15301, April 1980.